

Peristaltic Flows of Nanofluid with Compliant Walls



By

Zahid Nisar

**Department of Mathematics
Quaid-i-Azam University
Islamabad, Pakistan
2022**

Peristaltic Flows of Nanofluid with Compliant Walls



By

Zahid Nisar

Supervised By

Prof. Dr. Tasawar Hayat

**Department of Mathematics
Quaid-i-Azam University
Islamabad, Pakistan
2022**

Peristaltic Flows of Nanofluid with Compliant Walls



By

Zahid Nisar

A THESIS SUBMITTED IN THE PARTIAL FULFILLMENT OF THE REQUIREMENT FOR THE
DEGREE OF
DOCTOR OF PHILOSOPHY
IN
MATHEMATICS

Supervised By

Prof. Dr. Tasawar Hayat

**Department of Mathematics
Quaid-i-Azam University
Islamabad, Pakistan
2022**

Author's Declaration

I **Zahid Nisar** hereby state that my PhD thesis titled **Peristaltic Flows of Nanofluid with Compliant Walls** is my own work and has not been submitted previously by me for taking any degree from the Quaid-I-Azam University Islamabad, Pakistan or anywhere else in the country/world.

At any time if my statement is found to be incorrect even after my graduate the university has the right to withdraw my PhD degree.

Name of Student: **Zahid Nisar**

Date: **06-06-2022**

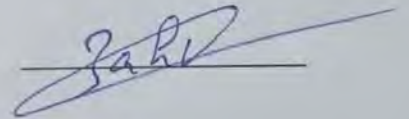
Plagiarism Undertaking

I solemnly declare that research work presented in the thesis titled "Peristaltic Flows of Nanofluid with Compliant Walls" is solely my research work with no significant contribution from any other person. Small contribution/help wherever taken has been duly acknowledged and that complete thesis has been written by me.

I understand the zero tolerance policy of the HEC and Quaid-I-Azam University towards plagiarism. Therefore, I as an Author of the above titled thesis declare that no portion of my thesis has been plagiarized and any material used as reference is properly referred/cited.

I undertake that if I am found guilty of any formal plagiarism in the above titled thesis even afterward of PhD degree, the University reserves the rights to withdraw/revoke my PhD degree and that HEC and the University has the right to publish my name on the HEC/University Website on which names of students are placed who submitted plagiarized thesis.

Student/Author Signature:

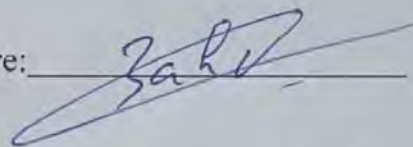


Name: Zahid Nisar

Certificate of Approval

This is to certify that the research work presented in this thesis entitled **Peristaltic Flows of Nanofluid with Compliant Walls** was conducted by Mr. **Zahid Nisar** under the kind supervision of **Prof. Dr. Tasawar Hayat**. No part of this thesis has been submitted anywhere else for any other degree. This thesis is submitted to the Department of Mathematics, Quaid-i-Azam University, Islamabad in partial fulfillment of the requirements for the degree of Doctor of Philosophy in field of Mathematics from Department of Mathematics, Quaid-i-Azam University Islamabad, Pakistan.

Student Name: **Zahid Nisar**

Signature: 

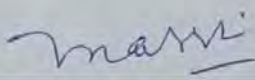
External committee:

a) **External Examiner 1:**

Name: **Dr. Nasir Ali**

Designation: Professor

Office Address: Department of Mathematics & Statistics,
International Islamic University, Islamabad.

Signature: 

b) **External Examiner 2:**

Name: **Dr. Maryiam Javed**

Designation: Associate Professor

Office Address: Department of Applied Mathematics and Statistics,
Institute of Space Technology (IST), Islamabad.

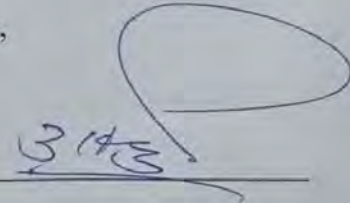
Signature: 

c) **Internal Examiner**

Name: **Dr. Tasawar Hayat**

Designation: Professor

Office Address: Department of Mathematics, QAU Islamabad.

Signature: 

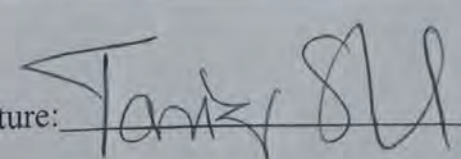
Supervisor Name:

Prof. Dr. Tasawar Hayat

Signature: 

Name of Dean/HOD:

Prof. Dr. Tariq Shah

Signature: 

Peristaltic Flows of Nanofluid with Compliant Walls

By

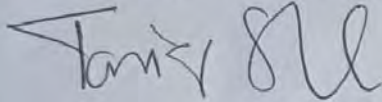
Zahid Nisar

CERTIFICATE

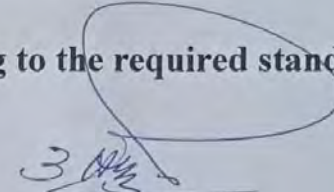
A THESIS SUBMITTED IN THE PARTIAL FULFILLMENT OF THE
REQUIREMENTS FOR THE DEGREE OF THE

DOCTOR OF PHILOSOPHY IN MATHEMATICS

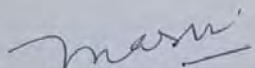
We accept this dissertation as conforming to the required standard

1. 

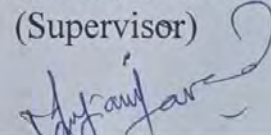
Prof. Dr. Tariq Shah
(Chairman)

2. 

Prof. Dr. Tasawar Hayat
(Supervisor)

3. 

Prof. Dr. Nasir Ali

4. 

Dr. Maryiam Javed
Associate Professor

Department of Mathematics & Statistics
International Islamic University,
Islamabad

(External Examiner)

Department of Applied Mathematics and
Statistics, Institute of Space Technology
(IST), Islamabad

(External Examiner)

Department of Mathematics

Quaid-I-Azam University

Islamabad, Pakistan

2022

DEDICATED
TO
MY BELOVED PARENTS
AND
MY DAUGHTER
ALISHA ZAHID

Acknowledgment

In the name of **Allah** the most beneficent and the most merciful, who granted me the ability and potential to fulfill the requirements of my dissertation. I offer my humblest gratitude to the **Holy Prophet Muhammad (S. A. W)** who is forever a torch of guidance and knowledge for humanity.

I express my deepest gratitude to my respected, affectionate, and devoted supervisor **Prof. Dr. Tasawar Hayat** for his intellectual guidance, constant encouragement, suggestions, and inexhaustible inspiration throughout my research work. I am certain that the guidance and training provided by him to me have laid a foundation for my future success. Many thanks to **Prof. Dr. Tariq Shah** (Chairman) and **Prof. Dr. Sohail Nadeem** (ex-chairman) for providing me an opportunity to learn and seek knowledge in an educated environment.

My deepest gratitude goes to my father **Nisar Ahmed** and mother **Rehana Kousar**, for their love, support and encouragement. I am very thankful to my Grandfather **Nazir Ahmed (Late)** for their love and prayers for me. Also, I would like to thank my younger brother **Shahid Ishaq** and **Tahir Usman** for their love and support. I wish to express my devoted thanks to My wife **Amna Mehboob** who supported and encouraged me at every tough moment of my life.

I am extremely thankful to my honorable seniors **Dr. Fahad Munir Abbasi**, **Dr. Humaira Yasmin** and **Dr. M. Bilal Ashraf** for their cooperation and suggestions throughout the research work.

I would extend my sincere and heartily thanks and appreciation to my colleagues **Dr. Bilal Ahmed**, **Dr. Arsalan Aziz** and **Dr. Khursheed Muhammad** they always encouraged and cooperated with me and made every possible effort to provide the invaluable input for the improvement of this study.

With tremendous pride and love, I am cordially thankful to my friends **Dr. Zahid Ahmed, Dr. Zakir Hussain, Dr. Faisal Shah, Dr. M. Asif, Dr. Sajjad Husain, Dr. Sohail Khan, Dr. Naeem Ullah, Mr. Waqar** and **Mr. Fakhar Abbas** for providing me nice company during my research work.

Zahid Nisar

June 9, 2022

Preface

It is well established fact that peristalsis is employed in esophagus, intestine and stomach. This phenomenon is also used in blood pump machines, chyme in the gastrointestinal tract, sanitary materials transportation, roller and finger pumps and many others. Thermal management is major issue in a variety of industries including transportation, microelectronics, manufacturing and metrology. One of the most important approaches to accomplish faster cooling for many applications is to improve the heat transfer capabilities of standard heat transfer fluids. Scientists have recently concentrated on nanofluid for an increase about the heat transportability of traditional fluids by adding tiny nanoparticles. Nanofluids with high thermal conductivity and low viscosity, even at low particle concentrations, are important for heat transport applications. In addition the peristalsis of non-Newtonian fluids in channel with compliant walls has significance in biomechanics and engineering. We therefore focus about this topic here. This thesis has ten chapters.

Relations of Cauchy stress tensors of non-Newtonian fluids and background information about literature review are given in chapter one.

Chapter two examines peristalsis of nanoliquid in a compliant wall channel. Mixed convection and Hall current analysis are present. Partial slip and convective conditions are simultaneously discussed. Numerical computations have been executed for the velocity, nanoparticles concentration, temperature, and coefficient of heat transfer. Graphical analysis is presented. This chapter are published in **International Communications in Heat and Mass Transfer 121 (2021) 105121**.

Chapter three elaborates the bioconvective peristaltic transport of nanoliquid with gyrotactic microorganisms. Channel walls are considered symmetric and elastic nature. Partial slip

conditions are imposed. Thermal radiation is present in the energy equation. The results for velocity, concentration, temperature, heat transfer coefficient and density of motile microorganism are examined graphically. Results of this chapter are available in **International Communications in Heat and Mass Transfer 129 (2021) 105693**.

Chapter four addresses MHD peristaltic motion of couple stress nanofluid in a channel with compliant walls. Influences of Ohmic heating and viscous dissipation are analyzed. Zero mass nanoparticle flux and convective condition are also imposed on channel walls. A numerical solution is obtained for large wavelength and small Reynolds numbers. The impacts of pertinent parameters of interest on concentration, temperature, and coefficient of heat transfer are scrutinized graphically. The result of this research is submitted in **Mathematical Methods in the Applied Sciences**.

Chapter five describes impacts of wall flexibility on MHD peristaltic flow of Eyring–Powell nanofluid. Convective conditions are employed. No slip conditions are imposed on channel walls. Nanofluid model is considered by taking the impacts of thermophoresis and Brownian motion. Influences of pertinent variables on axial velocity, temperature, concentration and coefficient of heat transfer are inspected graphically. Material here is published in **Journal of Thermal Analysis and Calorimetry 144 (2021) 1199-1208**.

Sixth chapter explores first-order chemical reactions and activation energy on MHD peristaltic activity of Eyring-Powell nanomaterial. Mathematical modelling for generation/absorption is organized. Velocity slip is imposed. Numerical results for velocity, concentration, temperature, rate of heat transfer and trapping are analyzed. Material of this study is published in **International Communications in Heat and Mass Transfer 116 (2020) 104655**.

Chapter seven discusses slips aspects for peristaltic motion of fourth-grade nanoliquid. Elastic characteristics of channel walls are studied. Velocity, concentration and thermal slip effects are imposed. Thermal radiation and dissipation are studied. Comprehensive study for heat transfer coefficient, velocity, concentration of nanoparticles, temperature, velocity and trapping is arranged. Moreover the results for skin friction coefficient and Sherwood number are focused. The contents here are published in **International Communications in Heat and Mass Transfer** **119 (2020) 1046976**.

Chapter eight addresses impacts of entropy generation and Joule heating on MHD peristaltic activity of fourth-grade nanofluid. Analysis carried out by taking the effects of radiation and Arrhenius activation energy. Numerical technique is used to solve the resulting problem. Detailed analysis of the emerging parameters of interest on velocity, temperature, concentration, coefficient of heat transfer and entropy are graphically examined. The findings of this study have been submitted for publication in **Applied Mathematics and Mechanics**.

Chapter nine inspected mixed convection peristaltic motion of tangent hyperbolic nanoliquid. Partial slip characteristics are imposed on flexible channel walls. We evaluated the transportation of heat for nonlinear thermal radiation. The roles of sundry variables on velocity, concentration, temperature and coefficient of heat transfer are examined graphically. Finally, key points of the analysis are organized. The results of this research have been submitted for publication in **The European Physical Journal Plus**.

Chapter ten addresses peristaltic flow of MHD Sutterby nanomaterial with entropy generation and Hall aspects. Convective conditions are imposed for flexible channel walls. Energy and concentration equations are arranged in presence of Joule heating, thermal radiation, dissipation and activation energy. Resulting nonlinear system is numerically solved. Graphical analysis for

velocity, temperature, concentration, heat transfer rate and entropy generation is analyzed. The contents of this chapter are published in **Journal of Thermal Analysis and Calorimetry 143 (2021) 1867-1880.**

Contents

1 Literature review and basic laws	6
1.1 Introduction	6
1.2 Literature survey	6
1.3 Basic equations	11
1.3.1 Mass conservation	11
1.3.2 Momentum conservation	12
1.3.3 Energy conservation	12
1.3.4 Concentration equation	12
1.4 Models of fluids	13
1.4.1 Viscous fluid	13
1.4.2 Non-Newtonian fluids	13
1.4.3 Compliant wall	15
2 Peristalsis of nanofluid by mixed convection and wall properties	17
2.1 Introduction	17
2.2 Physical model	17
2.3 Numerical method	20
2.4 Graphical findings	20
2.4.1 Velocity	20
2.4.2 Temperature	21
2.4.3 Concentration	21
2.4.4 Coefficient of heat transfer	22

2.5	Closing remarks	36
3	Bioconvection analysis for peristalsis of nanofluid	38
3.1	Introduction	38
3.2	Problem development	38
3.3	Numerical method	41
3.4	Graphical outcomes and discussion	42
3.4.1	Velocity	42
3.4.2	Temperature	42
3.4.3	Concentration	43
3.4.4	Coefficient of heat transfer	43
3.4.5	Density of motile microorganism	44
3.5	Conclusions	56
4	Peristalsis of couple stress nanofluid with wall characteristics	57
4.1	Introduction	57
4.2	Formulation	57
4.3	Numerical method and analysis	60
4.3.1	Temperature	60
4.3.2	Concentration	61
4.3.3	Coefficient of heat transfer	62
4.4	Concluding remarks	71
5	Significance of convective conditions for peristalsis of Eyring-Powell nanofluid	72
5.1	Introduction	72
5.2	Formulation	72
5.3	Results and discussion	76
5.3.1	Velocity	76
5.3.2	Temperature	76
5.3.3	Concentration	77

5.3.4	Heat transfer coefficient	78
5.4	Validation of the result	87
5.5	Conclusions	88
6	Peristalsis of Eyring-Powell nanofluid with activation energy and heat generation/absorption	89
6.1	Introduction	89
6.2	Formulation	89
6.3	Numerical outcomes and discussion	93
6.3.1	Velocity	93
6.3.2	Temperature	94
6.3.3	Concentration	94
6.3.4	Heat transfer coefficient	95
6.3.5	Trapping	95
6.4	Physical quantities	96
6.5	Conclusion	110
7	Peristaltic activity of fourth grade nanofluid with slip and radiation	112
7.1	Introduction	112
7.2	Formulation	112
7.3	Numerical outcomes and discussion	116
7.3.1	Velocity	116
7.3.2	Temperature	117
7.3.3	Concentration	117
7.3.4	Coefficient of heat transfer	118
7.3.5	Skin friction Coefficient	118
7.3.6	Sherwood number	118
7.3.7	Trapping	119
7.4	Conclusions	133

8	Entropy generation in mixed convective peristalsis of fourth grade nanofluid	135
8.1	Introduction	135
8.2	Formulation	135
8.3	Numerical results	138
8.3.1	Velocity	138
8.3.2	Temperature	138
8.3.3	Concentration	138
8.3.4	Heat transfer coefficient	139
8.3.5	Entropy	139
8.4	Expression for entropy generation	139
8.5	Conclusions	150
9	Peristaltic activity of hyperbolic tangent nanofluid with non-linear radiation	151
9.1	Introduction	151
9.2	Formulation	151
9.3	Results and discussion	155
9.3.1	Velocity	155
9.3.2	Temperature	156
9.3.3	Concentration	156
9.3.4	Heat transfer coefficient	157
9.4	Conclusions	169
10	Peristalsis of Sutterby nanofluid with Hall current and entropy generation	170
10.1	Introduction	170
10.2	Formulation	170
10.3	Expression for entropy generation	174
10.4	Numerical outcomes and discussion	175
10.4.1	Velocity	175
10.4.2	Temperature	176
10.4.3	Concentration	176
10.4.4	Coefficient of Heat transfer	176

10.4.5 Entropy generation	177
10.5 Validation of the problem	177
10.6 Conclusions	186

Chapter 1

Literature review and basic laws

1.1 Introduction

This chapter deals with the basic concept of equations and literature survey of peristalsis, nanofluid, non-Newtonian fluid models, compliant walls and mixed convection. Different types of constitutive relations for non-Newtonian fluid models like Couple-stress, Eyring-Powell, Fourth-grade, Sutterby and Hyperbolic tangent are included.

1.2 Literature survey

Peristalsis is the process of muscular tissue contraction and relaxation that enables for material movement. This mechanism has applications in physiology and engineering. These applications comprise like chewing of food via the esophagus, sanitary fluid transport, chyme activity in intestine and vasomotion of blood vessels. Many biological applications like heart-lung devices and blood pumps for dialysis are due to this activity. The subject has received considerable attention from researchers due to its widespread occurrence in medical, engineering and electronics. Latham [1] presented a seminal study for viscous fluid on peristalsis. Burns and Parkes [2] examined peristaltic flow of viscous fluid considering different geometries. Shapiro et al. [3] represented the fundamental principle and reflect the importance of this flow mechanism for various physical variables. This analysis was extensively explained employing long wavelength and low Reynold number. Dodds et al. [4] discussed peristaltic movement in the esophagus

with dry and wet swallows. Srivastava and Srivastava [5] addressed the peristaltic flow of viscous fluid through a two-layered model. Shehawy and Husseny [6] reported the peristalsis of incompressible viscous fluid filling porous space. Misra and Pandey [7] studied the mathematical modeling of peristaltic activity for Casson fluid. Mekheimer [8] examined peristaltic transport of blood flow by taking magnetic features in a non-uniform channel. Hayat et al. [9] discussed peristaltic transport of Jeffrey liquid with an endoscope aspect. Ali et al. [10] scrutinized features of slip in MHD peristalsis with variable viscosity. Peristalsis of Maxwell liquid is reported by Tripathi et al. [11]. Mustafa et al. [12] analyzed the peristaltic flow of nanofluid with partial slip effects. Abbasi et al. [13] examined numerical investigation for peristaltic activity of copper–water nanomaterial through porous space. Hayat et al. [14] analyzed impacts of thermal radiation and convective conditions for peristalsis of nanofluid. Ellahi et al. [15] explored peristaltic transport of couple stress fluid in a non-uniform rectangular duct. Size of trapped bolus declines for couple stress fluid variable. Sinnott et al. [16] discussed peristaltic activity in a small intestine through particulate suspension. From this study it is noted that high fluid pressures in advance of the moving contraction induce considerable wall dilatation shortly downstream inside the relaxation period for solely liquid content. Bhatti et al. [17] focused heat and mass transfer for MHD peristaltic flow of Sisko fluid by considering Darcy-Brinkman-Forchheimer porous space. Velocity enhances via Darcy aspect. Hayat et al. [18] examined peristaltic motion of nanoliquid in a curved channel with Hall aspects. Velocity of fluid enhances for Hall effect.

Nanofluids are significant due to their use in industry and thermal engineering. Nanofluids incorporate the nanoparticles that are suspended with diameters ($<100\text{nm}$). These materials are used for increased thermal conductivity. The nanoparticles normally used are usually made of oxides (TiO), carbides (SiC), metals (Cu, Ag), or non-metallic carbon nanotubes. Nanofluids have applications such as thermal absorption, machine processes, cooling and chillers heat transfer efficiency, microelectronics, boiling processes and nuclear reactor etc. These are often used in the delivery of medications and in patients with radiation. Choi [19] combined nanoparticles with base fluid and found that the resulting fluids had a significant difference in thermal conductivity. Kang et al. [20] experimentally examined this argument. Later on Buongiorno [21] studied a non-homogeneous equilibrium model. It shows that the presence of

thermophoresis and random diffusions improve the thermal conductivity of conventional fluids. Akbar et al. [22] analyzed peristalsis of nanofluid with slip aspects. Consequence of convective heat transfer of Al₂O₃/water nanofluid in a circular duct is studied by Heris et al. [23]. Ebaid and Aly [24] computed exact solution for peristaltic flow of nanofluid in an asymmetric channel with flexible boundaries. Numerical investigation for peristaltic activity of Carreau nanomaterial is studied by Akbar et al. [25]. Temperature of fluid increases through Brownian motion and thermophoresis variables. Tripathi and Bég [26] explored the mixed convection analysis in peristaltic pumping of nanofluid. This study is very much applicable in drug delivery structures. Hayat et al. [27] addressed slip aspects for peristaltic flow of nanofluid through Soret and Dufour effects. Kothandapani and Prakash [28] explored magnetic field and radiation aspects for peristaltic flow of nanomaterial filling porous space. Akbar et al. [29] investigated heat source/sink features in peristaltic flow by addition of nanoparticles. Reddy and Makinde [30] analyzed the characteristics of nanofluid with a peristaltic motion of Jeffrey material. Numerical simulation regarding peristaltic activity of water-based nanofluid considering temperature-dependent viscosity is studied by Hayat et al. [31]. Tripathi et al. [32] examined electroosmotically modulated peristalsis of nanomaterial. Ohmic heating aspects also present in this study. Abbasi et al. [33] developed numerical solution for peristaltic transport of nanofluid by considering boron nitride-ethylene glycol. In this study temperature rises via Hartman number. Mekheimer et al. [34] examined blood flow analysis by considering the gold nanoparticles in peristaltic motion. In this study, they examined how gold nanoparticles are useful in cancer treatment. Rafiq et al. [35] focused peristalsis of nanomaterial subject to ion-slip and Hall aspects. This study is useful for biomedical purposes.

Recently the researchers have concentrated their attention on investigating the features of non-Newtonian matters owing to their major usefulness in numerous chemical and mechanical industries. The functional implementations found in non-Newtonian fluids include processing cheap soft material, greases, paints, sugar solution, polymer melts and many more. The applications of non-Newtonian fluids in the fields of chemical industries, biomedical processes, particles mixing and filtration of devices etc. Various relations of non-Newtonian fluids are present considering different assumptions. Srivastava [36] discussed the peristaltic motion with couple-stress fluid. Ramesh [37] discussed the slip features in the peristalsis of couple stress

fluid filling porous space. Velocity and temperature are enhanced against Couple stress fluid parameter. Hayat et al. [38] studied the aspects of convective conditions in peristaltic activity through Eyring-Powell fluid with chemical reaction. Temperature is decayed with the increment of Biot number. Bhatti et al. [39] studied MHD peristaltic transport of Ree–Eyring liquid with flexible walls. Mehmood et al. [40] demonstrated peristaltic activity with fourth-grade material in an inclined channel. Soret and Dufour aspects in mixed convective peristaltic activity is due to Mustafa et al. [41]. Akbar et al. [42] explored peristalsis of Sutterby liquid within small intestines. Abbasi et al. [43] scrutinized comparative study of peristalsis of Sutterby and Eyring-Prandtl fluids. Akram and Nadeem [44] analyzed mixed convective peristaltic flow of hyperbolic tangent nanofluid. Velocity of fluid decline via magnetic variable. Abbasi et al. [45] developed the numerical solutions about MHD peristaltic flow of Carreau–Yasuda material through a curved channel with Hall current.

Mechanism of peristalsis through compliant channel is popular in applications regarding physiological flows and engineering. Hence Mitra and Prasad [46] firstly discussed the effect of wall properties in peristalsis. Radhakrishnamacharya and Srinivasulu [47] examined compliant wall aspects for peristaltic of heat transfer. Srinivas et al. [48] explored variations of slip conditions, wall properties and heat transfer on MHD peristaltic motion. Srinivas and Kothandapani [49] highlighted the influence of heat and mass transfer on MHD peristaltic flow through a porous space with compliant walls. Impacts of wall properties are reported by Hayat et al. [50]. Mustafa et al. [51] examined numerical investigation peristaltic transport of nanomaterial in a symmetric channel with wall properties. He compared the numerical solution with Homotopy(HAM) method through good agreement. Hayat et al. [52] studied the influence of compliant walls on peristalsis of power-law fluid. Gad [53] discussed influence of Hall current on peristalsis in a channel with wall effects. Nadeem et al. [54] scrutinized features regarding elastic walls for Williamson nanoliquid in a curved channel. Sucharitha et al. [55] reported MHD peristaltic transport of nanomaterial with compliant wall chrematistics. In this study the authors analyzed the aspects of Ohmic heating and viscous dissipation.

Forced convection might not be enough to evaporate all the heat in very high-power output devices. In these situations, the combination of natural convection and forced convection (mixed convection) can better produce the desired results. This mechanism refers to the process

of heat transmission in fluids in which the flow field is much different than it would be under normal circumstances of uniform density due to differences in gravitational body force associated with non-uniformity of density within the system. The mechanisms involved are typically viewed in terms of fluid buoyancy and the consequences are sometimes referred to as buoyancy effects on heat transmission. Mixed convection usually occurs in many industrial and technological applications. Examples of mixed convection phenomena include a low-speed heat exchanger, solar cells, ventilator-cooled electronic devices, and nuclear reactor cooling during an emergency shutdown. Umavathi et al. [56] explored the analysis of mixed convection through vertical porous medium. Brinkman–Forchheimer extended Darcy equations are employed to model flow in this study too. Akbarinia and Behzadmehr [57] have discussed the mixed convection analysis by considering the features of nanomaterial in curved tubes. Eldabe et al. [58] analyzed mixed convective peristalsis of Biviscosity liquid with viscosity dependence on temperature. Srinivas et al. [59] calculated exact solution for peristaltic activity with mixed convection. Akram et al. [60] investigated peristaltic flow of nonlinear liquid in an asymmetric channel subject to mixed convection. Hayat et al. [61] examined MHD peristaltic motion with mixed convection. Viscosity features are taken in this investigation as a variable. Slip impact for peristaltic transport of nanofluid with mixed convection is analyzed by Noreen et al. [62]. Magnetic field and dissipation have been accounted. Mokhtari et al. [63] developed numerical investigation for mixed convective flow considering different Fin arrangements with the horizontal channel. Turkyilmazoglu [64] calculated the exact solutions for MHD mixed convection flow with stretching walls.

The role of thermal radiation is very important in industrial operations and space technologies. Thermal radiation must be evaluated in the current study since it demonstrates a remarkable synchronization of system temperature/changing heat transfer rate. Thermal radiation is also used in medical treatments. Pal [65] examined the effects of radiation and heat sink/source for flow by unsteady stretching surface. Hayat and Alsaedi [66] studied Ohmic heating and thermal radiation for MHD Oldroyd-B fluid. Ara et al. [67] investigated the radiative analysis for flow of Powell- Eyring material. Kothandapani and Prakash [68] studied radiation effects on the peristaltic transport of nanofluids. Latif et al. [69] analyzed thermal radiation and viscous dissipation for peristaltic activity. Prakash and Tripathi [70] reported the

electroosmotic flow of Williamson fluid with peristaltic activity by taking the aspect of thermal radiation.

When a fluid comes in contact with a solid surface and takes on the velocity of that surface, this is referred to as a no-slip state. This is because fluids have a viscous characteristics. The no-slip requirement, on the other hand, is insufficient for fluid to pass through permeable walls, slotted plates, rough and coated surfaces, foam etc. The slip condition is applicable in such fluids. The fluid flows subject to partial slip are significant in polymers and polishing the valves of an artificial heart. Chu and Fang [71] introduced slip flow in peristalsis first time. Ali et al. [72] examined slip impacts on the peristaltic transport of MHD liquid. Chaube et al. [73] pointed out the slip features in peristalsis of micropolar liquid. Tripathi et al. [74] studied peristaltic activity through slip aspects in fractional Burger’s material. Impacts of slip and thermally radiation are reported by Akbar et al. [75]. Sucharitha et al. [76] discussed magnetic field and slip consequences on convective peristaltic flow of Bingham liquid with compliant wall.

1.3 Basic equations

Here we include some fundamental expressions which will be employed in modeling of problems.

1.3.1 Mass conservation

For a compressible liquid, the mathematical expression of continuity is

$$\nabla \cdot (\rho \mathbf{V}) + \frac{\partial \rho}{\partial t} = 0, \tag{1.1}$$

in which density, time and velocity are represented by ρ , t and \mathbf{V} respectively. For incompressible fluid ($\rho = \text{const}$) and one obtains

$$\nabla \cdot \mathbf{V} = 0. \tag{1.2}$$

1.3.2 Momentum conservation

Momentum expressions satisfies

$$\rho \frac{d\mathbf{V}}{dt} = \rho \mathbf{b} + \nabla \cdot \boldsymbol{\tau}, \quad (1.3)$$

where $\boldsymbol{\tau} = \mathbf{S} - p\mathbf{I}$ depicts Cauchy-stress tensor, \mathbf{I} the identity tensor, p the pressure, \mathbf{S} the extra stress tensor and $\rho \mathbf{b}$ depicts the body force.

1.3.3 Energy conservation

Energy expression for nanofluid is

$$\rho_f c_f \left(\frac{\partial}{\partial t} + \mathbf{V} \cdot \nabla \right) T = -\nabla \cdot \mathbf{q} + I_p \nabla \cdot \mathbf{j}_p \quad (1.4)$$

In above expression left hand side represent internal energy and I_p and \mathbf{j}_p represent specific enthalpy and diffusion mass flux of nanomaterials. Here

$$\mathbf{q} = -k \nabla T + I_p \mathbf{j}_p, \quad (1.5)$$

$$\mathbf{j}_p = -\rho_p D_T \frac{\nabla T}{T_m} - \rho_p D_B \nabla C, \quad (1.6)$$

where D_B and D_T shows Brownian and thermophoresis coefficients and T_m the mean temperature. By employing (1.6) and (1.7), the energy expression reduces to

$$\rho_f c_f \left(\frac{\partial}{\partial t} + \mathbf{V} \cdot \nabla \right) T = k \nabla^2 T + \rho_p c_p \left[\frac{D_T}{T_m} \nabla T \cdot \nabla T + D_B \nabla C \cdot \nabla T \right]. \quad (1.7)$$

1.3.4 Concentration equation

Equation of concentration for nanofluids is

$$\left(\frac{\partial}{\partial t} + \mathbf{V} \cdot \nabla \right) C = \frac{D_T}{T_m} \nabla^2 T + D_B \nabla^2 C, \quad (1.8)$$

where C shows the nanoparticles concentration.

1.4 Models of fluids

1.4.1 Viscous fluid

Cauchy stress tensor T for incompressible viscous fluid is represented by

$$\mathbf{T} = -p\mathbf{I} + \mu\mathbf{A}_1, \quad (1.9)$$

where \mathbf{I} the identity tensor, p the pressure, μ the dynamic viscosity and A_1 the first Rivlin-Ericksen tensor defined as

$$\mathbf{A}_1 = (\text{grad } \mathbf{V})^t + (\text{grad } \mathbf{V}), \quad (1.10)$$

where

$$\text{grad } \mathbf{V} = \begin{bmatrix} \frac{\partial u}{\partial x} & \frac{\partial u}{\partial y} & \frac{\partial u}{\partial z} \\ \frac{\partial v}{\partial x} & \frac{\partial v}{\partial y} & \frac{\partial v}{\partial z} \\ \frac{\partial w}{\partial x} & \frac{\partial w}{\partial y} & \frac{\partial w}{\partial z} \end{bmatrix} \quad (1.11)$$

and so

$$\mathbf{A}_1 = \begin{bmatrix} 2\frac{\partial u}{\partial x} & \frac{\partial u}{\partial y} + \frac{\partial v}{\partial x} & \frac{\partial u}{\partial z} + \frac{\partial w}{\partial x} \\ \frac{\partial u}{\partial y} + \frac{\partial v}{\partial x} & 2\frac{\partial v}{\partial y} & \frac{\partial w}{\partial y} + \frac{\partial v}{\partial z} \\ \frac{\partial u}{\partial z} + \frac{\partial w}{\partial x} & \frac{\partial w}{\partial y} + \frac{\partial v}{\partial z} & 2\frac{\partial w}{\partial z} \end{bmatrix} \quad (1.12)$$

1.4.2 Non-Newtonian fluids

Cauchy stress tensor for incompressible non-Newtonian fluid models is

$$\mathbf{T} = -p\mathbf{I} + S, \quad (1.13)$$

Extra stress tensor S varies for different models.

Eyring-Powell model

Extra stress tensor for Eyring-Powell model is defined by [38]

$$S_{ij} = \mu \frac{\partial u_i}{\partial x_j} + \frac{1}{\beta^{**}} \sinh^{-1} \left(\frac{1}{c^{**}} \frac{\partial u_i}{\partial x_j} \right), \quad i, j = 1, 2 \quad (1.14)$$

where $u = u_1$, $v = u_2$, $x = x_1$ and $y = x_2$.

$$\sinh^{-1} \left(\frac{1}{c^{**}} \frac{\partial u_i}{\partial x_j} \right) = \frac{1}{c^{**}} \frac{\partial u_i}{\partial x_j} - \frac{1}{6} \left(\frac{1}{c^{**}} \frac{\partial u_i}{\partial x_j} \right)^3, \quad \left| \frac{1}{c^{**}} \frac{\partial u_i}{\partial x_j} \right| \ll 1. \quad (1.15)$$

Here c^{**} and β^{**} are the material constants of Eyring-Powel liquid and μ the coefficient of viscosity.

Fourth grade model

For fourth-grade model extra stress tensor is [40]

$$\begin{aligned} S = & \mu \mathbf{A}_1 + \alpha'_1 \mathbf{A}_2 + \alpha'_2 \mathbf{A}_1^2 + \beta'_1 \mathbf{A}_3 + \beta'_2 (\mathbf{A}_1 \mathbf{A}_2 + \mathbf{A}_2 \mathbf{A}_1) + \beta'_3 (tr \mathbf{A}_1^2) \mathbf{A}_1 + \gamma'_1 \mathbf{A}_4 + \\ & \gamma'_2 (\mathbf{A}_1 \mathbf{A}_3 + \mathbf{A}_3 \mathbf{A}_1) + \gamma'_3 \mathbf{A}_2^2 + \gamma'_4 (\mathbf{A}_1^2 \mathbf{A}_2 + \mathbf{A}_2 \mathbf{A}_1^2) + \gamma'_5 (tr \mathbf{A}_2) \mathbf{A}_2 + \gamma'_6 (tr \mathbf{A}_2) \mathbf{A}_1^2 + \\ & (\gamma'_7 tr \mathbf{A}_3 + \gamma'_7 tr (\mathbf{A}_2 \mathbf{A}_1)) \mathbf{A}_1. \end{aligned} \quad (1.16)$$

where $\alpha'_i (i = 1, 2)$, $\beta'_i (i = 1 - 3)$ and $\gamma'_i (i = 1 - 8)$ are material constants of fourth-grade where and Rivlin-Ericksen tensors are [40]

$$\mathbf{A}_n = \frac{d\mathbf{A}_{n-1}}{dt} + (\text{grad } \mathbf{V}) \mathbf{A}_{n-1} + \mathbf{A}_{n-1} (\text{grad } \mathbf{V})^T, \quad n > 1. \quad (1.17)$$

Sutterby model

Extra stress tensor for Sutterby model is defined through [42]

$$S = \frac{\mu}{2} \left[\frac{\sinh^{-1}(\bar{b}\dot{\gamma})}{\bar{b}\dot{\gamma}} \right]^{m^*} \mathbf{A}_1, \quad (1.18)$$

$$\dot{\gamma} = \sqrt{\frac{1}{2} trace \mathbf{A}_1^2}, \quad (1.19)$$

where \bar{b} and m^* denote material constants, μ the fluid dynamic viscosity and \mathbf{A}_1 the first Rivlin Ericksen tensor.

Hyperbolic tangent model

Extra stress tensor for hyperbolic tangent model is defined [44]

$$S = \left[\mu_\infty + (\mu_\infty + \mu_0) \tanh(\Gamma/\dot{\gamma})^n \right] \dot{\gamma}, \quad (1.20)$$

$$\dot{\gamma} = \sqrt{\frac{1}{2} \text{trace} \mathbf{A}_1^2}, \quad (1.21)$$

We consider in this case the infinite shear rate viscosity $\mu_\infty = 0$ and $\Gamma/\dot{\gamma} < 1$. Thus S takes the form

$$S = \left[\mu_0 (\Gamma/\dot{\gamma})^n \right] \dot{\gamma} = \left[\mu_0 (1 + n(\Gamma/\dot{\gamma} - 1)) \right] \dot{\gamma}, \quad (1.22)$$

where $\Gamma/\dot{\gamma}$ denote material constants, n the power law index, μ_0 the zero shear rate viscosity and \mathbf{A}_1 the first Rivlin Ericksen tensor.

Couple-Stress fluid model

Constitutive equations for a couple-stress fluid are [37, 38]

$$\rho_f \frac{\partial v_i}{\partial t} = T_{ji,i} + \rho_f f_i, \quad (1.23)$$

$$e_{ijk} T_{ji}^A + M_{ji,j} + \rho_f C_i = 0, \quad (1.24)$$

$$S_{ij} = -p + 2\mu d_{ij}^*, \quad (1.25)$$

$$\mu_{ij} = 4\eta_1 \omega_{j,i} + 4\eta_1' \omega_{i,j} \quad (1.26)$$

Here v_i denotes velocity, f_i the body force per unit mass, C_i moment of body per unit mass, M_{ij} couple-stress tensor, d_{ij}^* symmetric part gradient of the velocity, ω_i the vorticity vector, and η_1 and η_1' are constants connected with the couple stress. T_{ji}^A and S_{ij} are antisymmetric and symmetric parts of the tensor T_{ij} respectively.

1.4.3 Compliant wall

When a compressing source is removed, the tendency of an organ to return to its previous pattern is measured. A compliant wall is one that is flexible, stretchable, dampening, and

elastic in nature. It's also capable of retaining fluid. When the pressure in the fluid is disturbed in such a way that the deflection of the wall is minimal, the rigid wall assumption remains valid in most physical events. However, if the channel wall is expected to be fragile (i.e., less than 0.05 of the radius) or constructed of deformable material, the compliant wall option produces excellent consequences.

For a flexible wall, the governing equation of motion is as follows:

$$L(\eta) = p - p_0,$$

$$L = \left[-\tau \frac{\partial^2}{\partial x^2} + m \frac{\partial^2}{\partial t^2} + d_1 \frac{\partial}{\partial t} \right], \quad (1.27)$$

where L denotes the operator for depicting the movements of a stressed membrane. Because of muscle tension, P_0 is the pressure outside the wall. We take $P_0 = 0$ for inextensible channel walls. Further m , τ and d_1 depicts mass per unit area, elastic tension and viscous damping coefficient respectively.

Chapter 2

Peristalsis of nanofluid by mixed convection and wall properties

2.1 Introduction

Present chapter highlights novel aspects of mixed convection and Hall current on the peristaltic movement of nanomaterial in a symmetric channel. Fluid through the porous medium is taken. Here channel boundaries are compliant. Moreover slip condition is employed for velocity. Convective conditions are imposed for temperature and concentration. Numerical solutions for resulting problems are obtained by shooting technique. Influences of variables of interest on concentration, temperature, velocity and heat transfer rate are graphically illustrated.

2.2 Physical model

Peristaltic flow of viscous nanofluid in a symmetric channel of width $2d_1$ is studied. Flow is induced by waves propagation along the boundaries of channel. Here the cartesian coordinates the x and y -axis appears are along and normal to the boundaries of channel.

The walls shapes are [51]

$$y = \pm\eta(x, t) = \pm\left[d_1 + a \sin \frac{2\pi}{\lambda}(x - ct)\right], \quad (2.1)$$

in which λ depicts the wavelength, a the amplitude of wave, t the time and c the wave speed. Fluid is conducted electrically with a constant strength through an applied magnetic field B_0 . Neglecting an induced magnetic field, the Hall current contribution is retained. Thus by generalized Ohm's expression [18]

$$\mathbf{J} = \sigma \left[-\frac{1}{n_e e} (\mathbf{J} \times \mathbf{B}) + \mathbf{E} + (\mathbf{V} \times \mathbf{B}) \right]. \quad (2.2)$$

Here σ denotes electrical conductivity, \mathbf{E} the electric field, \mathbf{V} the velocity, e the charge of electron and n_e the mass of electron. We have

$$\mathbf{J} \times \mathbf{B} = -\frac{\sigma B_0^2}{1 + m^2} [(u - mv), (v + mu), 0] \quad (2.3)$$

Expressions governing the proposed problem are

$$\frac{\partial u}{\partial x} + \frac{\partial v}{\partial y} = 0, \quad (2.4)$$

$$\begin{aligned} \frac{\partial u}{\partial t} + u \frac{\partial u}{\partial x} + v \frac{\partial u}{\partial y} = & -\frac{1}{\rho_f} \frac{\partial p}{\partial x} + \nu \left(\frac{\partial^2 u}{\partial x^2} + \frac{\partial^2 u}{\partial y^2} \right) - \frac{\sigma B_0^2}{\rho_f (1 + m^2)} (u - mv) \\ & - \frac{\mu}{\rho_f k_1} u + g\beta_T (T - T_0) + g\beta_C (C - C_0), \end{aligned} \quad (2.5)$$

$$\frac{\partial v}{\partial t} + u \frac{\partial v}{\partial x} + v \frac{\partial v}{\partial y} = -\frac{1}{\rho_f} \frac{\partial p}{\partial y} + \nu \left(\frac{\partial^2 v}{\partial x^2} + \frac{\partial^2 v}{\partial y^2} \right) - \frac{\sigma B_0^2}{\rho_f (1 + m^2)} (v + mu), \quad (2.6)$$

$$\begin{aligned} \frac{\partial T}{\partial t} + u \frac{\partial T}{\partial x} + v \frac{\partial T}{\partial y} = & \alpha \left(\frac{\partial^2 T}{\partial x^2} + \frac{\partial^2 T}{\partial y^2} \right) + \frac{\nu}{c_f} \left[2 \left(\frac{\partial u}{\partial x} \right)^2 + \left(\frac{\partial v}{\partial x} + \frac{\partial u}{\partial y} \right)^2 + 2 \left(\frac{\partial v}{\partial y} \right)^2 \right] \\ & + \tau \left[D_B \left(\frac{\partial C}{\partial x} \frac{\partial T}{\partial x} + \frac{\partial C}{\partial y} \frac{\partial T}{\partial y} \right) + \frac{D_T}{T_m} \left\{ \left(\frac{\partial T}{\partial y} \right)^2 + \left(\frac{\partial T}{\partial x} \right)^2 \right\} \right], \end{aligned} \quad (2.7)$$

$$\frac{\partial C}{\partial t} + u \frac{\partial C}{\partial x} + v \frac{\partial C}{\partial y} = \left(\frac{\partial^2 C}{\partial x^2} + \frac{\partial^2 C}{\partial y^2} \right) D_B + \left(\frac{\partial^2 T}{\partial x^2} + \frac{\partial^2 T}{\partial y^2} \right) \frac{D_T}{T_m}. \quad (2.8)$$

Relevant boundary conditions are

$$u \pm \beta \left(\frac{\partial v}{\partial x} + \frac{\partial u}{\partial y} \right) = 0, \quad -k \frac{\partial T}{\partial y} = h_1 \left\{ \frac{T_1 - T}{T - T_0} \right\}, \quad -D_B \frac{\partial C}{\partial y} = h_2 \left\{ \frac{C_1 - C}{C - C_0} \right\}, \text{ at } y = \pm \eta, \quad (2.9)$$

$$\left[-\tau_1 \frac{\partial^3}{\partial x^3} + m_1 \frac{\partial^3}{\partial x \partial t^2} + d \frac{\partial^2}{\partial t \partial x} \right] \eta = \mu \left(\frac{\partial^2 u}{\partial x^2} + \frac{\partial^2 u}{\partial y^2} \right) - \rho_f \left(\frac{\partial u}{\partial t} + u \frac{\partial u}{\partial x} + v \frac{\partial u}{\partial y} \right) - \frac{\sigma B_0^2}{\rho_f (1 + m^2)} (u - mv) - \frac{\mu}{k_1} u + g \rho_f \beta_T (T - T_0) + g \rho_f \beta_C (C - C_0) \quad \text{at } y = \pm \eta. \quad (2.10)$$

We consider the stream function $u = \psi_y$ and $v = -\delta \psi_x$ and the following non-dimensional variables

$$\begin{aligned} u^* &= \frac{u}{c}, \quad v^* = \frac{v}{c}, \quad x^* = \frac{x}{\lambda}, \quad y^* = \frac{y}{d_1}, \quad t^* = \frac{ct}{\lambda}, \quad \beta^* = \frac{\beta}{d_1} \\ \eta^* &= \frac{\eta}{d_1}, \quad p^* = \frac{d_1^2 p}{c \lambda \mu}, \quad \theta = \frac{T - T_0}{T_1 - T_0}, \quad \phi = \frac{C - C_0}{C_1 - C_0}, \end{aligned} \quad (2.11)$$

Incompressibility constrain (2.4) is trivially satisfied while the other equations after invoking lubrication approach and dropping asterisks yield

$$\frac{\partial^4 \psi}{\partial y^4} - \left(\frac{M^2}{1 + m^2} + \frac{1}{K} \right) \frac{\partial^2 \psi}{\partial y^2} + Gr \frac{\partial \theta}{\partial y} + Gc \frac{\partial \phi}{\partial y} = 0, \quad (2.12)$$

$$\frac{1}{Pr} \left(\frac{\partial^2 \theta}{\partial y^2} \right) + Nb \frac{\partial \theta}{\partial y} \frac{\partial \phi}{\partial y} + Nt \left(\frac{\partial \theta}{\partial y} \right)^2 + Ec \left(\frac{\partial^2 \psi}{\partial y^2} \right)^2 = 0, \quad (2.13)$$

$$\frac{\partial^2 \phi}{\partial y^2} + \frac{Nt}{Nb} \left(\frac{\partial^2 \theta}{\partial y^2} \right) = 0. \quad (2.14)$$

The boundary conditions are

$$\frac{\partial \psi}{\partial y} \pm \beta \frac{\partial^2 \psi}{\partial y^2} = 0 \quad \text{at } y = \pm \eta, \quad (2.15)$$

$$\begin{aligned} \left[E_1 \frac{\partial^3}{\partial x^3} + E_2 \frac{\partial^3}{\partial x \partial t^2} + E_3 \frac{\partial^2}{\partial x \partial t} \right] \eta &= \frac{\partial^3 \psi}{\partial y^3} - \left(\frac{M^2}{1 + m^2} + \frac{1}{K} \right) \frac{\partial \psi}{\partial y} + \\ Gr \theta + Gc \phi &\quad \text{at } y = \pm \eta, \end{aligned} \quad (2.16)$$

$$\frac{\partial \theta}{\partial y} = \left\{ \begin{array}{l} -Bi_1(1 - \theta) \\ -Bi_1 \theta \end{array} \right\}, \quad \frac{\partial \phi}{\partial y} = \left\{ \begin{array}{l} -Bi_2(1 - \phi) \\ -Bi_2 \phi \end{array} \right\}, \quad \text{at } y = \pm \eta, \quad (2.17)$$

with ϵ as the amplitude ratio, δ wave number, Nb the Brownian variable, Nt the thermophoresis parameter, Re Reynolds number, Sc the schmidt number, K the porosity parameter, Pr the Prandtl number, Ec the Eckert variable, Bi_1 thermal biot number, Bi_2 mass biot number, M the Hartman number, (E_1, E_2, E_3) the wall parameters, Gc concentration Grashof number,

Gr thermal Grashof number, β the velocity slip parameter defined below

$$\begin{aligned}
\epsilon &= \frac{a}{d_1}, \delta = \frac{d_1}{\lambda}, Nb = \frac{\tau D_B (C_1 - C_0)}{\nu}, Nt = \frac{\tau D_T (T_1 - T_0)}{T_m \nu}, Re = \frac{cd_1 \rho_f}{\mu} \\
Sc &= \frac{\nu}{D_B}, K = \frac{k_1}{d_1^2}, Pr = \frac{\nu}{\alpha}, Ec = \frac{c^2}{c_f (T_1 - T_0)}, Bi_1 = \frac{h_1 d_1}{k}, Bi_2 = \frac{h_2 d_1}{D_B}, \\
M &= \sqrt{\frac{\sigma}{\mu}} B_0 d_1, E_1 = \frac{-\tau d_1^3}{\lambda^3 \mu c}, E_2 = \frac{m_1 c d_1^3}{\lambda^3 \mu}, E_3 = \frac{d d_1^3}{\lambda^2 \mu}, Gc = \frac{g \rho_f \beta_C (C - C_0) d_1^2}{\mu c}, \\
Gr &= \frac{g \rho_f \beta_T (T - T_0) d_1^2}{\mu c}, \beta^* = \frac{\beta}{d_1}.
\end{aligned} \tag{2.19}$$

2.3 Numerical method

Expressions (2.12) – (2.14) with boundary conditions (2.15) – (2.17) are solved numerically. The technique works with minimum error for small step size. Thus both x and y are equally modified by a size of step 0.01. The outcomes are provided in the next section.

2.4 Graphical findings

This portion explored axial velocity, temperature, nanoparticles concentration and heat transfer rate. Figs. 2.1 – 2.28 are plotted for this purpose.

2.4.1 Velocity

In Figs. 2.1 – 2.7 the behaviors of distinct parameters on velocity are investigated. Fig. 2.1 shows that velocity grows when value of slip parameter β enhances. Clearly more velocity occurs in neighbourhood of channel walls. Influence of porosity (K) on velocity is indicated in Fig. (2.2). Velocity is increased by K . This happens because porous medium will provide less resistance to fluid flow (resulting in a rise of fluid velocity). In Fig. 2.3 opposite behavior is observed for velocity through different values of Hartman number M . In fact more resistive force through larger Lorentz force causes decrease in fluid motion. Behaviors of heat and mass Grashof numbers Gr and Gc are sketched in Figs. 2.4 and 2.5 respectively. Increase of these parameters means increased buoyancy forces (leading to higher velocity distribution). As expected the velocity is enhanced. Variation of Hall parameter m on velocity has been sketched

in Fig. 2.6. Clearly velocity is an increasing function of m . The Hall effects physically actually offset the magnetic force of the applied magnetic field. Influences of flexible wall variables (E_1 , E_2 , E_3) are presented in Fig. 2.7. Here larger E_1 and E_2 enhances the velocity. However there is velocity decay for E_3 . Velocity in all plots is of parabolic shape.

2.4.2 Temperature

Figs. 2.8 – 2.16 represent the influences of pertinent variables on temperature. Fig. 2.8 sketched effects of thermal Biot number Bi_1 on temperature. Here temperature is an increasing function of Bi_1 . Due to non-uniform temperature field within the fluid we considered large values of thermal Biot number. Fig. 2.9 depicts that temperature increases for larger Prandtl number Pr . The temperature increases efficiently when Pr enhances due to the existence of strong viscous dissipation impacts. In Fig. 2.10 we noticed that temperature reduces by an enhancement in Hall parameter m . By increasing the Hall parameter, the current density of the fluid increases, allowing the temperature to increase. Fig. 2.11 demonstrates that increasing K lead to temperature rise. Fig. 2.12 illustrates that for higher Eckert number the temperature is enhanced. For higher Ec , frictional heating collects additional kinetic energy in liquid particles. Temperature upgrades for rising Ec . In Fig. 2.13 we capture the combined effects of thermophoresis parameters Nt and Brownian motion Nb . Here temperature enhances for both parameters. It is due to the random movement of nanoliquid particles from channel walls to material. Impacts of thermal and concentration Grashof numbers are shown in Figs. 2.14 and 2.15. It is noted through these Figs. that temperature enhances for an increase in both the parameters. Such behaviors physical explanation is due to the buoyancy force resulting from the temperature difference within the flow domain. This force rapidly causes the fluid flow. The wall parameters E_1 and E_2 increase the temperature whereas E_3 reduces. (see Fig. 2.16).

2.4.3 Concentration

Figs. 2.17 – 2.22 have been organized for the outcomes of concentration with respect to mass Biot number Bi_2 , thermophoresis parameter Nt , thermal Grashof number Gr , concentration Grashof number Gc , porosity K and wall parameters E_1 , E_2 , E_3 . Fig. 2.17 is portrayed to see impacts of concentration Biot number Bi_2 . Here concentration increases for larger values

of Bi_2 . Fig. 2.18 reveals that concentration is an increasing function of Gr . Similar behavior for concentration Grashof number Gc is observed through Fig. 2.19. In Fig. 2.20 we noticed that concentration decays for porosity parameter K . Fig. 2.21 elucidates that concentration decreases by increasing thermophoresis parameter Nt . The intensity of thermophoretic impacts is rising gradually. This results in a greater mass flux due to the concentration gradient. This reduces the concentration of nanoparticles. Fig. 2.22 captures variation of compliant wall parameters E_1, E_2, E_3 on concentration. Here concentration has increasing behavior for E_1 and E_2 while opposite response observed for E_3 .

2.4.4 Coefficient of heat transfer

Impacts of several distinct variables on heat transfer coefficient $Z(x) = \eta_x \theta_y(\eta)$ are inspected by Figs. 2.23–2.28. Fig. 2.23 assures that larger thermal Biot number Bi_1 show a decrease in heat transfer rate. As Bi_1 rises, thermal conductivity at the wall will reduce and the heat transfer rate will decline. Fig. 2.24 depicts that Z decreases for thermal Grashof number Gr . Fig. 2.25 shows that heat transfer rate is reduced via concentration Grashof numbers Gc . Fig. 2.26 displays Z against porosity parameter K . Here heat transfer coefficient is increased with higher K . Effects of Hall parameter m is sketched in Fig. 2.27. Clearly Z is an increasing function of this parameter. A rise in heat transfer coefficient is because of Hall effects which tend to rise in fluid temperature. Influence of Brownian motion Nb and thermophoresis parameters Nt are displayed in Fig. (2.28). Heat transfer rate with respect to Nb and Nt is enhanced. As the Brownian motion effect strengthens, this correlates to the efficient migration of nanoparticles from the wall to liquid, and consequently the transfer enhances.

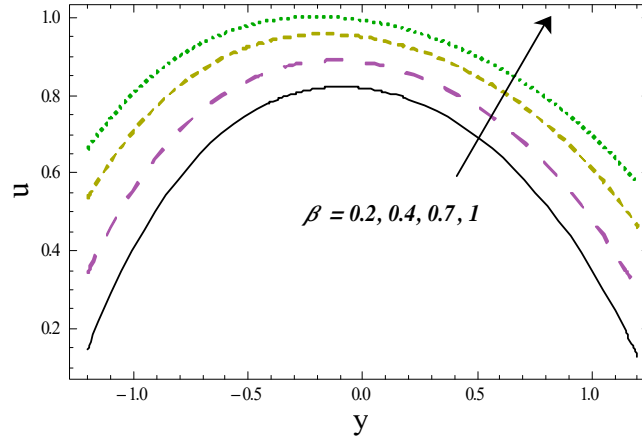


Fig. 2.1: Variation of β on velocity when $x = \epsilon = 0.2$, $t = 0.1$, $K = 0.6$, $M = 0.5$, $m = 2$, $\text{Pr} = 6.9$, $Ec = 1$, $Nb = Nt = 0.3$, $Gr = 0.4$, $Gc = 0.7$, $E_1 = 0.03$, $E_2 = 0.02$, $E_3 = 0.01$, $Bi_1 = 3$, $Bi_2 = 5$.

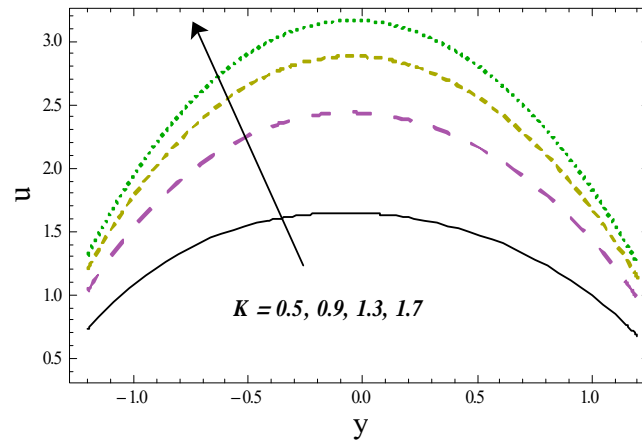


Fig. 2.2: Variation of K on velocity when $x = \epsilon = 0.2$, $t = 0.1$, $\beta = 0.2$, $M = 0.5$, $m = 2$, $\text{Pr} = 6.9$, $Ec = 1$, $Nb = Nt = 0.3$, $Gr = 0.4$, $Gc = 0.7$, $E_1 = 0.03$, $E_2 = 0.02$, $E_3 = 0.01$, $Bi_1 = 3$, $Bi_2 = 5$.

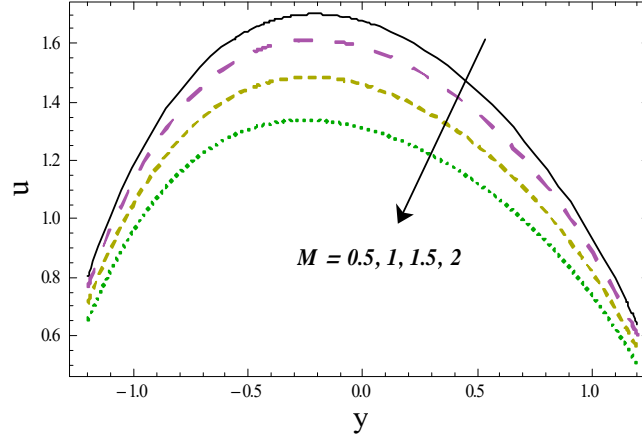


Fig. 2.3: Variation of M on velocity when $x = \epsilon = 0.2$, $t = 0.1$, $\beta = 0.2$, $K = 0.6$, $m = 2$, $\text{Pr} = 6.9$, $Ec = 1$, $Nb = Nt = 0.3$, $Gr = 0.4$, $Gc = 0.7$, $E_1 = 0.03$, $E_2 = 0.02$, $E_3 = 0.01$, $Bi_1 = 3$, $Bi_2 = 5$.

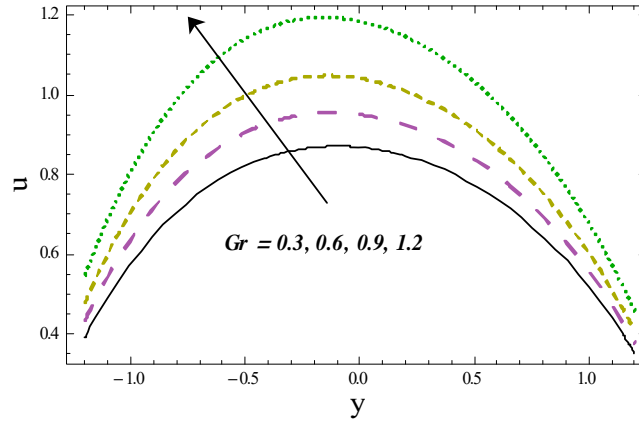


Fig. 2.4: Variation of Gr on velocity when $x = \epsilon = 0.2$, $t = 0.1$, $\beta = 0.2$, $K = 0.6$, $M = 0.5$, $m = 2$, $\text{Pr} = 6.9$, $Ec = 1$, $Nb = Nt = 0.3$, $Gc = 0.7$, $E_1 = 0.03$, $E_2 = 0.02$, $E_3 = 0.01$, $Bi_1 = 3$, $Bi_2 = 5$.

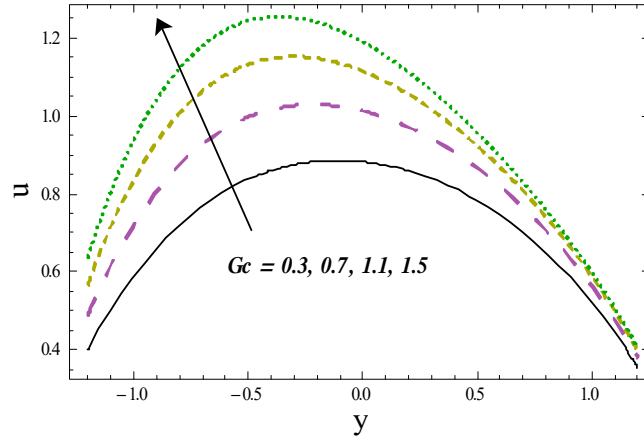


Fig. 2.5: Variation of Gc on velocity when $x = \epsilon = 0.2$, $t = 0.1$, $\beta = 0.2$, $K = 0.6$, $M = 0.5$, $m = 2$, $Pr = 6.9$, $Ec = 1$, $Nb = Nt = 0.3$, $Gr = 0.4$, $E_1 = 0.03$, $E_2 = 0.02$, $E_3 = 0.01$, $Bi_1 = 3$, $Bi_2 = 5$.

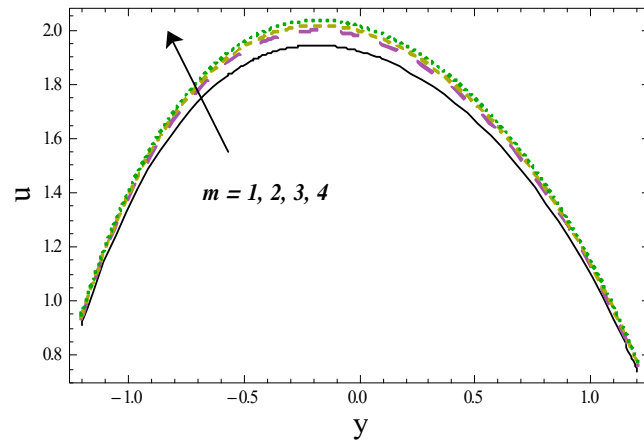


Fig. 2.6: Variation of m on velocity when $x = \epsilon = 0.2$, $t = 0.1$, $\beta = 0.2$, $K = 0.6$, $M = 0.5$, $m = 2$, $Pr = 6.9$, $Ec = 1$, $Nb = Nt = 0.3$, $Gr = 0.4$, $Gc = 0.7$, $E_1 = 0.03$, $E_2 = 0.02$, $E_3 = 0.01$, $Bi_1 = 3$, $Bi_2 = 5$.

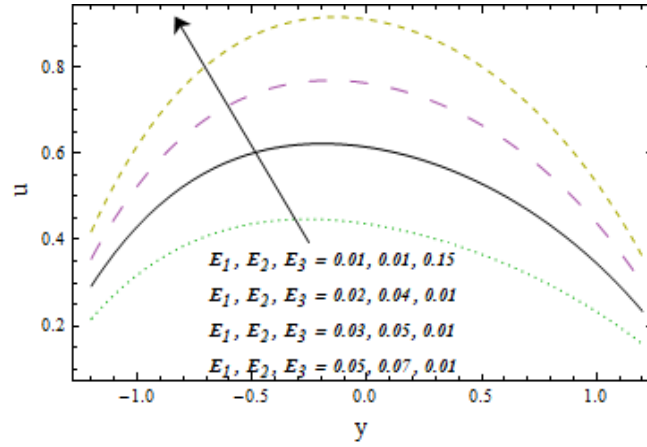


Fig. 2.7: Variation of E_1, E_2, E_3 on velocity when $x = \epsilon = 0.2, t = 0.1, \beta = 0.2, K = 0.6, M = 0.5, m = 2, \text{Pr} = 6.9, \text{Ec} = 1, \text{Nb} = \text{Nt} = 0.2, \text{Gr} = 0.5, \text{Gc} = 1.3, \text{Bi}_1 = 3, \text{Bi}_2 = 5.$

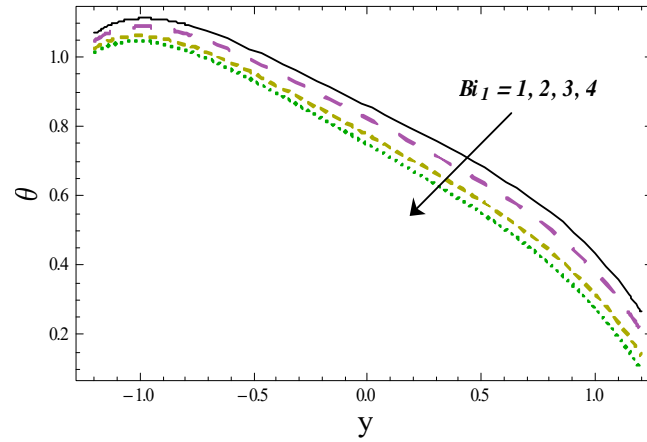


Fig. 2.8: Variation of Bi_1 on temperature when $x = \epsilon = 0.2, t = 0.1, \beta = 0.2, K = 0.6, M = 0.5, m = 2, \text{Pr} = 6.9, \text{Ec} = 1, \text{Nb} = \text{Nt} = 0.3, \text{Gr} = 0.4, \text{Gc} = 0.7, E_1 = 0.03, E_2 = 0.02, E_3 = 0.01, \text{Bi}_2 = 5.$

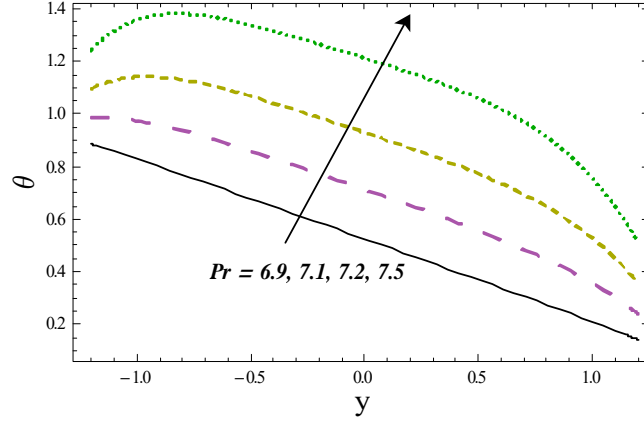


Fig. 2.9: Variation of Pr on temperature when $x = \epsilon = 0.2$, $t = 0.1$, $\beta = 0.2$, $K = 0.6$, $M = 0.5$, $m = 2$, $Ec = 1$, $Nb = Nt = 0.3$, $Gr = 0.4$, $Gc = 0.7$, $E_1 = 0.03$, $E_2 = 0.02$, $E_3 = 0.01$, $Bi_1 = 3$, $Bi_2 = 5$.

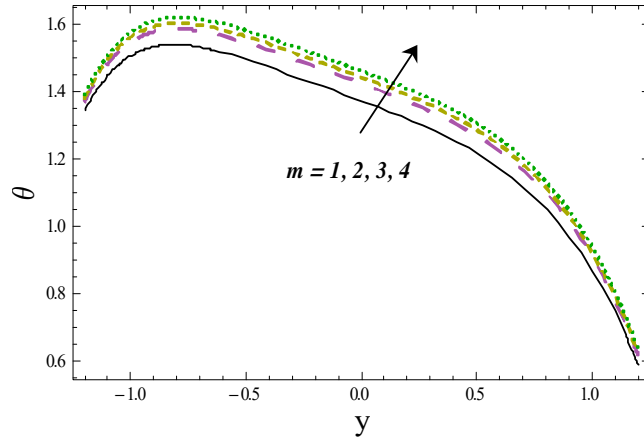


Fig. 2.10: Variation of m on temperature when $x = \epsilon = 0.2$, $t = 0.1$, $\beta = 0.2$, $M = 0.5$, $K = 0.6$, $Pr = 6.9$, $Ec = 1$, $Nb = Nt = 0.3$, $Gr = 0.4$, $Gc = 0.7$, $E_1 = 0.03$, $E_2 = 0.02$, $E_3 = 0.01$, $Bi_1 = 3$, $Bi_2 = 5$.

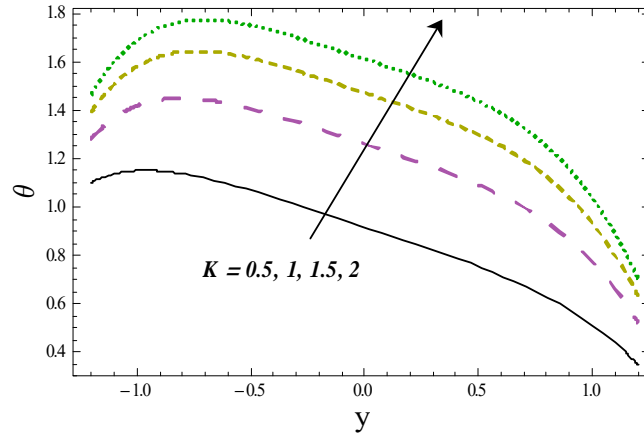


Fig. 2.11: Variation of K on temperature when $x = \epsilon = 0.2$, $t = 0.1$, $\beta = 0.2$, $M = 0.5$, $m = 2$, $\text{Pr} = 6.9$, $Ec = 1$, $Nb = Nt = 0.3$, $Gr = 0.4$, $Gc = 0.7$, $E_1 = 0.03$, $E_2 = 0.02$, $E_3 = 0.01$, $Bi_1 = 3$, $Bi_2 = 5$.

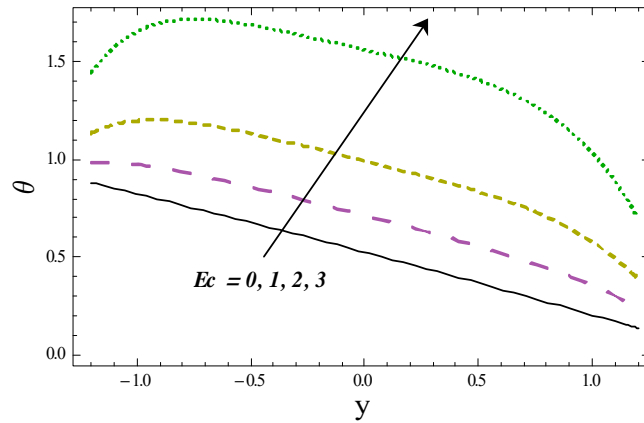


Fig. 2.12: Variation of Ec on temperature when $x = \epsilon = 0.2$, $t = 0.1$, $\beta = 0.2$, $K = 0.6$, $M = 0.5$, $m = 2$, $\text{Pr} = 6.9$, $Nb = Nt = 0.3$, $Gr = 0.4$, $Gc = 0.7$, $E_1 = 0.03$, $E_2 = 0.02$, $E_3 = 0.01$, $Bi_1 = 3$, $Bi_2 = 5$.

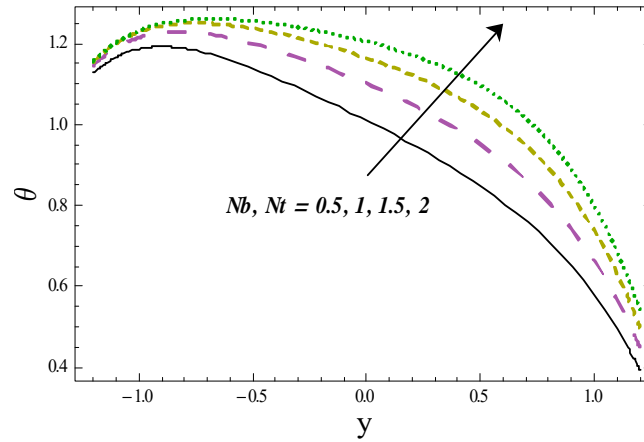


Fig.2.13: Variation of Nb, Nt on temperature when $x = \epsilon = 0.2, t = 0.1, \beta = 0.2, K = 0.6, M = 0.5, m = 2, Pr = 6.9, Ec = 1, Gr = 0.4, Gc = 0.7, E_1 = 0.03, E_2 = 0.02, E_3 = 0.01, Bi_1 = 3, Bi_2 = 5$.

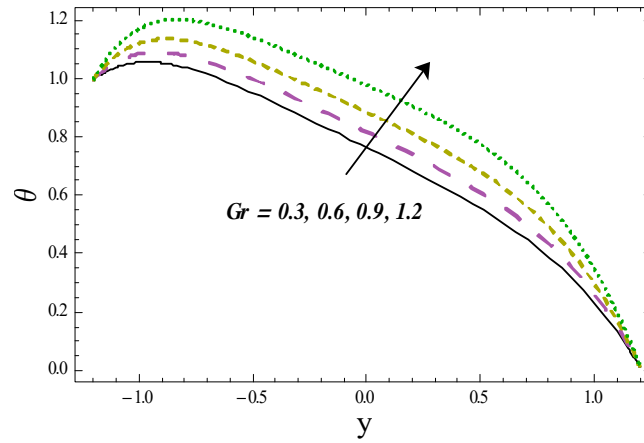


Fig. 2.14: Variation of Gr on temperature when $x = \epsilon = 0.2, t = 0.1, \beta = 0.2, K = 0.6, M = 0.5, m = 2, Pr = 6.9, Ec = 1, Nb = Nt = 0.3, Gc = 0.7, E_1 = 0.03, E_2 = 0.02, E_3 = 0.01, Bi_1 = 3, Bi_2 = 5$.

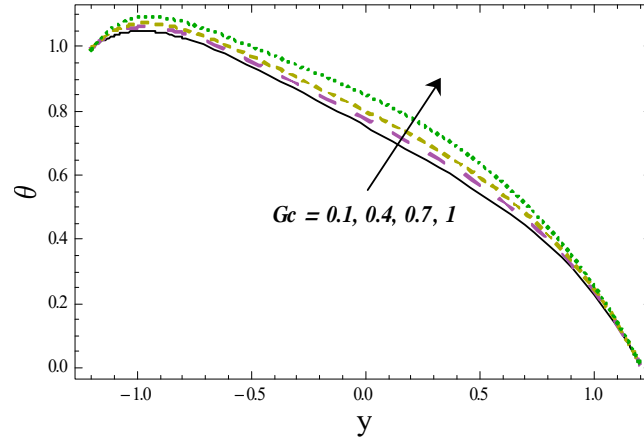


Fig. 2.15: Variation of Gc on temperature when $x = \epsilon = 0.2$, $t = 0.1$, $\beta = 0.2$, $K = 0.6$, $M = 0.5$, $m = 2$, $Pr = 6.9$, $Ec = 1$, $Nb = Nt = 0.3$, $Gr = 0.4$, $E_1 = 0.03$, $E_2 = 0.02$, $E_3 = 0.01$, $Bi_1 = 3$, $Bi_2 = 5$.

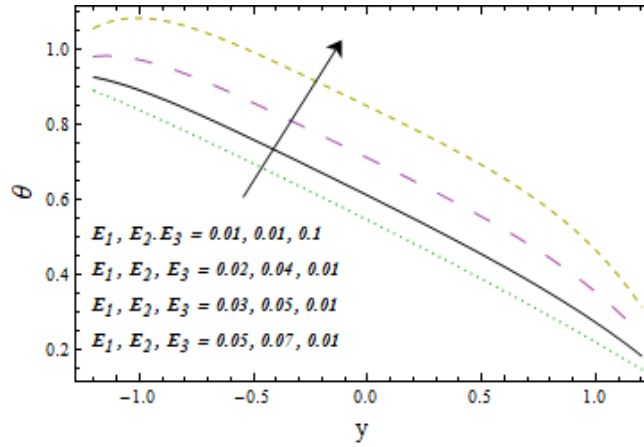


Fig. 2.16: Variation of E_1 , E_2 , E_3 on temperature when $x = \epsilon = 0.2$, $t = 0.1$, $\beta = 0.2$, $K = 0.6$, $M = 0.5$, $m = 2$, $Pr = 6.9$, $Ec = 1$, $Nb = Nt = 0.3$, $Gr = 0.4$, $Gc = 0.7$, $Bi_1 = 3$, $Bi_2 = 5$.

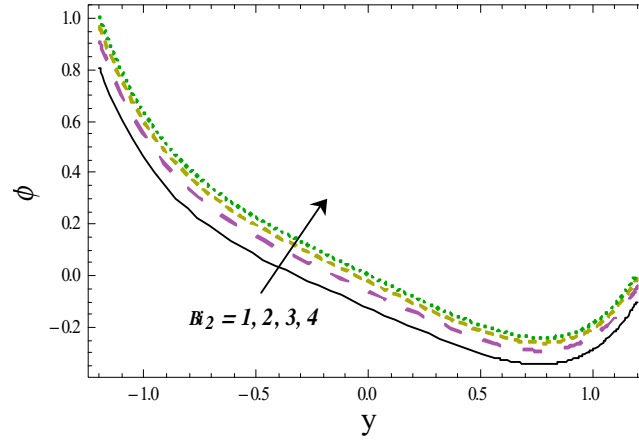


Fig. 2.17: Variation of Bi_2 on concentration when $x = \epsilon = 0.2$, $t = 0.1$, $\beta = 0.2$, $K = 0.6$, $M = 0.5$, $m = 2$, $Pr = 6.9$, $Ec = 1$, $Nb = Nt = 0.3$, $Gr = 0.4$, $Gc = 0.7$, $E_1 = 0.03$, $E_2 = 0.02$, $E_3 = 0.01$, $Bi_1 = 3$, $Bi_2 = 5$.

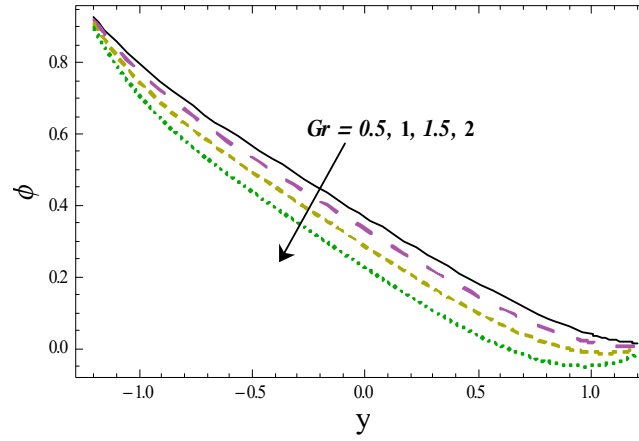


Fig. 2.18: Variation of Gr on concentration when $x = \epsilon = 0.2$, $t = 0.1$, $\beta = 0.2$, $K = 0.6$, $M = 0.5$, $m = 2$, $Pr = 6.9$, $Ec = 1$, $Nb = Nt = 0.3$, $Gc = 0.7$, $E_1 = 0.03$, $E_2 = 0.02$, $E_3 = 0.01$, $Bi_1 = 3$, $Bi_2 = 5$.

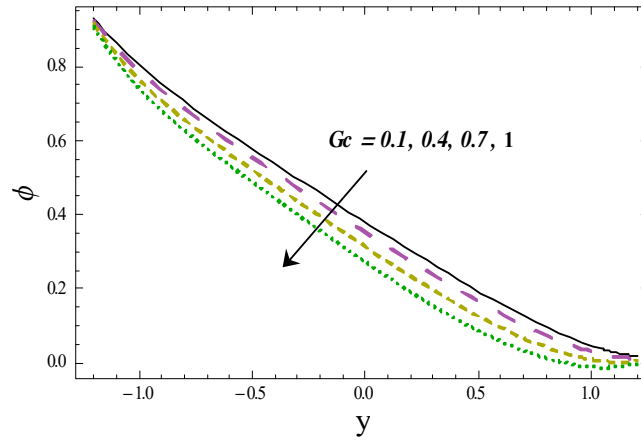


Fig. 2.19: Variation of Gc on concentration when $x = \epsilon = 0.2$, $t = 0.1$, $\beta = 0.2$, $K = 0.6$, $M = 0.5$, $m = 2$, $Pr = 6.9$, $Ec = 1$, $Nb = Nt = 0.3$, $Gr = 0.4$, $E_1 = 0.03$, $E_2 = 0.02$, $E_3 = 0.01$, $Bi_1 = 3$, $Bi_2 = 5$.

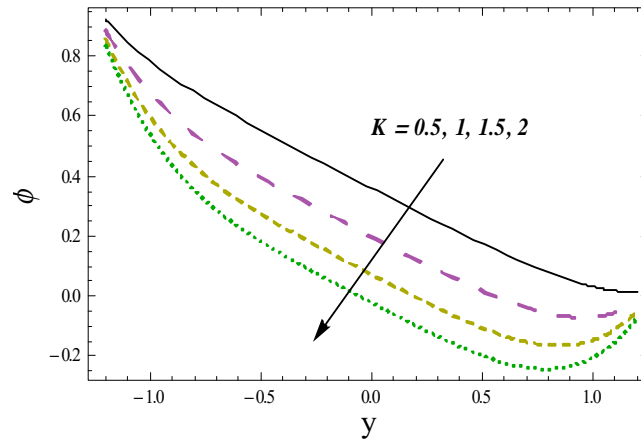


Fig. 2.20: Variation of K on concentration when $x = \epsilon = 0.2$, $t = 0.1$, $\beta = 0.2$, $M = 0.5$, $m = 2$, $Pr = 6.9$, $Ec = 1$, $Nb = Nt = 0.3$, $Gr = 0.4$, $Gc = 0.7$, $E_1 = 0.03$, $E_2 = 0.02$, $E_3 = 0.01$, $Bi_1 = 3$, $Bi_2 = 5$.

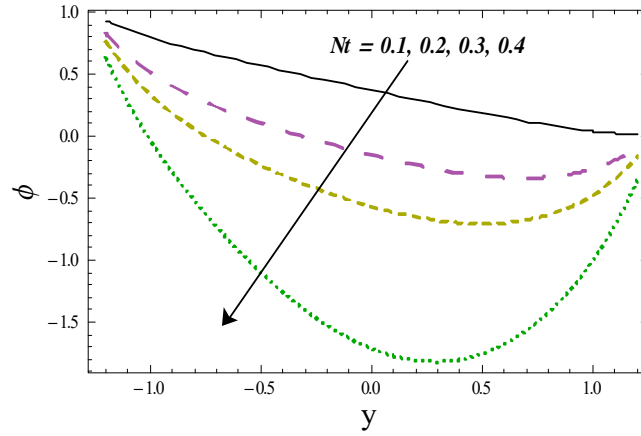


Fig. 2.21: Variation of Nt on concentration when $x = \epsilon = 0.2$, $t = 0.1$, $\beta = 0.2$, $K = 0.6$, $M = 0.5$, $m = 2$, $Pr = 6.9$, $Ec = 1$, $Nb = 0.3$, $Gr = 0.4$, $Gc = 0.7$, $E_1 = 0.03$, $E_2 = 0.02$, $E_3 = 0.01$, $Bi_1 = 3$, $Bi_2 = 5$.

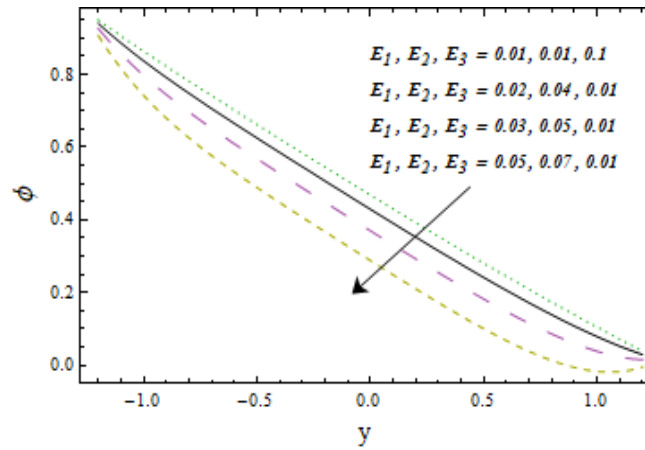


Fig. 2.22: Variation of E_1 , E_2 , E_3 on concentration when $x = \epsilon = 0.2$, $t = 0.1$, $\beta = 0.2$, $K = 0.6$, $M = 0.5$, $m = 2$, $Pr = 6.9$, $Ec = 1$, $Nb = Nt = 0.3$, $Gr = 0.4$, $Gc = 0.7$, $Bi_1 = 3$, $Bi_2 = 5$.

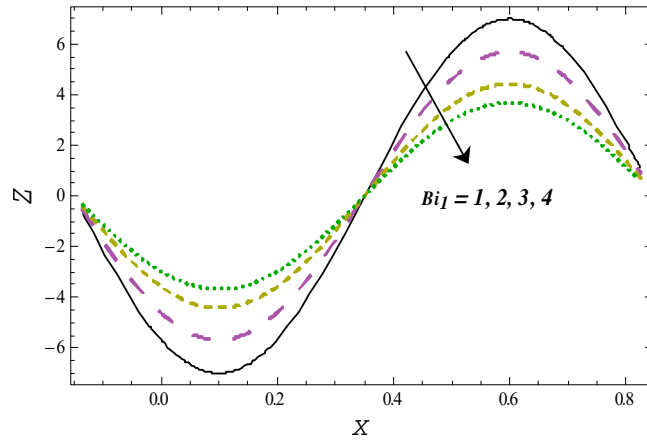


Fig. 2.23: Variation of Bi_1 on heat transfer coefficient when $x = \epsilon = 0.2$, $t = 0.1$, $\beta = 0.2$, $K = 0.6$, $M = 0.5$, $m = 2$, $Pr = 6.9$, $Ec = 1$, $Nb = Nt = 0.3$, $Gr = 0.4$, $Gc = 0.7$, $E_1 = 0.03$, $E_2 = 0.3$, $E_3 = 0.3$, $Bi_2 = 5$.

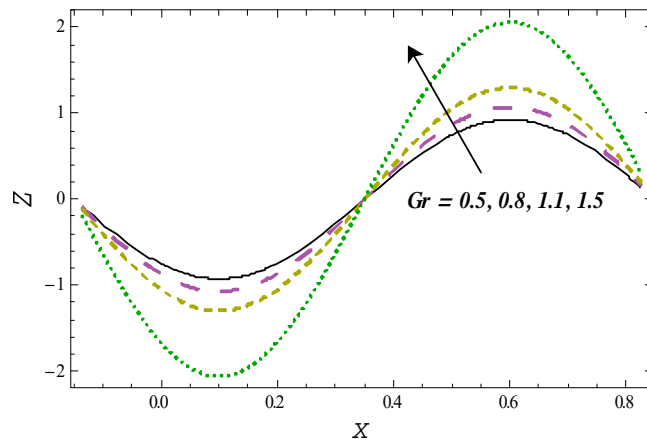


Fig. 2.24: Variation of Gr on heat transfer coefficient when $x = \epsilon = 0.2$, $t = 0.1$, $\beta = 0.2$, $K = 0.6$, $M = 0.5$, $m = 2$, $Pr = 6.9$, $Ec = 1$, $Nb = Nt = 0.3$, $Gc = 0.7$, $E_1 = 0.03$, $E_2 = 0.02$, $E_3 = 0.3$, $Bi_1 = 3$, $Bi_2 = 5$.

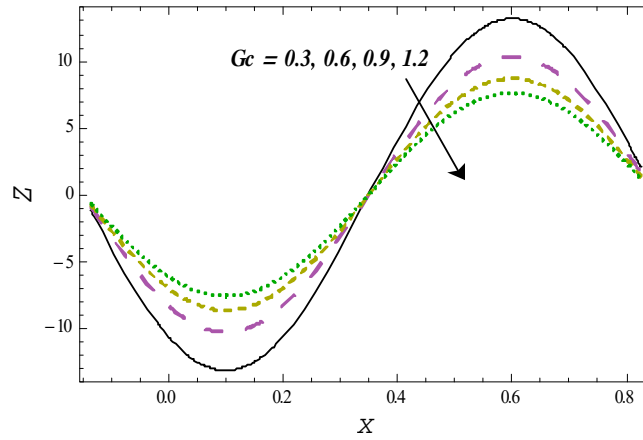


Fig. 2.25: Variation of Gc on heat transfer coefficient when $x = \epsilon = 0.2$, $t = 0.1$, $\beta = 0.2$, $K = 0.6$, $M = 0.5$, $m = 2$, $Pr = 6.9$, $Ec = 1$, $Nb = Nt = 0.3$, $Gr = 0.4$, $E_1 = 0.03$, $E_2 = 0.02$, $E_3 = 0.3$, $Bi_1 = 3$, $Bi_2 = 5$.

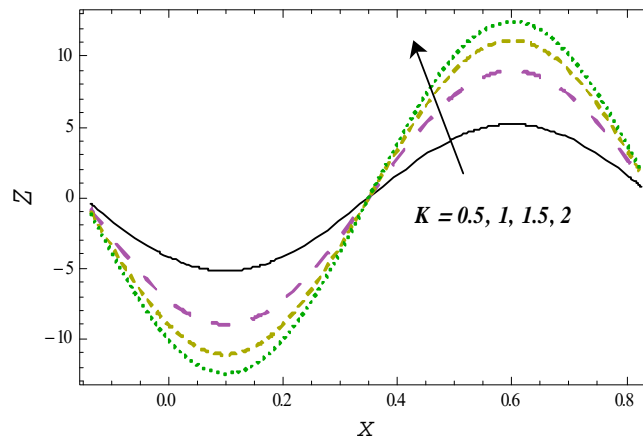


Fig. 2.26: Variation of K on heat transfer coefficient when $x = \epsilon = 0.2$, $t = 0.1$, $\beta = 0.2$, $M = 0.5$, $m = 2$, $Pr = 6.9$, $Ec = 1$, $Nb = Nt = 0.3$, $Gr = 0.4$, $Gc = 0.7$, $E_1 = 0.03$, $E_2 = 0.02$, $E_3 = 0.3$, $Bi_1 = 3$, $Bi_2 = 5$.

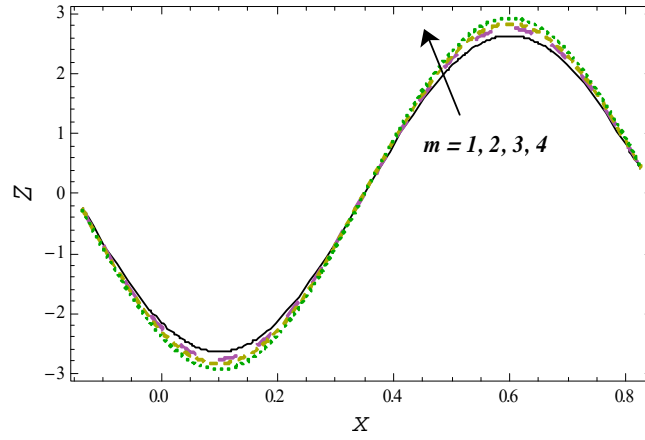


Fig. 2.27: Variation of m on heat transfer coefficient when $x = \epsilon = 0.2$, $t = 0.1$, $\beta = 0.2$, $M = 0.5$, $K = 0.6$, $\text{Pr} = 6.9$, $Ec = 1$, $Nb = Nt = 0.3$, $Gr = 0.4$, $Gc = 0.7$, $E_1 = 0.03$, $E_2 = 0.02$, $E_3 = 0.3$, $Bi_1 = 3$, $Bi_2 = 5$.

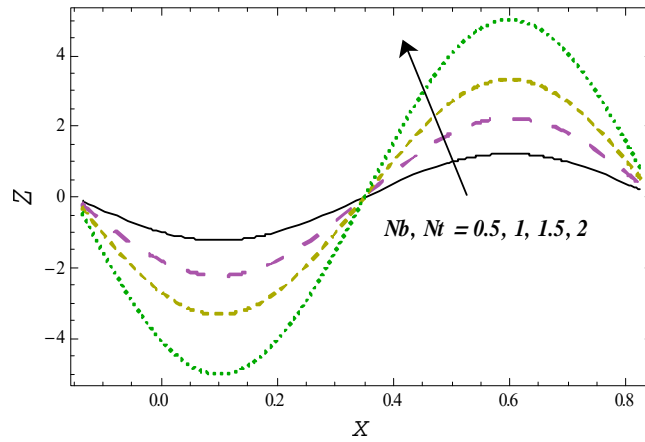


Fig. 2.28: Variation of Nb , Nt on heat transfer coefficient when $x = \epsilon = 0.2$, $t = 0.1$, $\beta = 0.2$, $K = 0.6$, $M = 0.5$, $m = 2$, $\text{Pr} = 6.9$, $Ec = 1$, $Gr = 0.4$, $Gc = 0.7$, $E_1 = 0.03$, $E_2 = 0.02$, $E_3 = 0.3$, $Bi_1 = 3$, $Bi_2 = 5$.

2.5 Closing remarks

Main points are listed below.

- Influences of β , Gr and Gc on velocity are similar.
- Effects of E_i ($i = 1, 2$) on concentration, temperature and velocity are quite opposite to that of E_3 .
- Hartman M and Hall m variables on temperature and velocity have reverse outcomes.
- Temperature is qualitatively similar for Nb and Nt .
- Temperature is reduced by thermal Biot number Bi_1 .
- Concentration and temperature have opposite impacts for Gr and Gc .
- Effects of K and Nt on concentration are quite reverse when compared with Bi_2 .
- Outcomes of Bi_1 and Gc on heat transfer coefficient are quite opposite than Gr , K and m .

Chapter 3

Bioconvection analysis for peristalsis of nanofluid

3.1 Introduction

The current chapter examined the aspects of bioconvecitve MHD peristaltic flow of nanofluid containing gyrotactic organisms. Impacts of Hall current and thermal radiation are also examined in the present study. Velocity, thermal and concentration slip conditions are imposed on elastic channel. Numerical solutions are obtained foe velocity, temperature, concentration, heat transfer coefficient and motile organism density. Related graphs arranged the minor findings.

3.2 Problem development

Here we studied MHD peristaltic flow of viscous nanoliquid in a symmetric channel of width $2d_1$. Disturbance in fluid is due to sinusoidal wave train which propagates with constant speed c . Fluid is conducting by a constant magnetic field of strength B_0 . Electric field effects are neglected. Geometry of the wall surface with the wavelength λ and amplitude a is defined as

$$y = \pm \eta(x, t) = \pm \left[d_1 + a \sin \frac{2\pi}{\lambda} (x - ct) \right], \quad (3.1)$$

By Ohms law, the Lorentz force \mathbf{F}_B is calculated as follows:

$$\mathbf{F}_B = \left[-\frac{\sigma B_0^2}{1+m^2}(u-mv), -\frac{\sigma B_0^2}{1+m^2}(v+mu), 0 \right], \quad (3.2)$$

where σ denotes electrical conductivity and m is the Hall parameter. We have relavent expressions

$$\frac{\partial u}{\partial x} + \frac{\partial v}{\partial y} = 0, \quad (3.3)$$

$$\begin{aligned} \rho_f \left(\frac{\partial u}{\partial t} + u \frac{\partial u}{\partial x} + v \frac{\partial u}{\partial y} \right) &= -\frac{\partial p}{\partial x} + \mu \left(\frac{\partial^2 u}{\partial x^2} + \frac{\partial^2 u}{\partial y^2} \right) - \frac{\sigma B_0^2}{(1+m^2)}(u-mv) \\ +g(1-F_0)\rho_f\beta_T(T-T_0) - (\rho_p - \rho_f)g\beta_c(C-C_0) - (\rho_m - \rho_f)\gamma g(F-F_0), \end{aligned} \quad (3.4)$$

$$\rho_f \left(\frac{\partial v}{\partial t} + u \frac{\partial v}{\partial x} + v \frac{\partial v}{\partial y} \right) = -\frac{\partial p}{\partial y} + \mu \left(\frac{\partial^2 v}{\partial x^2} + \frac{\partial^2 v}{\partial y^2} \right) - \frac{\sigma B_0^2}{(1+m^2)}(v+mu), \quad (3.5)$$

$$\begin{aligned} \rho_f c_f \left(\frac{\partial T}{\partial t} + u \frac{\partial T}{\partial x} + v \frac{\partial T}{\partial y} \right) &= k \left(\frac{\partial^2 T}{\partial x^2} + \frac{\partial^2 T}{\partial y^2} \right) + \mu \left[\left(\frac{\partial v}{\partial x} + \frac{\partial u}{\partial y} \right)^2 + 2 \left(\frac{\partial v}{\partial y} \right)^2 + 2 \left(\frac{\partial u}{\partial x} \right)^2 \right] \\ + \rho_p c_p \left[D_B \left(\frac{\partial C}{\partial x} \frac{\partial T}{\partial x} + \frac{\partial C}{\partial y} \frac{\partial T}{\partial y} \right) + \frac{D_T}{T_m} \left\{ \left(\frac{\partial T}{\partial x} \right)^2 + \left(\frac{\partial T}{\partial y} \right)^2 \right\} \right] \\ - \frac{\partial q_r}{\partial y} + \frac{\sigma B_0^2}{(1+m^2)}(u^2 + v^2), \end{aligned} \quad (3.6)$$

$$\frac{\partial C}{\partial t} + u \frac{\partial C}{\partial x} + v \frac{\partial C}{\partial y} = D_B \left(\frac{\partial^2 C}{\partial x^2} + \frac{\partial^2 C}{\partial y^2} \right) + \left(\frac{\partial^2 T}{\partial x^2} + \frac{\partial^2 T}{\partial y^2} \right) \frac{D_T}{T_m}, \quad (3.7)$$

$$\frac{\partial F}{\partial t} + u \frac{\partial F}{\partial x} + v \frac{\partial F}{\partial y} = D_N \left(\frac{\partial^2 F}{\partial y^2} + \frac{\partial^2 F}{\partial x^2} \right) - \frac{bW_c}{(C_1 - C_0)} \left(\frac{\partial}{\partial y} \left(F \frac{\partial C}{\partial y} \right) + \frac{\partial}{\partial x} \left(F \frac{\partial C}{\partial x} \right) \right). \quad (3.8)$$

Boundary conditions are as follows:

$$u \pm \beta_1 \left(\frac{\partial v}{\partial x} + \frac{\partial u}{\partial y} \right) = 0 \text{ at } y = \pm\eta, \quad (3.9)$$

$$T \pm \beta_2 \frac{\partial T}{\partial y} = \left\{ \begin{matrix} T_1 \\ T_0 \end{matrix} \right\}, \quad C \pm \beta_3 \frac{\partial C}{\partial y} = \left\{ \begin{matrix} C_1 \\ C_0 \end{matrix} \right\}, \quad F = \left\{ \begin{matrix} F_0 \\ F_1 \end{matrix} \right\} \text{ at } y = \pm\eta, \quad (3.10)$$

$$\left[-\tau_1 \frac{\partial^3}{\partial x^3} + m_1 \frac{\partial^3}{\partial x \partial t^2} + d \frac{\partial^2}{\partial t \partial x} \right] \eta = \mu \left(\frac{\partial^2 u}{\partial x^2} + \frac{\partial^2 u}{\partial y^2} \right) - \rho_f \left(\frac{\partial u}{\partial t} + u \frac{\partial u}{\partial x} + v \frac{\partial u}{\partial y} \right) -$$

$$\begin{aligned} & \frac{\sigma B_0^2}{\rho_f(1+m^2)}(u-mv) - g(1-F_0)\rho_f\beta_T(T-T_0) + (\rho_p - \rho_f)g\beta_C(C-C_0) - \\ & (\rho_m - \rho_f)g\gamma(F-F_0) \text{ at } y = \pm\eta. \end{aligned} \quad (3.11)$$

Here (u, v) are components of velocity in (x, y) directions, k the thermal conductivity, μ the dynamic viscosity, p the pressure, ρ_f the nanofluid density, ρ_p the density of nanoparticles, ρ_m the density of motile microorganisms, g the gravity, D_T the thermophoretic coefficient of diffusion, D_B the Brownian movement, D_N the microorganisms diffusion coefficient, γ the average volume of microorganisms, T_m the mean temperature, m_1 mass per unit area, d the viscous damping coefficient, W_c the maximum cell swimming speed, τ_1 the elastic tension, $(\beta_1, \beta_2, \beta_3)$ the slip parameters, b the chemotaxis constant, (C_0, C_1) and (T_0, T_1) the lower and upper walls concentration and temperatures respectively. Further (F_0, F_1) the volume fraction at upper and lower walls.

Now we consider non-dimensional quantities and stream function ψ in above system of equations by

$$\begin{aligned} u^* &= \frac{u}{c}, \quad v^* = \frac{v}{c}, \quad x^* = \frac{x}{\lambda}, \quad y^* = \frac{y}{d_1}, \quad t^* = \frac{ct}{\lambda}, \quad \beta_i^* = \frac{\beta_i}{d_1} (i = 1-3) \\ \eta^* &= \frac{\eta}{d_1}, \quad p^* = \frac{d_1^2 p}{c\lambda\mu}, \quad \theta = \frac{T-T_0}{T_1-T_0}, \quad \phi = \frac{C-C_0}{C_1-C_0}, \quad \chi = \frac{F-F_0}{F_1-F_0}, \\ u &= \frac{\partial\psi}{\partial y}, \quad v = -\delta \frac{\partial\psi}{\partial x}. \end{aligned} \quad (3.12)$$

The incompressibility constraint (3.3) is easily satisfied, whereas the other equations after involving the lubrication technique and omitting asterisks yield [3].

$$\frac{\partial^4\psi}{\partial y^4} - \left(\frac{M^2}{1+m^2} \right) \frac{\partial^2\psi}{\partial y^2} + Gr \frac{\partial\theta}{\partial y} - Gc \frac{\partial\phi}{\partial y} - Gf \frac{\partial\chi}{\partial y} = 0, \quad (3.13)$$

$$\left(\frac{1}{Pr} + Rn \right) \frac{\partial^2\theta}{\partial y^2} + Nb \frac{\partial\theta}{\partial y} \frac{\partial\phi}{\partial y} + Nt \left(\frac{\partial\theta}{\partial y} \right)^2 + \frac{EcM^2}{1+m^2} \left(\frac{\partial\psi}{\partial y} \right)^2 + Ec \left(\frac{\partial^2\psi}{\partial y^2} \right)^2 = 0, \quad (3.14)$$

$$\frac{Nt}{Nb} \left(\frac{\partial^2\theta}{\partial y^2} \right) + \frac{\partial^2\phi}{\partial y^2} = 0. \quad (3.15)$$

$$\frac{\partial^2\chi}{\partial y^2} - Pe \frac{\partial\phi}{\partial y} \frac{\partial\chi}{\partial y} - Pe\chi \frac{\partial^2\phi}{\partial y^2} - Pe\xi \frac{\partial^2\phi}{\partial y^2} = 0 \quad (3.16)$$

The boundary conditions are expressed in the following way:

$$\frac{\partial\psi}{\partial y} \pm \beta_1 \frac{\partial^2\psi}{\partial y^2} = 0 \text{ at } y = \pm \eta, \quad (3.17)$$

$$\left[E_1 \frac{\partial^3}{\partial x^3} + E_2 \frac{\partial^3}{\partial x \partial t^2} + E_3 \frac{\partial^2}{\partial x \partial t} \right] \eta = \frac{\partial^3\psi}{\partial y^3} - \left(\frac{M^2}{1+m^2} \right) \frac{\partial\psi}{\partial y} + Gr\theta - Gc\phi - Gf\chi \text{ at } y = \pm\eta, \quad (3.18)$$

$$\theta \pm \beta_2 \frac{\partial\theta}{\partial y} = \begin{Bmatrix} 1 \\ 0 \end{Bmatrix}, \quad \phi \pm \beta_3 \frac{\partial\phi}{\partial y} = \begin{Bmatrix} 1 \\ 0 \end{Bmatrix}, \quad \chi = \begin{Bmatrix} 0 \\ 1 \end{Bmatrix} \text{ at } y = \pm\eta, \quad (3.19)$$

with ϵ as the amplitude ratio, δ wave number, Nb the Brownian variable, Nt the thermophoresis parameter, Re Reynolds number, Ec the Eckert variable, M the Hartman number, Gc buoyancy ratio parameter, Pr the Prandtl number, Gf bioconvection Rayleigh number, (E_1, E_2, E_3) the wall parameters, Gr local Grashof number, Pe bioconvection Peclet number, ξ the bioconvection constant and Rn the radiation parameter defined below

$$\begin{aligned} \epsilon &= \frac{a}{d_1}, \quad \delta = \frac{d_1}{\lambda}, \quad Nb = \frac{\tau D_B (C_1 - C_0)}{\nu}, \quad Nt = \frac{\tau D_T (T_1 - T_0)}{T_m \nu}, \quad Re = \frac{cd_1 \rho_f}{\mu}, \\ Ec &= \frac{c^2}{c_f (T_1 - T_0)}, \quad M = \sqrt{\frac{\sigma}{\mu}} B_0 d_1, \quad Gc = \frac{(\rho_p - \rho_f) g \beta_C (C_1 - C_0) d_1^2}{\mu c}, \quad Pr = \frac{\nu}{\alpha}, \\ Gf &= \frac{(\rho_p - \rho_f) \gamma g (F_1 - F_0) d_1^2}{\mu c}, \quad E_1 = \frac{-\tau d_1^3}{\lambda^3 \mu c}, \quad E_2 = \frac{m_1 c d_1^3}{\lambda^3 \mu}, \quad E_3 = \frac{d d_1^3}{\lambda^2 \mu}, \\ Gr &= \frac{g \beta_T (1 - F_0) \rho_f (T_1 - T_0) d_1^2}{\mu c}, \quad Pe = \frac{b W_c}{D_N}, \quad \xi = \frac{F_0}{F_1 - F_0}, \quad Rn = \frac{16 \bar{\sigma} T_0^3}{3kk}. \end{aligned} \quad (3.20)$$

3.3 Numerical method

Finding the exact solution to governing equations is extremely difficult. Thus here we employed NDSolve technique through Runge-Kutta method of fourth order (shooting technique). This makes it easy to acquire the solution of the governing problem. Therefore equations (3.13) – (3.16) with the related boundary conditions (3.17) – (3.19) are numerically solved. For small step sizes, this method works with minimal error. As a result, the size of step 0.01 affects both x and y equally. The next section contains the results.

3.4 Graphical outcomes and discussion

This portion investigated axial velocity, concentration, temperature, heat transfer coefficient and density of motile microorganism. Figures 1 – 34 are portrayed for this aim.

3.4.1 Velocity

Figs. 3.1 – 3.8 represent the influences of pertinent variables on axial velocity. Fig. 3.1 examined the consequences of velocity slip variable β_1 . The fluid's velocity intensifies via larger β_1 . Aspects of Grashof number Gr against velocity is revealed in Fig. 3.2. Velocity is shown to be strengthened by large amounts of Gr . Fig. 3.3 sketched effects of buoyancy ratio Gc on velocity. Here velocity enhances through Gc . Fig. 3.4 is portrayed to capture the outcomes of bioconvection Rayleigh variable Gf . Decaying behavior is observed via larger Gf . Consequence of Hartman variable M on axial velocity is revealed in Fig. 3.5. This figure reveals that velocity of the material decays. Actually, rise in M increases the Lorentz force that turns in direction contrary to flow. This resistance force reduces liquid motion that eventually reduced velocity. Fig. 3.6 shows the aspects of Hall parameter m against velocity. The velocity enlarges with the growing values of m . Influence of bioconvection Peclet number Pe on velocity profile is pointed out in Fig. 3.7. The plot shows that the bioconvection Peclet number Pe gains the velocity of fluid. Fig. 3.8 captures variation of compliant wall parameters E_1, E_2, E_3 against velocity. Related Fig. illustrates that the velocity for E_1 and E_2 is increasing, however the contrary response seen for E_3 .

3.4.2 Temperature

The role of various variables on temperature are addressed in Figs 3.9 – 3.17. Consequences of thermal slip variable β_2 against temperature are examined in Fig. 3.9. Through higher β_2 the temperature enhances. Fig. 3.10 assures that larger Prandtl number Pr show an increase in temperature of liquid. Significances of Brownian movement Nb and thermophoresis parameters Nt are portrayed in Fig 3.11. We witnessed from this figure that temperature enhances against both these variables. Fig. 3.12 is designed to see the influence of radiation variable Rn on temperature. The findings of this graph demonstrated that as Rn rises, the temperature of the

liquid decreases. Consequence of Grashof variable Gr on temperature is illustrated in Fig. 3.13. Outcomes of this result find that temperature of fluid rises via Gr . Fig. 3.14 represents outcome of Hall variable m on velocity. Temperature increases when m large. Fig. 3.15 demonstrates the influence of Eckert number Ec on temperature. This figure demonstrated that temperature increases for Eckert variable Ec . Influence of bioconvection Peclet number Pe on temperature is depicted in Fig. 3.16. When Pe increases the temperature rises. Fig. 3.17 is created to investigate consequence of wall parameters (E_1, E_2, E_3) on temperature. Here temperature of fluid enhances via larger E_1 and E_2 while it drops for E_3 .

3.4.3 Concentration

Impacts of several distinct variables on nanoparticle concentration are inspected by Figs. 3.18 – 3.23. Influence of thermophoresis parameters Nt is displayed in Fig. 3.18. A careful examination of this figure clearly reveals decrease in the concentration of nanoparticles. Fig. 3.19 illustrates influence of β_3 for concentration. It is noted that concentration of fluid declines for larger β_3 . From Fig. 3.20 we detected that concentration reduces for buoyancy ratio parameter Gc . Fig. 3.21 is sketched to elaborate the effect of ξ on concentration. Decaying behavior is observed for concentration against ξ . Fig. 3.22 is portrayed to see the outcome of bioconvection Peclet number Pe on concentration. An enhancement in Pe leads to decay of concentration of nanofluid. Fig. 3.23 simulates the features of wall variables (E_1, E_2, E_3) against concentration. It is found that the concentration displays rising trend with the enhancement of E_1 and E_2 and it declines for E_3 .

3.4.4 Coefficient of heat transfer

Fig. 3.24 – 3.30 represent the activity of coefficient of heat transfer Z . Effect of Grashof number Gr is demonstrated in Fig. 3.24. It is noticed that heat transfer coefficient improves with higher Grashof number Gr . Fig. 3.25 is depicted to examine the consequences of bioconvection Rayleigh variable Gf against Z . An increment in Z is seen due to Gf . Fig. 3.26 demonstrates that when β_2 increases, the heat transfer coefficient increments. Fig. 3.27 describes the results of Brownian motion Nb and thermophoresis parameters Nt . From this figure we noticed that coefficient of heat transfer enhances with increment both the parameters. Outcome of radiation

number Rn on the heat transfer rate is illustrated in Fig. 3.28. Decline behavior is witnessed from this graph. Fig. 3.29 visualizes the consequence of bioconvection Peclet number Pe on heat transfer coefficient. Higher Peclet number Pe increases Z . Fig. 3.30 portrays the heat transfer rate for different values of Hall variable m . With increasing m , the heat transfer coefficient highers.

3.4.5 Density of motile microorganism

Consequences of various distinct variables on motile microorganism χ are inspected through by Figs. 3.31 – 3.34. Effects of bioconvection Rayleigh variable Gf are depicted through Fig. 3.31. Clearly χ enhances against Gf . Fig. 3.32 is plotted to show the variations in motile microorganism for bioconvection parameter ξ . An increase is noticed in motile microorganism density. Fig. 3.33 explains the motile microorganism density against Peclet number Pe . It is found that enhancement of motile microorganism density occurs for Pe . Fig. 3.34 demonstrates the motile microorganism density versus thermophoresis parameters Nt . By increasing the thermophoresis parameters Nt the density of motile microorganism declines.

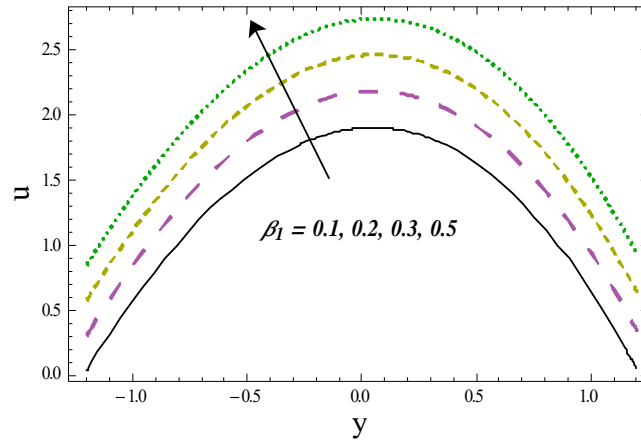


Fig. 3.1: Variation of β_1 on u

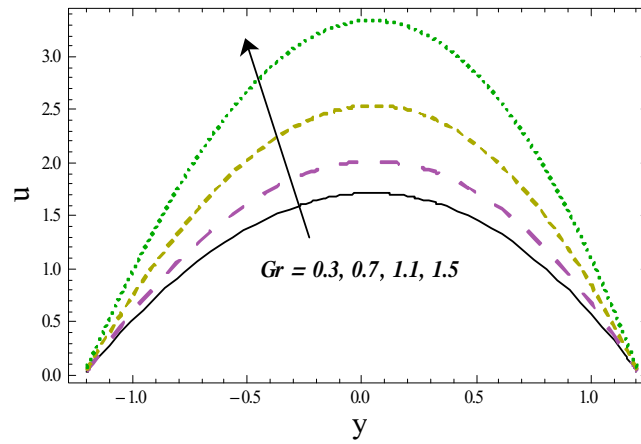


Fig. 3.2: Variation of Gr on u

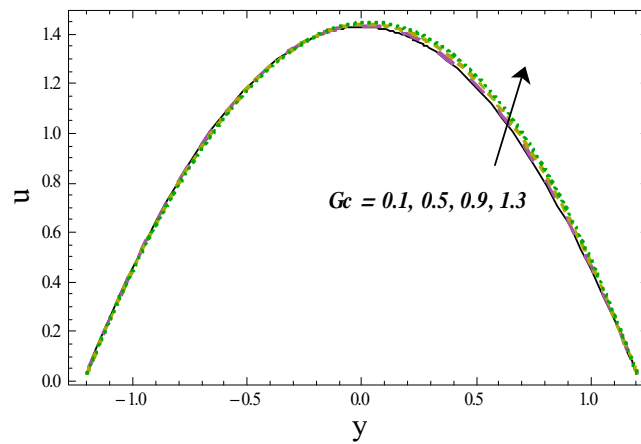


Fig. 3.3: Variation of Gc on u

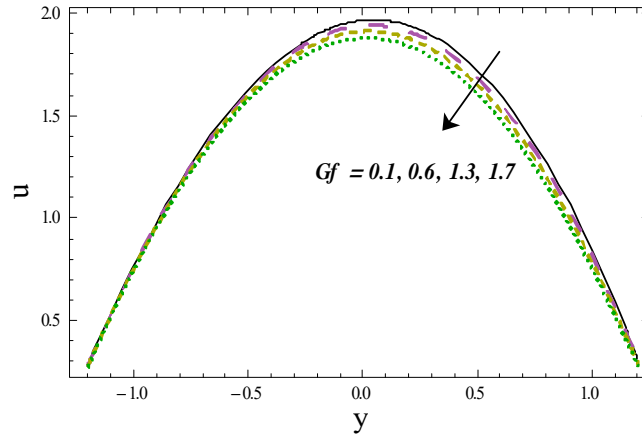


Fig. 3.4: Variation of Gf on u

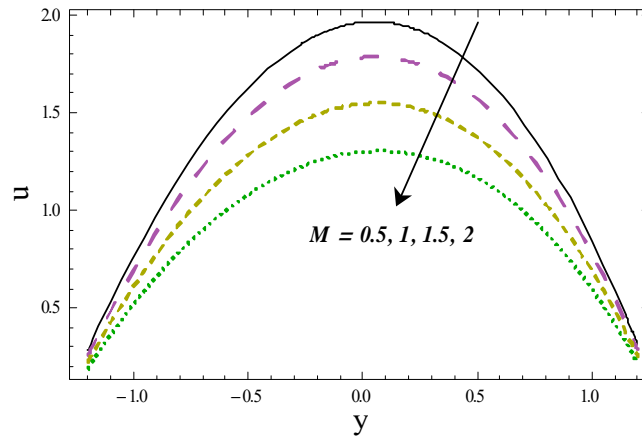


Fig. 3.5: Variation of M on u

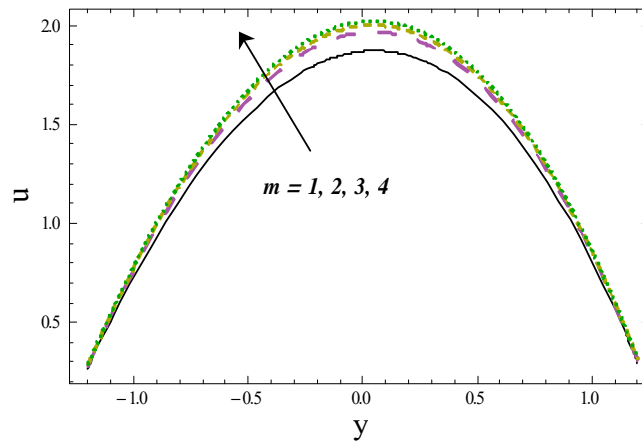


Fig. 3.6: Variation of m on u

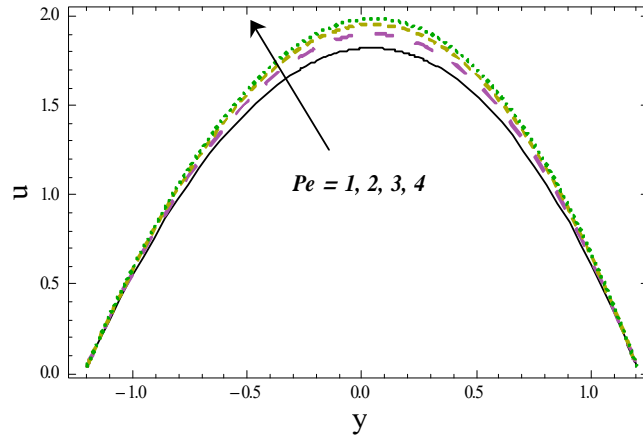


Fig. 3.7: Variation of Pe on u

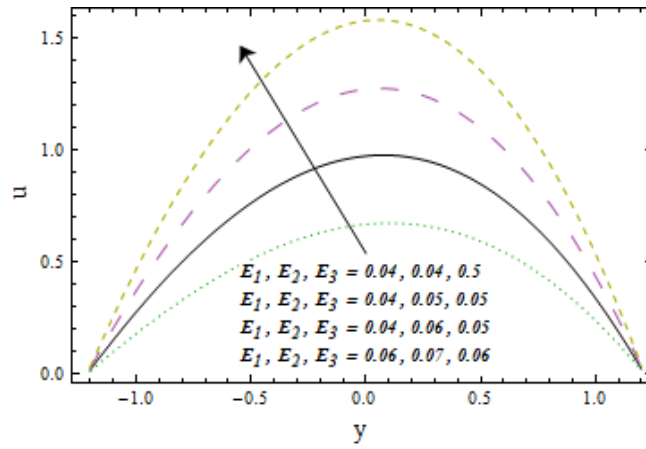


Fig. 3.8: Variations of E_1, E_2 and E_3 on u

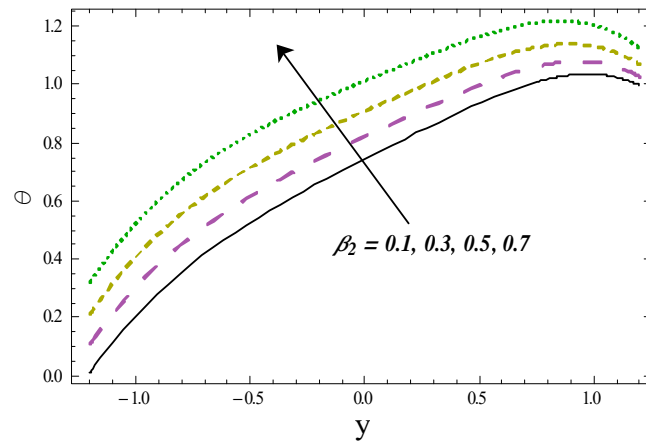


Fig. 3.9: Variation of β_2 on θ

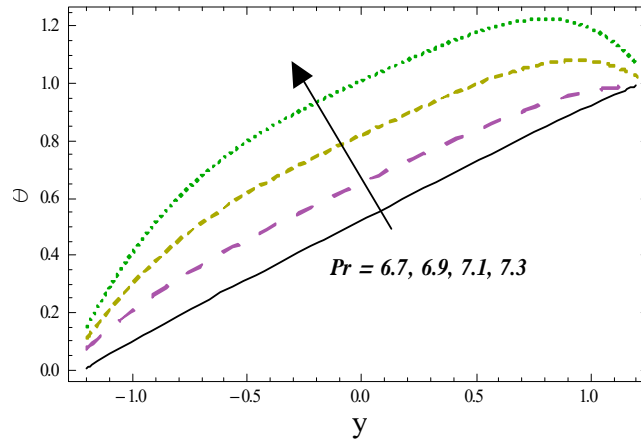


Fig. 3.10: Variation of Pr on θ

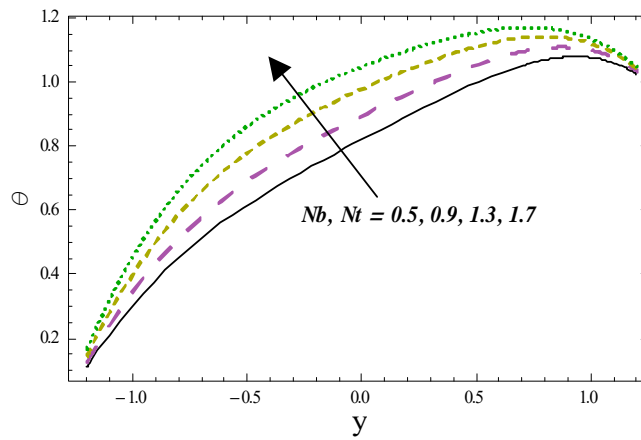


Fig. 3.11: Variations of Nb and Nt on θ

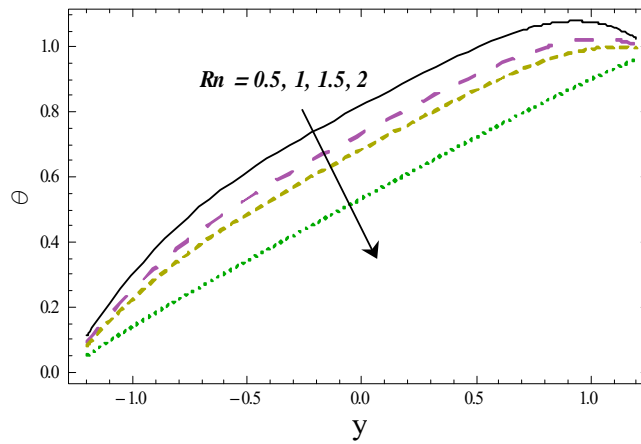


Fig. 3.12: Variation of Rn on θ

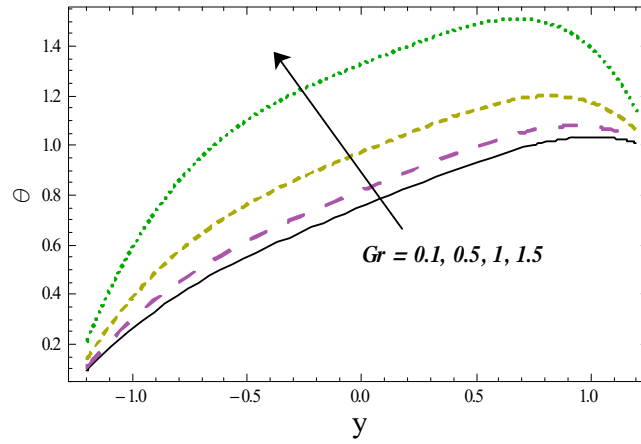


Fig. 3.13: Variation of Gr on θ

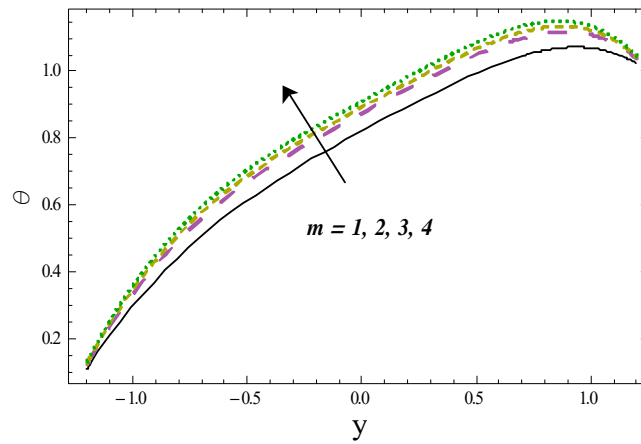


Fig. 3.14: Variation of m on θ

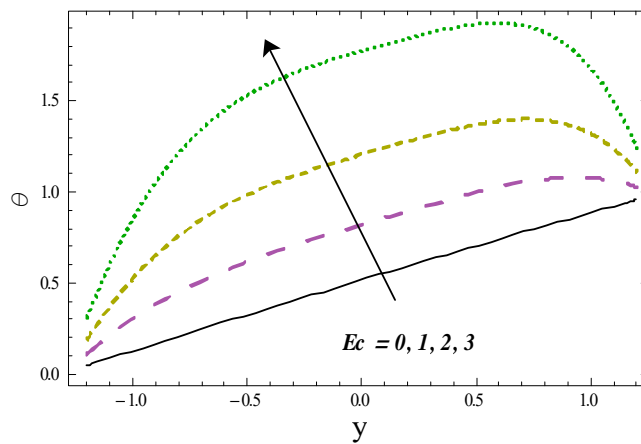


Fig. 3.15: Variation of Ec on θ

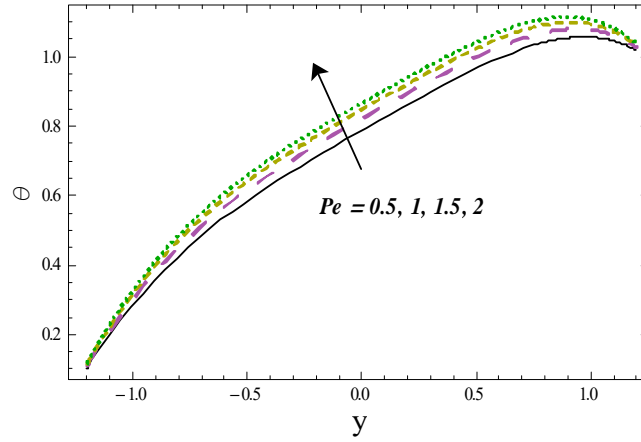


Fig. 3.16: Variation of Pe on θ

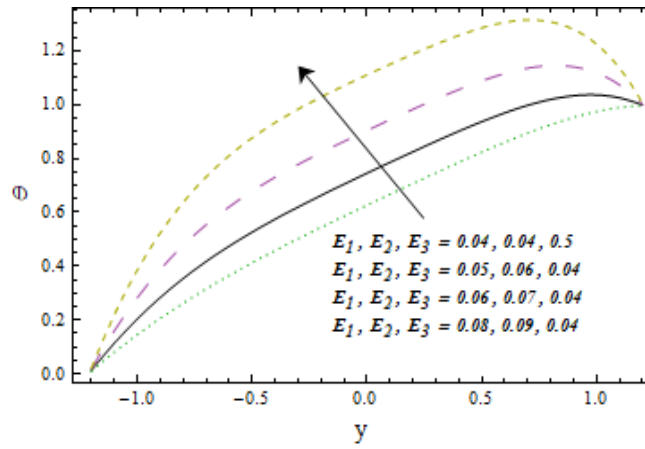


Fig. 3.17: Variations of E_1, E_2 and E_3 on θ

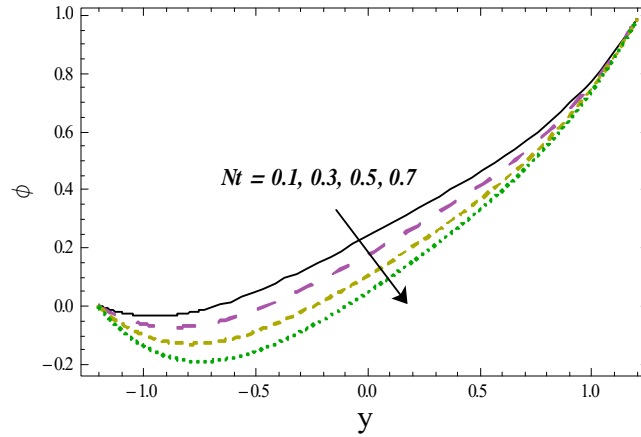


Fig. 3.18: Variation of Nt on ϕ

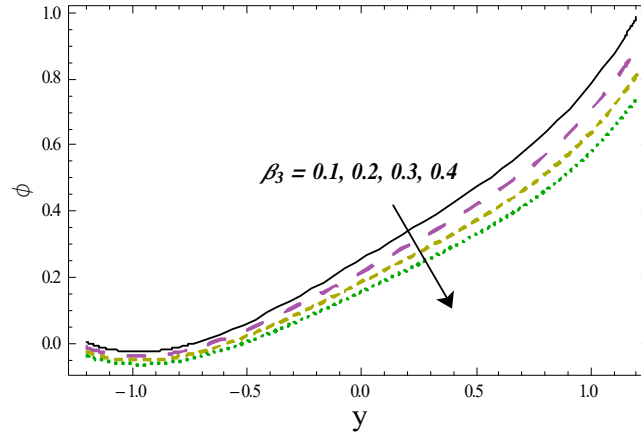


Fig. 3.19: Variation of β_3 on ϕ

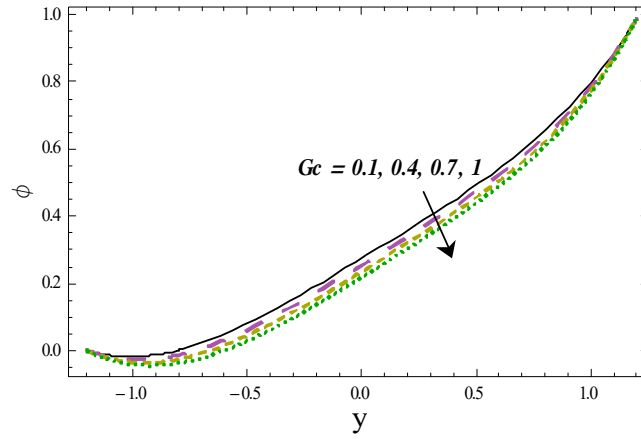


Fig. 3.20: Variation of Gc on ϕ

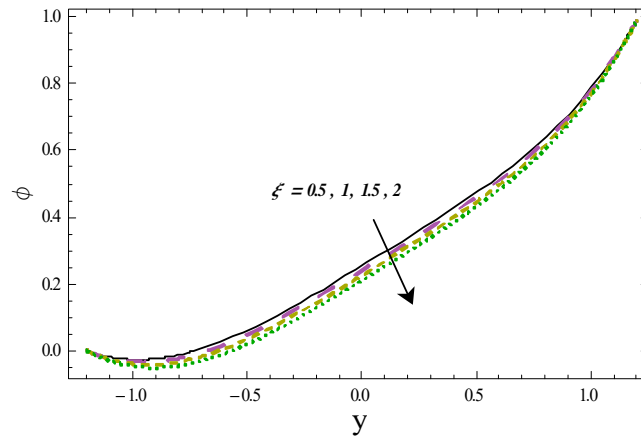


Fig. 3.21: Variation of ξ on ϕ

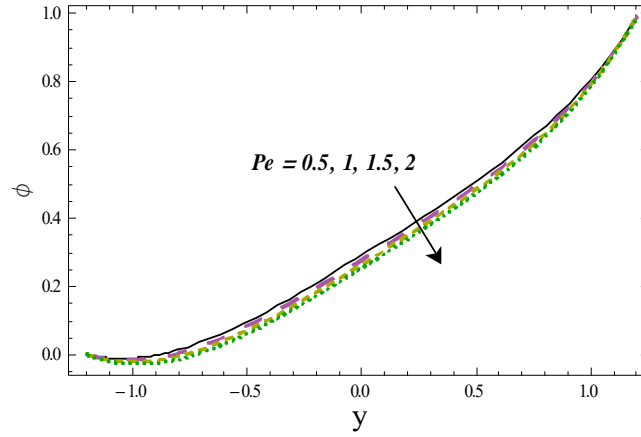


Fig. 3.22: Variation of Pe on ϕ

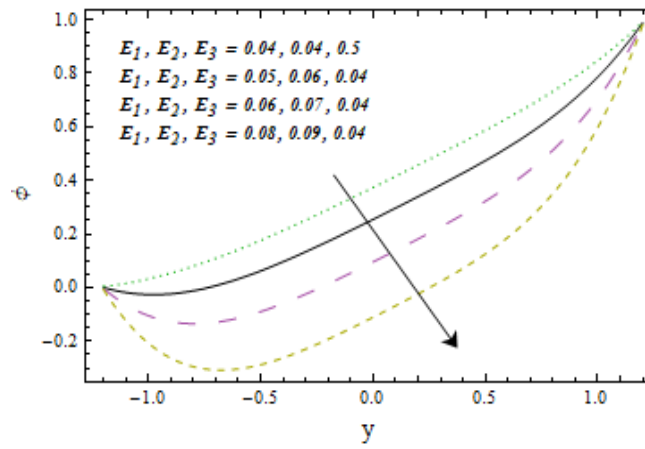


Fig. 3.23: Variations of E_1, E_2 and E_3 on ϕ

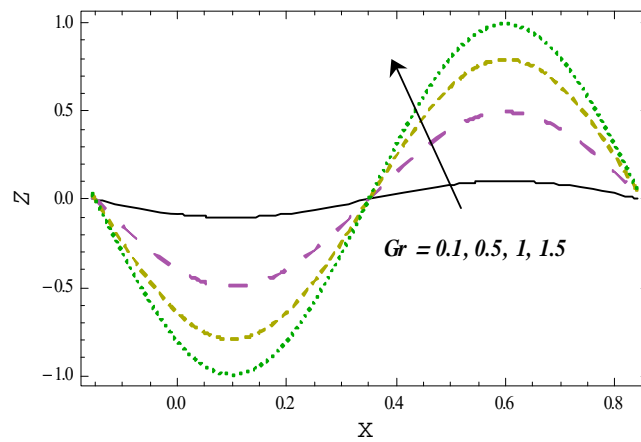


Fig. 3.24: Variation of Gr on Z

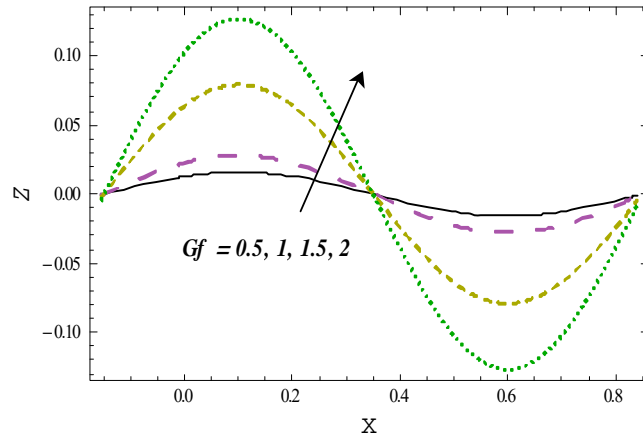


Fig. 3.25: Variation of Gf on Z

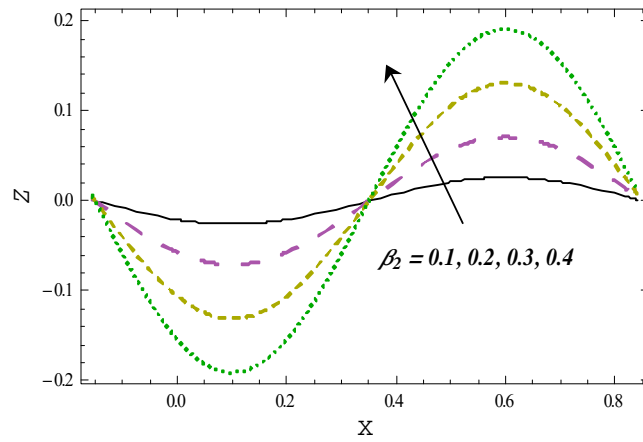


Fig. 3.26: Variation of β_2 on Z

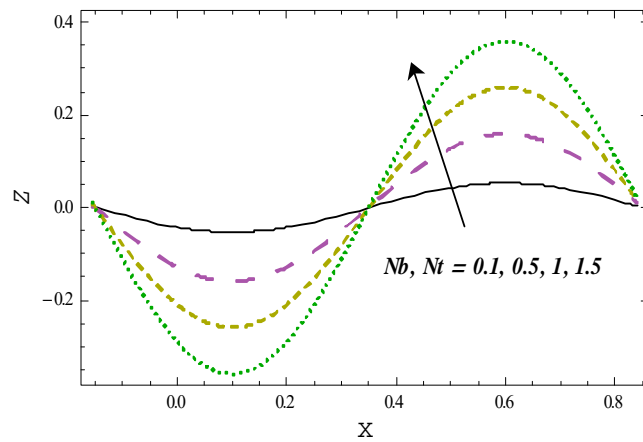


Fig. 3.27: Variations of Nb and Nt on Z

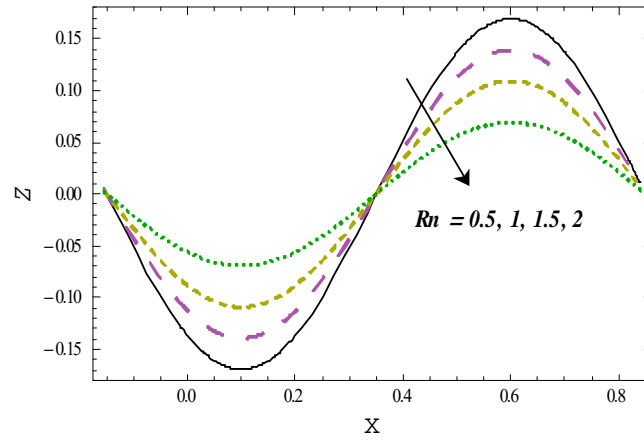


Fig. 3.28: Variation of Rn on Z

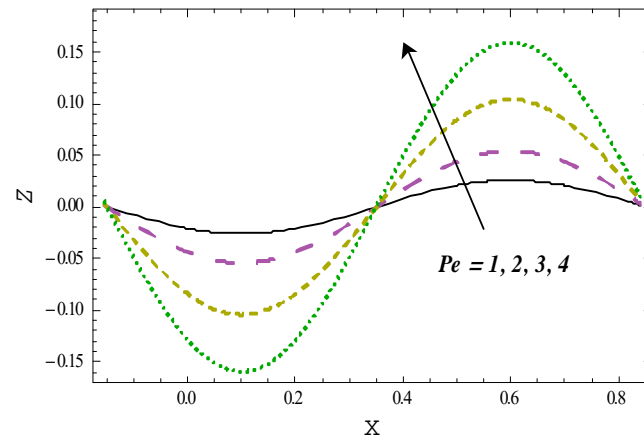


Fig. 3.29: Variation of Pe on Z

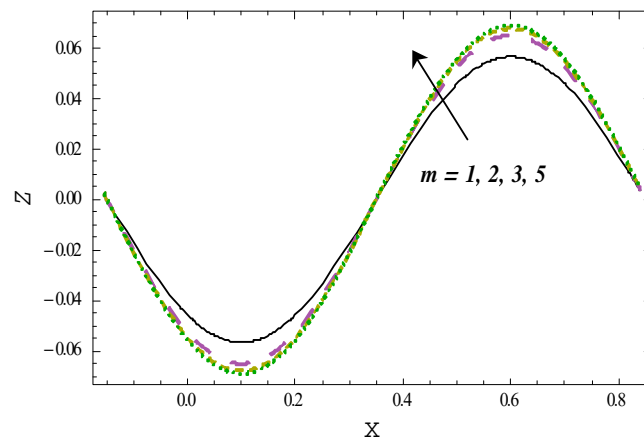


Fig. 3.30: Variation of m on Z

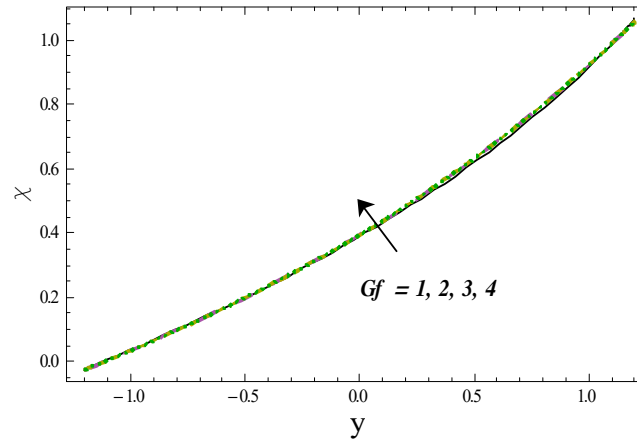


Fig. 3.31: Variation of Gf on χ

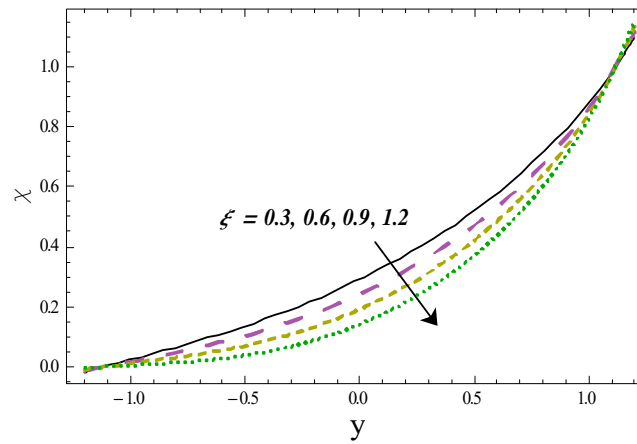


Fig. 3.32: Variation of ξ on χ

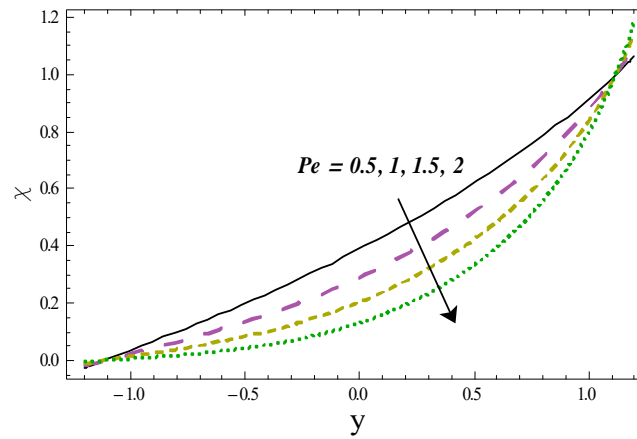


Fig. 3.33: Variation of Pe on χ

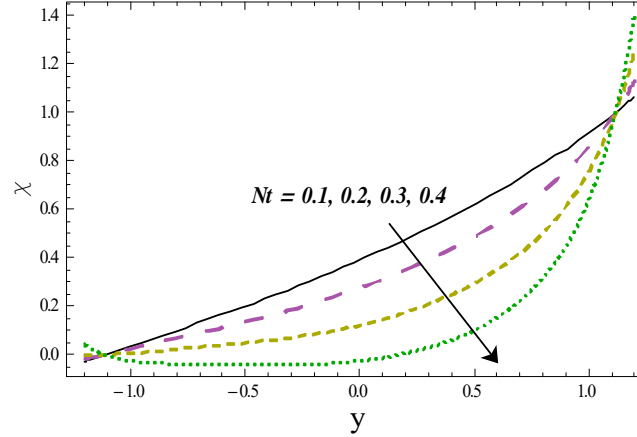


Fig. 3.34: Variation of Nt on χ

3.5 Conclusions

Majors outcomes are as follows.

- Velocity enhances for β_1 , Gr and Gc .
- Opposite behavior is observed for velocity agaianst Gf and Pe .
- Pr and Gr increase the temperature.
- Both thermophoresis Nt and Brownian motion Nb have rising impacts of temperature.
- Influences of Rn and Pe on temperature are dissimilar.
- Concentration of fluid declines for Nt and Gc .
- Velocity, temperature and concentration are increased with higher E_1 and E_2 while these quantities decrease for E_3 .
- Heat transfer coefficient enhances against larger Gf , β_2 and m .
- Effects of Pe on coefficient of heat transfer are reverse when compared with Rn .
- Density of motile microorganisms shows decreasing behavior of Pe and Nt .

Chapter 4

Peristalsis of couple stress nanofluid with wall characteristics

4.1 Introduction

Here examined the peristaltic motion of couple stress nanofluid. Energy equation is retained with viscous dissipation and thermal radiation aspects. Further chemical reaction between a chemical species and the nanofluid may be significant. Therefore we considered the Buongiorno nanofluid model with chemical reaction. Zero mass flux and thermal convective conditions are incorporated. Numerical solutions are developed for the governing problem. Finally the concentration, temperature and heat transfer coefficient are scrutinized through graphs.

4.2 Formulation

An incompressible couple-stress nanofluid in a channel of width $2d_1$ is taken. Flow generated is by sinusoidal waves propagating with uniform speed c . We select rectangular coordinate (x, y) such that x is parallel to wall and y is transverse to it. A magnetic field of strength of B_0 is exerted in y -direction. The wall shapes are

$$y = \pm \eta(x, t) = \pm \left[d_1 + a \sin \frac{2\pi}{\lambda} (x - ct) \right], \quad (4.1)$$

where a and λ denote amplitude and wavelength respectively. (See Fig. 4.1).

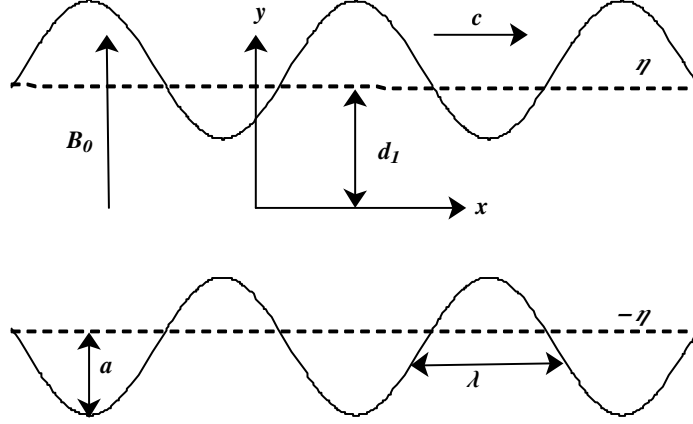


Fig. 4.1. Problem

The relevant equations for problem under consideration are

$$\frac{\partial u}{\partial x} + \frac{\partial v}{\partial y} = 0, \quad (4.2)$$

$$\frac{\partial u}{\partial t} + u \frac{\partial u}{\partial x} + v \frac{\partial u}{\partial y} = -\frac{1}{\rho_f} \frac{\partial p}{\partial x} + \nu \left(\frac{\partial^2 u}{\partial x^2} + \frac{\partial^2 u}{\partial y^2} \right) - \frac{\eta_1}{\rho_f} \left(\frac{\partial^4 u}{\partial x^4} + 2 \frac{\partial^4 u}{\partial x^2 \partial y^2} + \frac{\partial^4 u}{\partial y^4} \right) - \frac{\sigma B_0^2}{\rho_f} u, \quad (4.3)$$

$$\frac{\partial v}{\partial t} + u \frac{\partial v}{\partial x} + v \frac{\partial v}{\partial y} = -\frac{1}{\rho_f} \frac{\partial p}{\partial y} + \nu \left(\frac{\partial^2 v}{\partial x^2} + \frac{\partial^2 v}{\partial y^2} \right) - \frac{\eta_1}{\rho_f} \left(\frac{\partial^4 v}{\partial x^4} + 2 \frac{\partial^4 v}{\partial x^2 \partial y^2} + \frac{\partial^4 v}{\partial y^4} \right), \quad (4.4)$$

$$\begin{aligned} \frac{\partial T}{\partial t} + u \frac{\partial T}{\partial x} + v \frac{\partial T}{\partial y} = & \alpha \left(\frac{\partial^2 T}{\partial x^2} + \frac{\partial^2 T}{\partial y^2} \right) + \tau \left[\left\{ \left(\frac{\partial T}{\partial y} \right)^2 + \left(\frac{\partial T}{\partial x} \right)^2 \frac{D_T}{T_m} \right\} \right. \\ & \left. + \left(\frac{\partial C}{\partial y} \frac{\partial T}{\partial y} + \frac{\partial C}{\partial x} \frac{\partial T}{\partial x} \right) D_B \right] \\ & + \eta_1 \left[\left(\frac{\partial^2 v}{\partial x^2} + \frac{\partial^2 v}{\partial y^2} \right)^2 + \left(\frac{\partial^2 u}{\partial y^2} + \frac{\partial^2 u}{\partial x^2} \right)^2 \right] + \mu \left[\left(\frac{\partial v}{\partial x} + \frac{\partial u}{\partial y} \right)^2 + 2 \left\{ \left(\frac{\partial v}{\partial y} \right)^2 + \left(\frac{\partial u}{\partial x} \right)^2 \right\} \right] \\ & - \frac{\partial q_r}{\partial y} + \frac{\sigma B_0^2}{\rho_f c_f} u^2, \end{aligned} \quad (4.5)$$

$$\frac{\partial C}{\partial t} + u \frac{\partial C}{\partial x} + v \frac{\partial C}{\partial y} = D_B \left(\frac{\partial^2 C}{\partial x^2} + \frac{\partial^2 C}{\partial y^2} \right) + \left(\frac{\partial^2 T}{\partial x^2} + \frac{\partial^2 T}{\partial y^2} \right) \frac{D_T}{T_m} - k_1 (C - C_0). \quad (4.6)$$

Heat flux radiation q_r is defined as

$$q_r = -\frac{4\bar{\sigma}}{3k} \frac{\partial T^4}{\partial y}. \quad (4.7)$$

Expanding T^4 by using Taylor series we have

$$T^4 = 4T_0^3T - 3T_0^4. \quad (4.8)$$

Since the couple stress is presumed because of the suspended particles, the transparent fluid obviously cannot be sustained by couple stresses at the wall, we have therefore tacitly concluded that the couple stress tensor components vanish at the wall along with no slip and compliant walls i.e.

$$u = 0, \quad \frac{\partial^2 u}{\partial y^2} = 0 \quad \text{at } y = \pm\eta, \quad (4.9)$$

$$\left[-\tau_1 \frac{\partial^3}{\partial x^3} + m_1 \frac{\partial^3}{\partial x \partial t^2} + d \frac{\partial^2}{\partial t \partial x} \right] \eta = \mu \left(\frac{\partial^2 u}{\partial x^2} + \frac{\partial^2 u}{\partial y^2} \right) - \eta_1 \left(\frac{\partial^4 u}{\partial x^4} + 2 \frac{\partial^4 u}{\partial x^2 \partial y^2} + \frac{\partial^4 u}{\partial y^4} \right) - \rho_f \left(\frac{\partial u}{\partial t} + u \frac{\partial u}{\partial x} + v \frac{\partial u}{\partial y} \right) - \sigma B_o^2 u \quad \text{at } y = \pm\eta. \quad (4.10)$$

Further zero mass flux and thermal convective conditions are defined as

$$-k \frac{\partial T}{\partial y} = h \left\{ \begin{matrix} T - T_0 \\ T_0 - T \end{matrix} \right\}, \quad D_B \frac{\partial C}{\partial y} + \frac{D_T}{T_m} \frac{\partial T}{\partial y} = 0 \quad \text{at } y = \pm\eta. \quad (4.11)$$

Considering stream function $u = \psi_y$, $v = -\delta(\psi_x)$ and using the non-dimensional variables

$$\begin{aligned} cu^* &= u, \quad cv^* = v, \quad \lambda x^* = x, \quad d_1 y^* = y, \quad \lambda t^* = ct, \quad d_1 \eta^* = \eta, \\ c\lambda\mu p^* &= d_1^2 p, \quad T_0 \theta = T - T_0, \quad (C_1 - C_0)\phi = C - C_0. \end{aligned} \quad (4.12)$$

Now adopting low Reynolds number and large wavelength assumptions [3] in equations (4.3) – (4.6) we obtain after omitting asterisks

$$\frac{\partial^6 \psi}{\partial y^6} - \gamma^2 \frac{\partial^4 \psi}{\partial y^4} + M^2 \gamma^2 \frac{\partial^2 \psi}{\partial y^2} = 0, \quad (4.13)$$

$$\left(\frac{1}{\text{Pr}} + Rn \right) \frac{\partial^2 \theta}{\partial y^2} + Nb \left(\frac{\partial \phi}{\partial y} \frac{\partial \theta}{\partial y} \right) + Ec \left[\frac{1}{\gamma^2} \left(\frac{\partial^3 \psi}{\partial y^3} \right)^2 + \left(\frac{\partial^2 \psi}{\partial y^2} \right)^2 + M^2 \left(\frac{\partial \psi}{\partial y} \right)^2 \right] + \left(\frac{\partial \theta}{\partial y} \right)^2 Nt = 0, \quad (4.14)$$

$$\frac{Nt}{Nb} \left(\frac{\partial^2 \theta}{\partial y^2} \right) + \frac{\partial^2 \phi}{\partial y^2} - \zeta Sc \phi = 0, \quad (4.15)$$

The boundary conditions become

$$\frac{\partial \psi}{\partial y} = 0, \quad \frac{\partial^3 \psi}{\partial y^3} = 0 \quad \text{at } y = \pm \eta, \quad (4.16)$$

$$\left[E_1 \frac{\partial^3}{\partial x^3} + E_2 \frac{\partial^3}{\partial x \partial t^2} + E_3 \frac{\partial^2}{\partial x \partial t} \right] \eta = -\frac{1}{\gamma^2} \frac{\partial^5 \psi}{\partial y^5} + \frac{\partial^3 \psi}{\partial y^3} - M^2 \frac{\partial \psi}{\partial y} \quad \text{at } y = \pm \eta, \quad (4.17)$$

$$\frac{\partial \theta}{\partial y} = \begin{Bmatrix} -Bi\theta \\ Bi\theta \end{Bmatrix}, \quad Nb \frac{\partial \phi}{\partial y} + Nt \frac{\partial \theta}{\partial y} = 0 \quad \text{at } y = \pm \eta. \quad (4.18)$$

Continuity equation (4.2) is satisfied automatically. Here ϵ , δ , Pr , Ec , Re , Sc , M , Nb , Nt , Bi , γ , ζ , Rn , (E_1, E_2) and E_3 are amplitude ratio, wave number, Prandtl variable, Eckert variable, Reynolds number, Schmidt number, Hartman number, Brownian movement variable, thermophoresis variable, Biot number, couple-stress variable, chemical reaction variable, Radiation parameter, elasticity parameters and damping parameter, These are defined by

$$\begin{aligned} \epsilon &= \frac{a}{d_1}, \quad \delta = \frac{d_1}{\lambda}, \quad Pr = \frac{\nu}{\alpha}, \quad Ec = \frac{c^2}{c_f T_0}, \quad Re = \frac{\rho c d_1}{\mu}, \quad Sc = \frac{\nu}{D_B}, \\ M &= \sqrt{\frac{\bar{\sigma}}{\mu}} B_0 d_1, \quad Nb = \frac{D_B \tau (C_1 - C_0)}{\nu}, \quad Nt = \frac{D_T \tau T_0}{T_m \nu}, \quad Bi = \frac{h d_1}{k}, \quad \gamma = \sqrt{\frac{\mu}{\eta_1}} d_1, \\ \zeta &= \frac{k_1 d_1^2}{D_B}, \quad Rn = \frac{16 \bar{\sigma} T_0^3}{3 k k}, \quad E_1 = -\frac{d_1^3 \tau}{\lambda^3 \mu c}, \quad E_2 = \frac{c m_1 d_1^3}{\lambda^3 \mu}, \quad E_3 = \frac{d_1^3 d}{\lambda^2 \mu}. \end{aligned} \quad (4.19)$$

4.3 Numerical method and analysis

Problems (4.13) – (4.18) are tackled numerically by shooting technique via using NDSolve command with fourth order Runge-kutta technique in the MATHEMATICA. For boundary value problems, the performance of this technique is excellent. This method seems effective in small steps size and tiny errors. In addition, the y and x change in a step size of 0.01 uniformly. Set with 10^{-6} error tolerance. Graphical analysis of concentration, temperature and heat transfer rate against pertinent variables are examined in this section.

4.3.1 Temperature

Variations for physical variables on temperature θ have been displayed in Figs. 4.2 – 4.9. Fig. 4.2 indicates that temperature decreases against larger Hartman number M . This is

because the magnetic field functions as an agent of retardation. An effect of couple stress fluid variable γ is seen in Fig. 4.3. Distribution of temperature increments with the enhancement of variable couple-stress fluid γ . Temperature in Fig. 4.4 is decreased for higher values of radiation variable Rn . It's because fluid temperature is more than walls temperature. Due to dissipation of heat, the temperature drops here. Fig. 4.5 displays the outcomes of Eckert variable Ec on temperature. Temperature boosts by higher values of Eckert number. The change in temperature is observable due to the strong influence of viscous dissipation. Temperature enhances by increasing the values of Prandtl number Pr (see Fig. 4.6). It is because of the momentum's high diffusiveness. In Fig. 4.7 combination of Brownian motion Nb and thermophoresis Nt parameters are reported. As we increase values of both the parameters we can see that temperature increases. The increase in Brownian diffusion highers the average kinetic energy of fluid and fluid temperature enhances. Influence of thermal Biot number Bi against temperature is portrayed in Fig. 4.8. Here temperature decays when increased Bi . The Biot number Bi , improves the convective heating at the surface and reduces wall temperature. Biot number is more than one. This shows the non-uniform temperature fields inside the liquid. Fig. 4.9 is captured to see the behavior of compliant wall variables (E_1, E_2, E_3) on temperature. We observed that temperature enhances via E_1 and E_2 enhances it decays for E_3 .

4.3.2 Concentration

Impacts of different embedded parameters on concentration field ϕ are examined through Figs. 4.10–4.16. Fig. 4.10 is portrayed to analyze the variation of concentration for chemical reaction parameter ζ . Clearly large chemical reaction ζ gives enhancement in concentration profile ϕ . This happens because chemical reaction increases the rate of interfacial mass transfer which causes the increment of concentration. Concentration in Fig. 4.11 is diminished for large couple-stress fluid parameter γ . Fig. 4.12 reveals the influence of Brownian motion Nb parameter on concentration ϕ . In this Figure we noticed that by rising values of Nb concentration increases. Opposite behavior for concentration field ϕ is observed for thermophoresis parameter Nt in Fig. 4.13. Physically, higher strength of thermophoretical effects leads to the enhance volume flow by increasing the concentration of nanoparticles due to the temperature gradient. Fig. 4.14 prepared the concentration ϕ for larger Schmidt number Sc , the concentration rises when

the thermophoresis parameter enlarged. There is increase in concentration for E_1 and E_2 while concentration decreases for E_3 . (see Fig. 4.15). Radiation effect Rn is shown in the Fig. 4.16 for the field of concentration. It is evident that by increasing Rn concentration of nanofluid at the center of channel increases.

4.3.3 Coefficient of heat transfer

Figs. 4.17–4.24 show the variations of pertinent variables on coefficient of heat transfer $Z(x) = \eta_x \theta_y(\eta)$. Fig. 4.17 examined the effects of couple-stress fluid parameter γ . An increase of γ gives rise to heat transfer coefficient. The variation of Eckert number Ec on heat transfer coefficient Z is demonstrated by Fig. 4.18. Higher Eckert number Ec give rise to the heat transfer coefficient. Fig. 4.19 contains heat transfer coefficient with regard to radiation parameter Rn . For an improvement in Rn the heat transfer rate lessens. Fig. 4.20 is sketched to see the behavior of Prandtl number Pr on coefficient of heat transfer Z . The internal resistance of fluid particles increases because of Pr which enhances the rate of heat transfer. Fig. 4.21 includes the effect of Biot number Bi . Here heat transfer coefficient highers against Bi . Fig. 4.22 shows the variation of Hartman number against coefficient of heat transfer. It is evident from this Fig. that coefficient of heat of transfer declines. Fig. 4.23 depicts heat transfer coefficient Z via thermophoresis Nt parameter and Brownian movement parameter Nb . Here Z enhances when both Nb and Nt are increased. Such rise in coefficient of heat transfer Z is because the motion of nanoparticles to the fluid from the wall when both parameters are enhanced. In Fig. 4.24 the heat transfer coefficient rises by chemical reaction parameter ζ . Moreover, we observed that

Z has oscillating behavior because of the wave travelling along the boundaries of the channel.

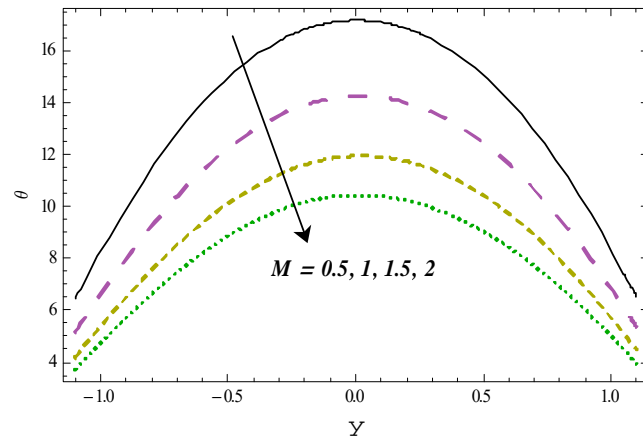


Fig. 4.2: Variation of M on θ

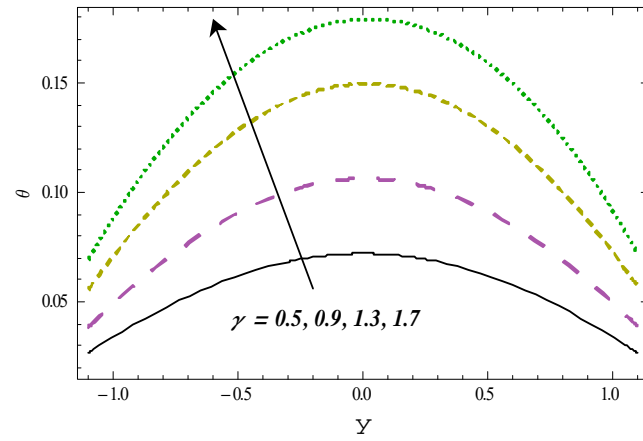


Fig. 4.3: Variation of γ on θ

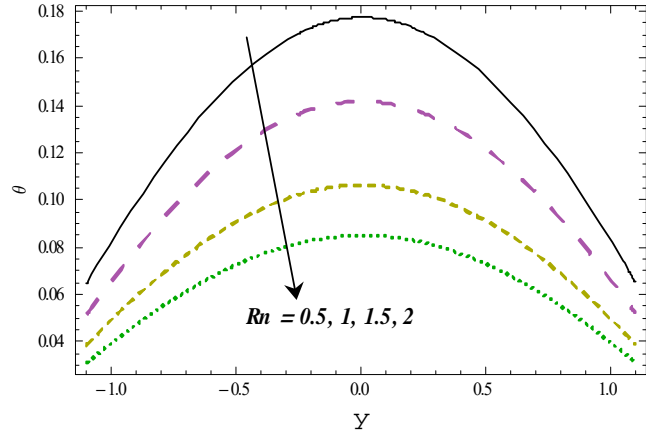


Fig. 4.4: Variation of Rn on θ

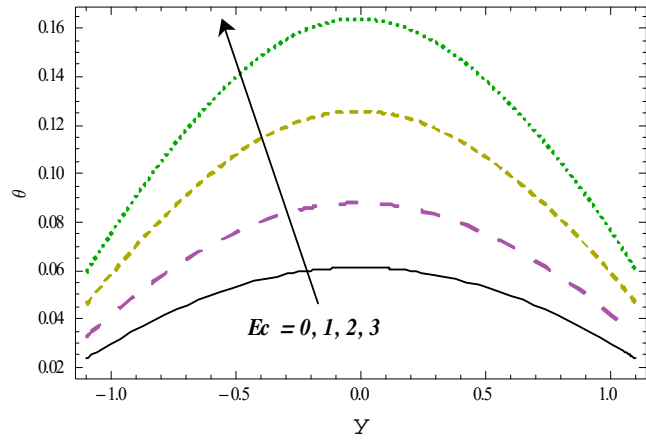


Fig. 4.5: Variation of Ec on θ

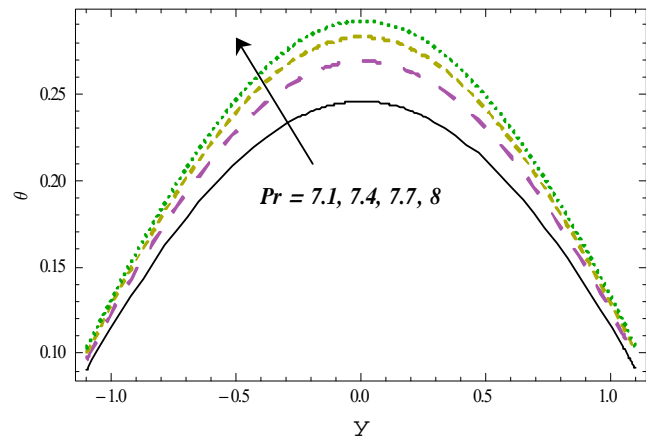


Fig. 4.6: Variation of Pr on θ

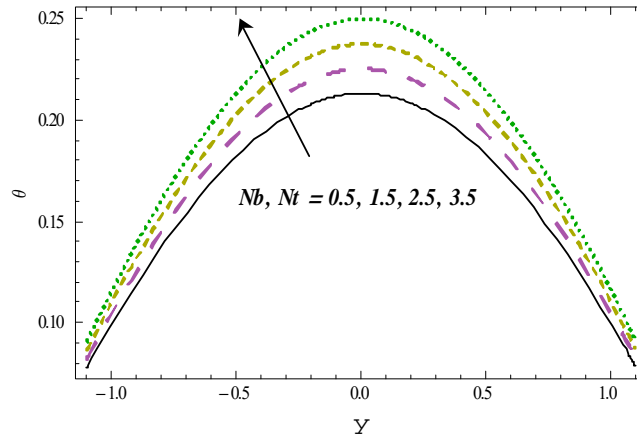


Fig. 4.7: Variations of Nb and Nt on θ

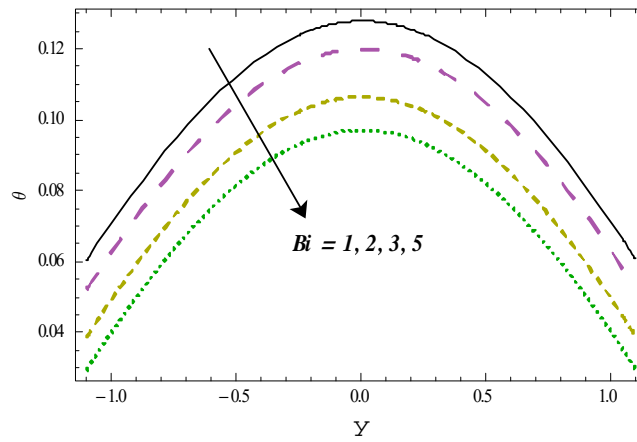


Fig. 4.8: Bi variation on θ

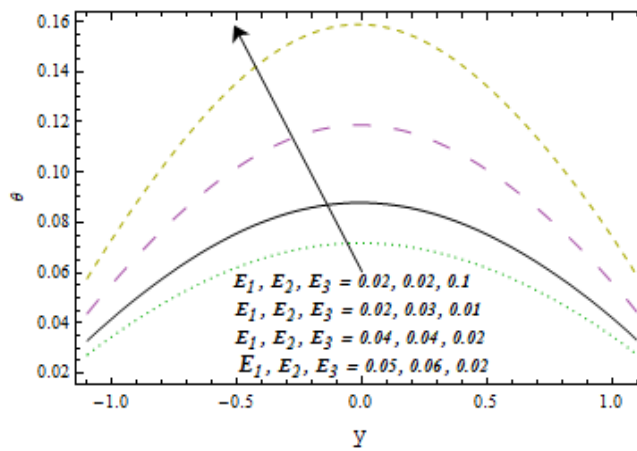


Fig. 4.9: Variations of E_1, E_2 and E_3 on θ

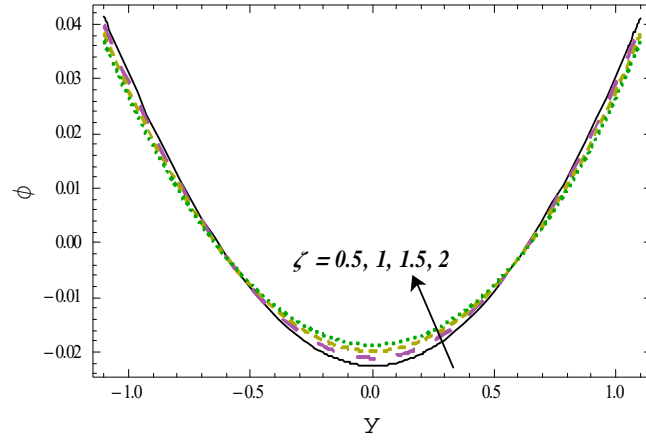


Fig. 4.10: Variation of ζ on ϕ

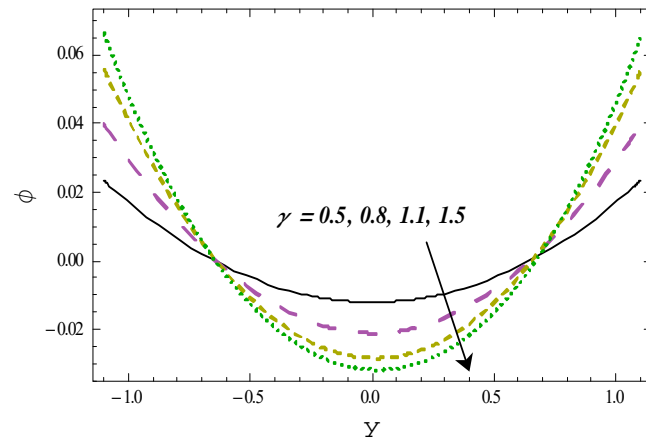


Fig. 4.11: Variation of γ on ϕ

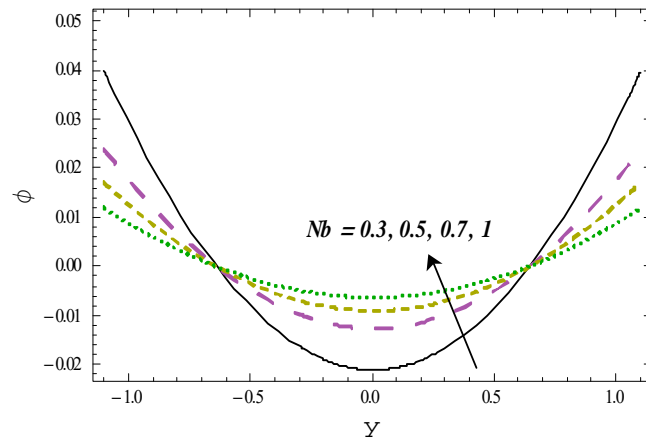


Fig. 4.12: Variation of Nb on ϕ

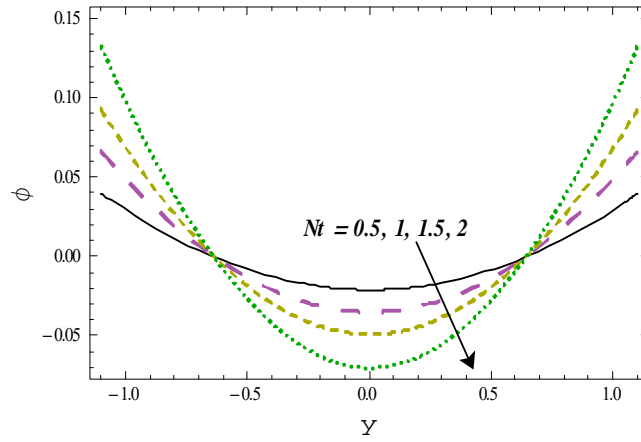


Fig. 4.13: Variation of Nt on ϕ

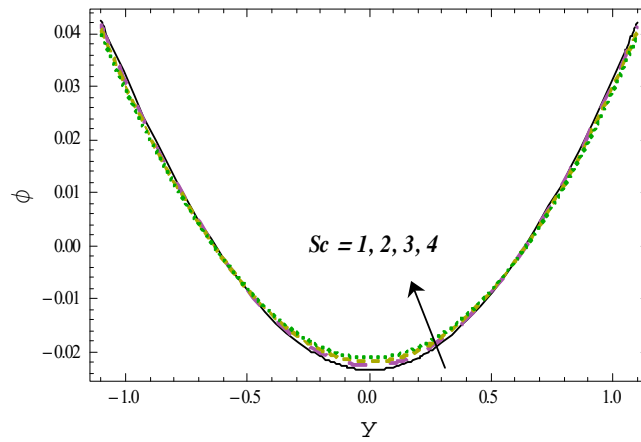


Fig. 4.14: Variation of Sc on ϕ

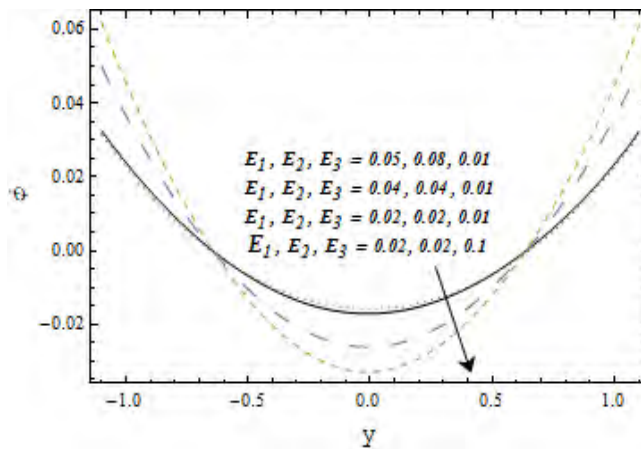


Fig. 4.15: Variations of E_1, E_2 and E_3 on ϕ

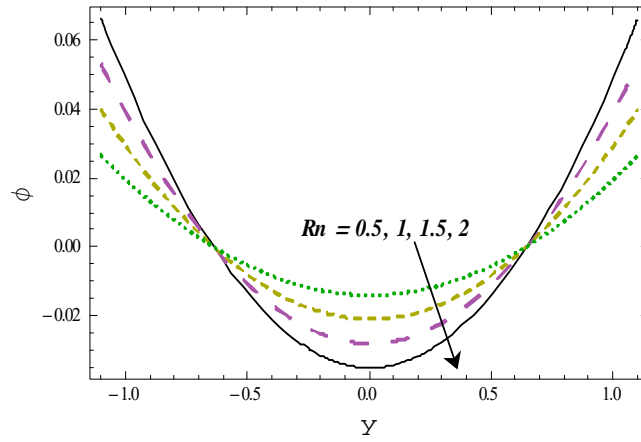


Fig. 4.16: Variation of Rn on ϕ

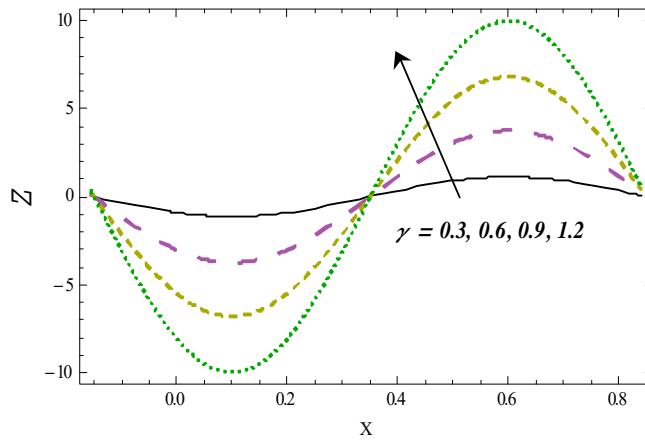


Fig. 4.17: Variation of γ on Z

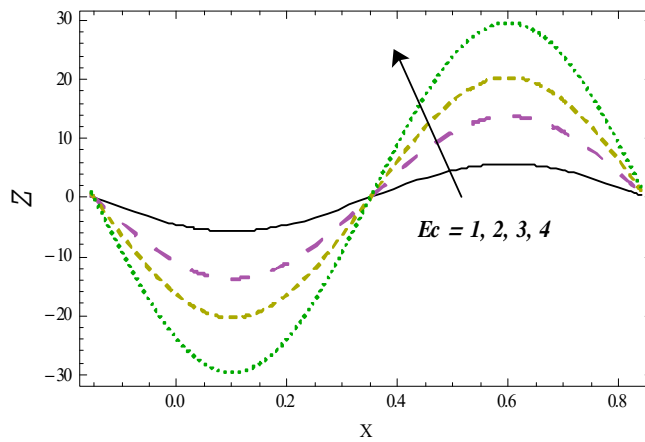


Fig. 4.18: Variation of Ec on Z

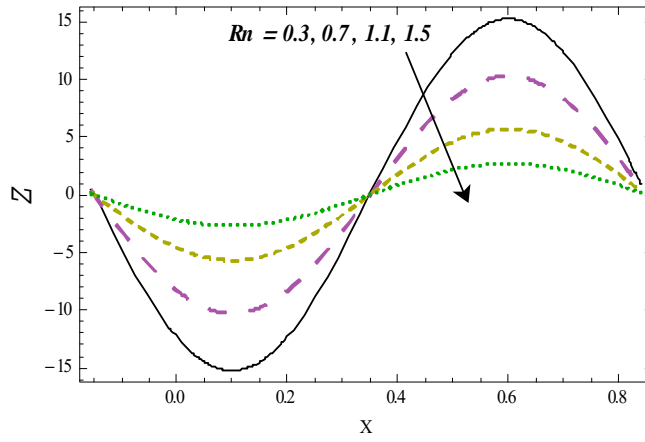


Fig. 4.19: Variation of Rn on Z

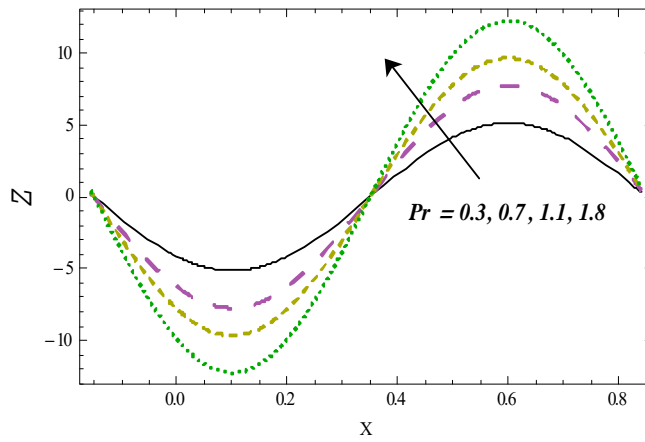


Fig. 4.20: Variation of Pr on Z

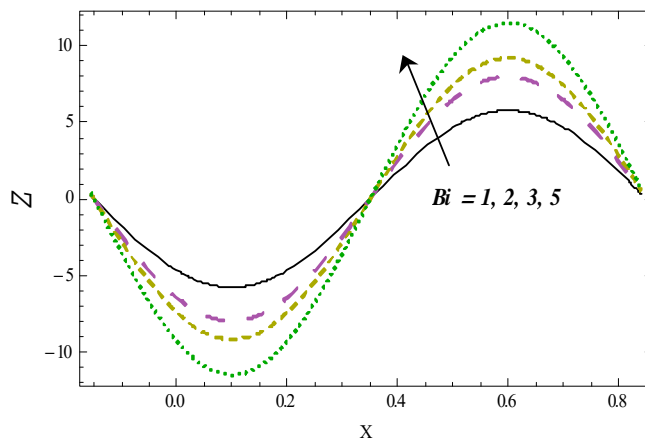


Fig. 4.21: Variation of Bi on Z

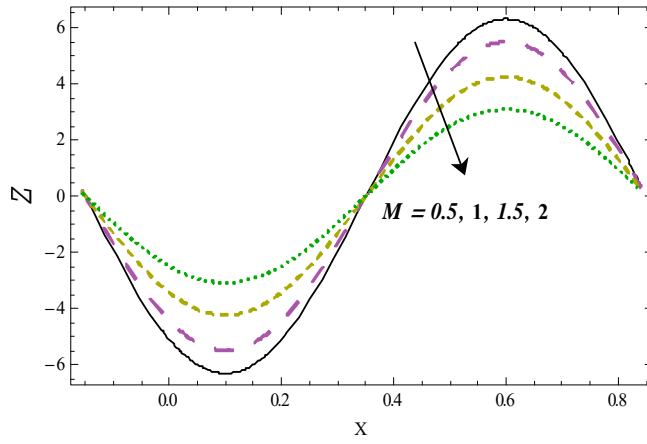


Fig. 4.22: Variation of M on Z

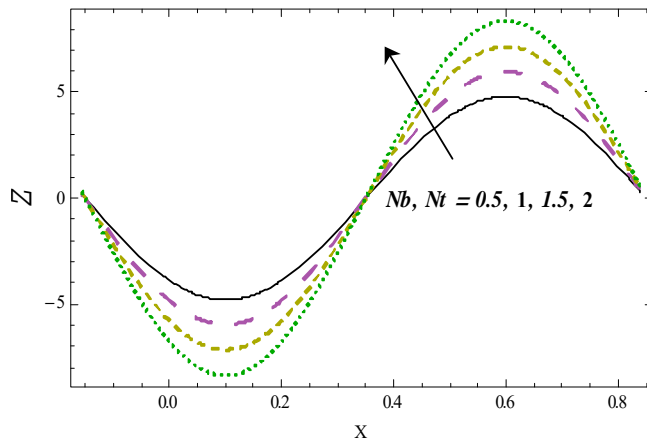


Fig. 4.23: Z against Nb and Nt

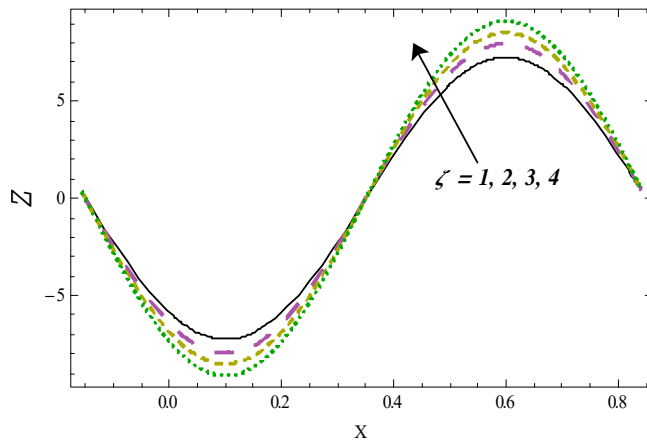


Fig. 4.24: Variation of ζ on Z

4.4 Concluding remarks

We noted the following key points.

- Outcomes of γ and ζ on temperature are reverse than Bi .
- Temperature for Prandtl Pr and Eckert Ec numbers are qualitatively similar.
- Impact of couple-stress fluid parameter γ and chemical reaction parameter ζ on concentration are opposite.
- Behavior of E_3 on concentration and temperature is opposite than E_1 and E_2 .
- Increment in Brownian movement Nb and thermophoresis Nt variables yields rise in temperature while decline observed for radiation parameter Rn .
- Outcome of ζ and Prandtl number Pr on Z are similar.
- Opposite trend is noted for heat transfer coefficient against Hartman number M and Biot number Bi .

Chapter 5

Significance of convective conditions for peristalsis of Eyring-Powell nanoliquid

5.1 Introduction

Main interest here to discuss radiative heat transfer in magnetohydrodynamic (MHD) peristaltic transport of Eyring-Powell nanofluid. Heat and mass convective conditions, Joule heating and dissipation are highlighted in modelling and discussion. Further the channel boundaries are taken of compliant nature. The nonlinear problem has been analyzed for the heat transfer coefficient, temperature, concentration and velocity. Fourth order Runge-Kutta algorithm through NDSolve of Mathematica is implemented. Major findings are concluded.

5.2 Formulation

Two-dimensional peristaltic flow of nanofluid in a compliant wall channel of width $2d_1$ is taken. Modeling is based upon relation of Eyring-Powell liquid. Peristaltic motion occurs due to sinusoidal waves with speed c and amplitude a . The x -axis is assumed parallel to channel walls and y -axis normal to it. Flow field is taken under the influence of uniform magnetic field B_0

towards y -axis. The waves shapes satisfies

$$y = \pm\eta(x, t) = \pm[d_1 + a \sin \frac{2\pi}{\lambda}(x - ct)], \quad (5.1)$$

where λ denotes wavelength and t the time. For Eyring-Powell liquid the extra stress tensor obeys:

$$S_{ij} = \mu \frac{\partial u_i}{\partial x_j} + \frac{1}{\beta^{**}} \sinh^{-1} \left(\frac{1}{c^{**}} \frac{\partial u_i}{\partial x_j} \right), \quad i, j = 1, 2 \quad (5.2)$$

where $u = u_1, v = u_2, x = x_1$ and $y = x_2$. Also

$$\sinh^{-1} \left(\frac{1}{c^{**}} \frac{\partial u_i}{\partial x_j} \right) = \frac{1}{c^{**}} \frac{\partial u_i}{\partial x_j} - \frac{1}{6} \left(\frac{1}{c^{**}} \frac{\partial u_i}{\partial x_j} \right)^3, \quad \left| \frac{1}{c^{**}} \frac{\partial u_i}{\partial x_j} \right| \ll 1, \quad (5.3)$$

in which c^{**} and β^{**} are the material constants of Eyring-Powell liquid and μ is the coefficient of shear viscosity. Related problems have statements in the forms

$$\frac{\partial u}{\partial x} + \frac{\partial v}{\partial y} = 0, \quad (5.4)$$

$$\rho_f \left(\frac{\partial u}{\partial t} + u \frac{\partial u}{\partial x} + v \frac{\partial u}{\partial y} \right) = -\frac{\partial p}{\partial x} + \frac{\partial S_{xx}}{\partial x} + \frac{\partial S_{xy}}{\partial y} - \sigma B_0^2 u, \quad (5.5)$$

$$\rho_f \left(\frac{\partial v}{\partial t} + u \frac{\partial v}{\partial x} + v \frac{\partial v}{\partial y} \right) = -\frac{\partial p}{\partial y} + \frac{\partial S_{yx}}{\partial x} + \frac{\partial S_{yy}}{\partial y}, \quad (5.6)$$

$$\begin{aligned} \rho_f c_f \left(\frac{\partial T}{\partial t} + u \frac{\partial T}{\partial x} + v \frac{\partial T}{\partial y} \right) &= k \left(\frac{\partial^2 T}{\partial x^2} + \frac{\partial^2 T}{\partial y^2} \right) + \frac{\partial u}{\partial x} S_{xx} + \frac{\partial v}{\partial y} S_{yy} + \left(\frac{\partial u}{\partial y} + \frac{\partial v}{\partial x} \right) S_{xy} + \\ \rho_p c_p \left[\frac{D_T}{T_m} \left\{ \left(\frac{\partial T}{\partial x} \right)^2 + \left(\frac{\partial T}{\partial y} \right)^2 \right\} + D_B \left(\frac{\partial C}{\partial x} \frac{\partial T}{\partial x} + \frac{\partial C}{\partial y} \frac{\partial T}{\partial y} \right) \right] &- \\ -\frac{\partial q_r}{\partial y} + \sigma B_0^2 u^2, & \end{aligned} \quad (5.7)$$

$$\frac{\partial C}{\partial t} + u \frac{\partial C}{\partial x} + v \frac{\partial C}{\partial y} = D_B \left(\frac{\partial^2 C}{\partial x^2} + \frac{\partial^2 C}{\partial y^2} \right) + \frac{D_T}{T_m} \left(\frac{\partial^2 T}{\partial x^2} + \frac{\partial^2 T}{\partial y^2} \right) \frac{D_T}{T_m}, \quad (5.8)$$

$$u = 0 \quad \text{at } y = \pm\eta, \quad (5.9)$$

$$\left[-\tau_1 \frac{\partial^3}{\partial x^3} + m_1 \frac{\partial^3}{\partial x \partial t^2} + d \frac{\partial^2}{\partial t \partial x} \right] \eta = \frac{\partial S_{xx}}{\partial x} + \frac{\partial S_{xy}}{\partial y} - \rho_f \left(\frac{\partial u}{\partial t} + u \frac{\partial u}{\partial x} + v \frac{\partial u}{\partial y} \right) - \sigma B_o^2 u \quad \text{at } y = \pm \eta. \quad (5.10)$$

$$-k \frac{\partial T}{\partial y} = h_1 \left\{ \begin{matrix} T_1 - T \\ T - T_0 \end{matrix} \right\}, \quad -D_B \frac{\partial C}{\partial y} = h_2 \left\{ \begin{matrix} C_1 - C \\ C - C_0 \end{matrix} \right\}, \quad \text{at } y = \pm \eta. \quad (5.11)$$

Here (u, v) denote the velocity components, (ρ_f) stands for density of nanofluid, (p) for pressure, (k) for thermal conductivity, (ν) for kinematic viscosity, (σ) for electric conductions of fluid and last two terms on R.H.S. of Eq. (5.7) represent radiation and Joule heating. Further (D_B) depicts Brownian movement (D_T) for thermophoresis diffusion coefficient, (m_1) for mass per unit area, (τ_1) for elastic tension, (T_m) for mean temperature, (d) for viscous damping coefficient, T_1, T_0 and C_1, C_0 respectively the upper and lower walls temperature and concentration. Further $S_{xx}, S_{yy}, S_{xy}, S_{yx}$ are the extra stress tensor.

In view of Rossland approximation, the radiative heat flow satisfies

$$q_r = -\frac{4\bar{\sigma}}{3\bar{k}} \frac{\partial T^4}{\partial y}, \quad (5.12)$$

in which \bar{k} and $\bar{\sigma}$ denote absorption and Stefan-Boltzmann constant coefficients respectively. After utilizing Taylor series for T^4 about T_0 and neglected the higher order expressions one has for

$$T^4 \approx 4T_0^3 T - 3T_0^4. \quad (5.13)$$

Energy equations now yields

$$\begin{aligned} \rho_f c_f \left(\frac{\partial T}{\partial t} + u \frac{\partial T}{\partial x} + v \frac{\partial T}{\partial y} \right) &= k \left(\frac{\partial^2 T}{\partial x^2} + \frac{\partial^2 T}{\partial y^2} \right) + \frac{\partial u}{\partial x} S_{xx} + \frac{\partial v}{\partial y} S_{yy} + \left(\frac{\partial u}{\partial y} + \frac{\partial v}{\partial x} \right) S_{xy} \\ &+ \rho_p c_p \left[\frac{D_T}{T_m} \left\{ \left(\frac{\partial T}{\partial x} \right)^2 + \left(\frac{\partial T}{\partial y} \right)^2 \right\} + D_B \left(\frac{\partial C}{\partial x} \frac{\partial T}{\partial x} + \frac{\partial C}{\partial y} \frac{\partial T}{\partial y} \right) \right] \\ &+ \frac{16\bar{\sigma}T_0^3}{3\bar{k}} \frac{\partial^2 T}{\partial y^2} + \sigma B_o^2 u^2. \end{aligned} \quad (5.14)$$

Writing stream functions $u = \frac{\partial\psi}{\partial y}$, $v = -\delta\frac{\partial\psi}{\partial x}$ and using

$$\begin{aligned} u &= cu^*, v = cv^*, x = \lambda x^*, y = d_1 y^*, ct = \lambda t^*, \eta = d_1 \eta^* \\ d_1^2 p &= c\lambda\mu p^*, (T_1 - T_0)\theta = T - T_0, (C_1 - C_0)\phi = C - C_0, \end{aligned} \quad (5.15)$$

one can write the following problems

$$(1 + B)\frac{\partial^4\psi}{\partial y^4} - \frac{A}{3}\frac{\partial^2}{\partial y^2}\left(\frac{\partial^2\psi}{\partial y^2}\right)^3 - M^2\frac{\partial^2\psi}{\partial y^2} = 0, \quad (5.16)$$

$$\begin{aligned} (1 + Rn\text{Pr})\frac{\partial^2\theta}{\partial y^2} + \text{Pr}Nb\left(\frac{\partial\phi}{\partial y}\right)\left(\frac{\partial\theta}{\partial y}\right) + \text{Pr}Nt\left(\frac{\partial\theta}{\partial y}\right)^2 \\ + \text{Pr}Ec\left[(1 + B)\left(\frac{\partial^2\psi}{\partial y^2}\right)^2 - A\left(\frac{\partial^2\psi}{\partial y^2}\right)^4 + M^2\left(\frac{\partial\psi}{\partial y}\right)^2\right] = 0, \end{aligned} \quad (5.17)$$

$$\frac{\partial^2\phi}{\partial y^2} + \frac{Nt}{Nb}\left(\frac{\partial^2\theta}{\partial y^2}\right) = 0, \quad (5.18)$$

with the boundary conditions

$$\frac{\partial\psi}{\partial y} = 0 \text{ at } y = \pm\eta, \quad (5.19)$$

$$\begin{aligned} \left[E_1\frac{\partial^3}{\partial x^3} + E_2\frac{\partial^3}{\partial x\partial t^2} + E_3\frac{\partial^2}{\partial x\partial t}\right]\eta = (1 + B)\frac{\partial^3\psi}{\partial y^3} - \frac{A}{3}\frac{\partial}{\partial y}\left(\frac{\partial^2\psi}{\partial y^2}\right)^3 \\ - M^2\frac{\partial\psi}{\partial y} \text{ at } y = \pm\eta, \end{aligned} \quad (5.20)$$

$$\frac{\partial\theta}{\partial y} = \begin{Bmatrix} -Bi_1(1 - \theta) \\ -Bi_1\theta \end{Bmatrix}, \quad \frac{\partial\phi}{\partial y} = \begin{Bmatrix} -Bi_2(1 - \phi) \\ -Bi_2\phi \end{Bmatrix}, \text{ at } y = \pm\eta. \quad (5.21)$$

Expression (5.3) is satisfied trivially. Note that in writing above problems, the assumptions of large wavelength and low numbers of Reynolds are invoked. Here $\epsilon, \delta, \alpha, \text{Re}, \text{Pr}, Ec, M, \tau, Sc, Nb, Nt, (B, A), Rn, Bi_1, Bi_2, (E_1, E_2)$ and E_3 amplitude ratio, wave number, thermal diffusivity, Reynolds number, Prandtl number, Eckert number, Hartman number, effective heat capacity ratio of nanoparticle material to liquid heat capacity, Schmidt number, thermophoresis parameter, Brownian diffusion parameter, Eyring fluid parameters, radiation parameter, thermal Biot number, mass Biot number, elasticity parameters and damping parameter, These are

defined by

$$\begin{aligned}
\epsilon &= \frac{a}{d_1}, \quad \delta = \frac{d_1}{\lambda}, \quad \alpha = \frac{k}{\rho_f c_f}, \quad \text{Re} = \frac{\rho_f c d_1}{\mu}, \quad \text{Pr} = \frac{\mu c_f}{K}, \quad \text{Ec} = \frac{c^2}{c_f (T_1 - T_0)}, \quad \text{Sc} = \frac{\nu}{D_B}, \\
M &= \sqrt{\frac{\sigma}{\mu}} B_0 d_1, \quad \tau = \frac{\rho_f c_p}{\rho_f c_f}, \quad \text{Nb} = \frac{D_B \tau (C_1 - C_0)}{\nu}, \quad \text{Nt} = \frac{D_T \tau (T_1 - T_0)}{T_m \nu}, \quad B = \frac{1}{\mu \beta^{**} c^{**}}, \quad A = \frac{B c^2}{6 d_1^2 c^{**2}}, \\
\text{Bi}_1 &= \frac{h_1 d_1}{k}, \quad \text{Bi}_2 = \frac{h_2 d_1}{D_B}, \quad \text{Rn} = \frac{16 \bar{\sigma} T_0^3}{3 k k}, \quad E_1 = -\frac{d_1^3 \tau}{\lambda^3 \mu c}, \quad E_2 = \frac{c m_1 d_1^3}{\lambda^3 \mu}, \quad E_3 = \frac{d_1^3 d}{\lambda^2 \mu}.
\end{aligned} \tag{5.22}$$

5.3 Results and discussion

Resulting problems consisting of Eqs. (5.16) – (5.21) are solved numerically by built-in function via shooting technique through the command NDSolve with Runge-kutta fourth order method in Mathematica.

5.3.1 Velocity

Here variation of velocity is presented through Figs. 5.1 – 5.5. Outcome for Eyring-Powell fluid parameter A on axial velocity is examined in Fig. 5.1. Here velocity rises for Eyring-Powell fluid parameter A . Fig. 5.2 demonstrates that the velocity decreases against Eyring-Powell liquid parameter B . It can be considered as characteristic of the Eyring-Powell fluid. Fig. 5.3 depicts the effects of E_1 , E_2 and E_3 on velocity. Velocity enhances for E_1 and E_2 whereas opposite happens via E_3 . Because walls are flexible, and possess elastic behavior causes less flow resistance. Fig. 5.4 illustrates variation of Hartman number M on velocity. Clearly higher Hartman number M yield decay of velocity. Actually the rate of transport declines by rising magnetic parameter since the Lorentz force resisted fluid motion. Fig. 5.5 develops velocity for different values of amplitude ratio ϵ . Investigation of this Fig. shows that by growing ϵ the velocity rises.

5.3.2 Temperature

Figs. 5.6 – 5.14 show the behaviour of temperature. Influence of Pr is shown in Fig. 5.6. This Fig. witnesses that temperature rises for higher Pr . It is due to the existence of strong momentum diffusivity. Effect of Eckert number Ec on temperature is displayed in Fig. 5.7.

Here temperature rises against Ec . This is due to increased internal fluid particle resistance which enhances fluid temperature. We next move to investigate the influences of Nb and Nt on temperature through Fig. 5.8. Random movement of nanoparticles increases for higher Brownian motion parameter and thus fluid temperature enhances. As a result of the collision of nanoparticles, the Brownian motion is produced (causing the particles to move at random). Particle collision whether collective or with liquid molecules is improved by inward contraction of elastic walls. Temperature against Eyring fluid parameter A is shown in Fig. 5.9. Clearly temperature strengthens when Eyring liquid parameter A rises. Figure 5.10 depicts Eyring fluid parameter B effects on temperature. Temperature by B is increased. Figure 5.11 displays temperature for different values of Hartman number M . Temperature decays for higher M . Figure 5.12 illustrates the effect of wall parameters (E_1, E_2, E_3) on temperature. Influences of E_1 and E_2 on temperature is quite opposite to that of E_3 . Figure 5.13 indicates temperature against radiation parameter Rn . Temperature decays when Rn increased. It is because the fluid temperature is higher than the walls, and due to the heat dissipation, the temperature is decreased. Higher Biot number Bi_1 give decay of temperature (see Fig. 5.14). This occurs due to non-uniform temperature of the fluid.

5.3.3 Concentration

Figs. 5.15 – 5.19 describe concentration for sundry variables. Concentration for Eyring-Powell fluid parameter B is shown in Figs. 5.15. It is observed that concentration decays for higher B . Radiation parameter Rn impact on concentration of nanoparticles is shown in Fig. 5.16. As observed from the figure, the concentration distribution of the nanofluid is seen higher with an increase in the radiation parameter Rn . Here concentration through higher Rn is enhanced. Fig. 5.17. witnessed that by increasing values of rigidity E_1 and stiffness E_2 variables the nanoparticle concentration enhances while it decreases against damping force parameter E_3 . Mass Biot parameter Bi_2 influence on nanoparticle concentration is presented in Fig. 5.18. An enhancement in concentration for Bi_2 is found. Concentration for Nt is shown in Fig. 5.19. Higher Nt leads to the concentration increases. Physically, a progressive rise in thermophoresical effect intensity would contribute to the larger mass flux due to the temperature gradient that increases the concentration of nanoparticles.

5.3.4 Heat transfer coefficient

Influence of coefficient of heat transfer $Z(x) = \eta_x \theta_y(\eta)$ is shown graphically in Figs. 5.20 – 5.24. Fig. 4.20 plots heat transfer coefficient Z versus Prandtl number Pr . Heat transfer coefficient Z for higher Pr is increased. It is because of the strong diffusiveness of momentum. Fig. 5.21 captures the effects of heat transfer coefficient Z for Brownian movement variable and the thermophoresis variable respectively. We witnessed that Z is an increasing function of both parameters Nb and Nt . Infact there is lead in effective motion of nanoparticles from the channel to the liquid as the influence of Brownian motion increases. As a result, there is a enormous increase in the rate of heat transfer. On the other hand the heat transfer coefficient Z decreases by radiation parameter Rn (see Fig. 5.22). Figure 5.23 is drawn for impact of thermal Biot variable Bi_1 on Z . An increasing behavior of Z is noticed for higher Bi_1 . Figure 5.24 shows heat transfer coefficient Z for distinct values of Hartman number M . It is apparent from this Fig. that heat transfer rate of fluid decays in view of Lorentz force resisting the heat transfer rate.

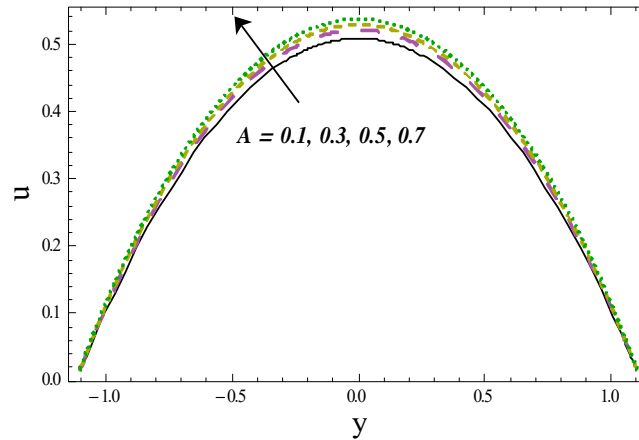


Fig. 5.1: Variation of A on u

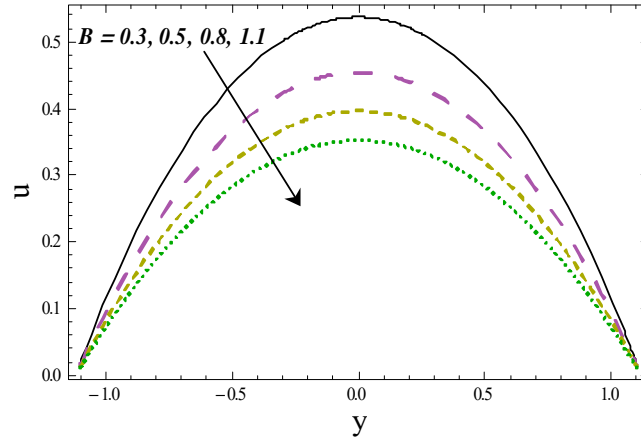


Fig. 5.2: Variation of B on u

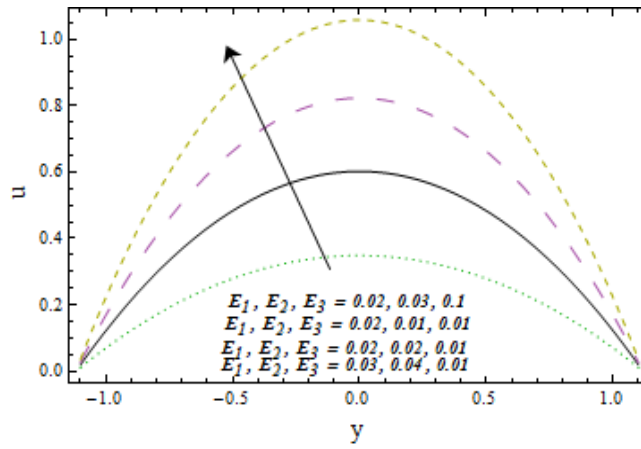


Fig. 5.3: E_1, E_2 and E_3 variations on u

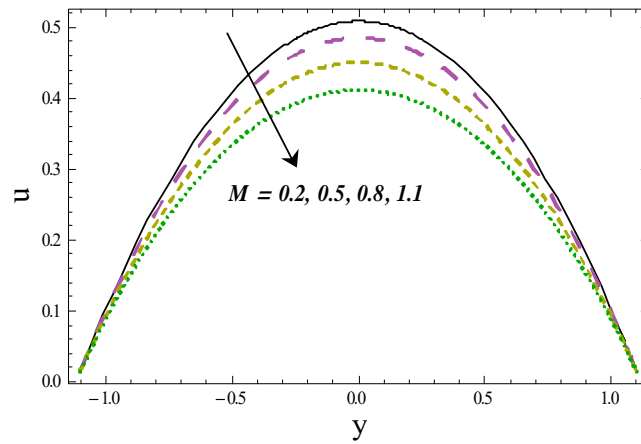


Fig. 5.4: Variation of M on u

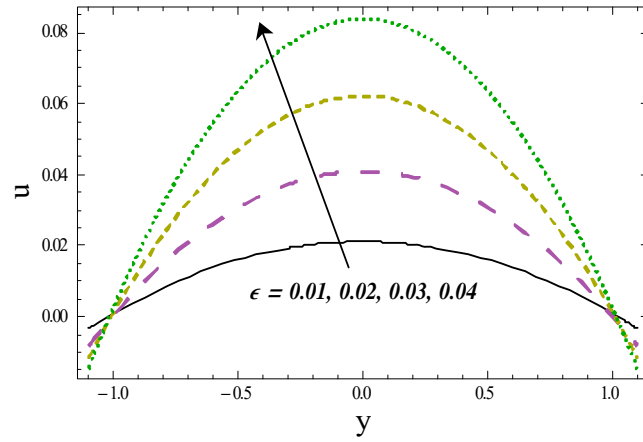


Fig. 5.5: Variation of ϵ on u

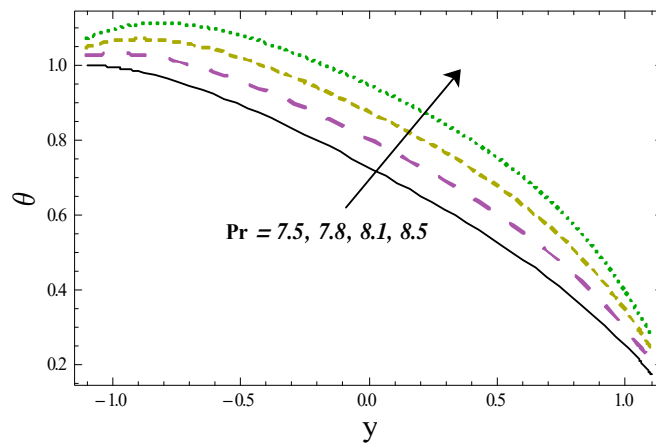


Fig. 5.6: Variation of Pr on θ

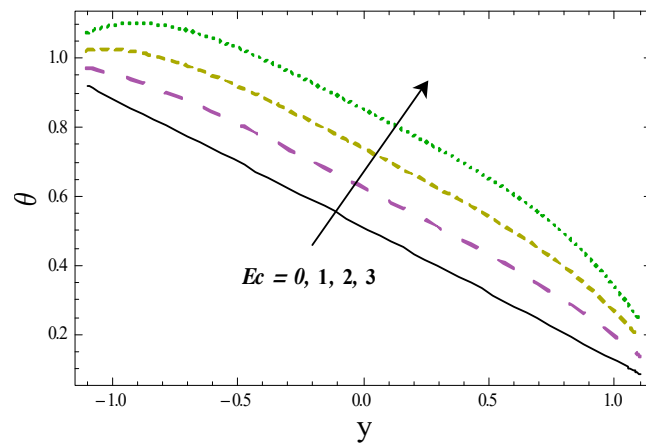


Fig. 5.7: Variation of Ec on θ

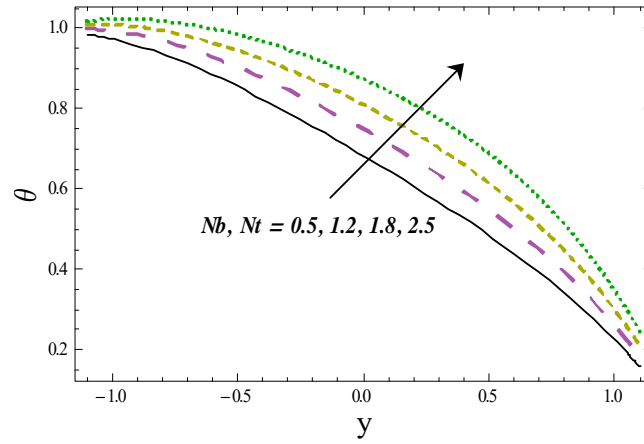


Fig. 5.8: Variation of Nb and Nt on θ

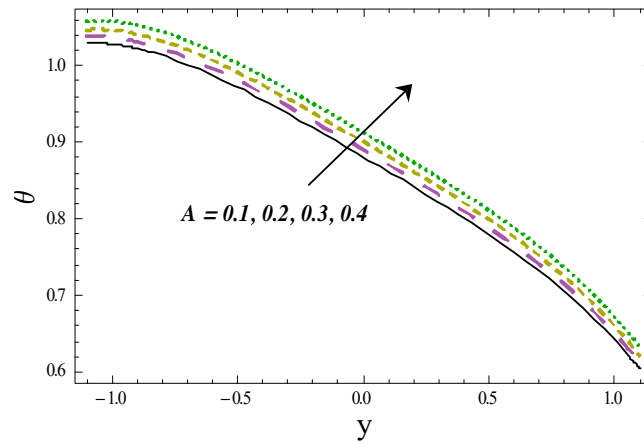


Fig. 5.9: Variation of A on θ

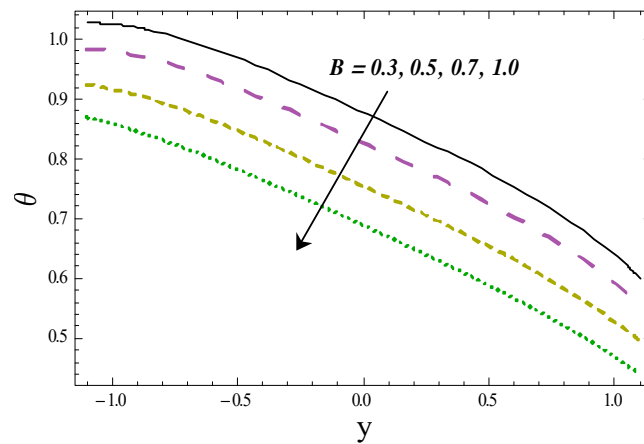


Fig. 5.10: Variation of B on θ

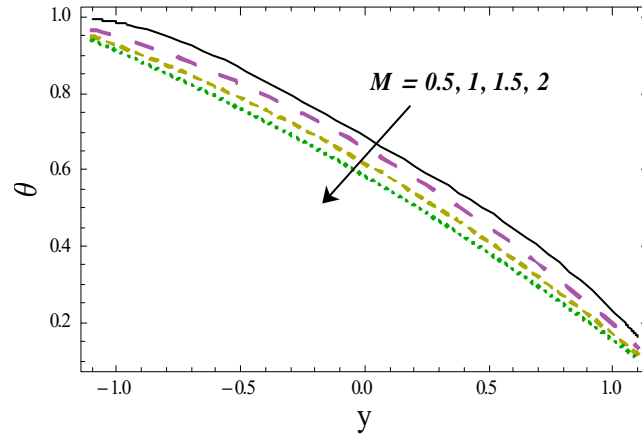


Fig. 5.11: M Variation on θ

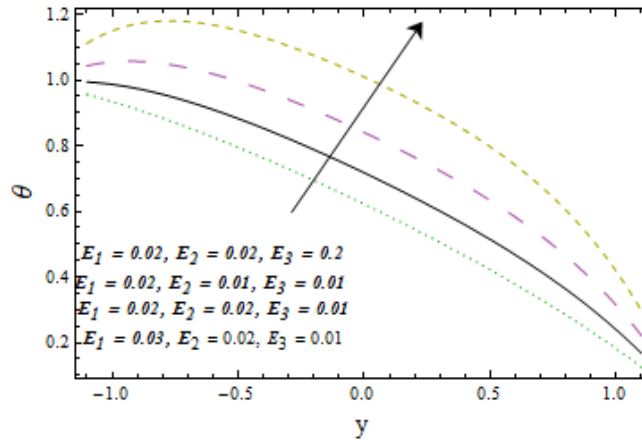


Fig. 5.12: Variation of E_1, E_2 and E_3 on θ

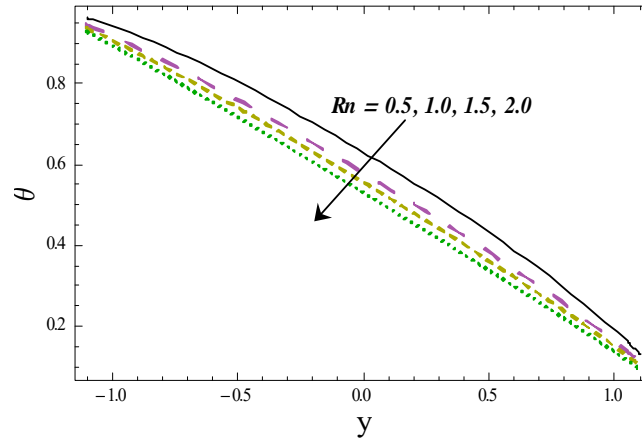


Fig. 5.13: Variation of Rn on θ

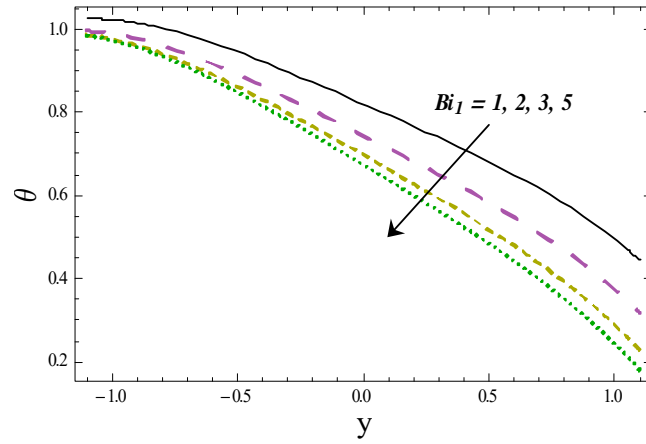


Fig. 5.14: Variation of Bi_1 on θ

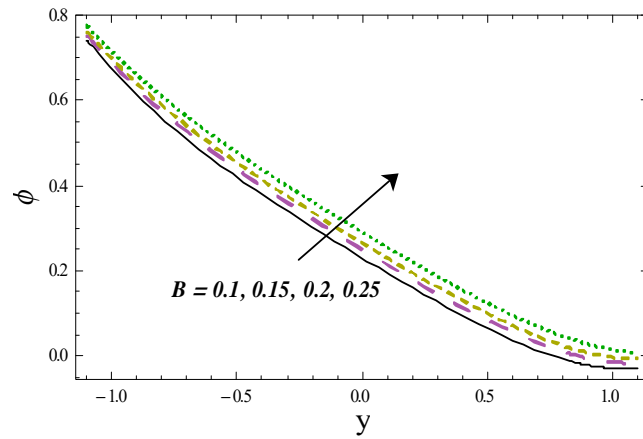


Fig. 5.15: Variation of B on ϕ

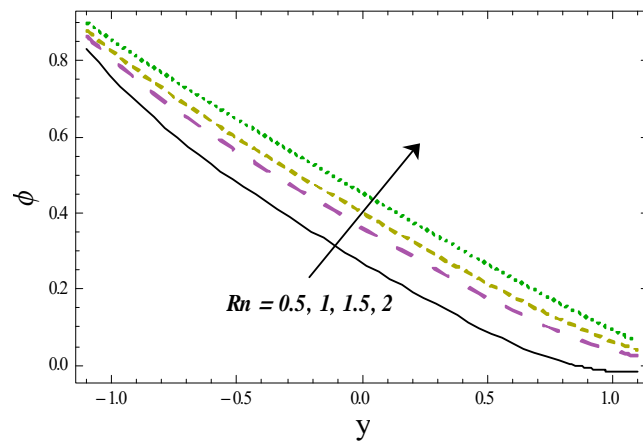


Fig. 5.16: Rn variation on ϕ

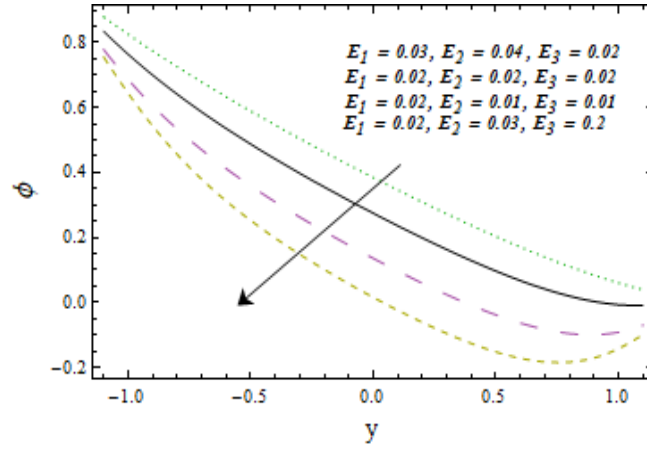


Fig. 5.17: E_1, E_2 and E_3 variations on ϕ

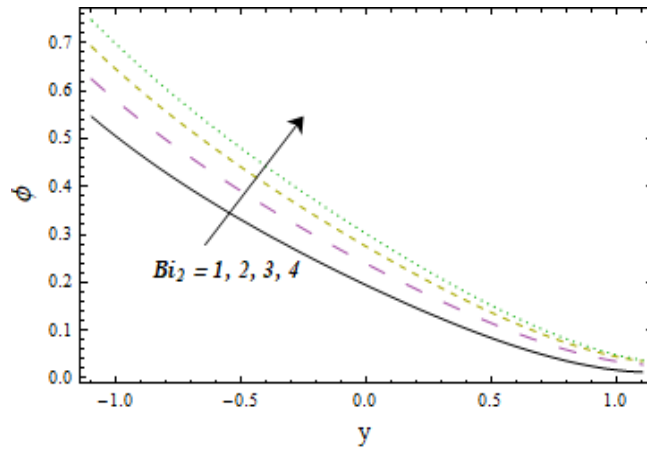


Fig. 5.18: Variation of Bi_2 on ϕ

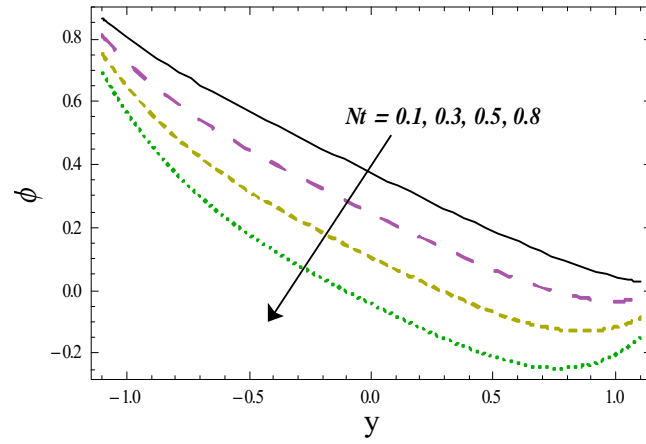


Fig. 5.19: Variation of Nt on ϕ

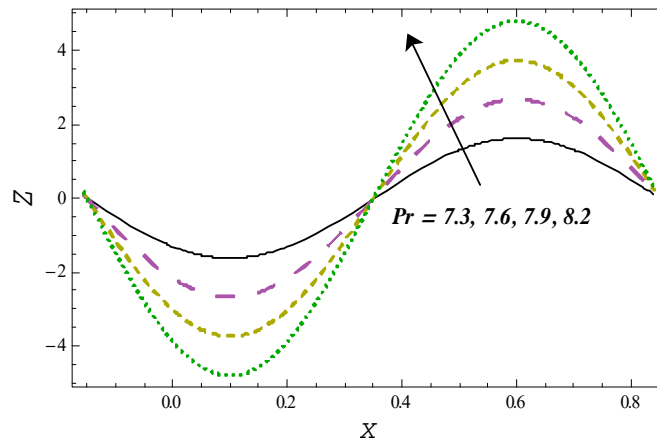


Fig. 5.20: Variation of Pr on Z

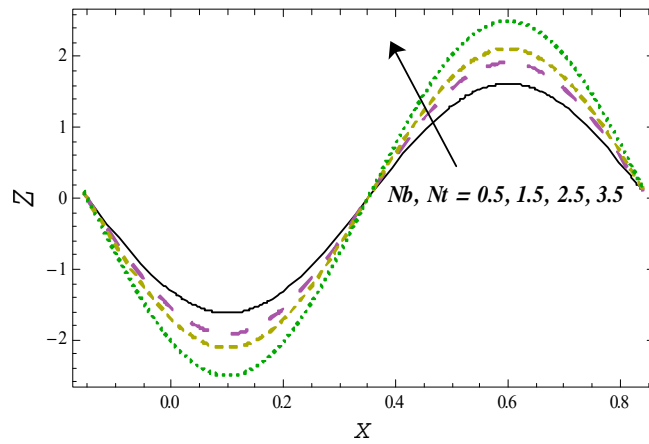


Fig. 5.21: Variations of Nb and Nt on Z

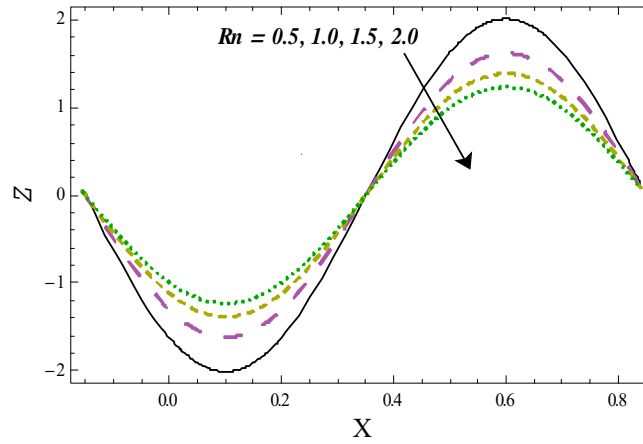


Fig. 5.22: Variation of Rn on Z

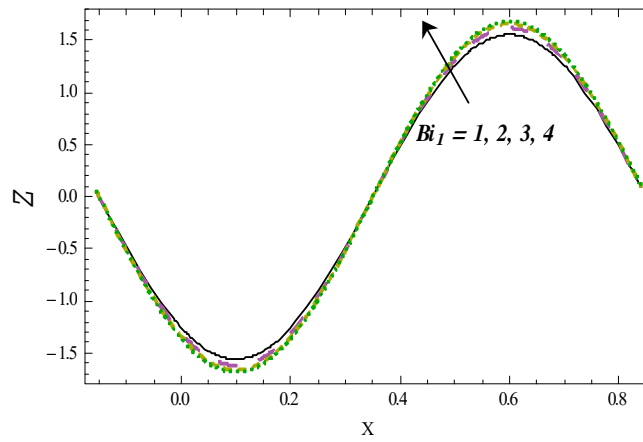


Fig. 5.23: Variation of Bi_1 on Z

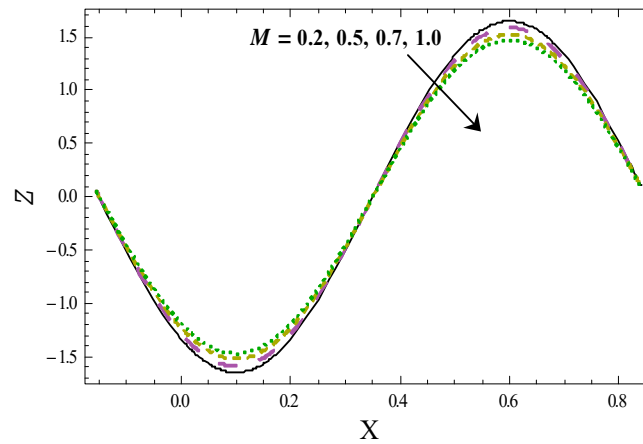


Fig. 5.24: Variation of M on Z

5.4 Validation of the result

To check the validation of our numerical result we construct Table. 5.1. It is obvious from this table the current results show good agreement with [51]when $(Bi_1, Bi_2) \rightarrow \infty$.

η	ϵ	Present Work	Present Work	Mustafa et al. [51]	Mustafa et al. [51]
		$A = B = M = Rn = 0$	$A = B = M = Rn = 0$		
		θ_y at $y = \eta$	ϕ_y at $y = \eta$	θ_y at $y = \eta$	ϕ_y at $y = \eta$
1.12	0.2	-0.211788	1.104649	-0.211789	1.104646
1.29	0.5	-5.523596	6.298794	-5.523598	6.298792

Table 5.1. Comparison of numerical results with ref. [51]

5.5 Conclusions

Following results are worth mentioning.

- Velocity rises for larger A and ϵ and it decreases by higher M .
- Behaviors of Pr and Ec on temperature are same.
- Temperature for Nb and Nt is enhanced.
- Increasing Rn shows temperature decay and enhancement of concentration.
- Behavior of E_3 on concentration and temperature is reverse than E_1 and E_2 .
- Rate of heat transfer intensifies for Nt , Nb and Bi_1 .
- Coefficient of heat transfer shows similar effects for M and Rn .

Chapter 6

Peristalsis of Eyring-Powell nanofluid with activation energy and heat generation/absorption

6.1 Introduction

This chapter addresses the effects of heat generation / absorption and activation energy on MHD peristalsis of Eyring-Powell nanofluid in a flexible channel. Velocity slip is taken. Energy equation is modeled by taking the effects of viscous dissipation, Joule heating and thermal radiation. Further the convective equations are imposed for temperature. Channel walls have different concentration. Problem with assumption of low Reynold number and long wavelength is presented. Governing problems have been solved by NDSolve technique. The velocity, concentration, temperature and heat transfer coefficient are explored.

6.2 Formulation

Peristaltic flow of Eyring-Powell fluid in a two-dimensional symmetric flexible channel is focused. Brownian motion and thermophoresis are accounted. Here channel width is $2d_1$. The flow considered for transversely applied constant magnetic field of strength B_0 . Induced magnetic

field is neglected. The waves form propagating along the channel walls are:

$$y = \pm\eta(x, t) = \pm[d_1 + a \sin \frac{2\pi}{\lambda}(x - ct)], \quad (6.1)$$

where a, λ, c and t are amplitude, wavelength, wave speed and time respectively. Extra stress tensor for Eyring-Powell model is defined by.

$$S_{ij} = \mu \frac{\partial u_i}{\partial x_j} + \frac{1}{\beta^{**}} \sinh^{-1} \left(\frac{1}{c^{**}} \frac{\partial u_i}{\partial x_j} \right), \quad i, j = 1, 2 \quad (6.2)$$

where $u = u_1, v = u_2, x = x_1$ and $y = x_2$.

$$\sinh^{-1} \left(\frac{1}{c^{**}} \frac{\partial u_i}{\partial x_j} \right) = \frac{1}{c^{**}} \frac{\partial u_i}{\partial x_j} - \frac{1}{6} \left(\frac{1}{c^{**}} \frac{\partial u_i}{\partial x_j} \right)^3, \quad \left| \frac{1}{c^{**}} \frac{\partial u_i}{\partial x_j} \right| \ll 1, \quad (6.3)$$

Here c^{**} and β^{**} are the material constants of Eyring-Powell liquid, μ the coefficient of viscosity. The appropriate equations for the current problem are listed below:

$$\frac{\partial u}{\partial x} + \frac{\partial v}{\partial y} = 0, \quad (6.4)$$

$$\rho_f \left(\frac{\partial u}{\partial t} + u \frac{\partial u}{\partial x} + v \frac{\partial u}{\partial y} \right) = -\frac{\partial p}{\partial x} + \frac{\partial S_{xx}}{\partial x} + \frac{\partial S_{xy}}{\partial y} - \sigma B_0^2 u, \quad (6.5)$$

$$\rho_f \left(\frac{\partial v}{\partial t} + u \frac{\partial v}{\partial x} + v \frac{\partial v}{\partial y} \right) = -\frac{\partial p}{\partial y} + \frac{\partial S_{yx}}{\partial x} + \frac{\partial S_{yy}}{\partial y}, \quad (6.6)$$

$$\begin{aligned} \rho_f c_f \left(\frac{\partial T}{\partial t} + u \frac{\partial T}{\partial x} + v \frac{\partial T}{\partial y} \right) &= k \left(\frac{\partial^2 T}{\partial x^2} + \frac{\partial^2 T}{\partial y^2} \right) + S_{xx} \frac{\partial u}{\partial x} + S_{yy} \frac{\partial v}{\partial y} + S_{xy} \left(\frac{\partial v}{\partial x} + \frac{\partial u}{\partial y} \right) \\ + \rho_p c_p \left[\left\{ \left(\frac{\partial T}{\partial x} \right)^2 + \left(\frac{\partial T}{\partial y} \right)^2 \right\} \frac{D_T}{T_m} + D_B \left(\frac{\partial C}{\partial y} \frac{\partial T}{\partial y} + \frac{\partial C}{\partial x} \frac{\partial T}{\partial x} \right) \right] &- \\ \frac{\partial q_r}{\partial y} + \sigma B_0^2 u^2 + Q_0 (T - T_0), & \end{aligned} \quad (6.7)$$

$$\begin{aligned} \frac{\partial C}{\partial t} + u \frac{\partial C}{\partial x} + v \frac{\partial C}{\partial y} &= D_B \left(\frac{\partial^2 C}{\partial x^2} + \frac{\partial^2 C}{\partial y^2} \right) + \frac{D_T}{T_m} \left(\frac{\partial^2 T}{\partial x^2} + \frac{\partial^2 T}{\partial y^2} \right) - \\ (C - C_0) \left(\frac{T}{T_0} \right)^n \exp \left(-\frac{E_a}{\kappa T} \right) k_r^2. & \end{aligned} \quad (6.8)$$

The boundary conditions are

$$u \pm \beta S_{xy} = 0 \quad \text{at } y = \pm\eta, \quad (6.9)$$

$$\begin{aligned} \left[-\tau_1 \frac{\partial^3}{\partial x^3} + m_1 \frac{\partial^3}{\partial x \partial t^2} + d \frac{\partial^2}{\partial t \partial x} \right] \eta &= \frac{\partial S_{xx}}{\partial x} + \frac{\partial S_{xy}}{\partial y} - \\ \rho_f \left(\frac{\partial u}{\partial t} + u \frac{\partial u}{\partial x} + v \frac{\partial u}{\partial y} \right) - \sigma B_o^2 u &\text{ at } y = \pm\eta. \end{aligned} \quad (6.10)$$

$$-k \frac{\partial T}{\partial y} = h \left\{ \begin{matrix} T_1 - T \\ T - T_0 \end{matrix} \right\}, \quad C = \left\{ \begin{matrix} C_1 \\ C_0 \end{matrix} \right\}, \quad \text{at } y = \pm\eta, \quad (6.11)$$

where (u, v) i the velocities in (x, y) directions, p pressure, k the thermal conductivity, ν the kinematic viscosity, σ the electric conductions, D_B the Brownian movement, D_T the thermophoretic diffusion coefficient, ρ_f the density of the nanofluid, Q_0 the heat generation/absorption parameter, m_1 the mass per unit area, τ_1 the elastic tension, T_m the mean temperature, d coefficient of viscous damping, β the velocity slip parameter, k_r the chemical reaction rate, E_a the activation energy, κ the Boltzmann constant, n the fitted rate constant, (T_1, T_0) and (C_1, C_0) respectively the upper and lower walls temperature and concentration and extra stress tensor components $S_{xx}, S_{yy}, S_{yx}, S_{xy}$ for the Eyring-Powell can be defined through expression (6.2). Last term in equation (6.8) appeared due to chemical reaction and activation energy.

By following approximation of Rosseland, the radiative heat flux q_r is described as

$$q_r = -\frac{4\bar{\sigma}}{3\bar{k}} \frac{\partial T^4}{\partial y}, \quad (6.12)$$

in which $\bar{\sigma}$ represents the constant Stefan – Boltzmann, and \bar{k} the coefficient of absorption.

We expect that the changes in temperature inside the flow are lower enough to characterize T^4 as a function of temperature in linear form. Considering Taylor series for T^4 about T_0 and ignoring the expressions of higher order one has

$$T^4 = 4T_0^3 T - 3T_0^4, \quad (6.13)$$

and thus

$$\begin{aligned}
\rho_f c_f \left(\frac{\partial T}{\partial t} + u \frac{\partial T}{\partial x} + v \frac{\partial T}{\partial y} \right) &= k \left(\frac{\partial^2 T}{\partial x^2} + \frac{\partial^2 T}{\partial y^2} \right) + S_{xx} \frac{\partial u}{\partial x} + S_{xy} \left(\frac{\partial u}{\partial y} + \frac{\partial v}{\partial x} \right) + S_{yy} \frac{\partial v}{\partial y} + \\
&\rho_p c_p \left[\left\{ \left(\frac{\partial T}{\partial x} \right)^2 + \left(\frac{\partial T}{\partial y} \right)^2 \right\} \frac{D_T}{T_m} + D_B \left(\frac{\partial C}{\partial x} \frac{\partial T}{\partial x} + \frac{\partial C}{\partial y} \frac{\partial T}{\partial y} \right) \right] + \\
&\frac{16\bar{\sigma}T_0^3}{3k} \frac{\partial^2 T}{\partial y^2} + \sigma B_o^2 u^2 + Q_0 (T - T_0). \tag{6.14}
\end{aligned}$$

Now introducing stream functions $u = \psi_y$, $v = -\delta\psi_x$ and invoking non-dimensional variables

$$\begin{aligned}
u^* &= \frac{u}{c}, \quad v^* = \frac{v}{c}, \quad x^* = \frac{x}{\lambda}, \quad y^* = \frac{y}{d_1}, \quad t^* = \frac{ct}{\lambda}, \quad \eta^* = \frac{\eta}{d_1}, \quad \beta^* = \frac{\beta}{d_1} \\
p^* &= \frac{d_1^2 p}{c\lambda\mu}, \quad \theta = \frac{T - T_0}{T_1 - T_0}, \quad \phi = \frac{C - C_0}{(C_1 - C_0)}, \quad S_{ij}^* = \frac{d_1}{\mu c} S_{ij}, \tag{6.15}
\end{aligned}$$

we obtain after dropping asterisks

$$(1 + B) \frac{\partial^4 \psi}{\partial y^4} - \frac{A}{3} \frac{\partial^2}{\partial y^2} \left(\frac{\partial^2 \psi}{\partial y^2} \right)^3 - M^2 \frac{\partial^2 \psi}{\partial y^2} = 0, \tag{6.16}$$

$$\begin{aligned}
&\left(\frac{1}{Pr} + Rn \right) \frac{\partial^2 \theta}{\partial y^2} + Nb \left(\frac{\partial \theta}{\partial y} \right) \left(\frac{\partial \phi}{\partial y} \right) + Nt \left(\frac{\partial \theta}{\partial y} \right)^2 + \\
&Ec \left[(1 + B) \left(\frac{\partial^2 \psi}{\partial y^2} \right)^2 - \frac{A}{3} \left(\frac{\partial^2 \psi}{\partial y^2} \right)^4 + M^2 \left(\frac{\partial \psi}{\partial y} \right)^2 \right] + Q\theta = 0 \tag{6.17}
\end{aligned}$$

$$\frac{\partial^2 \phi}{\partial y^2} + \frac{Nt}{Nb} \left(\frac{\partial^2 \theta}{\partial y^2} \right) - Sc\zeta (1 + (\Omega - 1)\theta)^n \exp \left(-\frac{E}{1 + (\Omega - 1)\theta} \right) \phi = 0. \tag{6.18}$$

The boundary conditions become

$$\frac{\partial \psi}{\partial y} \pm \beta \left[\{1 + B\} \frac{\partial^2 \psi}{\partial y^2} - \frac{A}{3} \left(\frac{\partial^2 \psi}{\partial y^2} \right)^3 \right] = 0 \text{ at } y = \pm\eta, \tag{6.19}$$

$$\begin{aligned}
&\left[E_1 \frac{\partial^3}{\partial x^3} + E_2 \frac{\partial^3}{\partial x \partial t^2} + E_3 \frac{\partial^2}{\partial x \partial t} \right] \eta = (1 + B) \frac{\partial^3 \psi}{\partial y^3} - \frac{A}{3} \frac{\partial}{\partial y} \left(\frac{\partial^2 \psi}{\partial y^2} \right)^3 \\
&M^2 \frac{\partial \psi}{\partial y} \text{ at } y = \pm\eta, \tag{6.20}
\end{aligned}$$

$$\frac{\partial \theta}{\partial y} = \left\{ \begin{array}{l} -Bi(1 - \theta) \\ -Bi\theta \end{array} \right\}, \quad \phi = \left\{ \begin{array}{l} 1 \\ 0 \end{array} \right\}, \text{ at } y = \pm\eta, \tag{6.21}$$

in which small Reynolds number and large wavelength approximation are utilized. Continuity equation (6.3) is identically satisfied. Further $\epsilon \left(= \frac{a}{d_1} \right)$ is amplitude ratio, $\delta \left(= \frac{d_1}{\lambda} \right)$ wave number, $\alpha \left(= \frac{k}{\rho_f c_f} \right)$ thermal diffusivity, $Pr \left(= \frac{\mu c_f}{k} \right)$ the Prandtl number, $Re \left(= \frac{\rho_f c d_1}{\mu} \right)$ Reynolds number, $Ec \left(= \frac{c^2}{c_f(T_1 - T_0)} \right)$ the Eckert number, $Sc \left(= \frac{\nu}{D_B} \right)$ the Schmidt number, $M \left(= \sqrt{\frac{\sigma}{\mu}} B_0 d_1 \right)$ the Hartman number, $\tau \left(= \frac{\rho_f c_p}{\rho_f c_f} \right)$ the effective heat capacity ratio of nanoparticle material to liquid heat capacity, $Nb \left(= \frac{D_B \tau (C_1 - C_0)}{\nu} \right)$ the Brownian diffusion parameter, $Nt \left(= \frac{D_T \tau (T_1 - T_0)}{T_m \nu} \right)$ the thermophoresis parameter, $\left(A = \frac{Bc^2}{6d_1^2 c^{**2}}, B = \frac{1}{\mu \beta^{**} c^{**}} \right)$ the Eyring liquid parameters, $Rn \left(= \frac{16\bar{\sigma} T_0^3}{3kk} \right)$ the radiation parameter, $Bi \left(= \frac{hd_1}{k} \right)$ the thermal Biot number, $Q \left(= \frac{Q_0 d_1^2}{\rho_f c_f} \right)$ the heat generation/absorption parameter, $\zeta \left(= \frac{k_r d_1^2}{\nu} \right)$ the chemical reaction parameter, $\Omega \left(= \frac{T_1}{T_0} \right)$ the temperature ratio parameter, $E \left(= -\frac{E_a}{\kappa T_0} \right)$ the activation energy parameter and

$$\left(E_1 = -\frac{d_1^3 \tau}{\lambda^3 \mu c}, E_2 = \frac{cm_1 d_1^3}{\lambda^3 \mu}, E_3 = \frac{d_1^3 d}{\lambda^2 \mu} \right) \text{ the wall parameters.}$$

6.3 Numerical outcomes and discussion

In this study we employed MATHEMATICA tool NDSolve to compute system of Eqs. (6.16) – (6.18) subject to (6.19) – (6.21). This technique is built-in which is based on Runge-Kutta fourth method. Efficiency of this technique is good for boundary value problems.

6.3.1 Velocity

Figs. 6.2 – 6.6 organize behavior of velocity for numerous pertinent parameters. Fig. 6.2 depicts outcome of Eyring-Powell fluid parameter A on velocity. Here velocity rises when A is increased. The velocity against Eyring fluid parameter B has been depicted through Fig. 6.3. Velocity reduces when Eyring liquid parameter B enhances. Fig. 6.4 portrays β outcome on the velocity field. This Fig. shows increasing behavior of velocity with respect to β . In fact more velocity occurs near walls of channel. Fig. 6.5 clarifies that for higher M the velocity decays. In fact more resistance offered to the fluid particles and so velocity decreases. Fig. 6.6 illustrates the effect of wall variables (E_1, E_2, E_3) on velocity. This Fig. show that velocity increases with higher E_1 and E_2 whereas as opposite behavior holds for E_3 .

6.3.2 Temperature

Influence of various physical variables on temperature is revealed in Figs. 6.7 – 6.16. Outcome for thermal Biot number Bi on temperature is shown in Fig. 6.7. As expected higher values of Bi give decline in temperature. Variation for Pr versus temperature is shown in Fig. 6.8. We have seen the increasing behavior of temperature with higher Pr . Larger Pr has lower thermal diffusivity and thus fluid becomes more viscous. It leads to an enhancement of temperature. Fig. 6.9 portrays the outcome of temperature for various values of Eckert number Ec . Temperature increases because high Eckert numbers strengthens the viscous dissipation effects. In Fig. 6.10 the consequence of radiation variable Rn on temperature is illustrated. It is found that with increasing thermal radiation the temperature falls. Figs. 6.11 and 6.12 show how heat generation/absorption variable Q influenced the temperature distribution. Here heat generation corresponds to $Q > 0$ and for heat absorption $Q < 0$. From Fig. 6.11 temperature enhances for heat generation $Q > 0$ while opposite behavior holds for heat absorption $Q < 0$ (see Fig. 6.12). Fig. 6.13 depicts consequence for Hartman number M on temperature. There is a reduction in temperature is for higher Hartman number M . Magnetic force is a resistive force that slows down the liquid particle drift. Fig. 6.14 shows the effects of temperature for rigidity parameter E_1 , the stiffness parameter E_2 and the viscous damping force parameter E_3 . It is noticed that an increase in E_1 and E_2 parameters rises the temperature but it reduces through higher E_3 . Fig. 6.15 represents impacts of Brownian movement Nb and thermophoresis Nt variables. It is apparent from these Figs. that higher values of these parameters correspond to temperature enhancement. Such increase in temperature is due to the occurrence of nanofeatures when enhancing the effects of both parameters. Fig. 6.16 elucidates the influence of E against temperature. We observed that temperature increases for higher E .

6.3.3 Concentration

Variation of pertinent variables on concentration is presented in Figs. 6.17 – 6.23. Fig. 6.17 presents that concentration is an increasing function of thermophoresis parameter Nt . Fig. 6.18 elaborates effects of nanoparticle concentration for radiation Rn . Here concentration of nanoparticles is observed to diminish when radiation effect intensifies. Fig. 6.19 depicts decay of concentration for Sc . Mathematically Sc is ratio of rate of momentum to the rate of mass

diffusions. For higher Sc the rate of mass diffusion is smaller. It leads to decay of concentration. Decay in concentration is found for higher chemical reaction parameter ζ in Fig. 6.20. Nanoparticle concentration versus activation energy E is depicted in Fig. 6.21. Here we observed that concentration enhances via higher E . Fig. 6.22 shows concentration for distinct values of temperature ratio parameter Ω . Concentration decreases against Ω . Fig. 6.23 elaborates consequences of wall parameter E_1, E_2 and E_3 on concentration. These Figs. show that concentration enhances with increasing E_1 and E_2 but reverse holds against E_3 .

6.3.4 Heat transfer coefficient

Figs. 6.24 – 6.32 are sketched for coefficient of heat transfer $Z(x) = \eta_x \theta_y(\eta)$ for the involved parameters. Fig. 6.24 explores influence of Biot parameter B_i on heat transfer coefficient Z . Z enhances for higher B_i . Fig. 6.25 summarized effects of radiation parameter Rn on heat transfer coefficient Z . A decreasing trend is noted for Z when Rn rises. Influence of Pr on Z is visualized in Fig. 6.26. It evidently displays that coefficient of heat transfer Z rises for higher Pr . Outcomes of Ec on Z is investigated in Fig. 6.27. It is found that rise in Ec increases the coefficient of heat transfer Z . Figs. 6.28 and 6.29 represent how coefficient of heat transfer Z is affected through the heat generation / absorption Q . Here we witnessed that Z increases for $Q > 0$ while it decreases when $Q < 0$. Fig. 6.30 indicates heat transfer coefficient Z against activation energy parameter E . Here Z enhances for higher E . Fig. 6.31 reveals the influence of ratio of temperature variable Ω on coefficient of heat transfer Z . Fig. 6.32 depicts Z against larger Brownian motion parameter Nb . We noticed that larger Nb shows an improvement of heat transfer coefficient Z . Activity of Z is also oscillatory.

6.3.5 Trapping

Plots for trapping are drawn in Figs. 6.33 – 6.35. Fig. 6.33 (a, b) is plotted for Eyring-Powell fluid parameter A . In this Fig. we noticed that trapped bolus size tends to decrease for higher A . Influence of Eyring-Powell fluid parameter B on streamline is demonstrated in Figs.6.34(a, b). An increment in B results in increase of size of bolus. Hartman number M caused reduction in bolus size (see Fig. 6.35(a, b)). It is also observed that bolus disappears for larger M .

6.4 Physical quantities

The skin friction, Nusselt number and Sherwood number denoted by (C_f) , (N_u) and (S_h) are defined as

$$C_f = (1 + B) \frac{\partial^2 \psi}{\partial y^2} - \frac{A}{3} \left(\frac{\partial^2 \psi}{\partial y^2} \right)^3, \quad N_u = -(1 + Rn) \frac{\partial \theta}{\partial y}, \quad S_h = -\frac{\partial \phi}{\partial y} \text{ at } y = \eta \quad (6.22)$$

Parameters								Results		
A	B	M	Nb	Nt	Ec	ζ	E	C_f	N_u	S_h
0.1	0.2	0.1	0.1	0.1	1	1	0.5	-0.732675	-0.834599	-1.06642
0.2	0.2	0.1	0.1	0.1	1	1	0.5	-0.729784	-0.834318	-1.06674
0.1	0.3	0.1	0.1	0.1	1	1	0.5	-0.733158	-0.846092	-1.06181
0.1	0.4	0.1	0.1	0.1	1	1	0.5	-0.733567	-0.855874	-1.05788
0.1	0.2	0.3	0.1	0.1	1	1	0.5	-0.698864	-0.834225	-1.06601
0.1	0.2	0.5	0.1	0.1	1	1	0.5	-0.640051	-0.835298	-1.06476
0.1	0.2	0.1	0.5	0.5	1	1	0.5	-0.732675	-0.610371	-1.15343
0.1	0.2	0.1	0.8	0.8	1	1	0.5	-0.732675	-0.474901	-1.21069
0.1	0.2	0.1	0.1	0.1	1.5	1	0.5	-0.732675	-0.76107	-1.09585
0.1	0.2	0.1	0.1	0.1	2	1	0.5	-0.732675	-0.687527	-1.12531
0.1	0.2	0.1	0.1	0.1	1	1.5	0.5	-0.732675	-0.833448	-1.27126
0.1	0.2	0.1	0.1	0.1	1	2	0.5	-0.732675	-0.832703	-1.39404
0.1	0.2	0.1	0.1	0.1	1	1	1	-0.732675	-0.83550	-0.983048
0.1	0.2	0.1	0.1	0.1	1	1	2	-0.732675	-0.836973	-0.854028

Table 6.1. Numerical outcomes of (C_f) , (N_u) and (S_h) when $(x = 0.2, t = 0.1, \epsilon = 0.2, \beta = 0.2, E_1 = 0.01, E_2 = 0.02, E_3 = 0.01, Rn = 0.9, Q = 0.3, Sc = 1, \Omega = 2, Bi = 3)$.

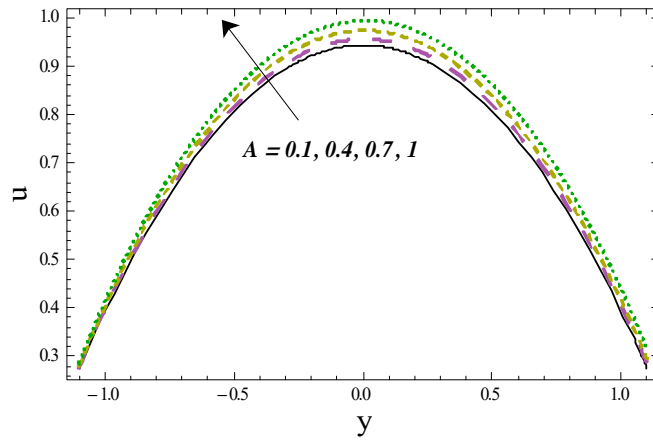


Fig. 6.2: Variation of A on u

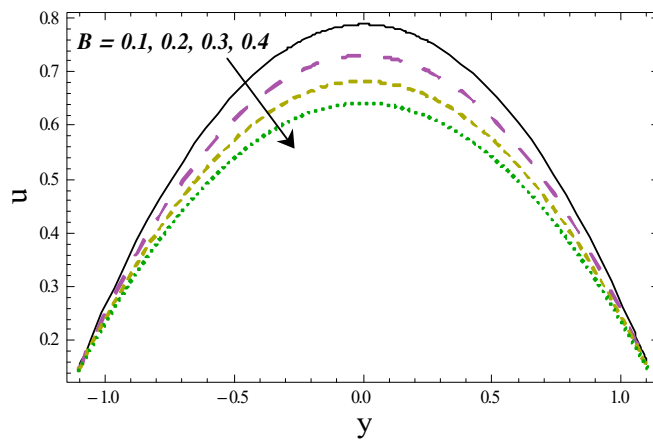


Fig. 6.3: Variation of B on u

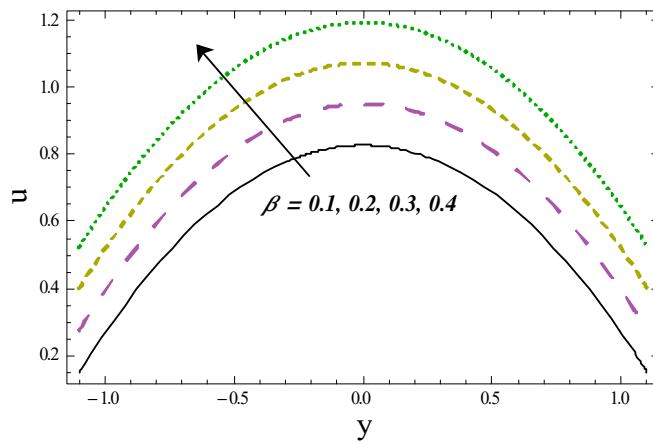


Fig. 6.4: Variation of β on u

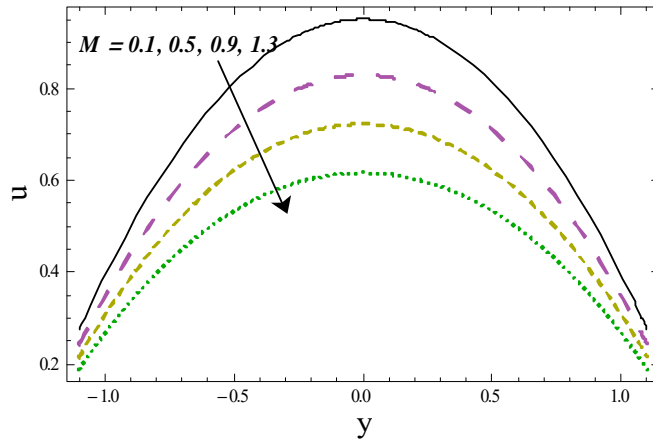


Fig. 6.5: Variation of M on u

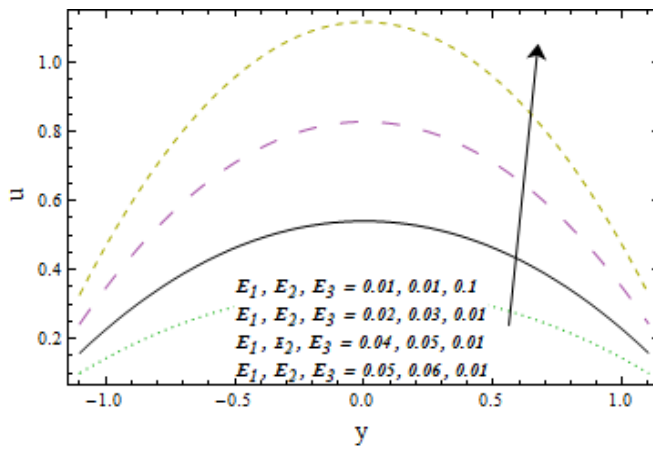


Fig. 6.6: Variations of E_1, E_2 and E_3 on u

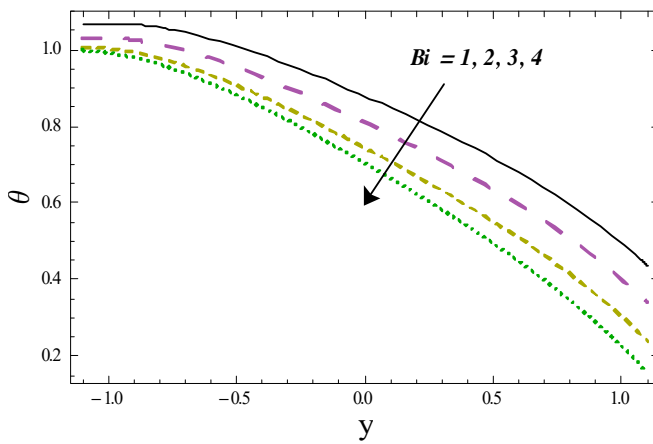


Fig. 6.7: Variation of Bi on θ

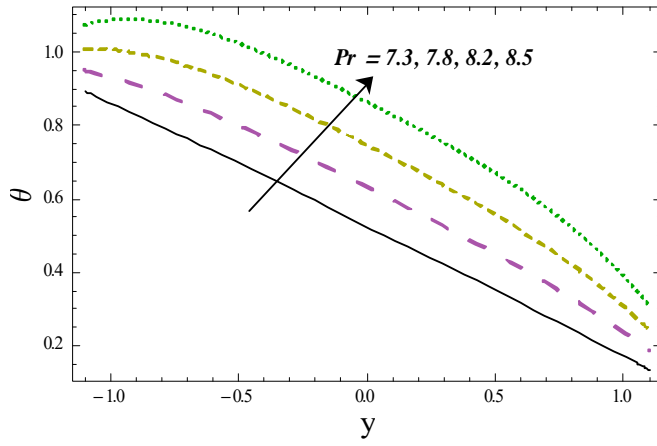


Fig. 6.8: Variation of Pr on θ

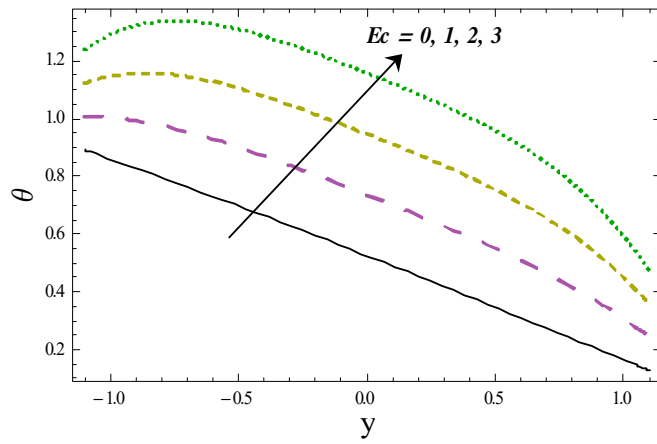


Fig. 6.9: Variation of Ec on θ

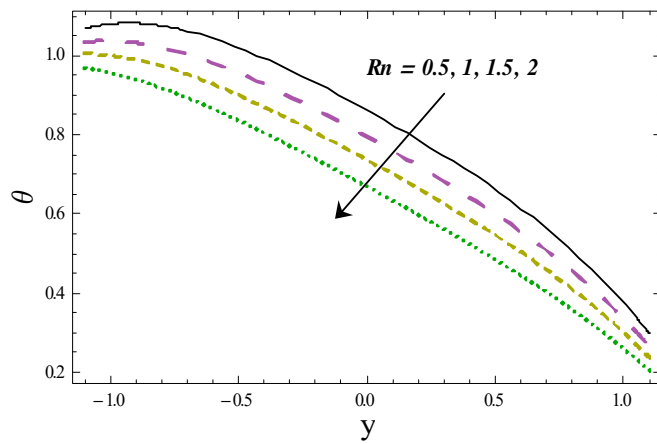


Fig. 6.10: Variation of Rn on θ

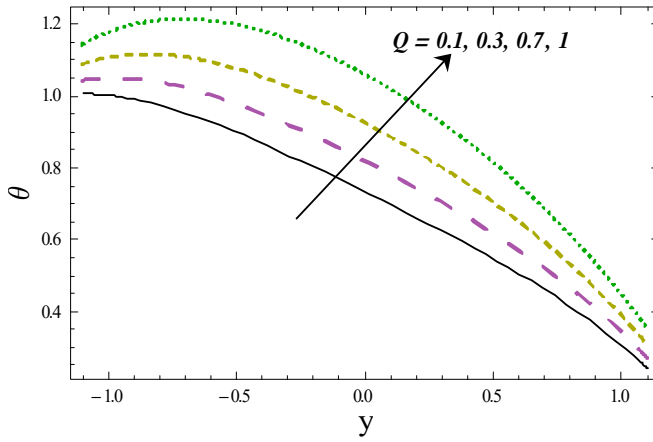


Fig. 6.11: Variation of $Q > 0$ on θ

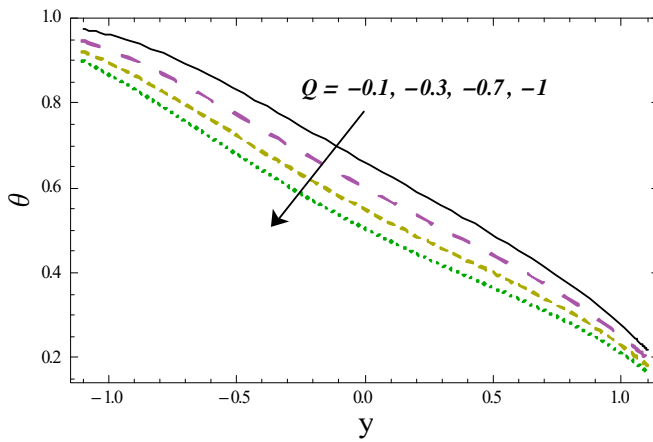


Fig. 6.12: Variation of $Q < 0$ on θ

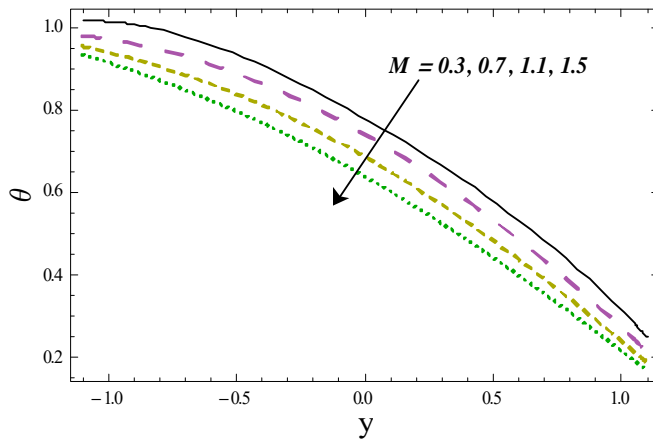


Fig. 6.13: θ against M

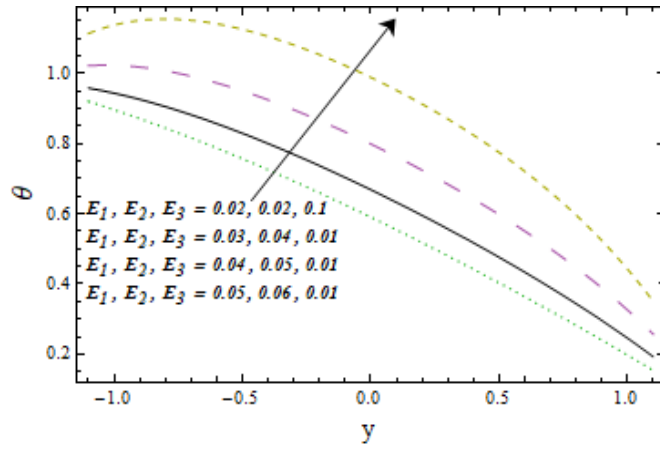


Fig. 6.14: E_1, E_2 and E_3 Variation for θ

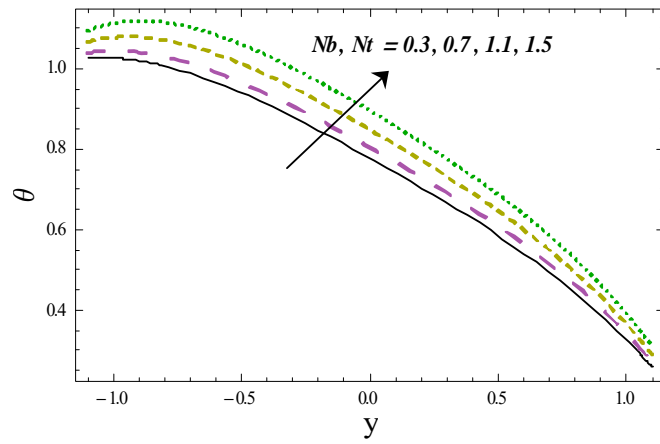


Fig. 6.15: Variations of Nb and Nt on θ

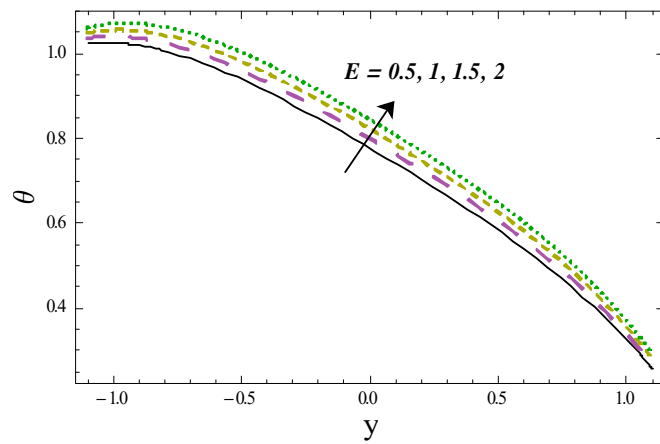


Fig. 6.16: Variation of E on θ

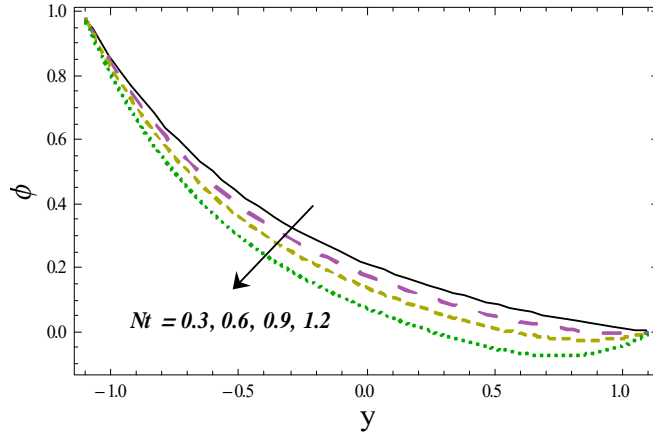


Fig. 6.17: Nt variation on ϕ

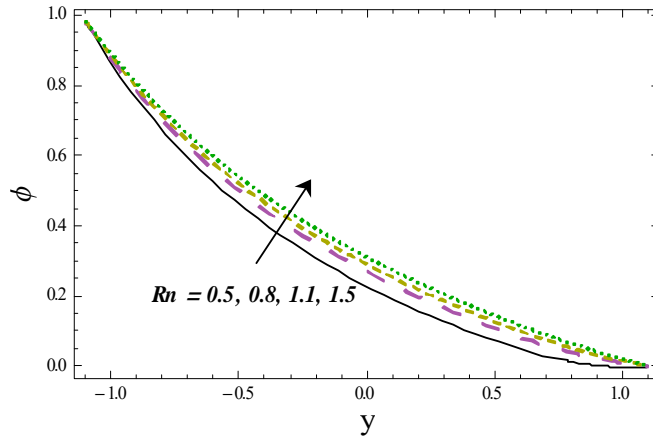


Fig. 6.18: Variation of Rn on ϕ

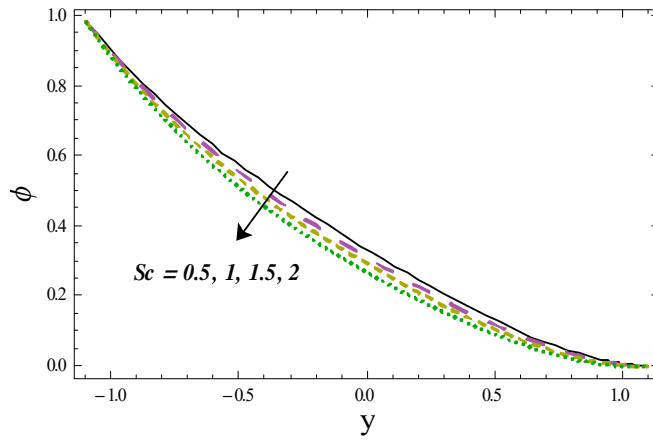


Fig. 6.19: Variation of Sc on ϕ

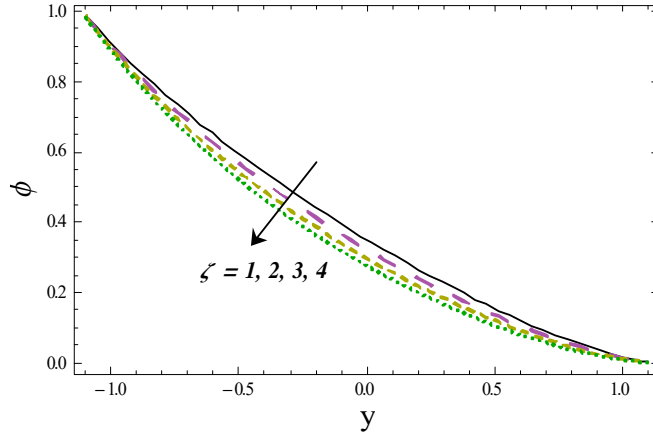


Fig. 6.20: Variation of ζ on ϕ

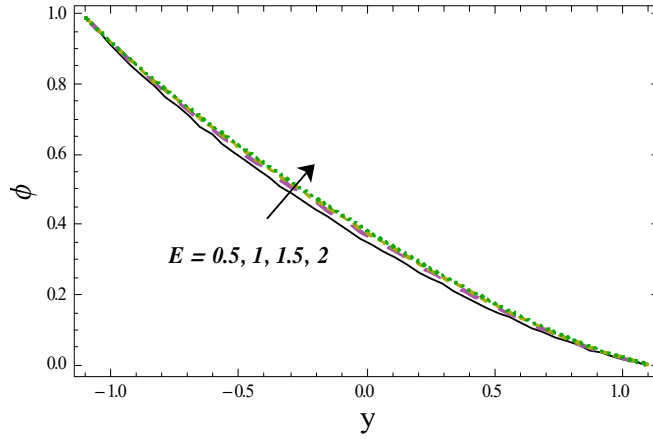


Fig. 6.21: Variation of E on ϕ

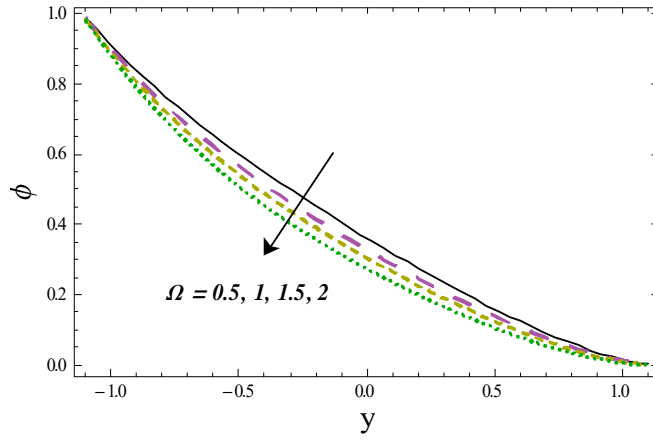


Fig. 6.22: ϕ against Ω

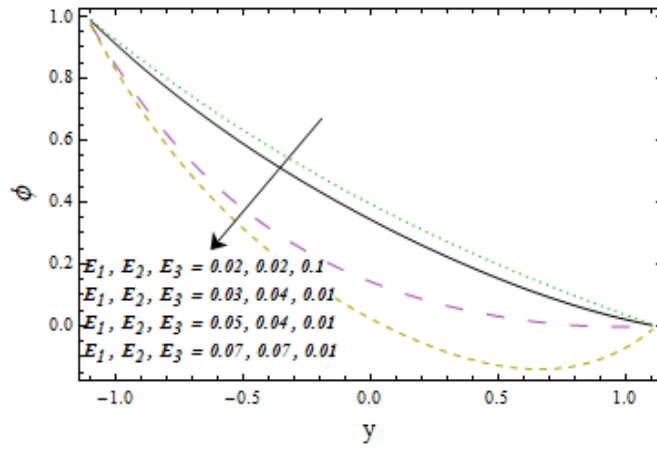


Fig. 6.23: E_1, E_2 and E_3 variation on ϕ

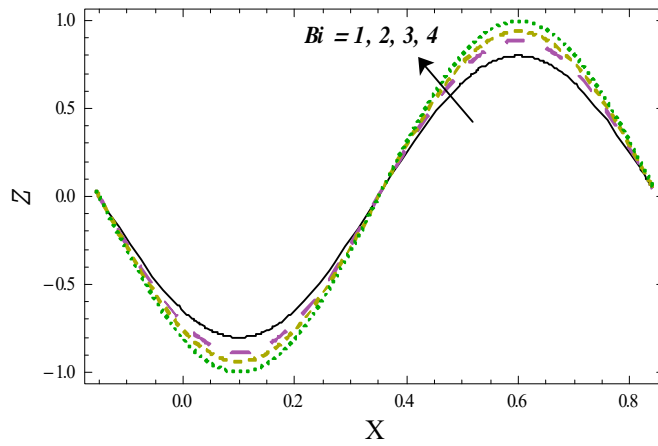


Fig. 6.24: Variation of Bi on Z

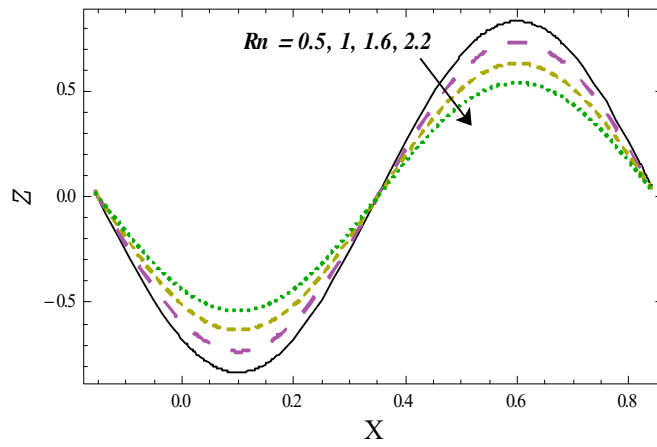


Fig. 6.25: Variation of Rn on Z

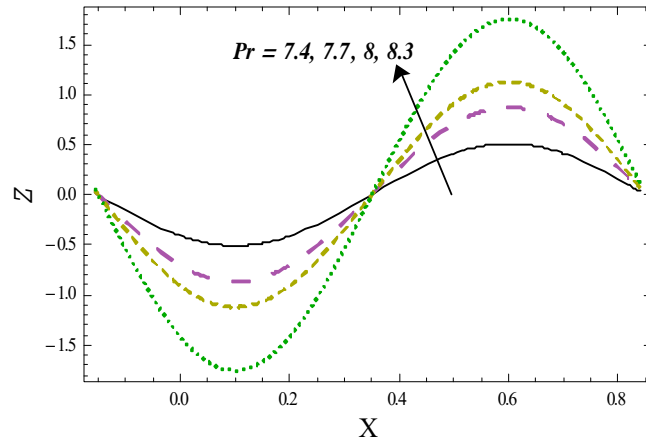


Fig. 6.26: Variation of Pr on Z

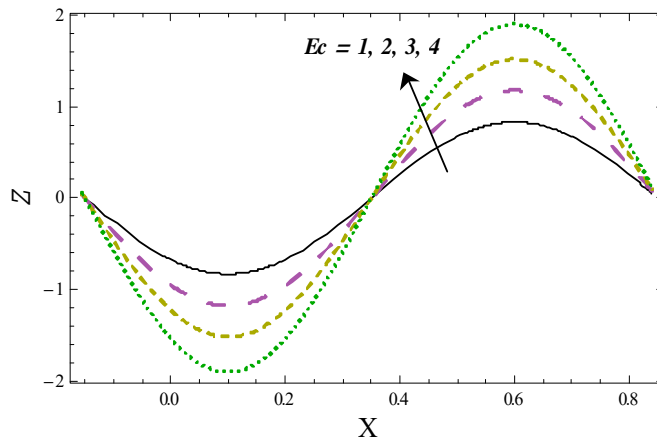


Fig. 6.27: Variation of Ec on Z

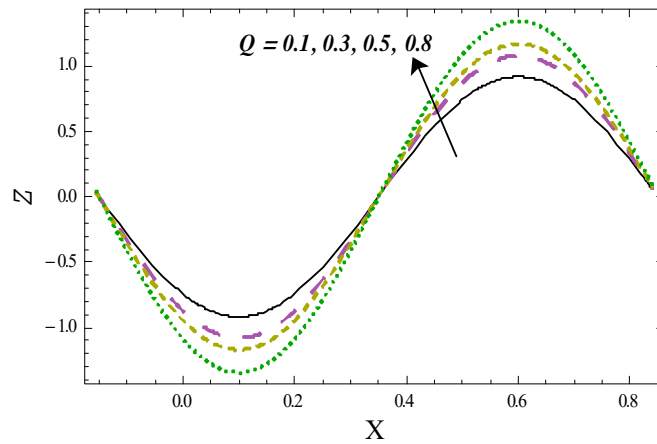


Fig. 6.28: Variation of $Q > 0$ on Z

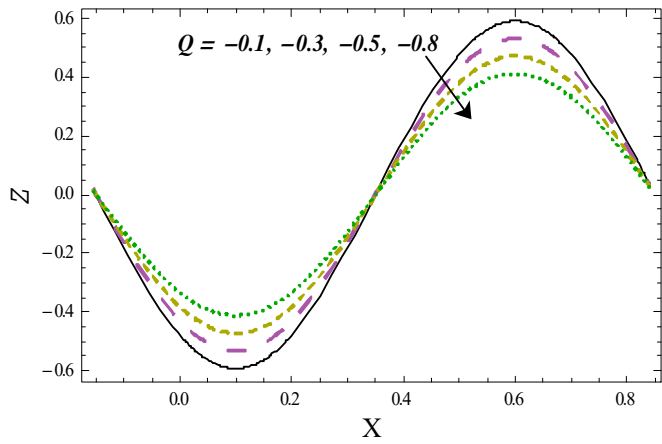


Fig. 6.29: Variation of $Q < 0$ on Z

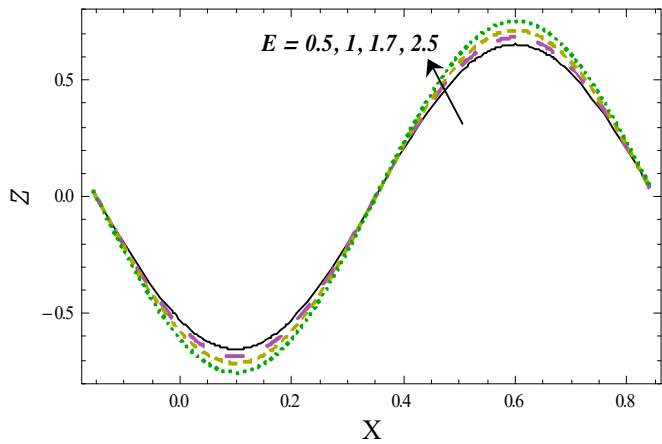


Fig. 6.30: Variation of E on Z

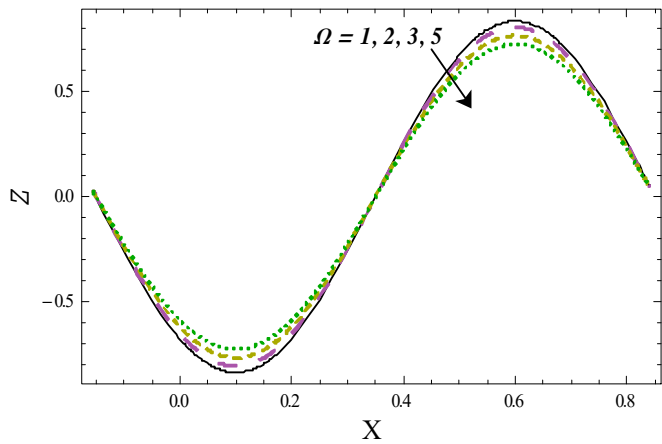


Fig. 6.31: Variation of Ω on Z

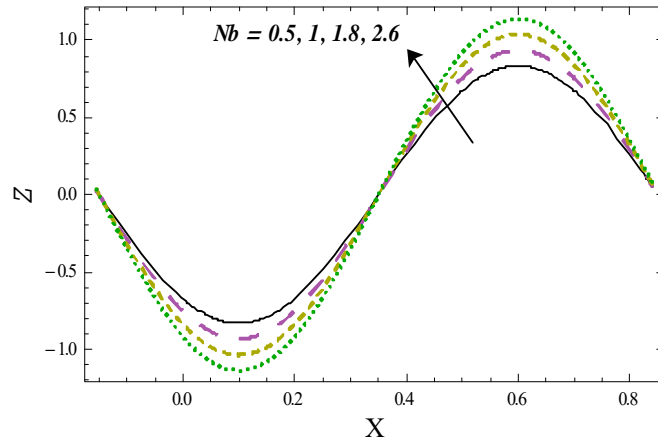


Fig. 6.32: Z against Nb

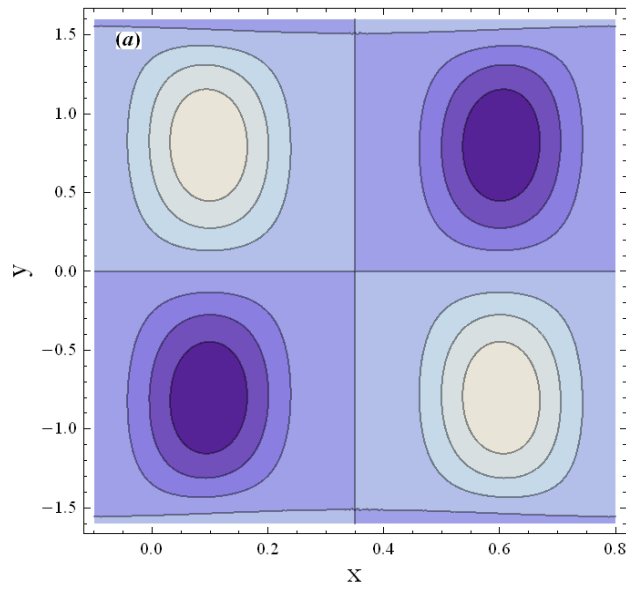


Fig. 6.33(a): Variation of ψ when $A = 0.1$.

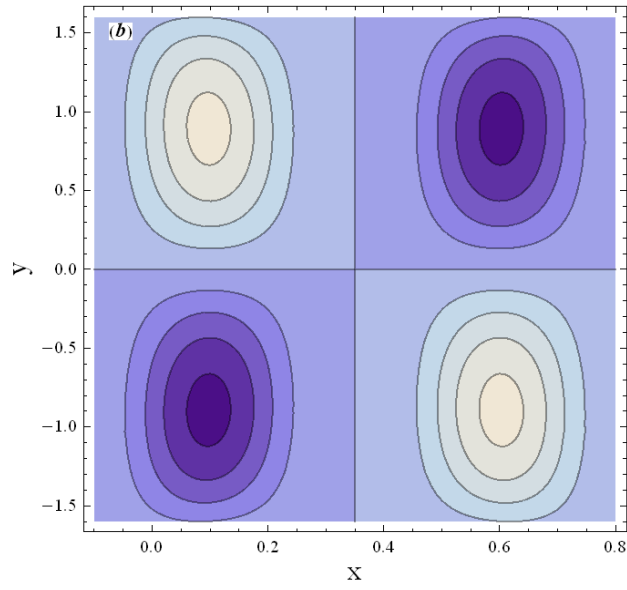


Fig. 6.33(b): Variation of ψ when $A = 0.2$.

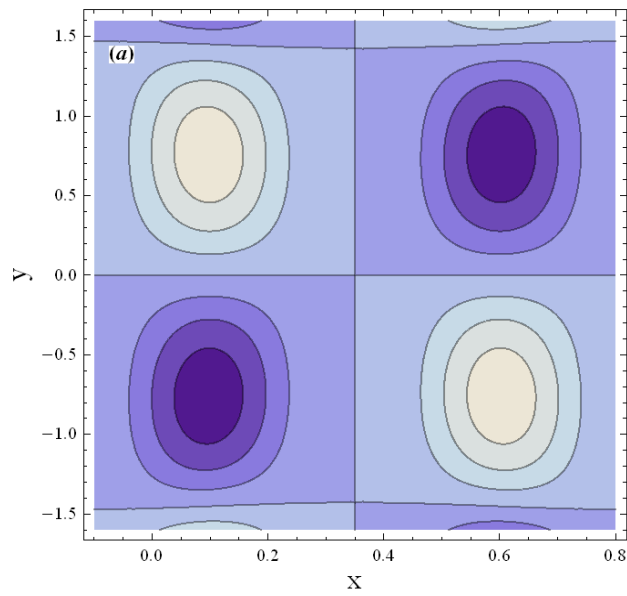


Fig. 6.34(a): Variation of ψ when $B = 0.3$.

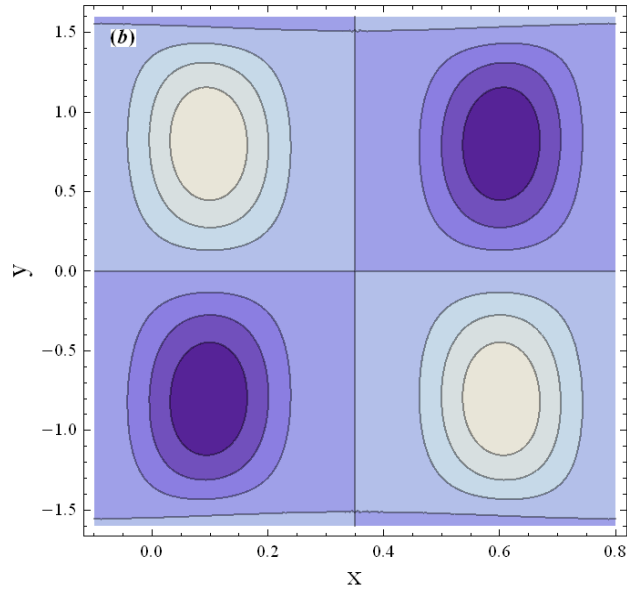


Fig. 6.34(b): Variation of ψ when $B = 0.5$.

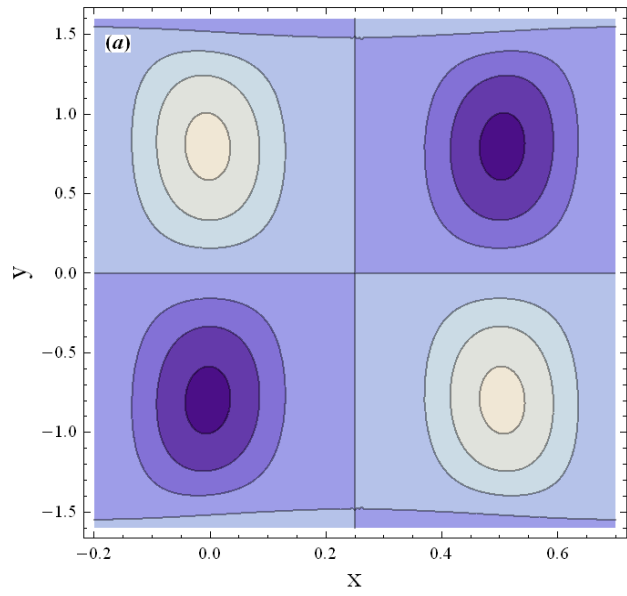


Fig. 6.35(a): Variation of ψ when $M = 0.7$.

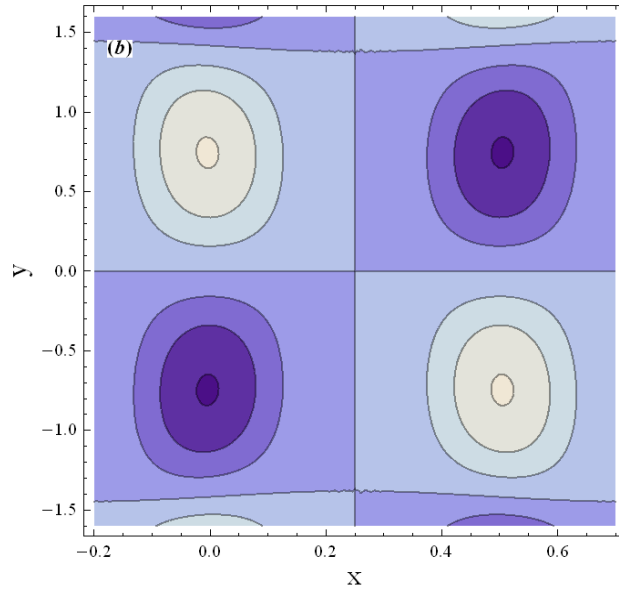


Fig. 6.35(b): Variation of ψ when $M = 1.2$.

6.5 Conclusion

The key consequences for the current analysis are summarized below.

- Velocity rises for A and β and it reduces against B and M .
- Temperature is increased through Pr , Ec , Nb and Nt .
- Temperature decreases by increasing Bi while it increases for E .
- Impacts of Rn on concentration and temperature are reverse.
- Higher Sc , Nt and ζ lead to decay of concentration.
- Concentration has reverse behavior for both E and Ω .
- Higher E_1 and E_2 enhance the temperature and concentration while these decay for E_3 .
- Behaviors of Prandtl Pr and Eckert Ec numbers on heat transfer coefficient are qualitatively similar.
- Coefficient of heat transfer boosts for both E and Bi .

- Effects of Eyring-Powell fluid variables B and A are opposite for trapping.
- Reverse behavior is noticed for skin friction coefficient against A and B .
- Nusselt number reduces for higher Nb and Nt . Similar trend is found for Sherwood number against E .

Chapter 7

Peristaltic activity of fourth grade nanofluid with slip and radiation

7.1 Introduction

This chapter intends to examine the peristalsis of fourth grade nanomaterial with chemical reaction. Thermal radiation, Ohmic heating and dissipation are present in the energy equations. Heat source/sink is also accounted. Slip constrains for velocity, temperature and concentration are invoked. Problem is evaluated for low Reynolds number and long wavelength. The reduced nonlinear systems are solved numerically. Detailed analysis is arranged for velocity, concentration, temperature, heat transfer coefficient and trapping. Key observations are concluded.

7.2 Formulation

Two-dimensional radiative peristaltic motion of magnetohydrodynamic(MHD) fourth-grade nanofluid is taken into account in a channel. Here channel of width $2d_1$ has flexible walls, λ the wavelength, and c the speed of wave and a the amplitude. Cartesian coordinates (x, y) are implemented such that x -axis along the channel wall and y -axis orthogonal to it. Flow is conducted with magnetic field of strength B_0 . Here we neglected an induced magnetic field. Brownian motion, thermophoresis and Joule heating are examined. Chemical reaction is also

present. The waves propagating along the channel walls are defined below.

$$y = \pm\eta(x, t) = \pm[d_1 + a \sin \frac{2\pi}{\lambda}(x - ct)], \quad (7.1)$$

Fourth-grade model extra stress tensor is [41].

$$\begin{aligned} S = & \mu \mathbf{A}_1 + \alpha'_1 \mathbf{A}_2 + \alpha'_2 \mathbf{A}_1^2 + \beta'_1 \mathbf{A}_3 + \beta'_2 (\mathbf{A}_1 \mathbf{A}_2 + \mathbf{A}_2 \mathbf{A}_1) + \beta'_3 (\text{tr} \mathbf{A}_1^2) \mathbf{A}_1 + \gamma'_1 \mathbf{A}_4 + \\ & \gamma'_2 (\mathbf{A}_1 \mathbf{A}_3 + \mathbf{A}_3 \mathbf{A}_1) + \gamma'_3 \mathbf{A}_2^2 + \gamma'_4 (\mathbf{A}_1^2 \mathbf{A}_2 + \mathbf{A}_2 \mathbf{A}_1^2) + \gamma'_5 (\text{tr} \mathbf{A}_2) \mathbf{A}_2 + \gamma'_6 (\text{tr} \mathbf{A}_2) \mathbf{A}_1^2 + \\ & (\gamma'_7 \text{tr} \mathbf{A}_3 + \gamma'_7 \text{tr} (\mathbf{A}_2 \mathbf{A}_1)) \mathbf{A}_1, \end{aligned} \quad (7.2)$$

where the Rivlin-Ericksen tensors are [41]

$$\mathbf{A}_1 = (\text{grad } \mathbf{V})^T + \text{grad } \mathbf{V}, \quad (7.3)$$

$$\mathbf{A}_n = \frac{d\mathbf{A}_{n-1}}{dt} + (\text{grad } \mathbf{V}) \mathbf{A}_{n-1} + \mathbf{A}_{n-1} (\text{grad } \mathbf{V})^T, \quad n > 1. \quad (7.4)$$

The relevant equations for problem under consideration are

$$\frac{\partial u}{\partial x} + \frac{\partial v}{\partial y} = 0, \quad (7.5)$$

$$\rho_f \left(\frac{\partial u}{\partial t} + u \frac{\partial u}{\partial x} + v \frac{\partial u}{\partial y} \right) = -\frac{\partial p}{\partial x} + \frac{\partial S_{xx}}{\partial x} + \frac{\partial S_{xy}}{\partial y} - \sigma B_0^2 u, \quad (7.6)$$

$$\rho_f \left(\frac{\partial v}{\partial t} + u \frac{\partial v}{\partial x} + v \frac{\partial v}{\partial y} \right) = -\frac{\partial p}{\partial y} + \frac{\partial S_{yx}}{\partial x} + \frac{\partial S_{yy}}{\partial y}, \quad (7.7)$$

$$\begin{aligned} \rho_f c_f \left(\frac{\partial T}{\partial t} + u \frac{\partial T}{\partial x} + v \frac{\partial T}{\partial y} \right) = & k \left(\frac{\partial^2 T}{\partial x^2} + \frac{\partial^2 T}{\partial y^2} \right) + S_{xx} \frac{\partial u}{\partial x} + S_{yy} \frac{\partial v}{\partial y} + S_{xy} \left(\frac{\partial v}{\partial x} + \frac{\partial u}{\partial y} \right) \\ & + \left[D_B \left(\frac{\partial C}{\partial y} \frac{\partial T}{\partial y} + \frac{\partial C}{\partial x} \frac{\partial T}{\partial x} \right) + \frac{D_T}{T_m} \left\{ \left(\frac{\partial T}{\partial y} \right)^2 + \left(\frac{\partial T}{\partial x} \right)^2 \right\} \right] \rho_p c_p + \\ Q_0 - \frac{\partial q_r}{\partial y} + \sigma B_0^2 u^2, \end{aligned} \quad (7.8)$$

$$\frac{\partial C}{\partial t} + u \frac{\partial C}{\partial x} + v \frac{\partial C}{\partial y} = D_B \left(\frac{\partial^2 C}{\partial x^2} + \frac{\partial^2 C}{\partial y^2} \right) + \frac{D_T}{T_m} \left(\frac{\partial^2 T}{\partial x^2} + \frac{\partial^2 T}{\partial y^2} \right) - k_1(C - C_0). \quad (7.9)$$

The appropriate boundary conditions are

$$u \pm \beta_1 S_{xy} = 0 \quad \text{at } y = \pm \eta, \quad (7.10)$$

$$\left[-\tau_1 \frac{\partial^3}{\partial x^3} + m_1 \frac{\partial^3}{\partial x \partial t^2} + d \frac{\partial^2}{\partial t \partial x} \right] \eta = \frac{\partial S_{xx}}{\partial x} + \frac{\partial S_{xy}}{\partial y} - \rho_f \left(\frac{\partial u}{\partial t} + u \frac{\partial u}{\partial x} + v \frac{\partial u}{\partial y} \right) - \sigma B_o^2 u \quad \text{at } y = \pm \eta. \quad (7.11)$$

$$T \pm \beta_2 \frac{\partial T}{\partial y} = \left\{ \begin{matrix} T_1 \\ T_0 \end{matrix} \right\}, \quad C \pm \beta_3 \frac{\partial C}{\partial y} = \left\{ \begin{matrix} C_1 \\ C_0 \end{matrix} \right\} \quad \text{at } y = \pm \eta, \quad (7.12)$$

where (u, v) are the velocity components in (x, y) directions, p the pressure, ρ_f the density of nanofluid, ν the kinematic viscosity, k the thermal conductivity, σ the electric conductions, D_B the Brownian movement, D_T the thermophoretic diffusion coefficient, $Q_0 > 0$ and $Q_0 < 0$ for the heat generation and heat absorption, d coefficient of viscous damping, $(\beta_1, \beta_2, \beta_3)$ the slip parameters, m_1 mass per unit area, T_m the mean temperature, τ_1 elastic tension, k_1 the chemical reaction rate and (T_1, T_0) and (C_1, C_0) respectively the upper and lower walls temperature and concentration. Material constants of fourth-grade are $\alpha'_i (i = 1, 2)$, $\beta'_i (i = 1-3)$ and $\gamma'_i (i = 1-8)$. Further extra stress tensor components S_{xx} , S_{yy} , S_{yx} , S_{xy} for the fourth-grade fluid can be defined through expression (7.2). Last term in Eq. (7.9) is due the effect of chemical reaction. Radiative heat flux q is depicted as follows:

$$q_r = -\frac{4\bar{\sigma}}{3\bar{k}} \frac{\partial T^4}{\partial y}, \quad (7.13)$$

in which $\bar{\sigma}$ represents the Stefan – Boltzmann constant, and \bar{k} the constant of absorption.

Expanding T^4 about T_0 by using Taylor expansion and ignoring the expressions of higher order we have

$$T^4 = 4T_0^3 T - 3T_0^4. \quad (7.14)$$

Using (7.14) into (7.13) one has

$$q_r = \frac{16\bar{\sigma}T_0^3}{3k} \frac{\partial T}{\partial y}. \quad (7.15)$$

Now if $\psi(x, y, t)$ represents the stream function then by defining $u = \psi_y, v = -\delta\psi_x$ and following non-dimensional variables

$$\begin{aligned} u &= cu^*, v = cv^*, x = \lambda x^*, y = d_1 y^*, ct = \lambda t^*, \eta = d_1 \eta^* \\ d_1^2 p &= c\lambda\mu p^*, (T_1 - T_0)\theta = T - T_0, (C_1 - C_0)\phi = C - C_0, \\ c\mu S_{ij}^* &= d_1 S_{ij}, d_1 \beta_i^* = \beta_i (i = 1 - 3), \mu d_1 \alpha_i'^* = \alpha_i' c, \\ \mu d_1^2 \beta_i'^* &= \beta_i' c^2, \mu d_1^3 \gamma_i'^* = \gamma_i' c^3, \end{aligned} \quad (7.16)$$

we get after utilizing long wavelength (i.e. wave number $\simeq 0$) and low Reynolds number approximations the following problems

$$\frac{\partial^2}{\partial y^2} \left(\frac{\partial^2 \psi}{\partial y^2} + 2\Gamma \left(\frac{\partial^2 \psi}{\partial y^2} \right)^3 \right) - M^2 \frac{\partial^2 \psi}{\partial y^2} = 0, \quad (7.17)$$

$$\begin{aligned} (1 + \text{Pr} Rn) \frac{\partial^2 \theta}{\partial y^2} + Nb \text{Pr} \left(\frac{\partial \theta}{\partial y} \right) \left(\frac{\partial \phi}{\partial y} \right) + \left(\frac{\partial \theta}{\partial y} \right)^2 Nt \text{Pr} + \\ Ec \text{Pr} \frac{\partial^2 \psi}{\partial y^2} \left[\frac{\partial^2 \psi}{\partial y^2} + M^2 \left(\frac{\partial \psi}{\partial y} \right)^2 + 2\Gamma \left(\frac{\partial^2 \psi}{\partial y^2} \right)^3 \right] + \text{Pr} Q = 0 \end{aligned} \quad (7.18)$$

$$\frac{Nt}{Nb} \left(\frac{\partial^2 \theta}{\partial y^2} \right) + \frac{\partial^2 \phi}{\partial y^2} - \zeta S c \phi = 0, \quad (7.19)$$

$$\frac{\partial \psi}{\partial y} \pm \beta_1 \left[\frac{\partial^2 \psi}{\partial y^2} + 2\Gamma \left(\frac{\partial^2 \psi}{\partial y^2} \right)^3 \right] = 0 \text{ at } y = \pm \eta, \quad (7.20)$$

$$\begin{aligned} \left[E_1 \frac{\partial^3}{\partial x^3} + E_2 \frac{\partial^3}{\partial x \partial t^2} + E_3 \frac{\partial^2}{\partial x \partial t} \right] \eta = \frac{\partial^3 \psi}{\partial y^3} + 6\Gamma \left(\left(\frac{\partial^2 \psi}{\partial y^2} \right)^2 \frac{\partial^3 \psi}{\partial y^3} \right) \\ - M^2 \frac{\partial \psi}{\partial y} \text{ at } y = \pm \eta, \end{aligned} \quad (7.21)$$

$$\theta \pm \beta_2 \frac{\partial \theta}{\partial y} = \begin{Bmatrix} 1 \\ 0 \end{Bmatrix}, \phi \pm \beta_3 \frac{\partial \phi}{\partial y} = \begin{Bmatrix} 1 \\ 0 \end{Bmatrix} \text{ at } y = \pm \eta. \quad (7.22)$$

Equation of continuity (7.5) is identically satisfied. Here ϵ shows amplitude ratio, α the thermal diffusivity, δ the wave number, Pr the Prandtl number, Re the Reynolds number, Ec the Eckert variable, Sc the Schmidt variable, M the Hartman variable, τ the efficient heat capacity ratio of nanoparticulate material to fluid heat capacity, Nb the Brownian diffusion variable, Nt the thermophoresis parameter, Rn the radiation number, Q the heat source/sink variable, ζ the chemical reaction number, (E_1, E_2, E_3) the wall variables and Γ the Deborah parameter. We have

$$\begin{aligned} \epsilon &= \frac{a}{d_1}, \quad \delta = \frac{d_1}{\lambda}, \quad \alpha = \frac{k}{\rho_f c_f}, \quad Pr = \frac{\mu c_f}{k}, \quad Re = \frac{\rho_f c d_1}{\mu}, \quad Ec = \frac{c^2}{c_f (T_1 - T_0)}, \quad Sc = \frac{\nu}{D_B}, \\ M &= \sqrt{\frac{\sigma}{\mu}} B_0 d_1, \quad \tau = \frac{\rho_f c_p}{\rho_f c_f}, \quad Nb = \frac{D_B \tau (C_1 - C_0)}{\nu}, \quad Nt = \frac{D_T \tau (T_1 - T_0)}{T_m \nu}, \quad Rn = \frac{16 \bar{\sigma} T_0^3}{3 k k}, \\ Q &= \frac{Q_0 d_1^2}{k(T_1 - T_0)}, \quad \zeta = \frac{k_1 d_1^2}{\nu}, \quad E_1 = -\frac{d_1^3 \tau}{\lambda^3 \mu c}, \quad E_2 = \frac{c m_1 d_1^3}{\lambda^3 \mu}, \quad E_3 = \frac{d_1^3 d}{\lambda^2 \mu}, \quad \Gamma = \beta'_2 + \beta'_3. \end{aligned}$$

7.3 Numerical outcomes and discussion

We employed MATHEMATICA tool NDSolve to compute system of Eqs. (7.17) – (7.22). This technique is built-in which based on Runge-Kutta fourth method. Efficiency of this technique is good for boundary value problems.

7.3.1 Velocity

Figs. 7.1 – 7.4 are organized to see variation of velocity against various relevant variables. The velocity against velocity slip variable β_1 is exhibited in Fig. 7.1. It is noted that velocity decreases when β_1 enhances. Impacts of wall variables (E_1, E_2, E_3) on velocity profile are shown in Fig. 7.2. From this Fig. the velocity rises for increasing values of (E_1, E_2) , whereas contrary trend is found for E_3 . Fig. 7.3 reveals consequence of Deborah number Γ on velocity profile. Here velocity profile increases for higher Γ . Fig. 7.4 displays the effect of magnetic variable M on velocity. Here an increment for M reduces the velocity.

7.3.2 Temperature

Effects of various thermo physical variables on temperature are illustrated in Figs. 7.5 – 7.14. Fig. 7.5 demonstrates the impacts of Brownian movement Nb and thermophoresis Nt parameters. It is clear that by enhancing the values of both the parameters the temperature enhances. Higher values of both parameters cause more randomness. This fact increases the temperature. Fig. 7.6 is drawn for analysis of temperature against Prandtl number Pr . Graph shows that rising behavior is observed in this case. Fig. 7.7 depicts effect of radiation Rn on temperature. Decaying behavior of temperature is witnessed. Fig. 7.8 elucidates thermal slip parameter β_2 impact. Clearly larger values of β_2 enhanced the temperature. Impact of magnetic parameter M is represented in Fig. 7.9. Obviously temperature declines when M increases. Eckert number effect on temperature is demonstrated in Fig. 7.10. Eckert variable in view of dissipation leads to growth of fluid temperature. Figs. 7.11 and 7.12 show how heat generation/absorption variable Q influenced the distribution of temperature. Temperature for heat generation ($Q > 0$) enhances while opposite scenario holds for heat absorption ($Q < 0$) in Fig. 7.12. Fig. 7.13 displays activity of wall properties on temperature. Temperature of fluid enhances with E_1 and E_2 and it decays against E_3 . Fig. 7.14 elaborates the consequences of Deborah number Γ on temperature. It can be concluded from this figure that higher values of Γ number give more fluid temperature.

7.3.3 Concentration

Influence of numerous parameters for concentration are reported in Figs 7.15 – 7.21. Effect of concentration slip parameter β_3 is sketched in Fig.7.15. Concentration is decreasing function of β_3 . Fig. 7.16 explores the influence of Deborah number Γ on concentration. Concentration of fluid is decreased for higher Γ . Impact of chemical reaction ζ on concentration is shown in Fig.7.17. Here we observed that concentration diminishes for higher ζ . Fig. 7.18 exposes influence of Brownian motion parameter Nb on concentration. Concentration grows for higher Nb . Fig. 7.19 describes the consequence of thermophoresis parameter Nt . Here concentration of nanoparticles is decreased when thermophoresis intensifies. Nanoparticle concentration against Schmidt number Sc is portrayed in Fig. 7.20. We noticed that larger Sc decreased concentration. Sc is the proportion of the dynamic diffusion to the rate of mass diffusion. Rate of mass

diffusion is decreases for larger Sc . It yields concentration declines. Variation of wall properties on concentration is depicted in Fig. 7.21. Clearly the concentration is enhanced by increasing E_1 and E_2 while reverse holds for E_3 .

7.3.4 Coefficient of heat transfer

Outcomes of $Z(x) = \theta_y(\eta)\eta_x$ are shown in Figs. 7.22 – 7.31. Consequence of Prandtl variable Pr on Z is investigated in Fig. 7.22. It is found that rise in Pr increases the coefficient of heat transfer Z . Outcome of Hartman number M on Z is portrayed in Fig. 7.23. Coefficient of heat transfer decreases against higher M . Fig. 7.24 elucidates the thermal slip parameter β_2 on heat transfer coefficient Z . We have seen the increasing behavior of Z against higher β_2 . A decreasing trend is noted for Z when chemical reaction parameter ζ higher (see Fig. 7.25). Fig. 7.26 portrays heat transfer rate Z for larger Brownian movement Nb and thermophoresis parameters Nt . Here we observed that higher Nb and Nt indicate an enhancement of heat transfer coefficient Z . Fig. 7.27 is made for the outcome of Deborah number Γ on Z . It is seen that an enhancement of Γ leads to rise in Z . Heat transfer coefficient Z against heat generation absorption Q is shown in Figs. 7.28 and 7.29. Here Z rises with ($Q > 0$) while it declines for ($Q < 0$). Role of Rn on the heat transfer coefficient Z is illustrated in Fig. 7.30. In this case the findings indicate decline in Z . Fig. 7.31. depicts the effects of Eckert number Ec on coefficient of heat transfer Z . Enhancement in Z is observed via larger Ec .

7.3.5 Skin friction Coefficient

Impact of skin friction coefficient $C_f = \eta_x \left(\psi_y(\eta) + 2\Gamma (\psi_y(\eta))^3 \right)$ is discussed through Figs. 7.32 – 7.34. Fig. 7.32 is plotted to see the effect of Deborah number Γ against C_f . Decaying behavior of C_f is noticed. Fig. 7.33 shows that for skin friction coefficient C_f diminishes when β_1 increments. Fig. 7.34 illustrates influence for Hartman number M on C_f . It is observed that C_f increases when M higher.

7.3.6 Sherwood number

Figs. 7.35 – 7.37 are portrayed to see effects of Sherwood number $S_h = \eta_x \phi_y(\eta)$ for different physical parameters. Fig. 7.35 demonstrates the impact of Nb on Sherwood number S_h . Larger

values of Nb caused decay of S_h . Figs. 7.36 and 7.37 display the impacts of thermophoresis Nt and chemical reaction parameters ζ respectively against S_h . Sherwood number S_h shows increasing trend for both parameters.

7.3.7 Trapping

Trapping is sketched through Figs. 7.38 and 7.39. Figs 7.38(a) and 7.38(b) we have plotted to see impacts for Deborah number Γ . As expected the trapped bolus size increases when Γ enhances. Effects of velocity slip variable β_1 on bolus size are given in Figs. 7.39 (a, b). Size of bolus decreases for higher β_1 .

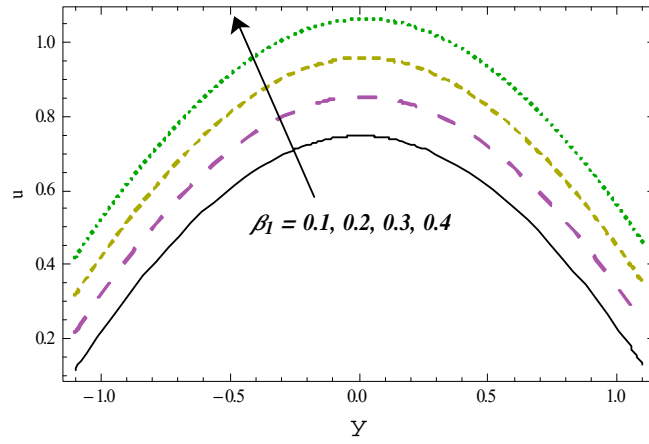


Fig. 7.1: Variation of β_1 on u

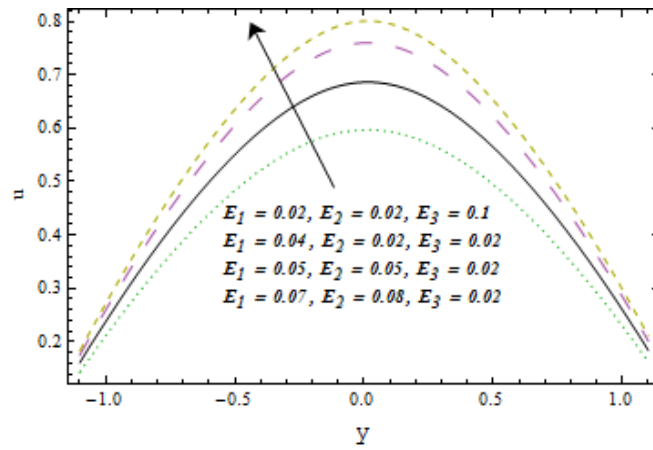


Fig. 7.2: Variations of E_1, E_2 and E_3 on u

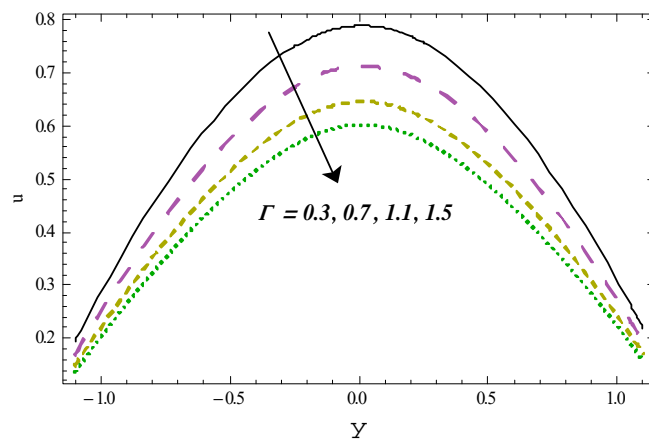


Fig. 7.3: Variation of Γ on u

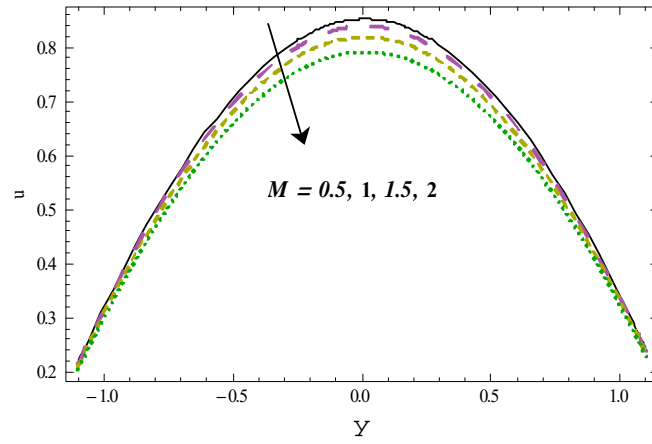


Fig. 7.4: Variation of M on u

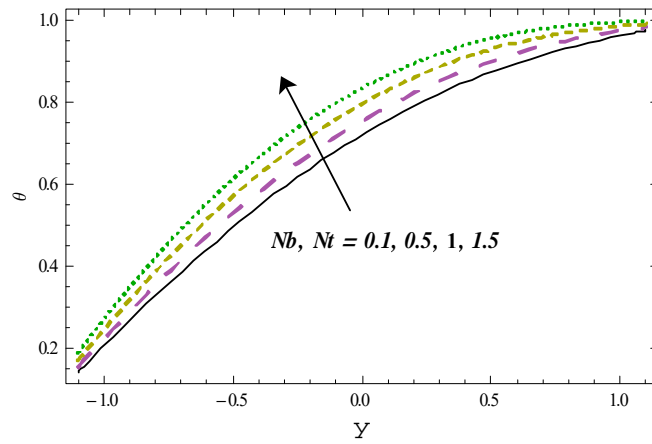


Fig. 7.5: Nb and Nt variation on θ

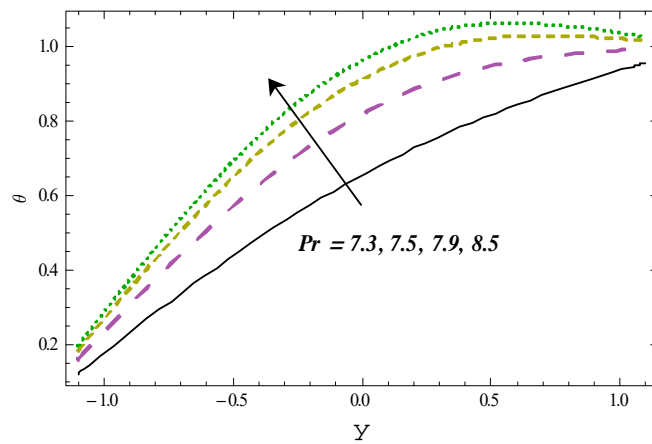


Fig. 7.6: Variation of Pr on θ

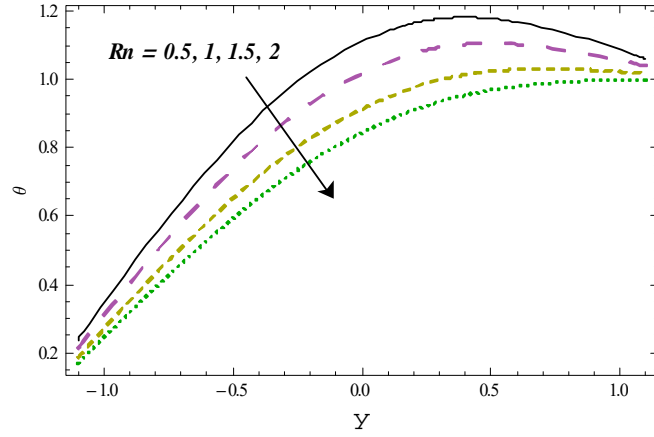


Fig. 7.7: Variation of Rn on θ

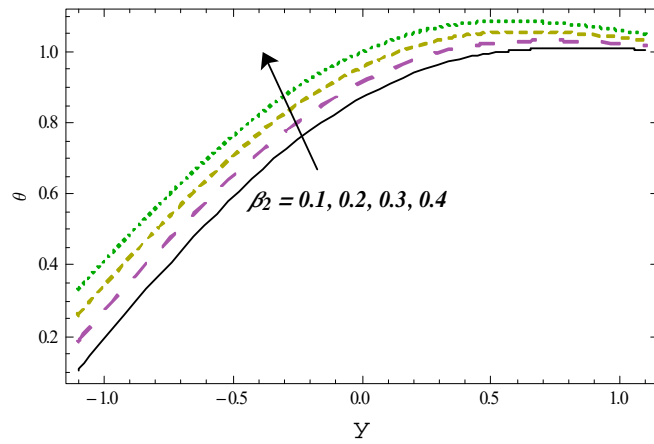


Fig. 7.8: Variation of β_2 on θ

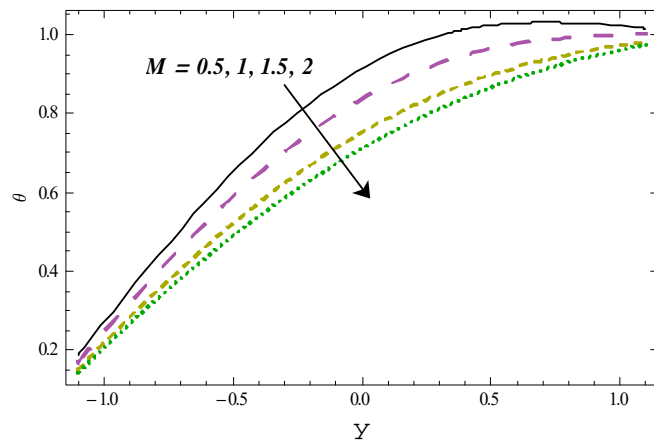


Fig. 7.9: Variation of M on θ

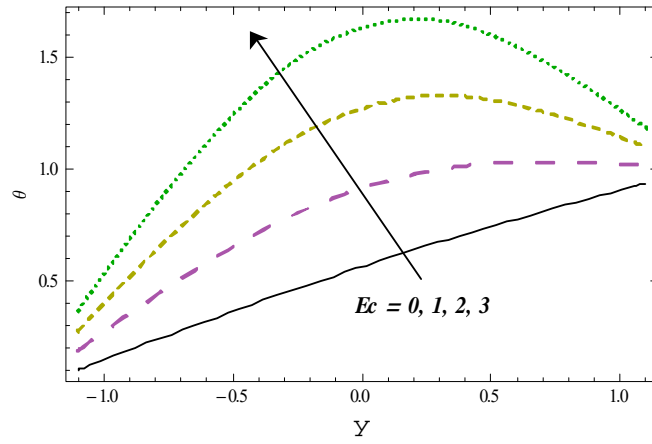


Fig. 7.10: Variation of Ec on θ

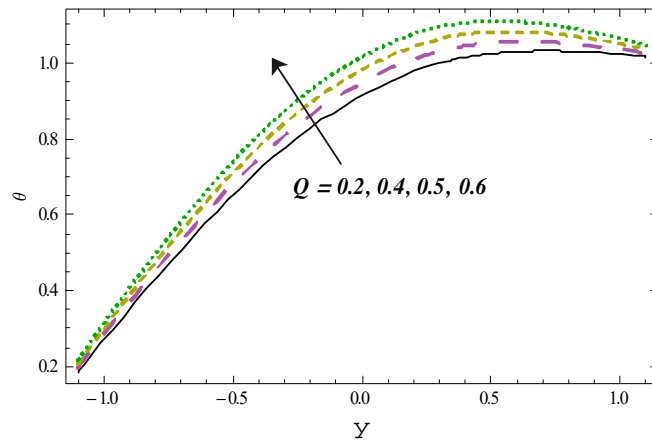


Fig. 7.11: Variation of $\dot{Q} > 0$ on θ

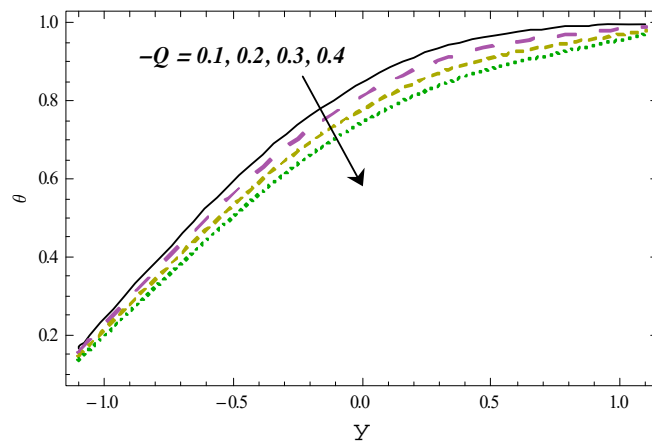


Fig. 7.12: Variation of $\dot{Q} < 0$ on θ

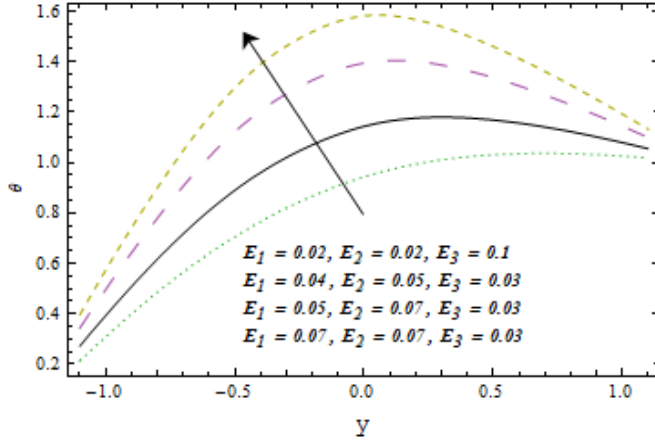


Fig. 7.13: Variations of E_1, E_2 and E_3 on θ

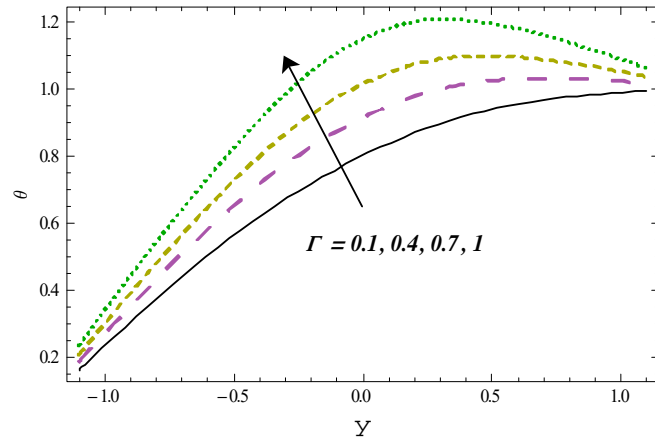


Fig. 7.14: Variation of Γ on θ

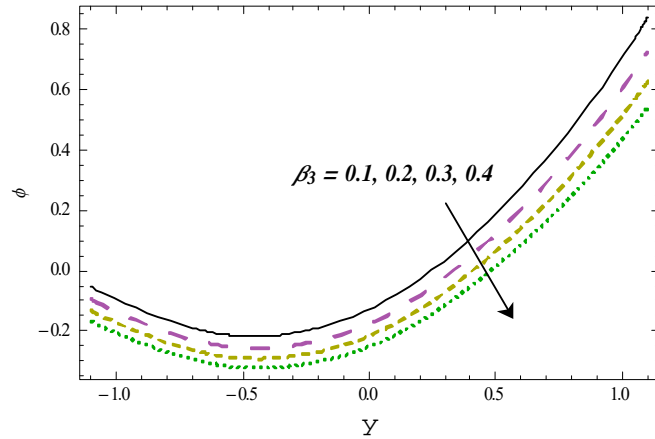


Fig. 7.15: Variation of β_3 on ϕ

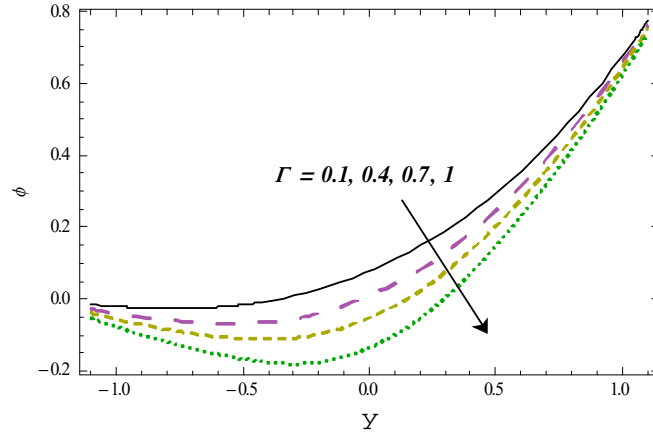


Fig. 7.16: Variation of Γ on ϕ

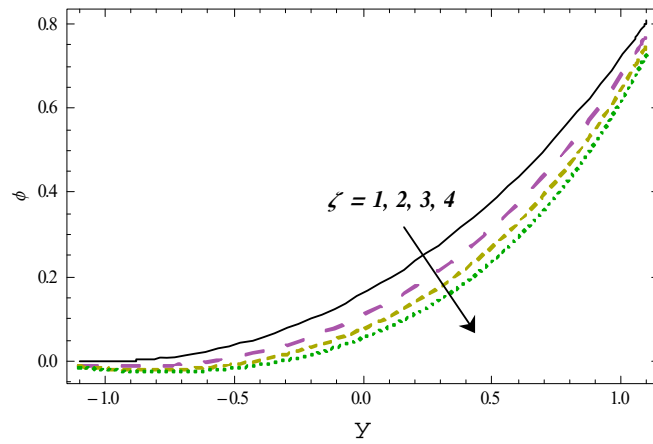


Fig. 7.17: Variation of ζ on ϕ

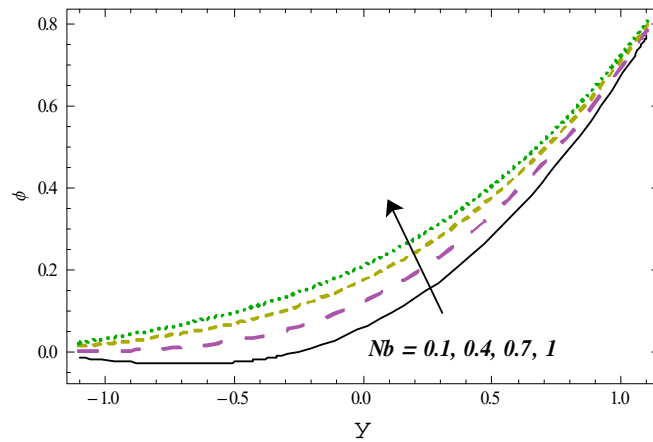


Fig. 7.18: Variation of Nb on ϕ

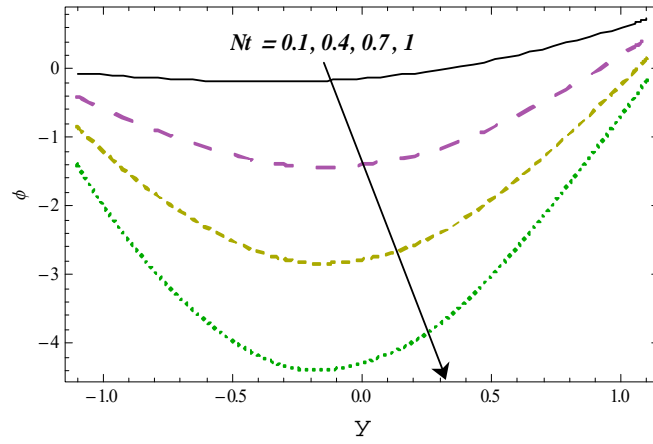


Fig. 7.19: Variation of Nt on ϕ

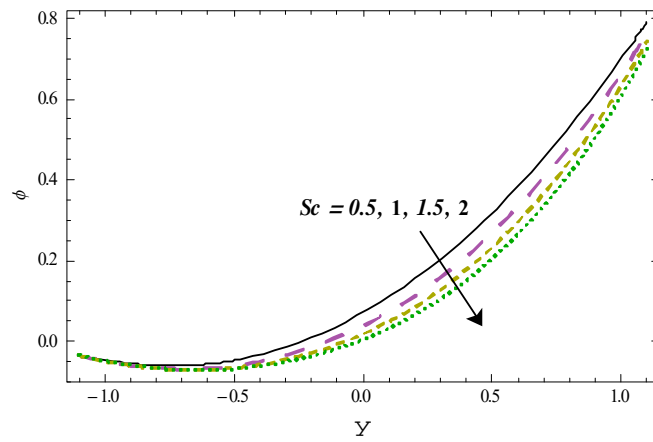


Fig. 7.20: Variation of Sc on ϕ

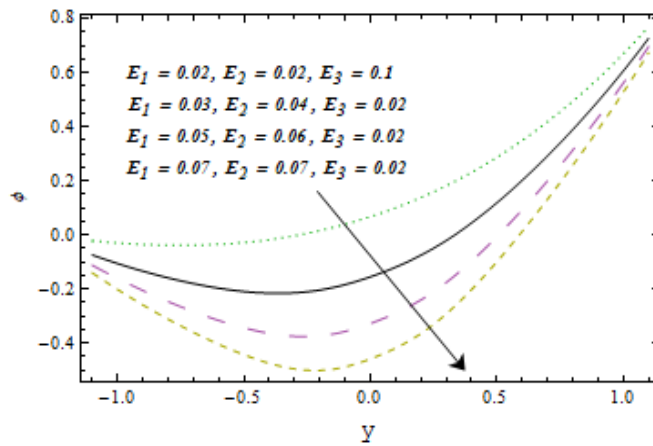


Fig. 7.21: Variations of E_1, E_2 and E_3 on ϕ

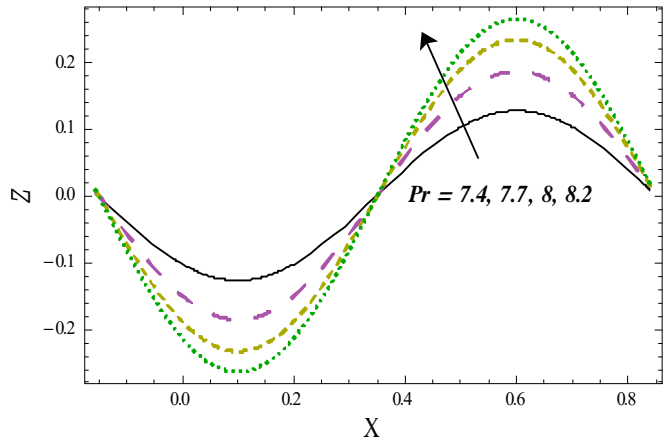


Fig. 7.22: Variation of Pr on Z

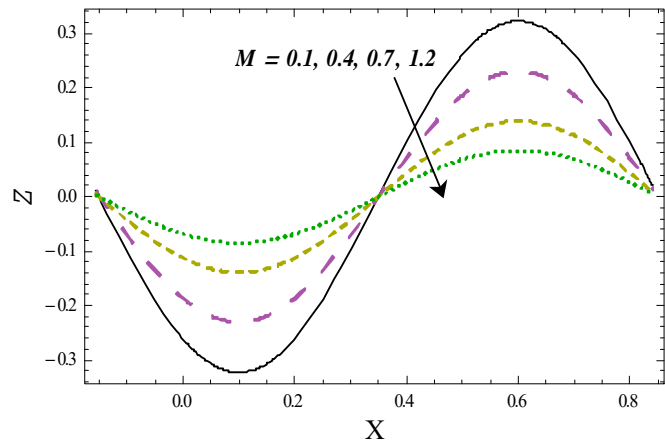


Fig. 7.23: Variation of M on Z

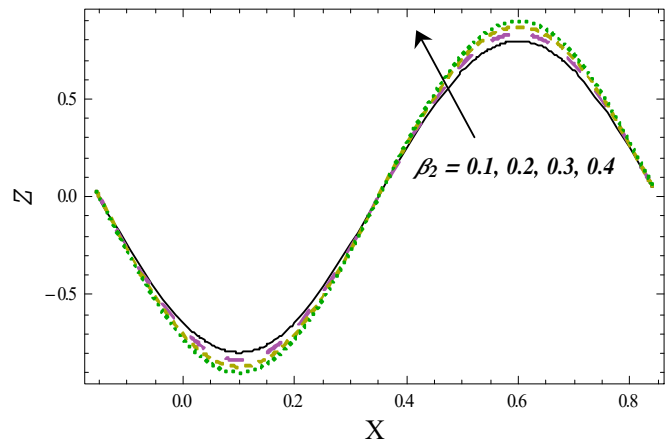


Fig. 7.24: Variation of β_2 on Z

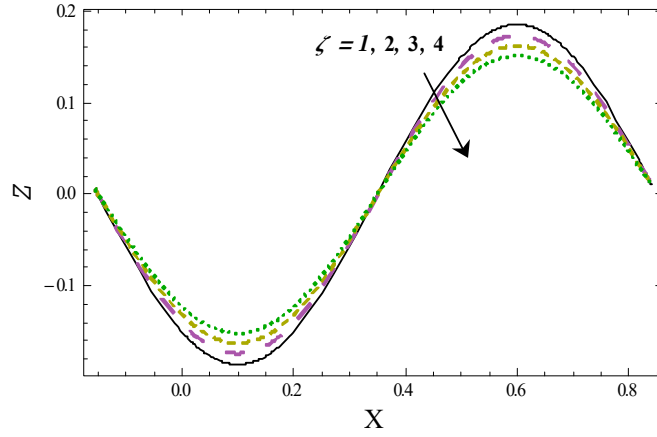


Fig. 7.25: Variation of ζ on Z

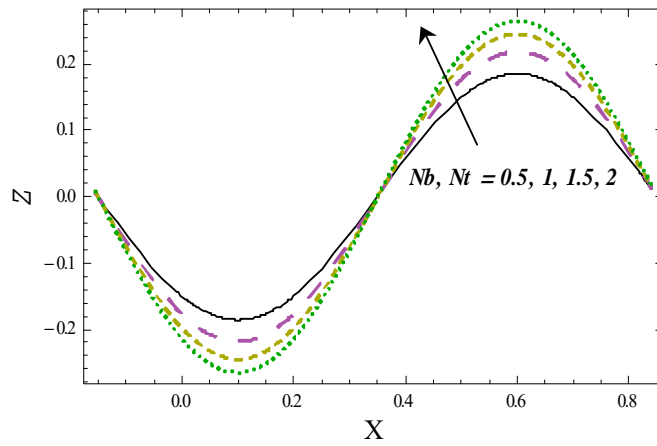


Fig. 7.27: Variations of Nb and Nt on Z

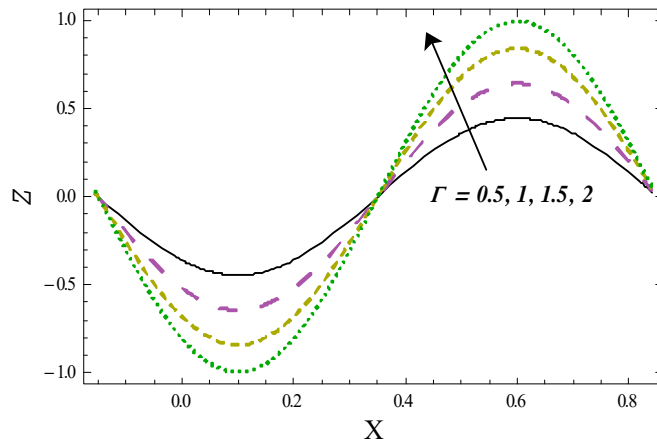


Fig. 7.28: Variation of Γ on Z

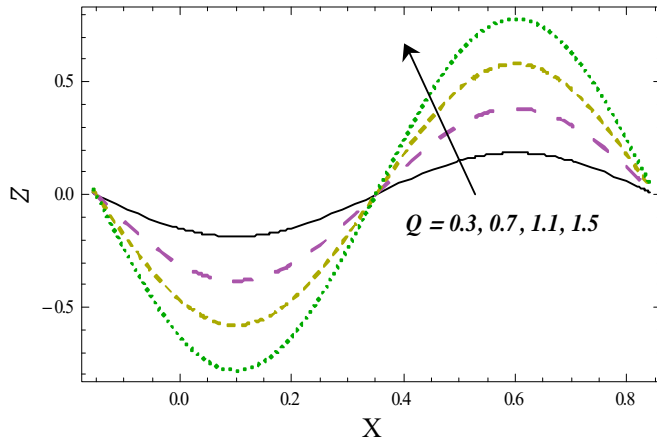


Fig. 7.29: Variation of $Q > 0$ on Z

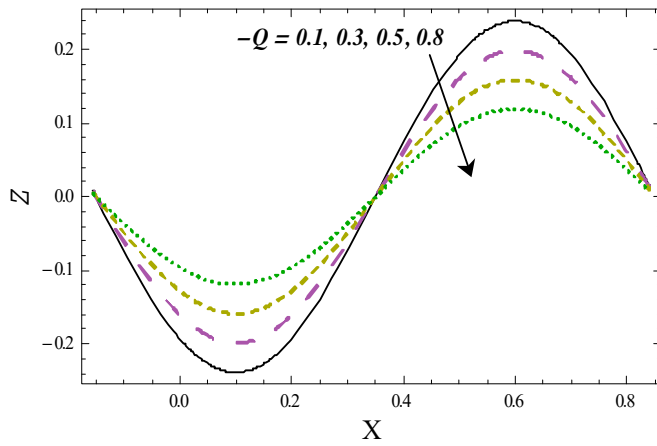


Fig. 7.30: Variation of $Q < 0$ on Z

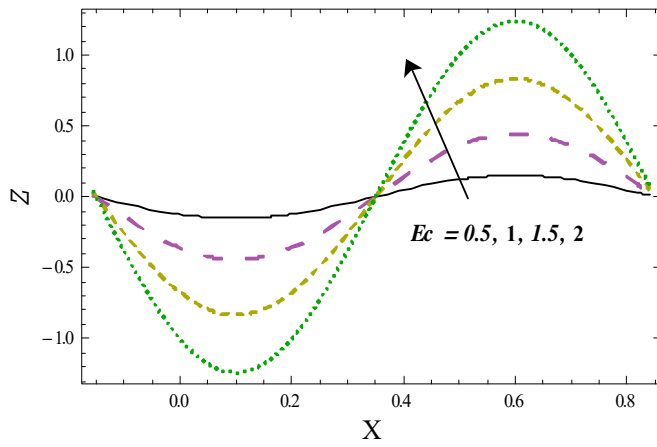


Fig. 7.31: Variation of Ec on Z

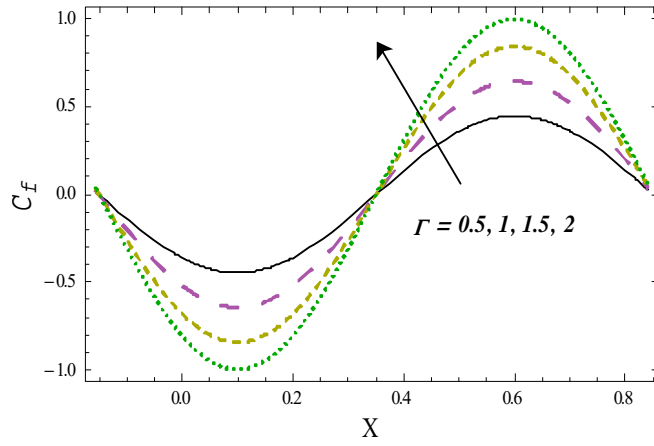


Fig. 7.32: Variation of Γ on C_f

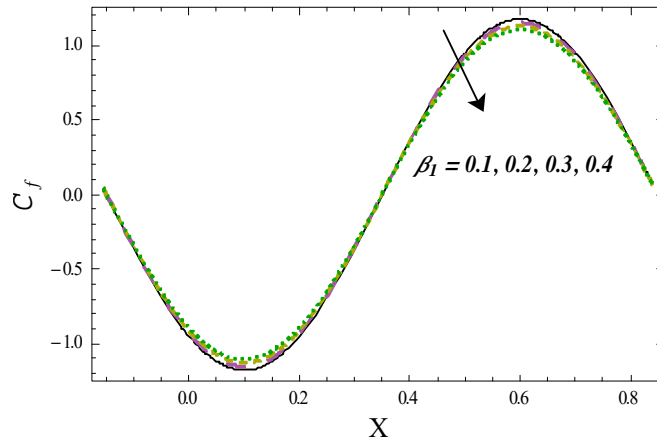


Fig. 7.33: Variation of β_1 on C_f

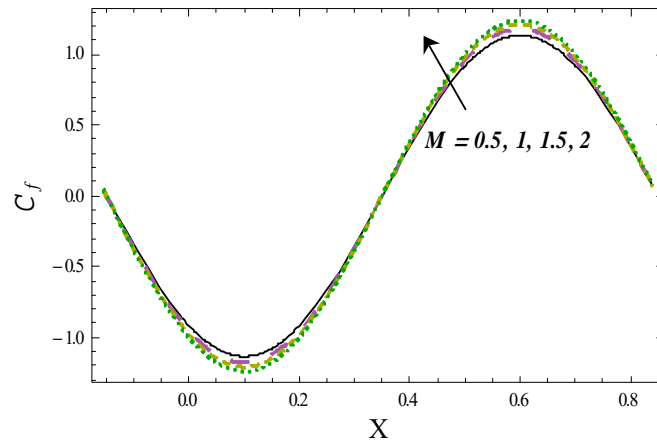


Fig. 7.34: Variation of M on C_f

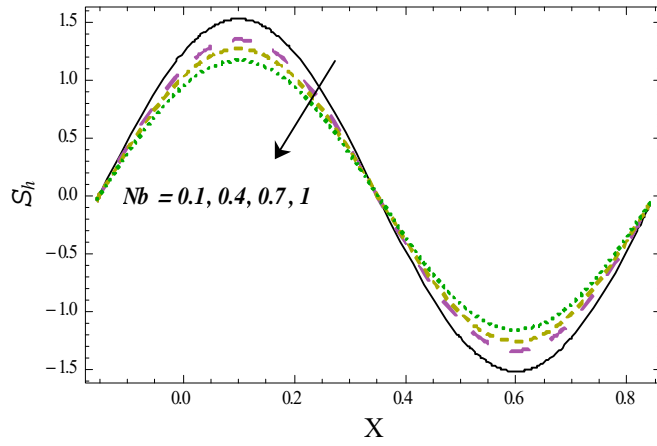


Fig. 7.35: Variation of Nb on S_h

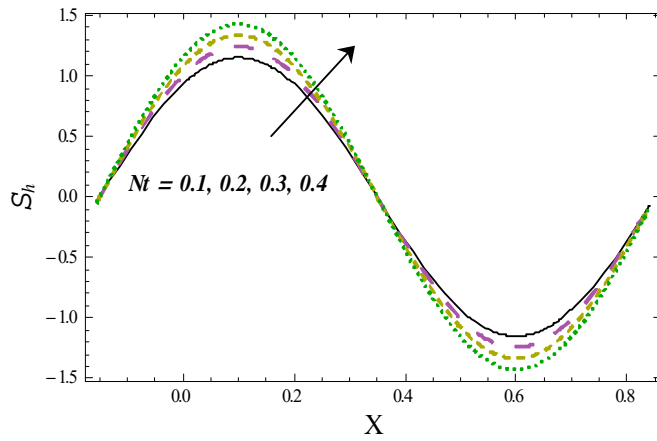


Fig. 7.36: Variation of Nt on S_h

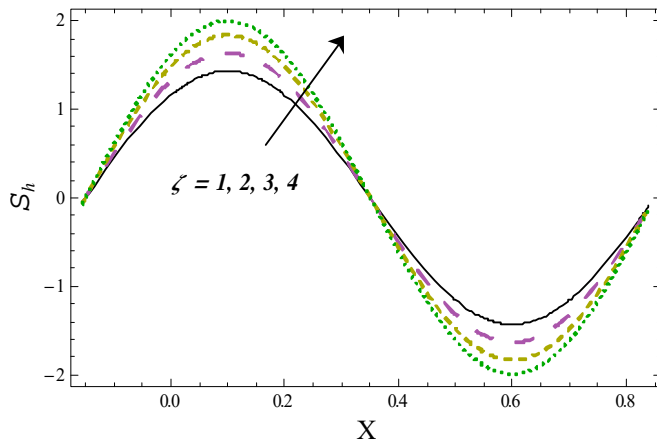


Fig. 7.37: Variation of ζ on S_h

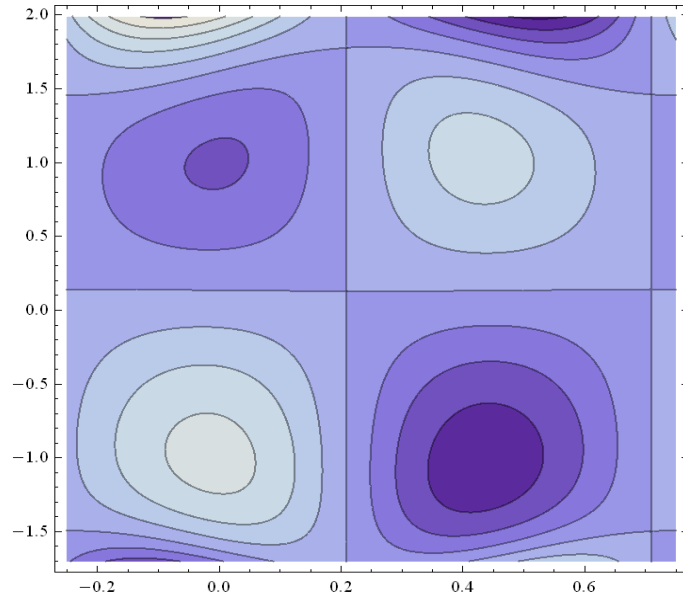


Fig. 7.38(a): Variation of ψ when $\Gamma = 0.1$.

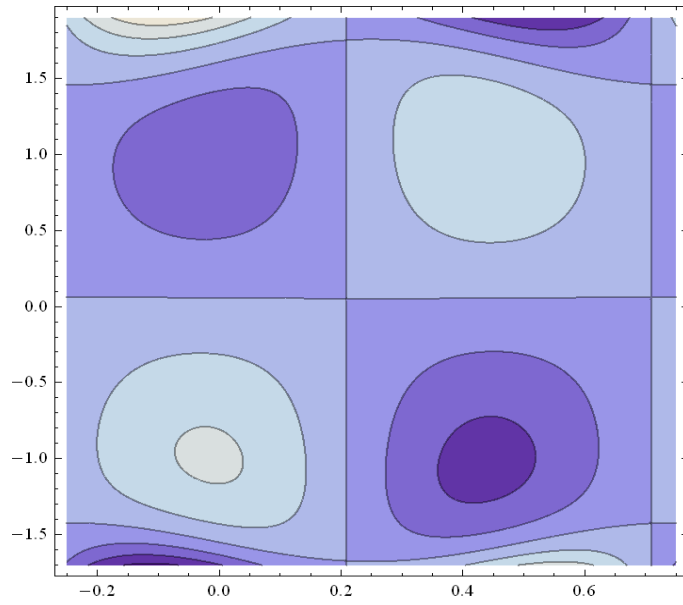


Fig. 7.38(b): Variation of ψ when $\Gamma = 0.3$.

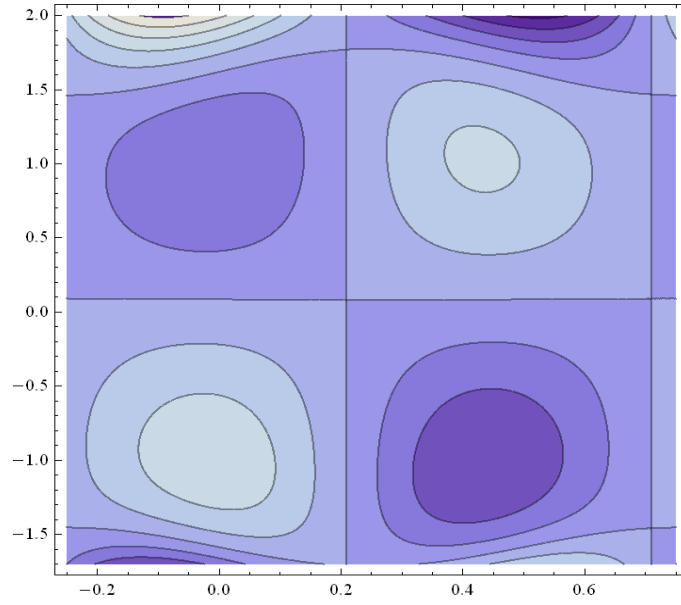


Fig. 7.39(a): Variation of ψ when $\beta_1 = 0.1$.

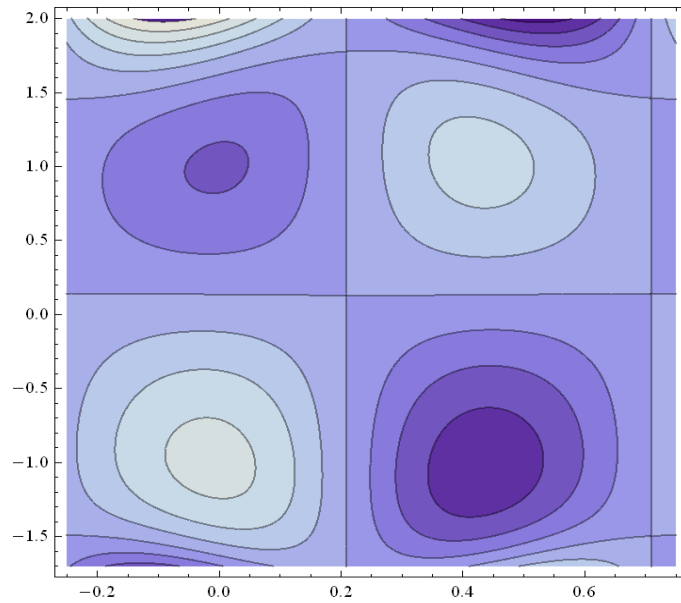


Fig. 7.39(b): Variation of ψ when $\beta_1 = 0.2$.

7.4 Conclusions

Following points are important.

- Velocity rfor M has reverse trend when compared with Γ and β_1 .

- Temperature and heat transfer coefficient increase with ($Q > 0$) while opposite holds for ($Q < 0$).
- Temperature for higher Nb and Nt has similar outcome.
- Temperature against Pr , Ec and Γ is enhanced.
- Effects of β_2 on temperature and β_3 on concentration are quite opposite.
- Higher ζ , Nt and Sc reduces the concentration.
- Heat transfer coefficient for Pr , Γ and β_2 is similar.
- Rn and M decreased heat transfer coefficient.
- Skin friction coefficient for Γ and β_1 is similar.
- Trapped bolus size declines for larger β_1 .

Chapter 8

Entropy generation in mixed convective peristalsis of fourth grade nanofluid

8.1 Introduction

The key emphasis here is to analyze of entropy generation in MHD peristaltic flow of fourth grade nanofluid. Activation energy, Hall current, mixed convection and slip features are considered. Related nonlinear differential system is solved numerically and analyzed.

8.2 Formulation

We have an interest to analyze the mixed convective peristalsis flow of fourth-grade nanofluid for outcomes of activation energy and Hall current. Following the notations of previous chapter we write directly the related system

$$\frac{\partial u}{\partial x} + \frac{\partial v}{\partial y} = 0, \quad (8.1)$$

$$\rho_f \left(\frac{\partial u}{\partial t} + u \frac{\partial u}{\partial x} + v \frac{\partial u}{\partial y} \right) = -\frac{\partial p}{\partial x} + \frac{\partial S_{xx}}{\partial x} + \frac{\partial S_{xy}}{\partial y} - \frac{\sigma B_0^2}{(1+m^2)}(u - mv) + g\rho_f\beta_T(T - T_0) + g\rho_f\beta_C(C - C_0), \quad (8.2)$$

$$\rho_f \left(\frac{\partial v}{\partial t} + u \frac{\partial v}{\partial x} + v \frac{\partial v}{\partial y} \right) = -\frac{\partial p}{\partial y} + \frac{\partial S_{yx}}{\partial x} + \frac{\partial S_{yy}}{\partial y} - \frac{\sigma B_0^2}{(1+m^2)}(v + mu), \quad (8.3)$$

$$\begin{aligned} \rho_f c_f \left(\frac{\partial T}{\partial t} + u \frac{\partial T}{\partial x} + v \frac{\partial T}{\partial y} \right) &= k \left(\frac{\partial^2 T}{\partial x^2} + \frac{\partial^2 T}{\partial y^2} \right) + \frac{\partial u}{\partial x} S_{xx} + \frac{\partial v}{\partial y} S_{yy} + \left(\frac{\partial u}{\partial y} + \frac{\partial v}{\partial x} \right) S_{xy} + \\ &\rho_p c_p \left[\left\{ \left(\frac{\partial T}{\partial x} \right)^2 + \left(\frac{\partial T}{\partial y} \right)^2 \frac{D_T}{T_m} \right\} + D_B \left(\frac{\partial C}{\partial x} \frac{\partial T}{\partial x} + \frac{\partial C}{\partial y} \frac{\partial T}{\partial y} \right) \right] + \\ &\frac{16\bar{\sigma}T_0^3}{3k} \frac{\partial^2 T}{\partial y^2} + \frac{\sigma B_0^2}{(1+m^2)}(u^2 + v^2). \end{aligned} \quad (8.4)$$

$$\begin{aligned} \frac{\partial C}{\partial t} + u \frac{\partial C}{\partial x} + v \frac{\partial C}{\partial y} &= D_B \left(\frac{\partial^2 C}{\partial x^2} + \frac{\partial^2 C}{\partial y^2} \right) + \frac{D_T}{T_m} \left(\frac{\partial^2 T}{\partial x^2} + \frac{\partial^2 T}{\partial y^2} \right) - \\ &k_r^2 (C - C_0) \left(\frac{T}{T_0} \right)^n \exp \left(-\frac{E_a}{\kappa T} \right). \end{aligned} \quad (8.5)$$

The boundary conditions are

$$u \pm \beta_1 S_{xy} = 0 \quad \text{at } y = \pm\eta, \quad (8.6)$$

$$\begin{aligned} \left[-\tau_1 \frac{\partial^3}{\partial x^3} + m_1 \frac{\partial^3}{\partial x \partial t^2} + d \frac{\partial^2}{\partial t \partial x} \right] \eta &= \frac{\partial S_{xx}}{\partial x} + \frac{\partial S_{xy}}{\partial y} - \rho_f \left(\frac{\partial u}{\partial t} + u \frac{\partial u}{\partial x} + v \frac{\partial u}{\partial y} \right) - \\ &\frac{\sigma B_0^2}{(1+m^2)}u + g\rho_f\beta_T(T - T_0) + g\rho_f\beta_C(C - C_0) \quad \text{at } y = \pm\eta. \end{aligned} \quad (8.7)$$

$$T \pm \beta_2 \frac{\partial T}{\partial y} = \left\{ \begin{matrix} T_1 \\ T_0 \end{matrix} \right\}, \quad C \pm \beta_3 \frac{\partial C}{\partial y} = \left\{ \begin{matrix} C_1 \\ C_0 \end{matrix} \right\} \quad \text{at } y = \pm\eta, \quad (8.8)$$

in which $(\beta_1, \beta_2, \beta_3)$ the slip parameters, T_m the mean temperature, E_a the activation energy, k_r the chemical reaction rate, n the fitted rate constant, κ the Boltzmann constant and (T_1, T_0) and (C_1, C_0) respectively the upper and lower walls temperature and concentration. Here m the Hall parameter.

Taking stream functions $u = \psi_y$, $v = -\delta\psi_x$ and setting

$$\begin{aligned}
u &= cu^*, \quad v = cv^*, \quad x = \lambda x^*, \quad y = d_1 y^*, \quad ct = \lambda t^*, \quad \eta = d_1 \eta, \\
d_1^2 p &= c\lambda\mu p^*, \quad d_1 \beta_i^* = \beta_i (i = 1 - 3), \quad (T_1 - T_0)\theta = T - T_0, \\
c\mu S_{ij}^* &= d_1 S_{ij}, \quad \mu d_1 \alpha_i^* = \alpha_i' c, \quad \mu d_1^2, \quad (C_1 - C_0)\phi = C - C_0, \\
\beta_i^* &= \beta_i' c^2, \quad \mu d_1^3 \gamma_i^* = \gamma_i' c^3.
\end{aligned} \tag{8.9}$$

one arrives at

$$\frac{\partial^2}{\partial y^2} \left(\frac{\partial^2 \psi}{\partial y^2} + 2\Gamma \left(\frac{\partial^2 \psi}{\partial y^2} \right)^3 \right) - \left(\frac{M^2}{1+m^2} \right) \frac{\partial^2 \psi}{\partial y^2} + Gr \frac{\partial \theta}{\partial y} + Gc \frac{\partial \phi}{\partial y} = 0, \tag{8.10}$$

$$\begin{aligned}
&\left(\frac{1}{Pr} + Rn \right) \frac{\partial^2 \theta}{\partial y^2} + Nb \left(\frac{\partial \phi}{\partial y} \right) \left(\frac{\partial \theta}{\partial y} \right) + Nt \left(\frac{\partial \theta}{\partial y} \right)^2 + \\
&Ec \frac{\partial^2 \psi}{\partial y^2} \left[\frac{\partial^2 \psi}{\partial y^2} + 2\Gamma \left(\frac{\partial^2 \psi}{\partial y^2} \right)^3 \right] + \frac{M^2 Ec}{1+m^2} \left(\frac{\partial \psi}{\partial y} \right)^2 = 0,
\end{aligned} \tag{8.11}$$

$$\frac{\partial^2 \phi}{\partial y^2} + \left(\frac{\partial^2 \theta}{\partial y^2} \right) \frac{Nt}{Nb} - Sc\zeta(1 + (\Omega - 1)\theta)^n \exp \left(-\frac{E}{1 + (\Omega - 1)\theta} \right) \phi = 0, \tag{8.12}$$

boundary conditions become

$$\frac{\partial \psi}{\partial y} \pm \beta_1 \left[\frac{\partial^2 \psi}{\partial y^2} + 2\Gamma \left(\frac{\partial^2 \psi}{\partial y^2} \right)^3 \right] = 0 \text{ at } y = \pm \eta, \tag{8.13}$$

$$\begin{aligned}
&\left[E_1 \frac{\partial^3}{\partial x^3} + E_2 \frac{\partial^3}{\partial x \partial t^2} + E_3 \frac{\partial^2}{\partial x \partial t} \right] \eta = \frac{\partial^3 \psi}{\partial y^3} + 6\Gamma \left(\left(\frac{\partial^2 \psi}{\partial y^2} \right)^2 \frac{\partial^3 \psi}{\partial y^3} \right) \\
&- \left(\frac{M^2}{1+m^2} \right) \frac{\partial \psi}{\partial y} + Gr\theta + Gc\phi \text{ at } y = \pm \eta,
\end{aligned} \tag{8.14}$$

$$\theta \pm \beta_2 \frac{\partial \theta}{\partial y} = \left\{ \begin{matrix} 1 \\ 0 \end{matrix} \right\}, \quad \phi \pm \beta_3 \frac{\partial \phi}{\partial y} = \left\{ \begin{matrix} 1 \\ 0 \end{matrix} \right\} \text{ at } y = \pm \eta. \tag{8.15}$$

Here $Gr \left(= \frac{g\rho_f \beta_T (\Gamma - T_0) d_1^2}{\mu c} \right)$ thermal Grashof number, $Gc \left(= \frac{g\rho_f \beta_C (C - C_0) d_1^2}{\mu c} \right)$ concentration Grashof number, $\left(\Gamma = \beta_2' + \beta_3' \right)$ the Deborah number, $\Omega \left(= \frac{T_1}{T_0} \right)$ the temperature ratio parameter, $E \left(= -\frac{E_a}{\kappa T_0} \right)$ the activation energy parameter and $\zeta \left(= \frac{k_1 d_1^2}{\nu} \right)$ the chemical reaction parameter.

8.3 Numerical results

The system (8.10) – (8.12) with appropriate conditions (8.13) – (8.15) is simulated by NDSolve in MATHEMATICA.

8.3.1 Velocity

The impacts of various physical variables on velocity are shown in Figs. 8.1 – 8.5. Fig. 8.1 exhibits that velocity of fluid enhances by increasing thermal Grashof parameter Gr . Fig. 8.2 shows consequence of velocity for several values of mass Grashof number Gc . Decreasing trend is noticed for velocity via larger Gc . Fig. 8.3 describes velocity against Hall variable m . It is obvious from this Fig. that velocity increases by rising values of m . The consequences of β_1 via velocity is portrayed in Fig. 8.4. Velocity of the fluid increases by higher β_1 . Fig. 8.5 shows the relationship between Deborah number Γ and velocity. We noticed decreasing activity of velocity with higher Γ .

8.3.2 Temperature

Variation of pertinent variables on temperature is presented in Figs. 8.6 – 8.9. Consequence of thermal Grashof variable Gr is demonstrated in Fig. 8.6. Here temperature increases via larger Gr . Hall parameter m versus temperature is portrayed in Fig. 8.7. We found that temperature is more via higher m . Fig. 8.8. is plotted to see the effect of thermal slip variable β_2 against temperature. Result shows an increment of temperature. Influence of fourth grade fluid variable Γ is exhibited in Fig. 8.9. Larger values of Γ shows an increase in temperature.

8.3.3 Concentration

Figs. 8.10 – 8.12 are sketched for behavior of concentration. Fig. 8.10 reveals the influence of activation energy parameter E . It is evident from this Fig. that concentration is enhanced via larger E . Fig. 8.11 summarized effects of mass Grashof number Gc on concentration ϕ . A decreasing trend is noted for ϕ when Gc rises. The inspiration of concentration slip parameter β_3 over concentration is scrutinized in Fig. 8.12. An increment in β_3 causes declines of concentration.

8.3.4 Heat transfer coefficient

Figs. 8.13–8.15 are portrayed to see the impacts of coefficient of heat transfer $Z(x) = \eta_x \theta_y(\eta)$. Influence of activation energy parameter E on Z is pictured in Fig. 8.13. Here Z is enhanced for larger E . Fig. 8.14 showed the impact of thermal Grashof number Gr on coefficient of heat transfer. We observed that higher Gr leads to an enhancement of Z . Fig. 8.15 represents the impact of Hall parameter m on Z . An increase in Z is observed for higher m .

8.3.5 Entropy

Entropy is explored here. Impact of coefficient of diffusion L is displayed in Fig. 8.16. Increased L causes thermal conductivity to decrease. The temperature and entropy increase is apparent. Impacts of Hall parameter m versus entropy is displayed in Fig. 8.17. There is a decreasing trend in entropy. Variation of temperature difference variable Λ on entropy is outlined in Fig. 8.18. Entropy of fluid decreases when Λ rises. Influence of concentration difference variable γ^* on entropy Ns is revealed in Fig. 8.19. This Fig. designates that the entropy of fluid increased. Fig. 8.20 is plotted to see the consequence of thermal Grashof number Gr . Here Ns enhances for higher Gr . Entropy Ns versus activation energy E is depicted in Fig. 8.21. Here we found entropy increase through larger E . Fourth-grade fluid parameter Γ outcome on entropy is notified in Fig. 8.22. Entropy of fluid enhances for larger Γ . Implementation of entropy with a Brinkman number Br is illustrated in Fig. 8.23. We found that increasing Br enhanced entropy. Fig. 8.24 is prepared for radiation parameter Rn against entropy. By higher Rn the entropy of fluid boosts.

8.4 Expression for entropy generation

Mathematically the entropy generation satisfies:

$$\begin{aligned}
 S'''_{gen} = & \frac{k}{T_m^2} \left(\left(\frac{\partial T}{\partial x} \right)^2 + \left(\frac{\partial T}{\partial y} \right)^2 + \frac{16\sigma^* T_0^3}{3k^* k} \left(\frac{\partial T}{\partial y} \right)^2 \right) + \frac{\sigma B_0^2}{T_m(1+m^2)} u^2 + \frac{\Phi}{T_m} \\
 & + \frac{RD}{C_m} \left(\left(\frac{\partial C}{\partial x} \right)^2 + \left(\frac{\partial C}{\partial y} \right)^2 \right) + \frac{RD}{T_m} \left(\frac{\partial C}{\partial x} \frac{\partial T}{\partial x} + \frac{\partial C}{\partial y} \frac{\partial T}{\partial y} \right). \quad (8.16)
 \end{aligned}$$

Viscous dissipation Φ is given by

$$\Phi = S_{xx} \frac{\partial u}{\partial x} + S_{yy} \frac{\partial v}{\partial y} + S_{xy} \left(\frac{\partial v}{\partial x} + \frac{\partial u}{\partial y} \right). \quad (8.17)$$

In dimensionless form we have

$$\begin{aligned} Ns &= \frac{S_{gen}'''}{S_G'''} = (1 + Rn) \left(\frac{\partial \theta}{\partial y} \right)^2 + \frac{L}{\Lambda} \left(\frac{\partial \theta}{\partial y} \right) \left(\frac{\partial \phi}{\partial y} \right) + \frac{L\gamma^*}{\Lambda^2} \left(\frac{\partial \phi}{\partial y} \right)^2 \\ &\quad + \frac{Br}{\Lambda} S_{xy} \frac{\partial^2 \psi}{\partial y^2} + \frac{BrM^2}{\Lambda(1+m^2)} \left(\frac{\partial \psi}{\partial y} \right)^2, \end{aligned} \quad (8.18)$$

where

$$S_G''' = \frac{k(T_1 - T_0)^2}{T_m^2 a^2}, \quad \Lambda = \frac{T_1 - T_0}{T_m}, \quad \gamma^* = \frac{C_1 - C_0}{C_m}, \quad L = \frac{RD(C_1 - C_0)}{k}. \quad (8.19)$$

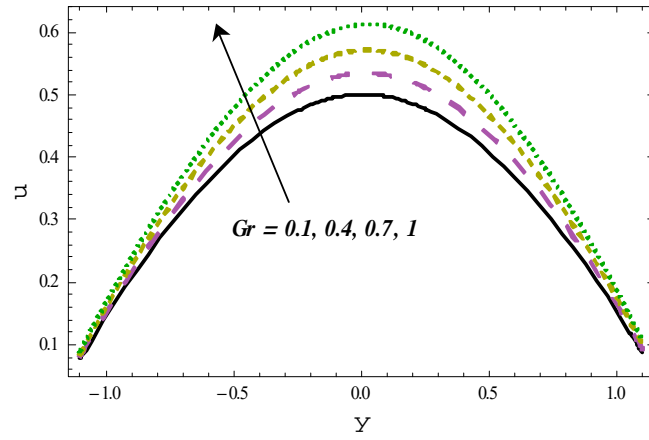


Fig. 8.1: Variation of Gr on u

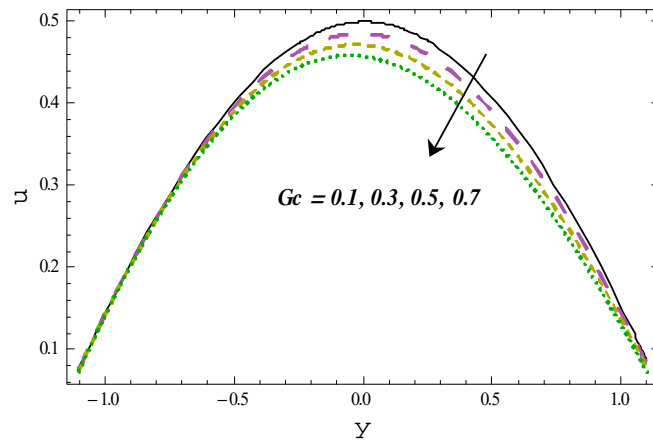


Fig. 8.2: Variation of Gc on u

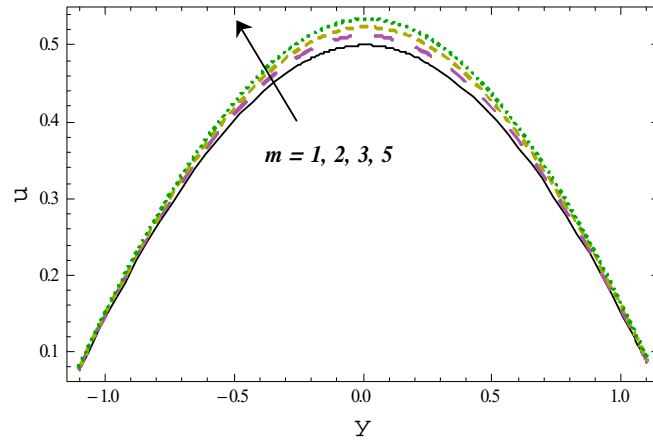


Fig. 8.3: Variation of m on u

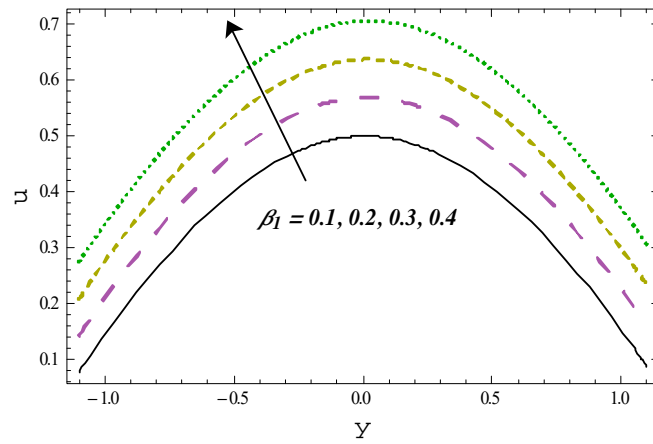


Fig. 8.4: Variation of β_1 on u

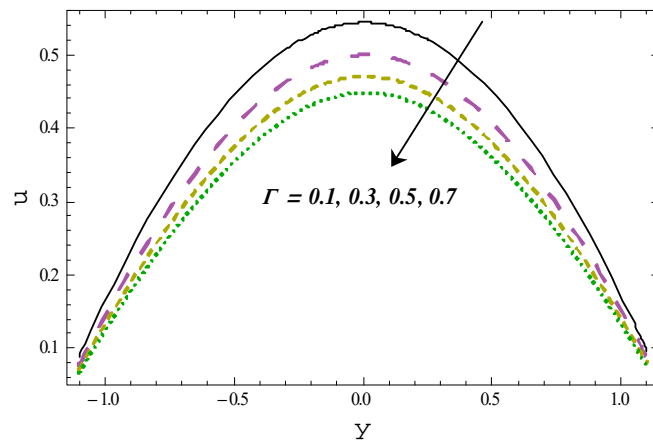


Fig. 8.5: Variation of Γ on u

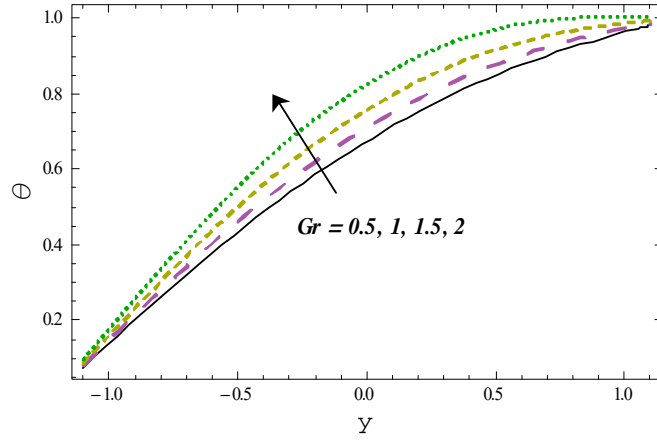


Fig. 8.6: Variation of Gr on θ

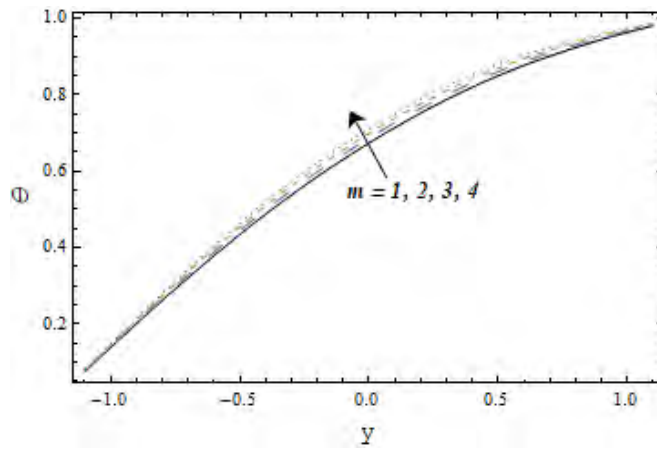


Fig. 8.7: Variation of m on θ

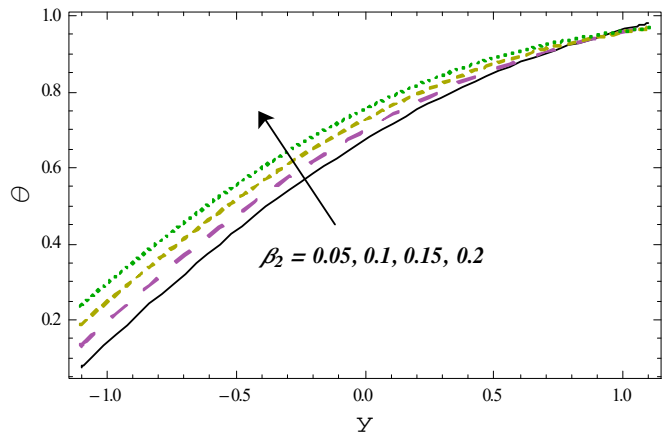


Fig. 8.8: Variation of β_2 on θ

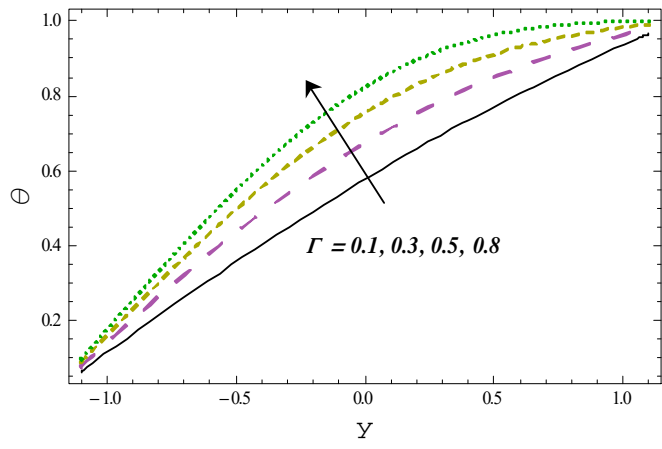


Fig. 8.9: Variation of Γ on θ

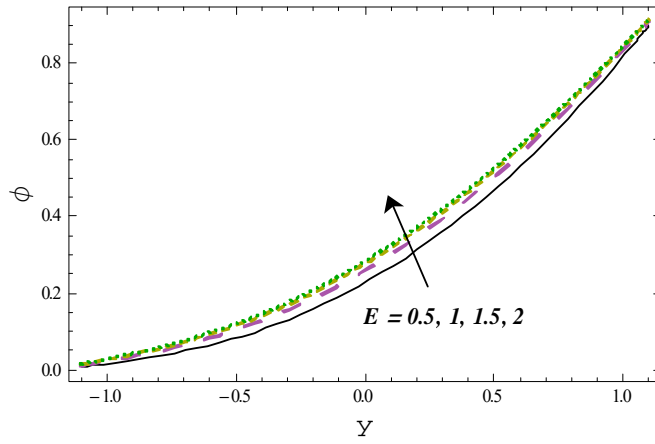


Fig. 8.10: Variation of E on ϕ

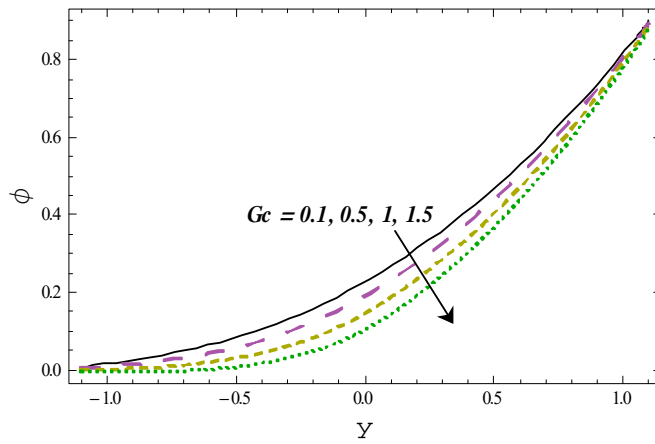


Fig. 8.11: Variation of Gc on ϕ

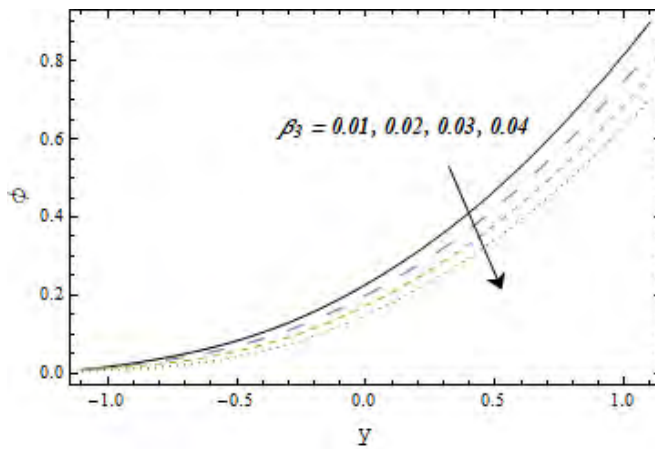


Fig. 8.12: Variation of β_3 on ϕ

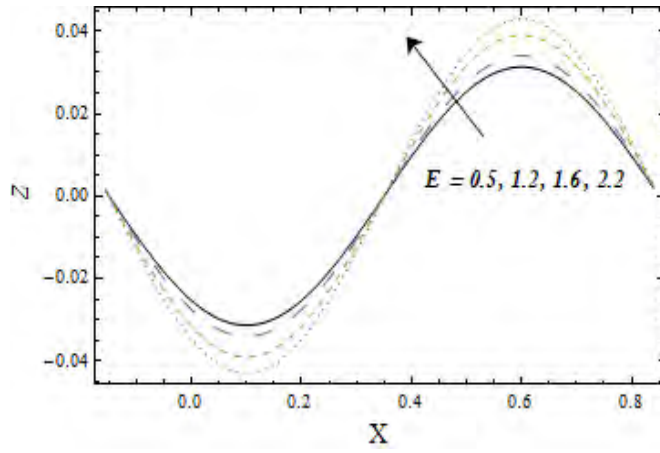


Fig. 8.13: Variation of E on Z

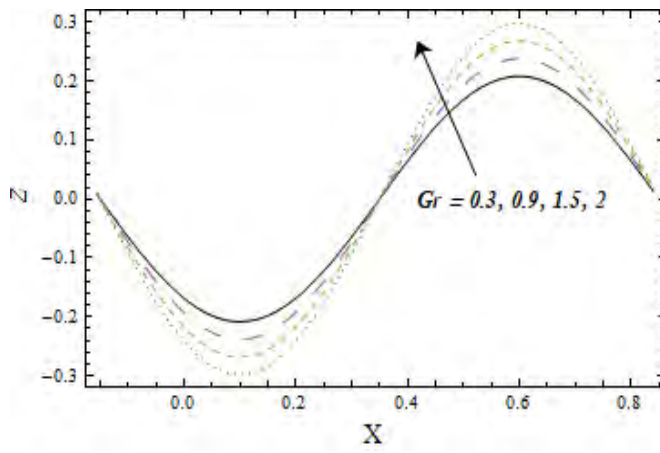


Fig. 8.14: Variation of Gr on Z

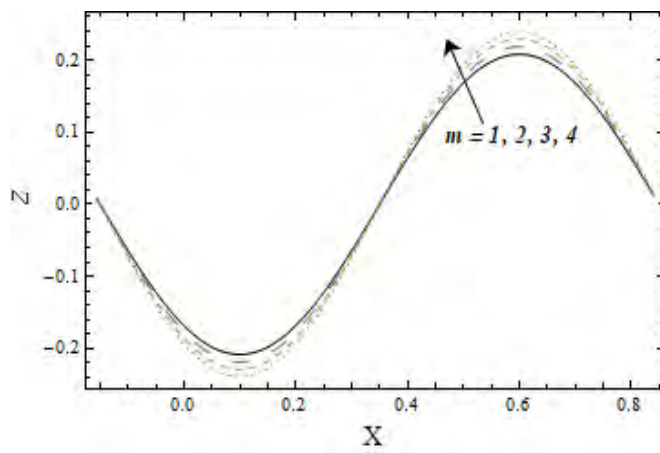


Fig. 8.15: Variation of m for Z

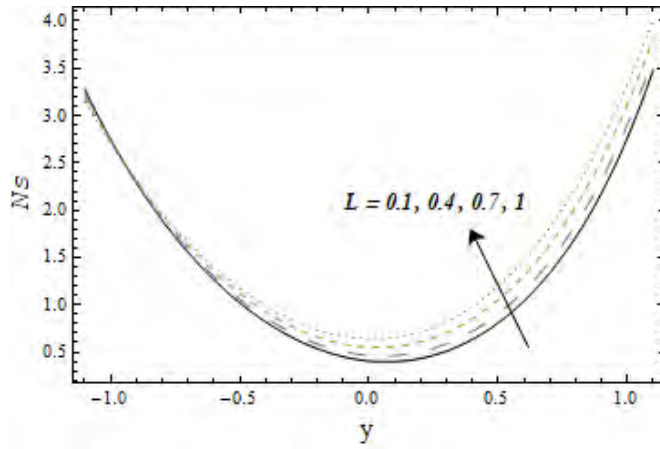


Fig. 8.16: Variation of L on Ns

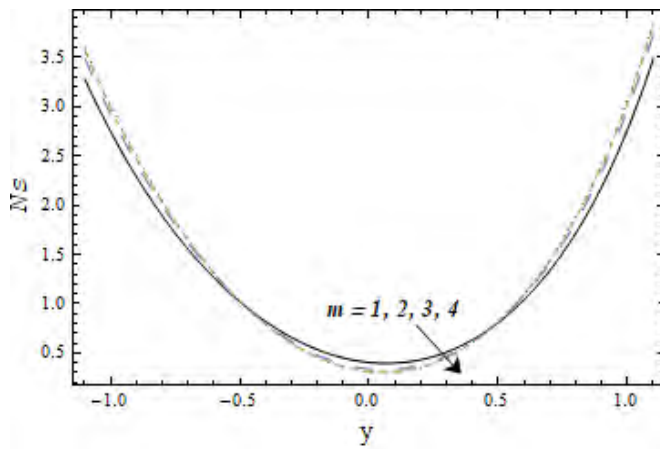


Fig. 8.17: Variation of m on Ns

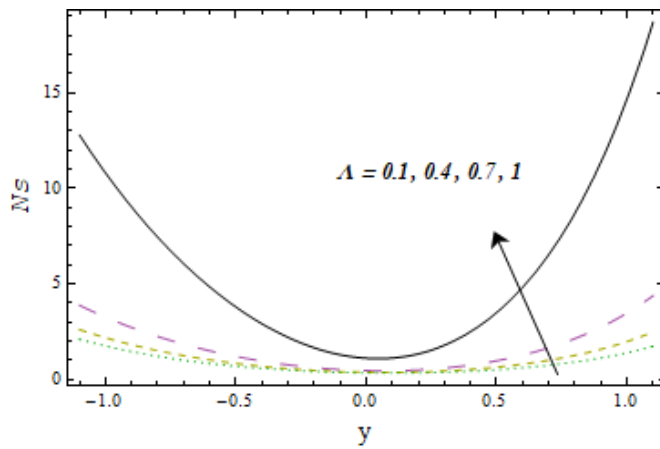


Fig. 8.18: Variation of Λ on Ns

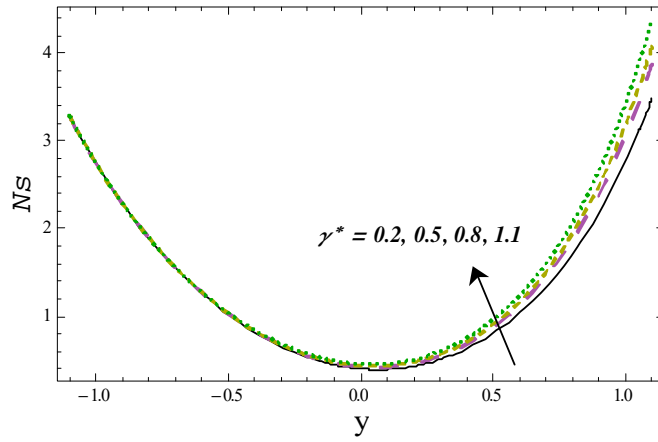


Fig. 8.19: Variation of γ^* on Ns

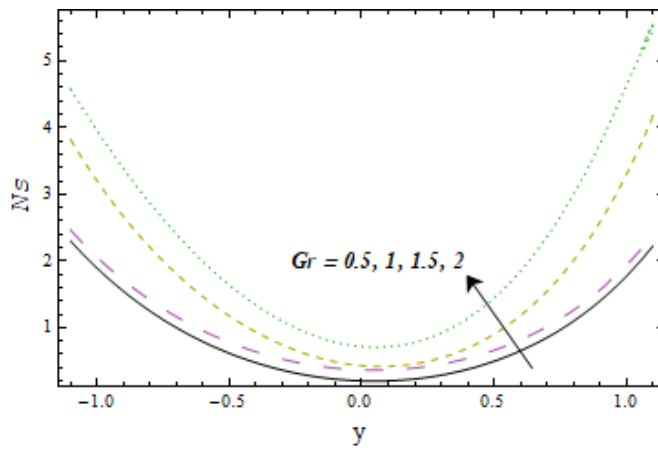


Fig. 8.20: Variation of Gr on Ns

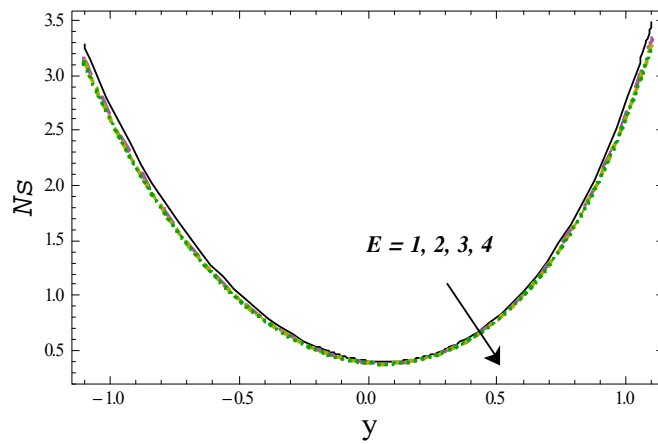


Fig. 8.21: Variation of E on Ns

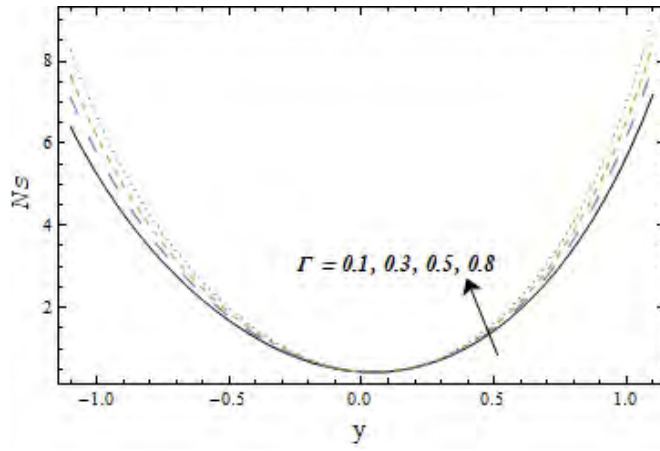


Fig. 8.22: Variation of Γ on Ns

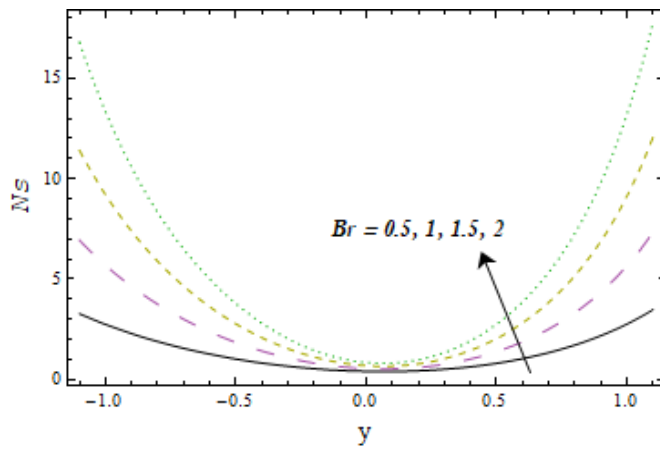


Fig. 8.23: Variation of Br on Ns

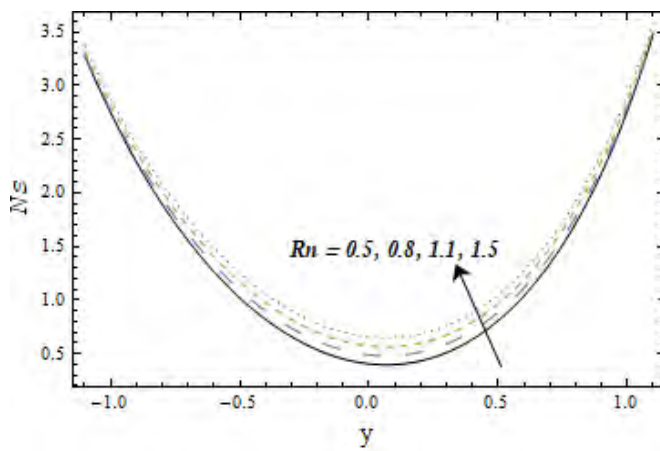


Fig. 8.24: Variation of Rn on Ns

8.5 Conclusions

The salient points about current study are given below.

- Velocity for Γ is opposite when compared with Gr and β_1 .
- Temperature enhances for m .
- Temperature of the fluid decreases by Rn .
- Behaviors of activation energy E on ϕ and Z are similar.
- Higher Gc and β_3 lead to decay in concentration.
- Entropy enhances for larger L and γ .
- Reverse behavior of Ns is noticed for Gr and E .

Chapter 9

Peristaltic activity of hyperbolic tangent nanofluid with non-linear radiation

9.1 Introduction

Here we investigate magnetohydrodynamic (MHD) peristalsis of hyperbolic tangent nanomaterial with mixed convection. Partial slip constraints on flexible channel walls are employed. Heat transfer analysis is accounted with viscous dissipation and Ohmic heating. Chemical reaction and nonlinear thermal radiation are accounted. Buongiorno's nanoliquid model is employed by considering the aspects of Brownian movement and thermophoresis. Appropriate use of long wavelength and small Reynolds approximation is made. System is numerically solved. The outcomes for the velocity, concentration, temperature and heat transfer rate for different physical variables are addressed through graphs.

9.2 Formulation

Two-dimensional flow of tangent hyperbolic nanofluid in a symmetric channel of width $2d_1$ is considered. Here we choose Cartesian coordinates (x, y) . Waves are propagating in x -direction with constant speed c having amplitude a and wavelength λ . Channel boundaries are taken of

compliant nature. Fluid is conducted by involvement of a constant magnetic field of strength B_0 . Magnetic field induced is ignored. Velocity, thermal and concentration slip conditions are imposed on channel walls. The lower and upper walls have concentrations C_0, C_1 and temperatures T_0, T_1 respectively. Heat transfer analysis involved the effects of viscous dissipation, Brownian motion, thermophoresis along with nonlinear radiation. First order chemical reaction is present in the concentration equation. The channel walls are represented by:

$$y = \pm\eta(x, t) = \pm[d_1 + a \sin \frac{2\pi}{\lambda}(x - ct)]. \quad (9.1)$$

Stress tensor \mathbf{S} for hyperbolic tangent liquid is outlined by [44]

$$\mathbf{S} = \left[\mu_\infty + (\mu_\infty + \mu_0) \tanh(\Gamma/\dot{\gamma})^n \right] \dot{\gamma}, \quad (9.2)$$

$$\dot{\gamma} = \sqrt{\frac{1}{2} \text{trace} \mathbf{A}_1^2}, \quad (9.3)$$

$$\mathbf{A}_1 = (\text{grad } V) + (\text{grad } V)^t. \quad (9.4)$$

We consider in this case the infinite shear rate viscosity $\mu_\infty = 0$ and $\Gamma/\dot{\gamma} < 1$. Thus (9.2) takes the form

$$S = \left[\mu_0 (\Gamma/\dot{\gamma})^n \right] \dot{\gamma} = \left[\mu_0 (1 + n(\Gamma/\dot{\gamma} - 1)) \right] \dot{\gamma}, \quad (9.5)$$

where $\Gamma/\dot{\gamma}$ denote material constants, n the power law index, μ_0 the zero shear rate viscosity and \mathbf{A}_1 the first Rivlin Ericksen tensor. The related expressions are

$$\frac{\partial u}{\partial x} + \frac{\partial v}{\partial y} = 0, \quad (9.6)$$

$$\begin{aligned} \rho_f \left(\frac{\partial u}{\partial t} + u \frac{\partial u}{\partial x} + v \frac{\partial u}{\partial y} \right) &= -\frac{\partial p}{\partial x} + \frac{\partial S_{xx}}{\partial x} + \frac{\partial S_{xy}}{\partial y} - \sigma B_0^2 u \\ g\rho_f \beta_T (T - T_0) + g\rho_f \beta_C (C - C_0), \end{aligned} \quad (9.7)$$

$$\rho_f \left(\frac{\partial v}{\partial t} + u \frac{\partial v}{\partial x} + v \frac{\partial v}{\partial y} \right) = -\frac{\partial p}{\partial y} + \frac{\partial S_{yx}}{\partial x} + \frac{\partial S_{yy}}{\partial y}, \quad (9.8)$$

$$\begin{aligned}
\rho_f c_f \left(\frac{\partial T}{\partial t} + u \frac{\partial T}{\partial x} + v \frac{\partial T}{\partial y} \right) &= k \left(\frac{\partial^2 T}{\partial y^2} + \frac{\partial^2 T}{\partial x^2} \right) + \frac{\partial u}{\partial x} S_{xx} + \frac{\partial v}{\partial y} S_{yy} + \left(\frac{\partial u}{\partial y} + \frac{\partial v}{\partial x} \right) S_{xy} \\
+ \rho_p c_p \left[\frac{D_T}{T_m} \left\{ \left(\frac{\partial T}{\partial y} \right)^2 + \left(\frac{\partial T}{\partial x} \right)^2 \right\} + D_B \left(\frac{\partial C}{\partial x} \frac{\partial T}{\partial x} + \frac{\partial C}{\partial y} \frac{\partial T}{\partial y} \right) \right] &+ \\
\sigma B_o^2 u^2 - \frac{\partial q_r}{\partial y}, &
\end{aligned} \tag{9.9}$$

$$\frac{\partial C}{\partial t} + u \frac{\partial C}{\partial x} + v \frac{\partial C}{\partial y} = D_B \left(\frac{\partial^2 C}{\partial x^2} + \frac{\partial^2 C}{\partial y^2} \right) + \left(\frac{\partial^2 T}{\partial x^2} + \frac{\partial^2 T}{\partial y^2} \right) \frac{D_T}{T_m} - k_1 (C - C_0). \tag{9.10}$$

The related boundary conditions are

$$u \pm \beta_1 S_{xy} = 0 \quad \text{at } y = \pm \eta, \tag{9.11}$$

$$\begin{aligned}
\left[-\tau_1 \frac{\partial^3}{\partial x^3} + m_1 \frac{\partial^3}{\partial x \partial t^2} + d \frac{\partial^2}{\partial t \partial x} \right] \eta &= \frac{\partial S_{xx}}{\partial x} + \frac{\partial S_{xy}}{\partial y} - \rho_f \left(\frac{\partial u}{\partial t} + u \frac{\partial u}{\partial x} + v \frac{\partial u}{\partial y} \right) - \\
\sigma B_o^2 u + g \rho_f \beta_T (T - T_0) + g \rho_f \beta_C (C - C_0) &\text{ at } y = \pm \eta,
\end{aligned} \tag{9.12}$$

$$T \pm \beta_2 \frac{\partial T}{\partial y} = \left\{ \begin{matrix} T_1 \\ T_0 \end{matrix} \right\}, \quad C \pm \beta_3 \frac{\partial C}{\partial y} = \left\{ \begin{matrix} C_1 \\ C_0 \end{matrix} \right\} \quad \text{at } y = \pm \eta, \tag{9.13}$$

where u is the velocity component in x direction and v the velocity in y direction, p the pressure, ν the kinematic viscosity, k the thermal conductivity, σ the electrical conductivity, ρ_f the density of nanofluid, D_T the thermophoretic diffusion, D_B the Brownian movement, $(\beta_1, \beta_2, \beta_3)$ the slip parameters, τ_1 elastic stress, d viscous damping coefficient, m_1 mass per unit area, T_m the mean temperature, k_1 chemical reaction parameter, S_{ij} the stress tensor components for the hyperbolic tangent liquid and q_r defined by nonlinear radiated heat flux satisfies

$$q_r = -\frac{4\bar{\sigma}}{3\bar{k}} \frac{\partial T^4}{\partial y} = -\frac{16\bar{\sigma}}{3\bar{k}} \left(T^3 \frac{\partial T}{\partial y} \right). \tag{9.14}$$

Now we take the stream function ψ as $(u, v) = (\psi_y, -\delta\psi_x)$ and the following non-dimensional quantities

$$\begin{aligned}
\frac{u}{c} = u^*, \quad \frac{v}{c} = v^*, \quad \frac{x}{\lambda} = x^*, \quad \frac{y}{d_1} = y^*, \quad \frac{ct}{\lambda} = t^*, \quad \frac{\eta}{d_1} = \eta^*, \quad \frac{d_1 S_{ij}}{\mu_0 c} = S_{ij}^*, \\
\frac{d_1^2 p}{c \lambda \mu_0} = p^*, \quad \frac{T - T_0}{(T_1 - T_0)} = \theta, \quad \frac{C - C_0}{(C_1 - C_0)} = \phi, \quad \frac{\beta_i}{d_1} = \beta_i^* \quad (i = 2 - 3).
\end{aligned} \tag{9.15}$$

Utilizing aforementioned terms and then invoking the long wavelength and low Reynolds, we get the system of equations after dropping asterisks as follows

$$[1 + n(We\dot{\gamma} - 1)] \frac{\partial^4 \psi}{\partial y^4} - M^2 \frac{\partial^2 \psi}{\partial y^2} + Gr \frac{\partial \theta}{\partial y} + Gc \frac{\partial \phi}{\partial y} = 0, \quad (9.16)$$

$$\begin{aligned} & \frac{\partial^2 \theta}{\partial y^2} + Pr Nb \left(\frac{\partial \phi}{\partial y} \right) \left(\frac{\partial \theta}{\partial y} \right) + Pr Nt \left(\frac{\partial \theta}{\partial y} \right)^2 + Pr Ec S_{xy} \frac{\partial^2 \psi}{\partial y^2} + \\ & Pr Rn \frac{\partial}{\partial y} \left[(1 + (\varsigma - 1)\theta)^3 \frac{\partial \theta}{\partial y} \right] + Pr M^2 \left(\frac{\partial \psi}{\partial y} \right)^2 = 0, \end{aligned} \quad (9.17)$$

$$Nb \frac{\partial^2 \phi}{\partial y^2} + Nt \left(\frac{\partial^2 \theta}{\partial y^2} \right) - Nb \zeta Sc \phi = 0, \quad (9.18)$$

with the non-dimensional boundary conditions

$$\frac{\partial \psi}{\partial y} \pm \beta_1 [1 + n(We\dot{\gamma} - 1)] \frac{\partial^2 \psi}{\partial y^2} = 0 \text{ at } y = \pm \eta, \quad (9.19)$$

$$\begin{aligned} & \left[E_1 \frac{\partial^3}{\partial x^3} + E_2 \frac{\partial^3}{\partial x \partial t^2} + E_3 \frac{\partial^2}{\partial x \partial t} \right] \eta = \frac{\partial^3 \psi}{\partial y^3} [1 + n(We\dot{\gamma} - 1)] - \\ & M^2 \frac{\partial \psi}{\partial y} + Gr \theta + Gc \phi \text{ at } y = \pm \eta, \end{aligned} \quad (9.20)$$

$$\theta \pm \beta_2 \frac{\partial \theta}{\partial y} = \begin{Bmatrix} 1 \\ 0 \end{Bmatrix}, \quad \phi \pm \beta_3 \frac{\partial \phi}{\partial y} = \begin{Bmatrix} 1 \\ 0 \end{Bmatrix} \text{ at } y = \pm \eta. \quad (9.21)$$

Notice that the continuity equation (9.9) is satisfied automatically. Here δ depicts the wave number, ϵ amplitude ratio, α thermal diffusivity, Gc the concentration Grashof number, Gr the thermal Grashof number, Pr the Prandtl number, Re the Reynolds number, Ec the Eckert number, Sc the Schmidt variable, Nt the thermophoresis parameter, M the Hartman variable, Nb the Brownian diffusion parameter, We the Weissenberg number, Rn the radiation parameter, ς the temperature ratio variable, ζ the chemical reaction parameter β_1 is the velocity slip variable and (E_1, E_2, E_3) the wall parameters defined below

$$\begin{aligned}
\epsilon &= \frac{a}{d_1}, \delta = \frac{d_1}{\lambda}, \alpha = \frac{k}{\rho_f c_f}, Gc = \frac{g\rho_f\beta_C(C - C_0)d_1^2}{\mu_0 c}, Gr = \frac{g\rho_f\beta_T(T - T_0)d_1^2}{\mu_0 c}, \\
Pr &= \frac{\mu_0 c_f}{k}, Re = \frac{\rho_f c d_1}{\mu_0}, Ec = \frac{c^2}{c_f(T_1 - T_0)}, Sc = \frac{\nu}{D_B}, Nt = \frac{D_T\tau(T_1 - T_0)}{T_m\nu}, \\
M &= \sqrt{\frac{\sigma}{\mu_0}}B_0d_1, Nb = \frac{D_B\tau(C_1 - C_0)}{\nu}, We = \frac{c\Gamma'}{d_1^2}, Rn = \frac{16\bar{\sigma}T_0^3}{3kk}, \varsigma = \frac{T_1}{T_0}, \\
\zeta &= \frac{k_1d_1^2}{D_B}, \beta_1 = \frac{\beta_1^*\mu_0}{d_1}. E_1 = -\frac{d_1^3\tau}{\lambda^3\mu_0 c}, E_2 = \frac{cm_1d_1^3}{\lambda^3\mu_0}, E_3 = \frac{d_1^3d}{\lambda^2\mu_0}.
\end{aligned}$$

9.3 Results and discussion

The resulting problem is highly nonlinear. Exact solution to this problem seems difficult. Therefore we utilized numerical technique for the nonlinear problem. We employed the scheme built-in in MATHEMATICA called NDSolve. This technique is based on Runge-Kutta fourth order method. It is convenient-to-use and cares about convergence automatically.

9.3.1 Velocity

The impacts of various variables on velocity are shown in Figs. 9.1 – 9.7. Outcome of thermal Grashof number Gr on velocity is portrayed in Fig. 9.1. Here velocity rises when Gr increased. Impact of mass Grashof number Gc versus velocity is illustrated in Fig. 9.2. An increasing trend is observed for velocity when Gc highers. Outcome of Weissenberg number on velocity is demonstrated in Fig. 9.3. It is observed that velocity is higher against We . Fig. 9.4 is prepared for impacts of power law index n on velocity. Clearly velocity rises for larger n . Fig. 9.5 elucidates the variation of velocity slip parameter β_1 versus velocity. Velocity increases by β_1 . Fig. 9.6 elaborates consequences of wall parameters E_1, E_2 and E_3 on velocity. These Figs indicate that velocity enhances for E_1 and E_2 but opposite holds against E_3 . Fig. 9.7 shows Hartman number M effect on the velocity. Higher Hartman number M indicate a decrease in velocity.

9.3.2 Temperature

Plots for temperature against numerous physical variables are drawn in Figs. 9.8 – 9.17. Fig. 9.8. explores of thermal slip parameter β_2 on velocity. This Fig. reveals that velocity of fluid rises for larger β_2 . Impact of thermal Grashof number Gr against temperature is present in Fig. 9.9. Temperature of liquid rises for larger Gr . Fig. 9.10 illustrates effect of Prandtl number Pr versus temperature. Result shows that an enhancement is observed in this case. Fig. 9.11 depicts that larger Eckert number enhance the viscous dissipation effect. This rises the temperature. Fig. 9.12 demonstrated a combined study of Brownian movement Nb and thermophoresis Nt variables. Larger values of Nb are correlated with higher random movement of the nanoparticles via wall to liquid that takes to a temperature uprise. Fig. 9.13 depicts temperature for larger radiation parameter Rn . It indicates that temperature of fluid decreases when Rn rises. Fig. 9.14 shows that higher values of ζ diminish temperature. Consequences of Weissenberg number We are shown in Fig. 9.15. For higher We an enhancement in temperature of fluid is observed. Fig. 9.16 declares outcome of wall parameters (E_1, E_2, E_3) on temperature. Results show that temperature enhances with higher E_1 and E_2 where as opposite behavior occurs for E_3 . Fig. 9.17 is sketched to see the impacts of Hartman variable M via temperature. There is a decreasing trend when M increases.

9.3.3 Concentration

Figs. 9.18–9.25 portrayed the concentration for numerous pertinent parameters. Concentration against mass concentration slip parameter β_3 is portrayed in Fig. 9.18. We noticed a reduction in concentration through β_3 . Fig. 9.19 demonstrates that concentration decreases in absolute sense when Gc enlarges. Brownian motion parameter Nb against concentration is described in Fig. 9.20. Concentration enhances for higher estimation of Nb . On the other hand opposite trend is witnessed on concentration via thermophoresis variable Nt (see Fig. 9.21). Figs. 9.22 and 9.23 demonstrate features of chemical reaction parameter ζ and Schmidt variable Sc versus concentration. Both ζ and Sc causes reduction in concentration. Fig. 9.24 depicts the concentration for the rigidity parameter E_1 , the tension parameter E_2 and E_3 . It is observed that an increment in E_1 and E_2 variables boosts the concentration but it falls through larger E_3 . Plot for Weissenberg number We on concentration is captured in Fig. 9.25. We observed

that concentration decreases for larger We .

9.3.4 Heat transfer coefficient

Results of various physical variables on coefficient of heat transfer $Z(x) = \theta_y(\eta) \eta_x$ are revealed in Figs. 9.26 – 9.33. Fig. 9.26 investigated the significance β_2 for Z . It reveals that Z enhances via larger β_2 . Fig. 9.27 presents the impact of Weissenberg number We on Z . It is observed that rise in We decays coefficient of heat transfer Z . Impact of radiation variable Rn for Z is portrayed in Fig. 9.28. Z has reducing pattern when Rn highers. The decrease in coefficient of heat transfer Z is also noticed for ς (see Fig. 9.29). Fig. 9.30 demonstrates coefficient of heat transfer Z verses Prandtl number Pr . Here Z enhances for higher Pr . Fig. 9.31 describes Z for larger thermophoresis Nt and Brownian motion parameter Nb . We observed that higher values of both the variables show an enhancement in Z . Effect of thermal Grashof parameter Gr on coefficient of heat transfer Z is sketched in Fig. 9.32. Here Z rises for higher Gr . Variation of Hartman parameter M is elaborated in Fig. 9.33. We observed that Z diminishes with rise in M .

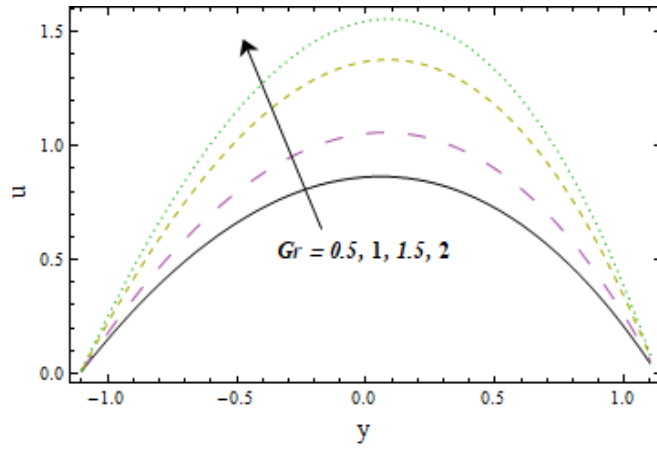


Fig. 9.1: Variation of Gr on u

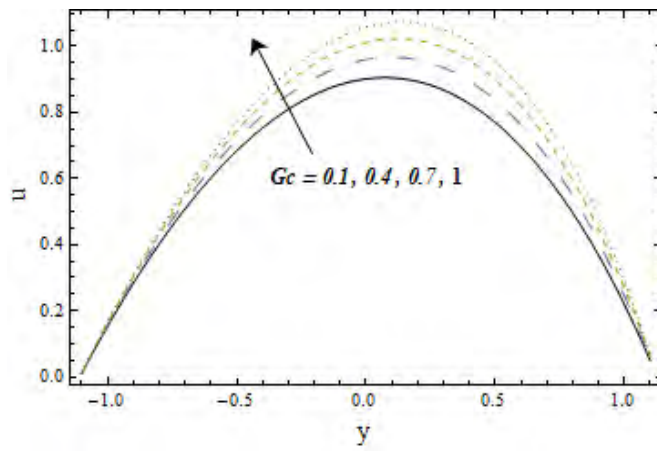


Fig. 9.2: Variation of Gc on u

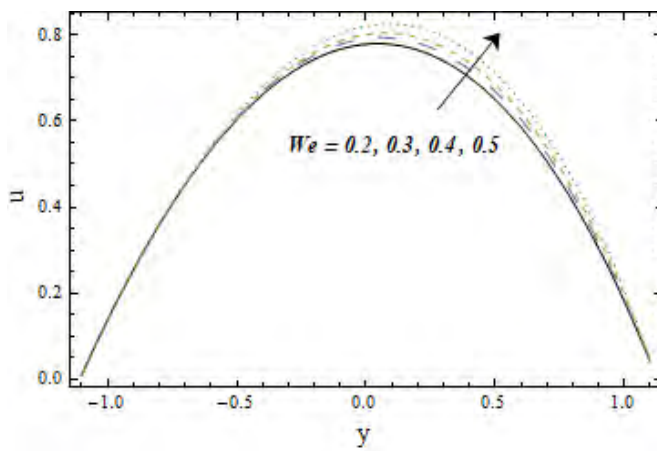


Fig. 9.3: Variation of We on u

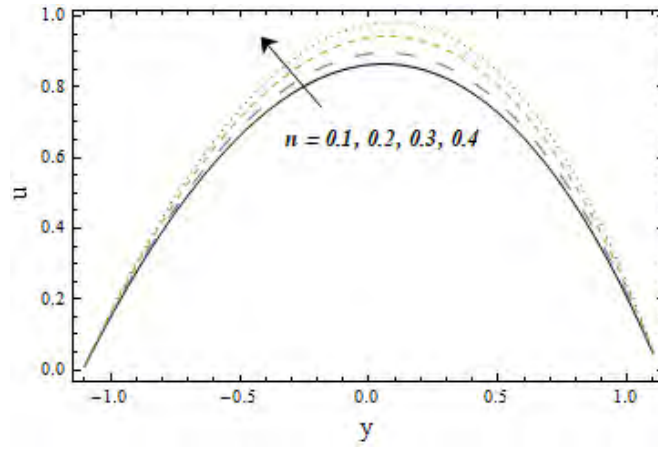


Fig. 9.4: Variation of n on u

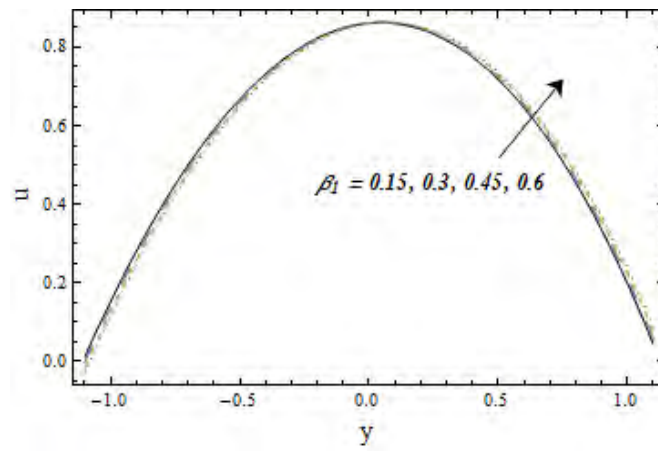


Fig. 9.5: Variation of β_1 on u

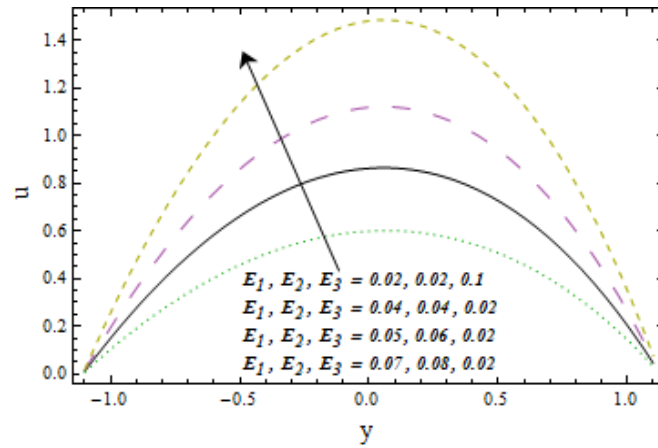


Fig. 9.6: Variations of E_1, E_2 and E_3 on u

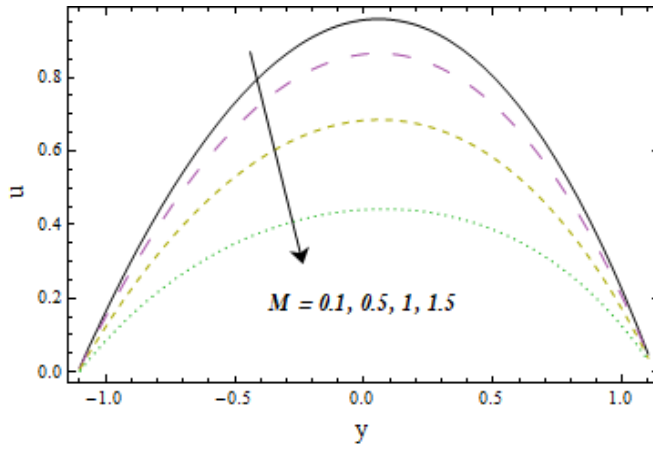


Fig. 9.7: Variation of M on u

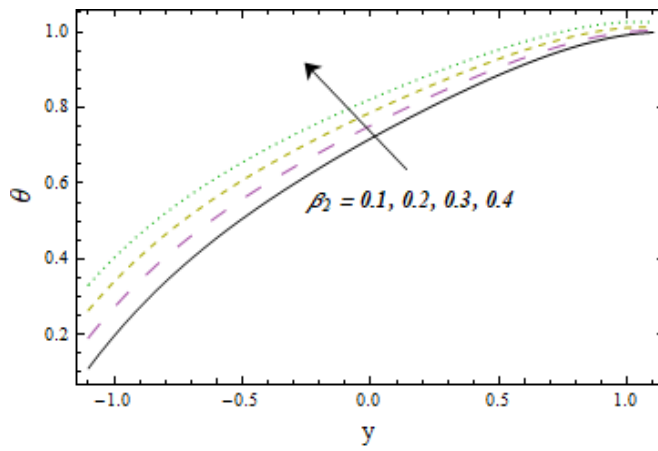


Fig. 9.8: Variation of β_2 on θ

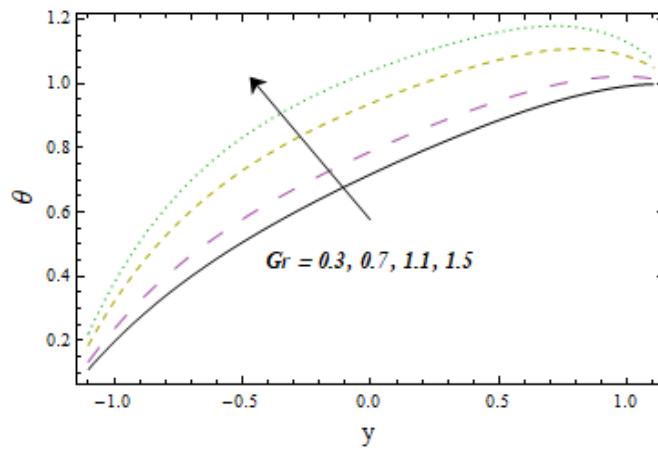


Fig. 9.9: Variation of Gr on θ

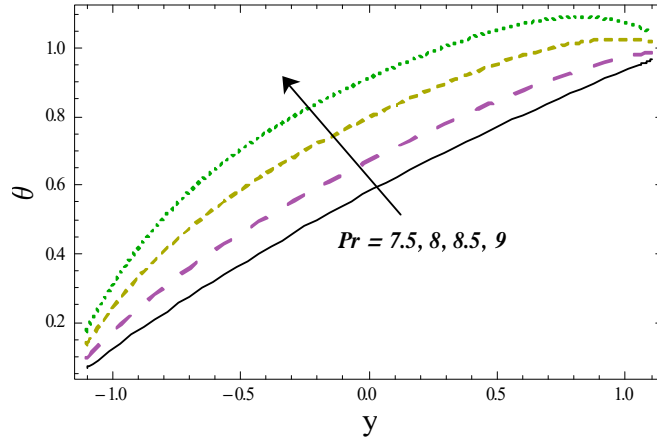


Fig. 9.10: Variation of Pr on θ

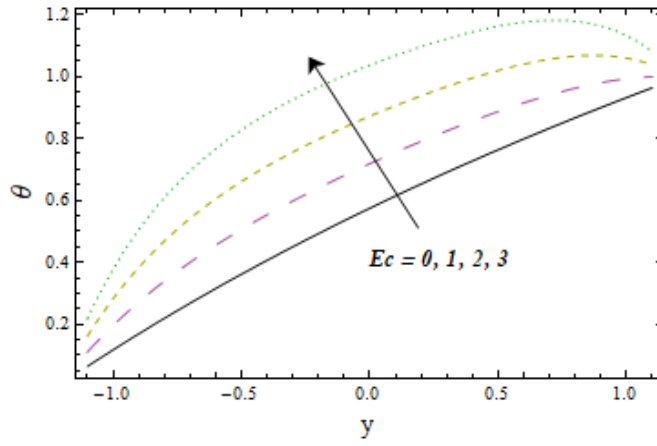


Fig. 9.11: Ec variation on θ

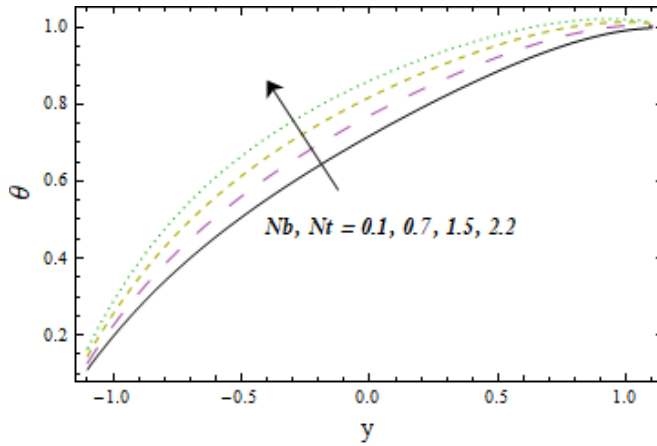


Fig. 9.12: Nb and Nt variation on θ

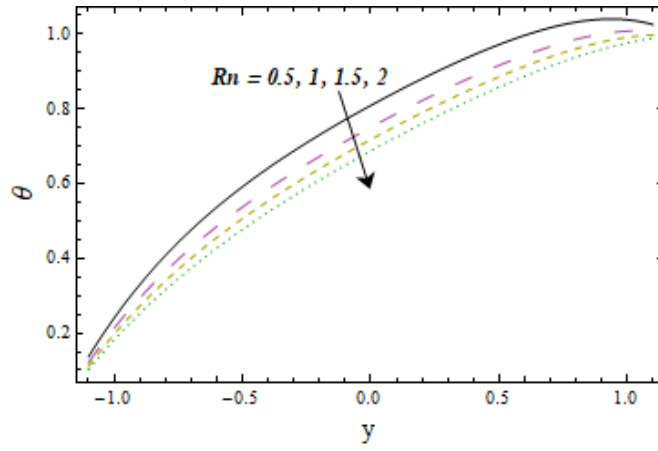


Fig. 9.13: Variation of Rn on θ

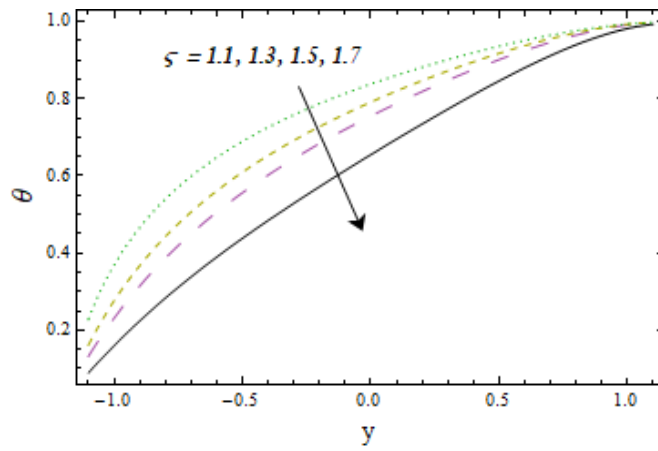


Fig. 9.14: Variation of ζ on θ

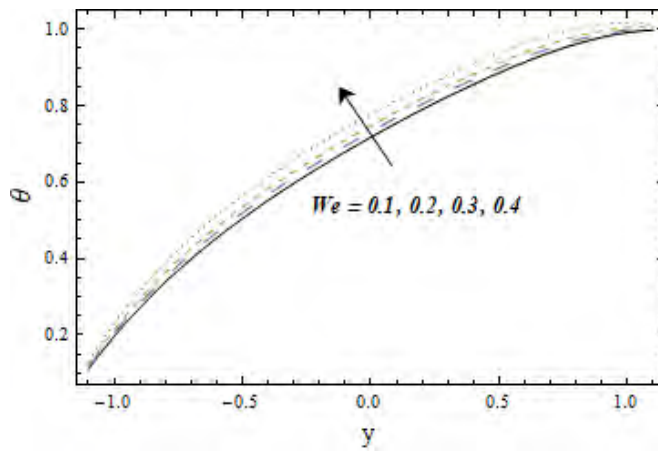


Fig. 9.15: Variation of We on θ

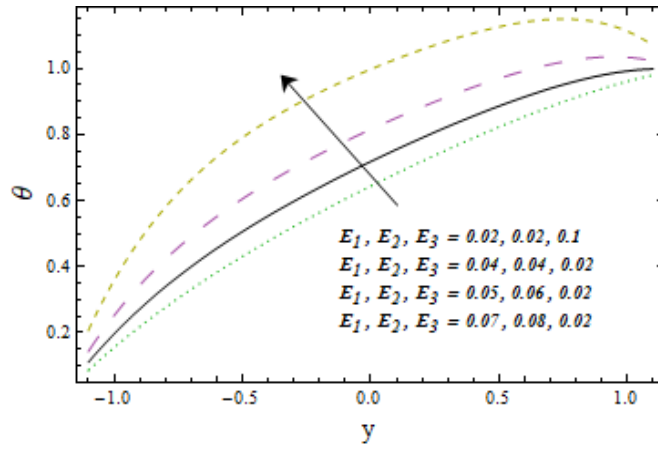


Fig. 9.16: Variations of E_1, E_2 and E_3 for θ

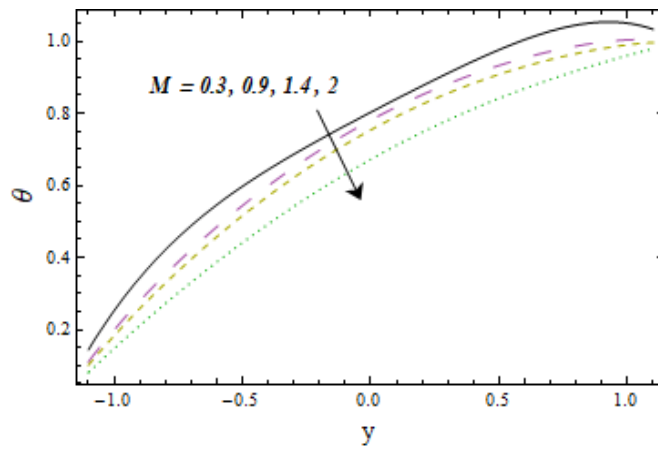


Fig. 9.17: Variation of M for θ

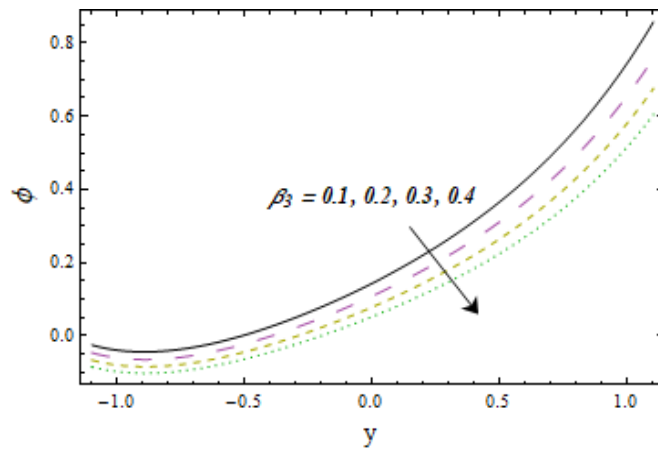


Fig. 9.18: Variation of β_3 on ϕ

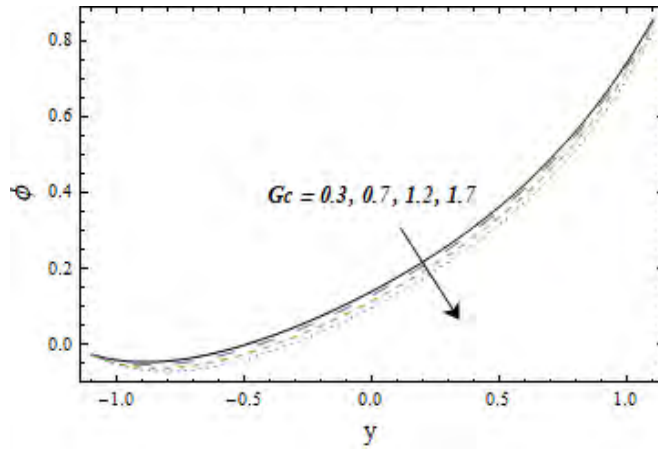


Fig. 9.19: Variation of Gc on ϕ

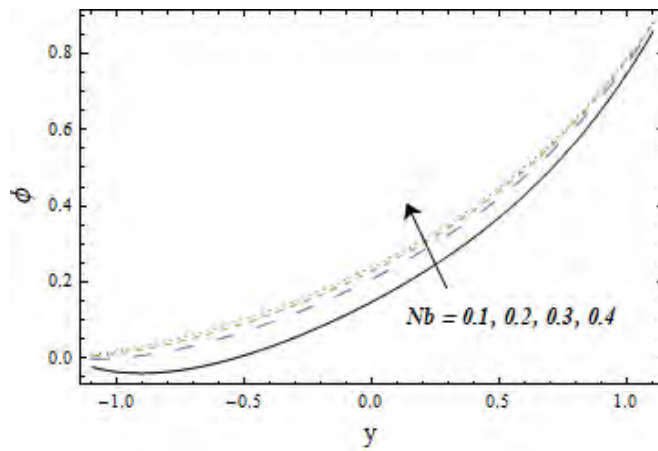


Fig. 9.20: Variation of Nb on ϕ

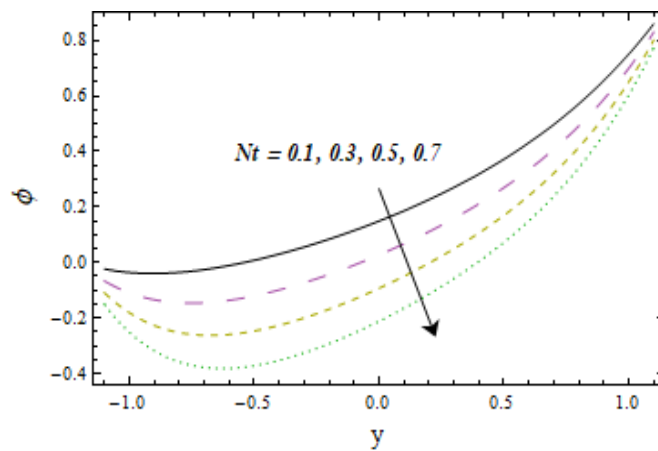


Fig. 9.21: Variation of Nt on ϕ

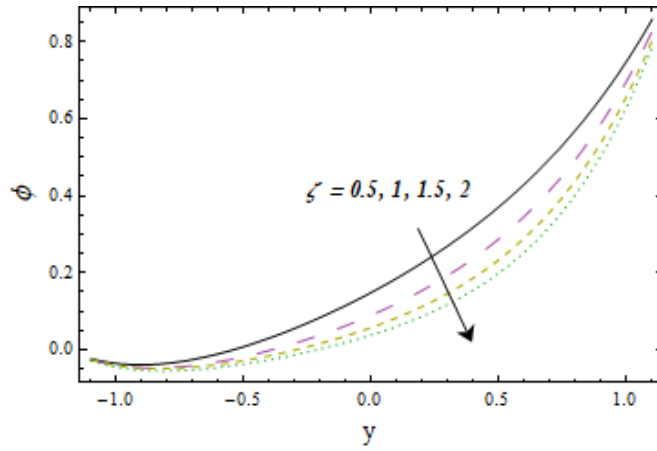


Fig. 9.22: Variation of ζ on ϕ

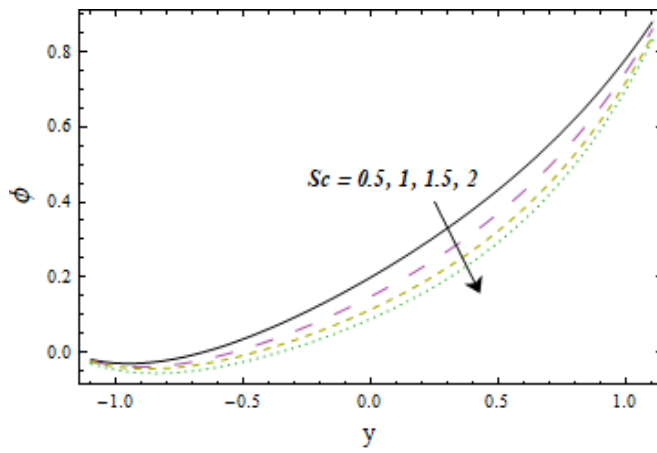


Fig. 9.23: Variation of Sc on ϕ

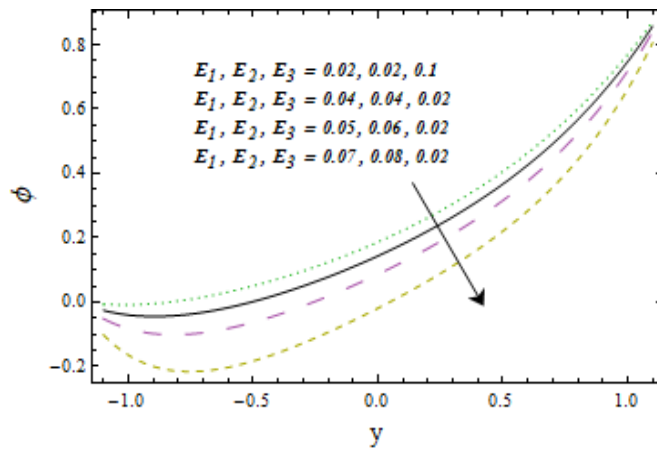


Fig. 9.24: Variations of E_1, E_2 and E_3 on ϕ

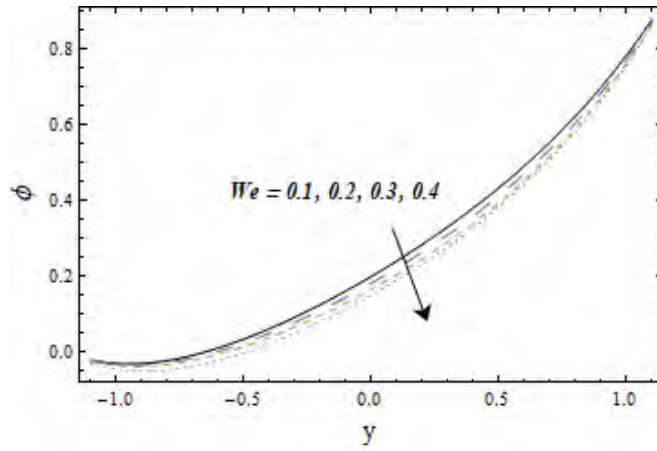


Fig. 9.25: Variation of We on ϕ

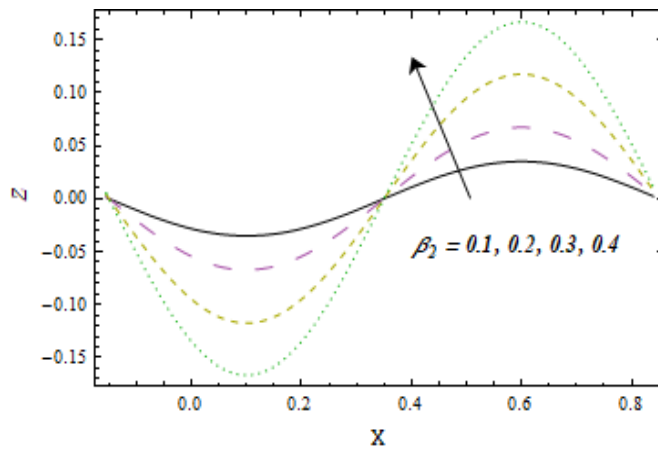


Fig. 9.26: Variation of β_2 on Z

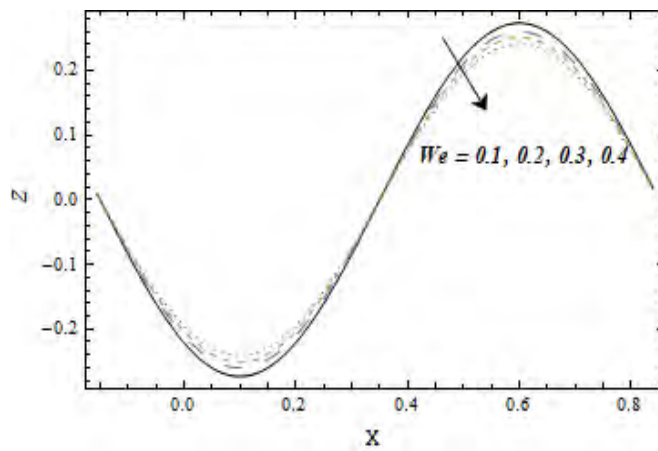


Fig. 9.27: Variation of We on Z

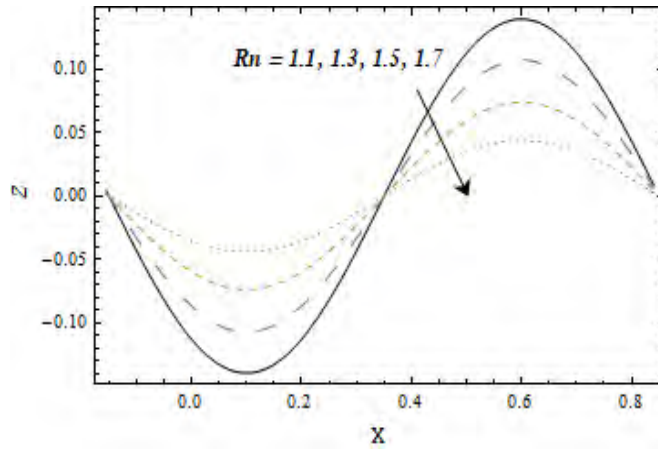


Fig. 9.28: Variation of Rn on Z

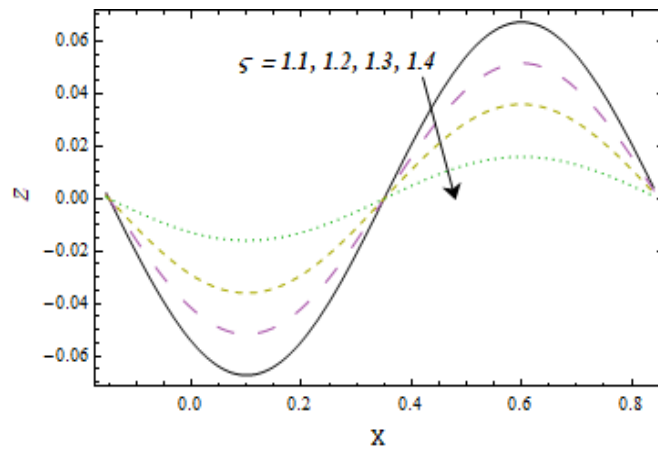


Fig. 9.29: Variation of ζ on Z

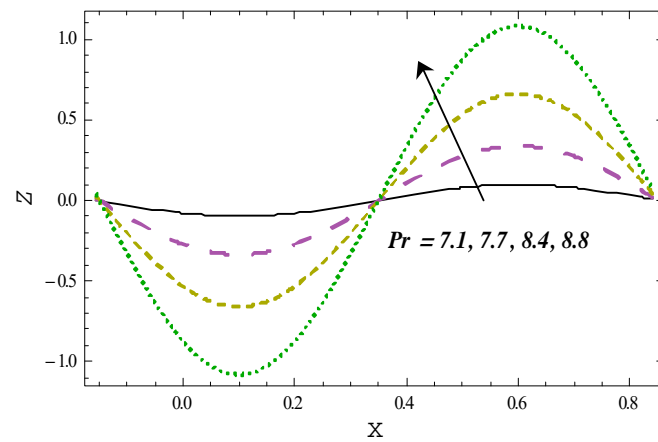


Fig. 9.30: Variation of Pr on Z

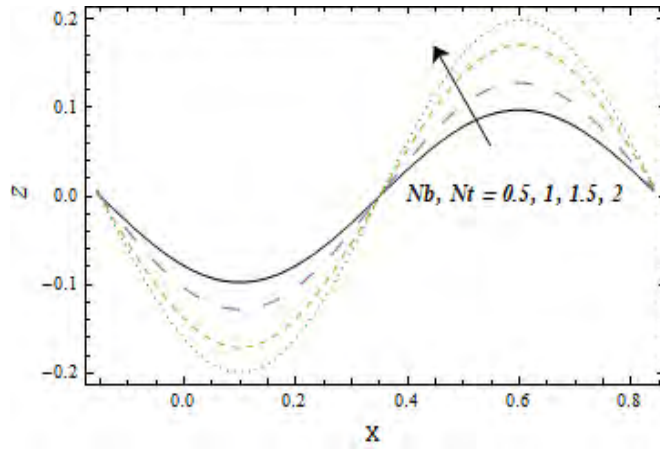


Fig. 9.31: Variation of Nb and Nt on Z

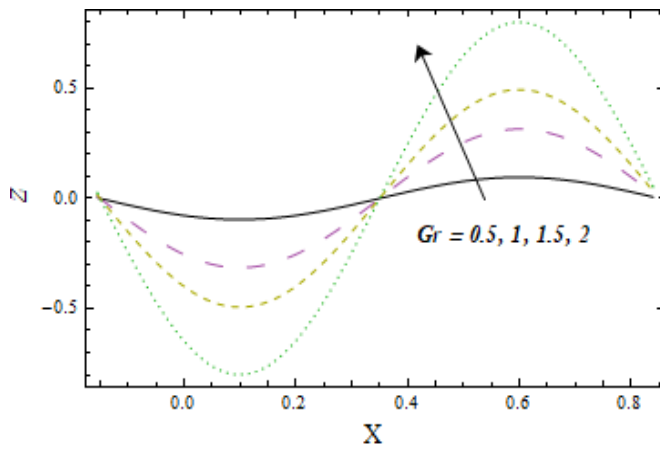


Fig. 9.32: Variation of Gr for Z

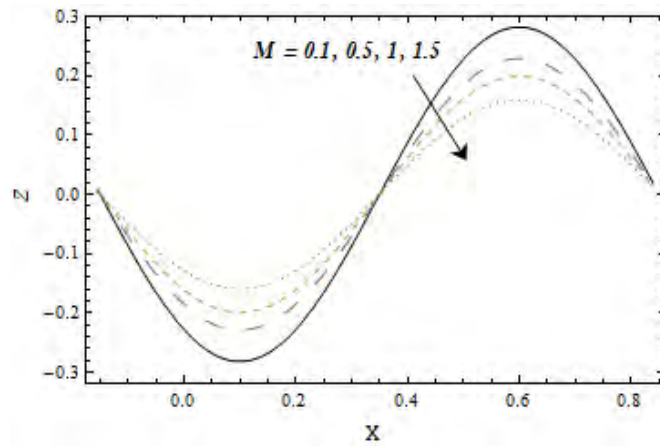


Fig. 9.33: Variation of M on Z

9.4 Conclusions

The key results of the present study are summarized as follows.

- Velocity rises through β_1 , Gr and Gc while it reduces against M .
- Impact of We on velocity and temperature is qualitatively same.
- Increasing outcomes of Pr , β_2 and Ec are noticed.
- Reduction in temperature and heat transfer coefficient for via Rn and ς is observed.
- Concentration is decreased through β_3 and ζ .
- Z against β_2 and Rn has reverse results
- Reduction is observed for Z against We and M .

Chapter 10

Peristalsis of Sutterby nanofluid with Hall current and entropy generation

10.1 Introduction

This chapter examined magnetohydrodynamic (MHD) mixed convection peristaltic flow of a Sutterby nanofluid with entropy generation. Convective conditions, Ohmic heating, mixed convection and radiation effects are considered. Brownian motion and thermophoresis are considered. A lubrication approach is employed. Governing problems are solved numerically with NDSolve. Physical quantities of interest are analyzed.

10.2 Formulation

We analyze two-dimensional peristaltic motion of Sutterby nanofluid in symmetric channel having width $2d_1$. Here x and y coordinates are perpendicular to each other. The wave propagates in the x -direction along channel wall. Flexible nature of channel walls is considered. Hall current, partial slip conditions for velocity and activation energy are also present. The walls shape satisfy:

$$y = \pm\eta(x, t) = \pm[d_1 + a \sin \frac{2\pi}{\lambda}(x - ct)], \quad (10.1)$$

where λ denotes wavelength, a the amplitude, t the time and c wave speed. Extra stress tensor for Sutterby model is [42]

$$S = \frac{\mu}{2} \left[\frac{\sinh^{-1}(\bar{b}\dot{\gamma})}{\bar{b}\dot{\gamma}} \right]^{m^*} \mathbf{A}_1, \quad (10.2)$$

$$\dot{\gamma} = \sqrt{\frac{1}{2} \text{trace} \mathbf{A}_1^2}, \quad (10.3)$$

$$\mathbf{A}_1 = (\text{grad } V) + (\text{grad } V)^t, \quad (10.4)$$

where \bar{b} and m^* denote material constants, μ the fluid dynamic viscosity and \mathbf{A}_1 the first Rivlin Ericksen tensor. The related expressions are

$$\frac{\partial u}{\partial x} + \frac{\partial v}{\partial y} = 0, \quad (10.5)$$

$$\rho_f \left(\frac{\partial u}{\partial t} + u \frac{\partial u}{\partial x} + v \frac{\partial u}{\partial y} \right) = -\frac{\partial p}{\partial x} + \frac{\partial S_{xx}}{\partial x} + \frac{\partial S_{xy}}{\partial y} - \frac{\sigma B_0^2}{(1+m^2)}(u - mv) + g\rho_f\beta_T(T - T_0) + g\rho_f\beta_C(C - C_0), \quad (10.6)$$

$$\rho_f \left(\frac{\partial v}{\partial t} + u \frac{\partial v}{\partial x} + v \frac{\partial v}{\partial y} \right) = -\frac{\partial p}{\partial y} + \frac{\partial S_{yx}}{\partial x} + \frac{\partial S_{yy}}{\partial y} - \frac{\sigma B_0^2}{(1+m^2)}(v + mu), \quad (10.7)$$

$$\begin{aligned} \rho_f c_f \left(\frac{\partial T}{\partial t} + u \frac{\partial T}{\partial x} + v \frac{\partial T}{\partial y} \right) &= k \left(\frac{\partial^2 T}{\partial x^2} + \frac{\partial^2 T}{\partial y^2} \right) + S_{xx} \frac{\partial u}{\partial x} + S_{yy} \frac{\partial v}{\partial y} + S_{xy} \left(\frac{\partial v}{\partial x} + \frac{\partial u}{\partial y} \right) \\ &+ \rho_p c_p \left[D_B \left(\frac{\partial T}{\partial x} \frac{\partial C}{\partial x} + \frac{\partial T}{\partial y} \frac{\partial C}{\partial y} \right) + \frac{D_T}{T_m} \left\{ \left(\frac{\partial T}{\partial x} \right)^2 + \left(\frac{\partial T}{\partial y} \right)^2 \right\} \right] + \\ &\frac{\sigma B_0^2}{(1+m^2)}(u^2 + v^2) - \frac{\partial q_r}{\partial y}, \end{aligned} \quad (10.8)$$

$$\frac{\partial C}{\partial t} + u \frac{\partial C}{\partial x} + v \frac{\partial C}{\partial y} = D_B \left(\frac{\partial^2 C}{\partial x^2} + \frac{\partial^2 C}{\partial y^2} \right) + \frac{D_T}{T_m} \left(\frac{\partial^2 T}{\partial x^2} + \frac{\partial^2 T}{\partial y^2} \right) - k_r^2 (C - C_0) \left(\frac{T}{T_0} \right)^n \exp \left(-\frac{E_a}{\kappa T} \right), \quad (10.9)$$

$$u \pm \beta S_{xy} = 0 \quad \text{at } y = \pm \eta, \quad (10.10)$$

$$\left(-\tau_1 \frac{\partial^3}{\partial x^3} + m_1 \frac{\partial^3}{\partial x \partial t^2} + d \frac{\partial^2}{\partial t \partial x} \right) \eta = \frac{\partial S_{xx}}{\partial x} + \frac{\partial S_{xy}}{\partial y} - \rho_f \left(\frac{\partial u}{\partial t} + u \frac{\partial u}{\partial x} + v \frac{\partial u}{\partial y} \right) - \frac{\sigma B_0^2}{(1+m^2)} u + g \rho_f \beta_T (T - T_0) + g \rho_f \beta_C (C - C_0) \quad \text{at } y = \pm \eta. \quad (10.11)$$

$$-k \frac{\partial T}{\partial y} = h_1 \left\{ \begin{matrix} T_1 - T \\ T - T_0 \end{matrix} \right\}, \quad -D_B \frac{\partial T}{\partial y} = h_2 \left\{ \begin{matrix} C_1 - C \\ C - C_0 \end{matrix} \right\} = 0, \quad \text{at } y = \pm \eta, \quad (10.12)$$

where (u, v) are the velocity component in (x, y) directions, p the pressure, k the thermal conductivity, ν the kinematic viscosity, ρ_f the density of nanoliquid, σ electrical conductivity, D_B Brownian movement, D_T thermophoresis diffusion coefficient, m the Hall parameter, β the slip parameter, d coefficient of viscous damping, k_r the chemical reaction rate, τ_1 the elastic tension, E_a the activation energy, m_1 mass per unit area, κ the Boltzmann constant, n fitted rate constant, (C_1, C_0) and (T_1, T_0) are the concentration and temperature at the upper and lower walls respectively and stress tensor components $S_{xx}, S_{yy}, S_{yx}, S_{xy}$ for the Sutterby material can be determined through expression (10.2). Last term in equation (10.9) appeared due to chemical reaction and activation energy.

By using the approximation of Rosseland, the radiative heat flux q_r obeys

$$q_r = -\frac{4\bar{\sigma}}{3\bar{k}} \frac{\partial T^4}{\partial y}, \quad (10.13)$$

in which $\bar{\sigma} = 5.6697 \times 10^{-8} W m^{-2} K^{-4}$ represents the constant Stefan – Boltzmann, and \bar{k} the coefficient of absorption. We expect that the changes in temperature inside the flow are lower enough to characterize T^4 as a temperature function in linear form. Using Taylor series for T^4 about T_0 and ignoring the expressions of higher order one obtains

$$T^4 = T_0^4 + 4T_0^3(T - T_0) + 6T_0^2(T - T_0)^2. \quad (10.14)$$

Thus (10.14) reduces to

$$T^4 \simeq 4T_0^3(T - T_0). \quad (10.15)$$

From (10.13) and (10.15) one can write

$$q_r = -\frac{16\sigma T_0^3}{3k} \frac{\partial T}{\partial y}. \quad (10.16)$$

Consider stream function ψ as $u = \psi_y$, $v = -\delta\psi_x$ and non-dimensional variables are

$$\begin{aligned} u^* &= \frac{u}{c}, \quad v^* = \frac{v}{c}, \quad x^* = \frac{x}{\lambda}, \quad y^* = \frac{y}{d_1}, \quad t^* = \frac{ct}{\lambda}, \quad \eta^* = \frac{\eta}{d_1}, \\ S_{ij}^* &= \frac{d_1 S_{ij}}{\mu c}, \quad \beta^* = \frac{\beta}{d_1}, \quad p^* = \frac{d_1^2 p}{c\lambda\mu}, \quad \theta = \frac{T - T_0}{T_1 - T_0}, \quad \phi = \frac{C - C_0}{C_1 - C_0}. \end{aligned} \quad (10.17)$$

By lubrication approach and above definitions we can obtain

$$\begin{aligned} &\left[1 - 3B \left(\frac{\partial^2 \psi}{\partial y^2}\right)^2\right] \frac{\partial^4 \psi}{\partial y^4} - 6B^* \frac{\partial^2 \psi}{\partial y^2} \left(\frac{\partial^3 \psi}{\partial y^3}\right)^2 - \left(\frac{M^2}{1+m^2}\right) \frac{\partial^2 \psi}{\partial y^2} + \\ &Gr \frac{\partial \theta}{\partial y} + Gc \frac{\partial \phi}{\partial y} = 0, \end{aligned} \quad (10.18)$$

$$\begin{aligned} &(1 + \text{Pr} Rn) \frac{\partial^2 \theta}{\partial y^2} + \text{Pr} Nb \left(\frac{\partial \theta}{\partial y}\right) \left(\frac{\partial \phi}{\partial y}\right) + \text{Pr} Nt \left(\frac{\partial \theta}{\partial y}\right)^2 + \\ &\text{Pr} Ec \left[\frac{M^2}{1+m^2} \left(\frac{\partial \psi}{\partial y}\right)^2 - B^* \left(\frac{\partial^2 \psi}{\partial y^2}\right)^4 + \left(\frac{\partial^2 \psi}{\partial y^2}\right)^2\right] = 0. \end{aligned} \quad (10.19)$$

$$\frac{\partial^2 \phi}{\partial y^2} + \frac{Nt}{Nb} \left(\frac{\partial^2 \theta}{\partial y^2}\right) - Sc\zeta(1 + (\Omega - 1)\theta)^n \exp\left(-\frac{E}{1 + (\Omega - 1)\theta}\right) \phi = 0, \quad (10.20)$$

$$\frac{\partial \psi}{\partial y} \pm \beta \left[\frac{\partial^2 \psi}{\partial y^2} - B^* \left(\frac{\partial^2 \psi}{\partial y^2}\right)^3\right] = 0 \text{ at } y = \pm \eta, \quad (10.21)$$

$$\begin{aligned} &\left(E_1 \frac{\partial^3}{\partial x^3} + E_2 \frac{\partial^3}{\partial x \partial t^2} + E_3 \frac{\partial^2}{\partial x \partial t}\right) \eta = \frac{\partial^3 \psi}{\partial y^3} - 3B \frac{\partial^3 \psi}{\partial y} \left(\frac{\partial^2 \psi}{\partial y^2}\right)^3 - \\ &\left(\frac{M^2}{1+m^2}\right) \frac{\partial \psi}{\partial y} + Gr\theta + Gc\phi \text{ at } y = \pm \eta, \end{aligned} \quad (10.22)$$

$$\frac{\partial \theta}{\partial y} = \left\{ \begin{array}{l} -Bi_1(1 - \theta) \\ -Bi_1\theta \end{array} \right\}, \quad \frac{\partial \phi}{\partial y} = \left\{ \begin{array}{l} -Bi_2(1 - \phi) \\ -Bi_2\phi \end{array} \right\}, \quad \text{at } y = \pm\eta, \quad (10.23)$$

in which asterisk has been suppressed for simplicity. Note that equation of continuity (10.5) is satisfied identically. Further $\epsilon \left(= \frac{a}{d_1} \right)$ depicts amplitude ratio, $\delta \left(= \frac{d_1}{\lambda} \right)$ wave number, $\alpha \left(= \frac{k}{\rho_f c_f} \right)$ thermal diffusivity, $Gr \left(= \frac{g\rho_f\beta_T(T-T_0)d_1^2}{\mu c} \right)$ thermal Grashof number, $Gc \left(= \frac{g\rho_f\beta_C(C-C_0)d_1^2}{\mu c} \right)$ concentration Grashof number, $Pr \left(= \frac{\mu c_f}{k} \right)$ the Prandtl number, $Re \left(= \frac{\rho_f c d_1}{\mu} \right)$ Reynolds number, $Ec \left(= \frac{c^2}{c_f(T_1-T_0)} \right)$ the Eckert number, $Br = Pr Ec$ the Brinkman number, $Sc \left(= \frac{\nu}{D_B} \right)$ the Schmidt variable, $\tau \left(= \frac{\rho_f c_p}{\rho_f c_f} \right)$ the effective heat capacity ratio of nanoparticle material to liquid heat capacity, $Nb \left(= \frac{D_B\tau(C_1-C_0)}{\nu} \right)$ the Brownian diffusion parameter, $Nt \left(= \frac{D_T\tau(T_1-T_0)}{T_m\nu} \right)$ the thermophoresis parameter, $B^* \left(= \frac{c^2 m^* b}{6d_1^2} \right)$ the Sutterby liquid parameter, $M \left(= \sqrt{\frac{\sigma}{\mu}} B_0 d_1 \right)$ the Hartman number, $Rn \left(= \frac{16\bar{\sigma}T_0^3}{3kk} \right)$ the radiation parameter, $Bi_1 \left(= \frac{h_1 d_1}{k} \right)$ the thermal Biot number, $Bi_2 \left(= \frac{h_2 d_1}{D_B} \right)$ the mass Biot number, $\zeta \left(= \frac{k_1 d_1^2}{\nu} \right)$ the chemical reaction parameter, $\Omega \left(= \frac{T_1}{T_0} \right)$ the temperature ratio parameter, $E \left(= -\frac{E_a}{\kappa T_0} \right)$ the activation energy parameter $\beta \left(= \frac{\beta^* \mu}{2d_1} \right)$ the velocity slip parameter and $\left(E_1 = -\frac{d_1^3 \tau}{\lambda^3 \mu c}, E_2 = \frac{cm_1 d_1^3}{\lambda^3 \mu}, E_3 = \frac{d_1^3 d}{\lambda^2 \mu} \right)$ the wall parameters.

10.3 Expression for entropy generation

Mathematically the entropy generation is defined as:

$$\begin{aligned} S_{gen}''' &= \frac{k}{T_m^2} \left(\left(\frac{\partial T}{\partial x} \right)^2 + \left(\frac{\partial T}{\partial y} \right)^2 + \frac{16\bar{\sigma}}{3kk} \left(\frac{\partial T}{\partial y} \right)^2 \right) + \frac{\sigma B_0^2}{T_m(1+m^2)} u^2 + \frac{\Phi}{T_m} \\ &+ \frac{RD}{C_m} \left(\left(\frac{\partial C}{\partial x} \right)^2 + \left(\frac{\partial C}{\partial y} \right)^2 \right) + \frac{RD}{T_m} \left(\frac{\partial C}{\partial x} \frac{\partial T}{\partial x} + \frac{\partial C}{\partial y} \frac{\partial T}{\partial y} \right). \end{aligned} \quad (10.24)$$

Here viscous dissipation Φ given by

$$\Phi = S_{xx} \frac{\partial u}{\partial x} + S_{yy} \frac{\partial v}{\partial y} + S_{xy} \left(\frac{\partial u}{\partial y} + \frac{\partial v}{\partial x} \right). \quad (10.25)$$

In dimensionless form we have

$$\begin{aligned}
Ns = \frac{S_{gen}'''}{S_G'''} &= (1 + Rn) \left(\frac{\partial \theta}{\partial y} \right)^2 + \frac{L}{\Lambda} \left(\frac{\partial \theta}{\partial y} \right) \left(\frac{\partial \phi}{\partial y} \right) + \frac{L\gamma^*}{\Lambda^2} \left(\frac{\partial \phi}{\partial y} \right)^2 \\
&+ \frac{Br}{\Lambda} S_{xy} \frac{\partial^2 \psi}{\partial y^2} + \frac{BrM^2}{\Lambda(1+m^2)} \left(\frac{\partial \psi}{\partial y} \right)^2,
\end{aligned} \tag{10.26}$$

where

$$S_G''' = \frac{k(T_1 - T_0)^2}{T_m^2 d_1^2}, \quad \Lambda = \frac{T_1 - T_0}{T_m}, \quad \gamma^* = \frac{C_1 - C_0}{C_m}, \quad L = \frac{RD(C_1 - C_0)}{k}. \tag{10.27}$$

10.4 Numerical outcomes and discussion

In this study we employed the MATHEMATICA tool NDSolve to solve system of Eqs. (10.18) – (10.20) with the relevant boundary condition (10.21) – (10.23). This method is useful for small steps with small errors. Further more, both x and y modify uniformly through a step size of 0.01. Error tolerance is fixed upto 10^{-6} .

10.4.1 Velocity

Influence of various physical variables on velocity is revealed through Figs. 10.1 – 10.7. Here larger β give rise to an enhancement of velocity (see Fig. 10.1). Higher velocity appears in the neighbourhood of walls. Fig. 10.2 depicts outcome of Sutterby fluid parameter B^* on velocity. Velocity rises when B is increased. In Fig. 10.3 the consequence of Gr on velocity is illustrated. It is found that with increasing Gr the velocity enhances. Increase of this parameter means higher buoyancy forces, which lead to higher velocity distribution. Fig. 10.4 portrays mass Grashof number Gc on the velocity. Velocity of fluid decreases for higher Gc . Fig. 10.5 illustrates the outcome of wall parameters (E_1, E_2, E_3) on velocity. This Fig. shows that velocity increases with higher E_1 and E_2 whereas opposite behavior for E_3 . Infact the walls are compliant in nature and have elastic attitude. This activity creates less resistance to the flow and therefore increases the velocity. Fig. 10.6 shows outcome of velocity for Hall parameter m . Velocity enhanced for m .

10.4.2 Temperature

Fig. 10.7 is sketched to see the Effect of thermal Biot number Bi_1 is shown in Fig 10.7. on temperature. It reveals that temperature falls for higher Bi_1 . Biot number lessens thermal conductivity, which leads to reduce the temperature of fluid. In Fig. 10.8 we observed that temperature increases with higher Sutterby fluid parameter B^* . This means that the Sutterby fluid temperature is stronger than that of the viscous fluid. Fig. 10.9 represents temperature for various values of thermal Grashof parameter Gr . It depicts from Fig. that when Gr increases then temperature of fluid enhances. Fig. 10.10 explains effect of Hall parameter m on temperature. Clearly temperature rises with higher m . An enhancement in Hall parameter corresponds to increase of velocity and consequently temperature.

10.4.3 Concentration

Influence of various physical variables on concentration is revealed in Figs. 10.11 – 10.14. Effect of Sutterby fluid variable B is presented in Fig. 10.11. It is evident from this Fig. that concentration increases. Fig 10.12. shows the plots of mass Grashof number Gc on concentration. It indicates an increasing trend of concentration. Nanoparticles concentration versus mass Biot number Bi_2 is depicted in Fig. 10.13. Here we observed that concentration enhances via higher Bi_2 . Fig. 10.14 depicts the consequence of activation energy E on concentration. Outcome shows that an enhancement is noticed in this case. Larger E enabled the Arrhenius activation energy factor to decrease. As a result of which the chemical reaction rate increases.

10.4.4 Coefficient of Heat transfer

Figs. 10.15–10.18 portrayed the heat transfer coefficient $Z(x) = \theta_y(\eta)\eta_x$ for numerous pertinent parameters. Effect of Sutterby fluid parameter B on heat transfer coefficient Z is investigated through Fig. 10.15. Result found that rise in B declines the coefficient of heat transfer Z . Fig. 10.16 demonstrates that larger values of thermal Grashof number Gr tend to increase the Z . Fig. 10.17 summarized effects of thermal Biot number Bi_1 on heat transfer coefficient Z . An increasing trend is noted for Z when Bi_1 highers. Fig. 10.18 depicts heat transfer coefficient Z verses activation energy parameter E . Here Z increases for higher E .

10.4.5 Entropy generation

Plots for entropy generation are drawn in Figs. 10.19 – 10.25. Fig. 10.19 is developed to see the impact of radiation parameter on entropy generation Ns . It shows that entropy increases near center of channel for higher Rn . Fig. 10.20 reveals the increasing response of Ns for higher Brinkman number Br . In Fig 10.21 an enhancement is observed in entropy Ns for higher concentration difference parameter γ^* . Fig. 10.22 shows the behavior of temperature difference parameter Λ on entropy Ns . Decreasing behavior for Ns is noticed. Fig. 10.23 depicts impacts on entropy Ns for diffusion coefficient parameter L . It is revealed from this Fig. that decreasing behavior of entropy occurs for raising L . Outcome of Sutterby fluid variable B^* on entropy is plotted in Fig. 10.24. Entropy rises for larger B . Impacts of Hall parameter m is sketched in Fig. 10.25. It is noted that entropy for m reduces.

10.5 Validation of the problem

We provide Table. 10.1. to verify the validation of our results. This table shows good agreement of the current results with [51] when $(B^* = M = Rn = Gr = Gc = \zeta = 0$ and $((Bi_1, Bi_2) \rightarrow \infty)$.

ϵ	η	Current work	Current work	ref. [51]	ref. [51]
		θ_y at $y = \eta$	ϕ_y at $y = \eta$	θ_y at $y = \eta$	ϕ_y at $y = \eta$
0.2	1.12	-0.211788	1.104649	-0.211789	1.104646
0.5	1.29	-5.523596	6.298794	-5.523598	6.298792

Table 10.1. Comparison of numerical results.

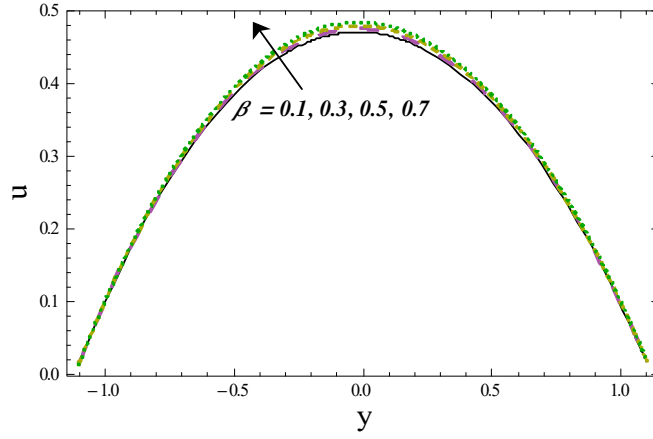


Fig. 10.1: Variation of β on u

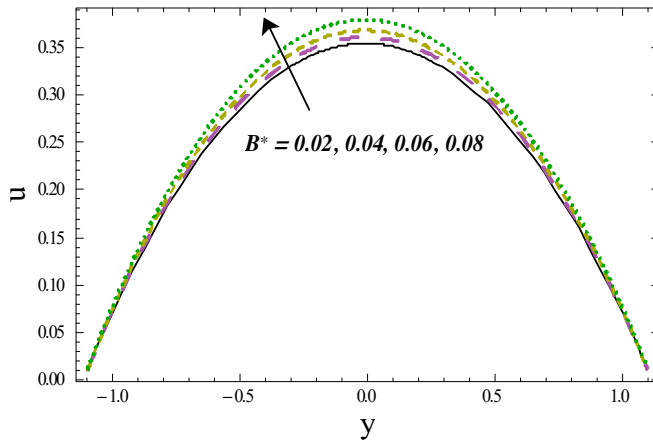


Fig. 10.2: Variation of B^* on u

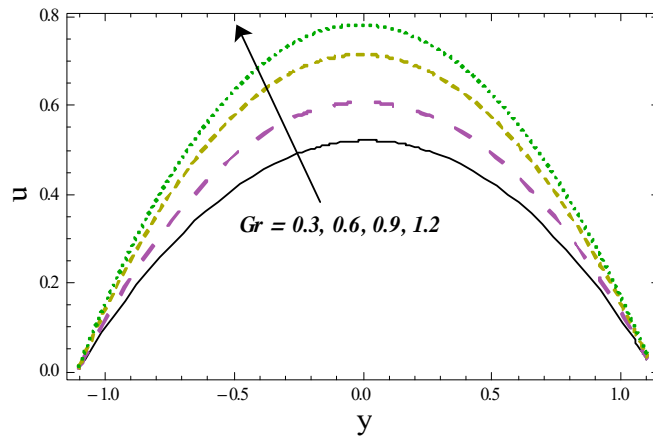


Fig. 10.3: Variation of Gr on u

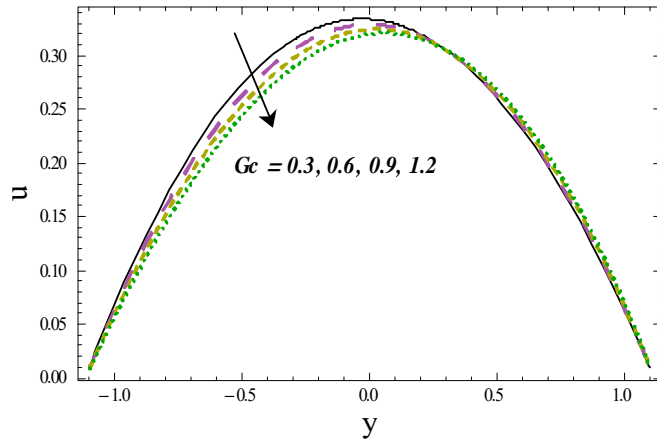


Fig. 10.4: Gc variation on u

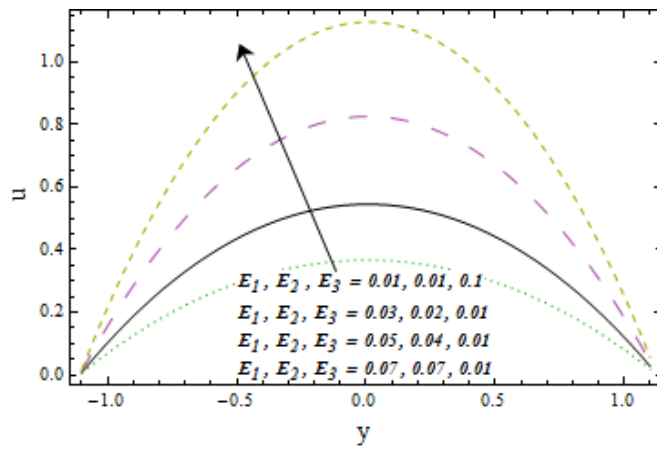


Fig. 10.5: Variations of E_1, E_2 and E_3 on u

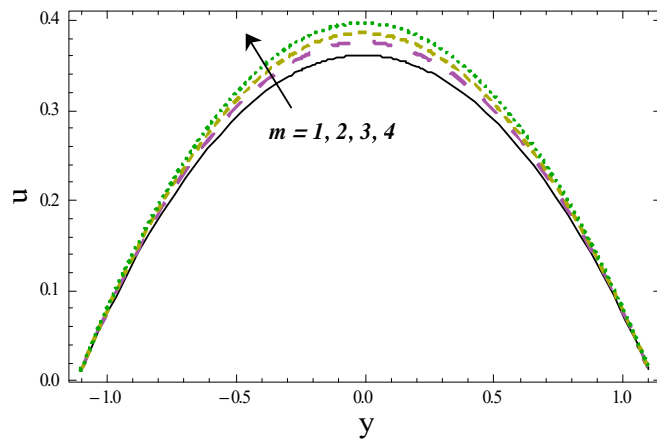


Fig. 10.6: Variation of m on u

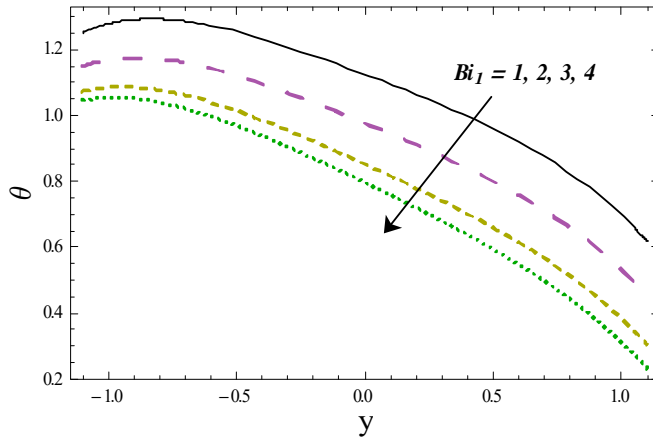


Fig. 10.7: Variation of Bi_1 on θ

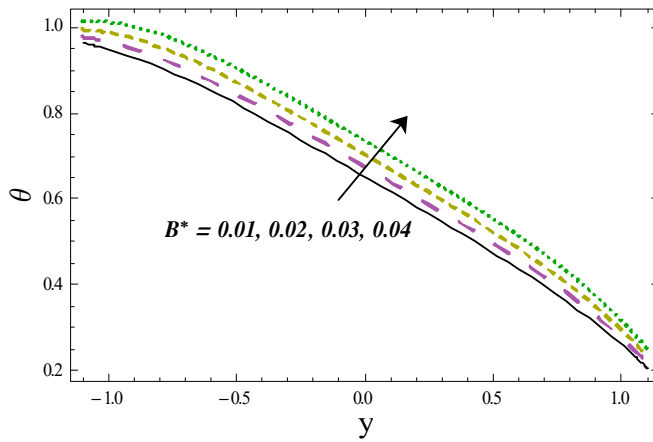


Fig. 10.8: Variation of B^* on θ

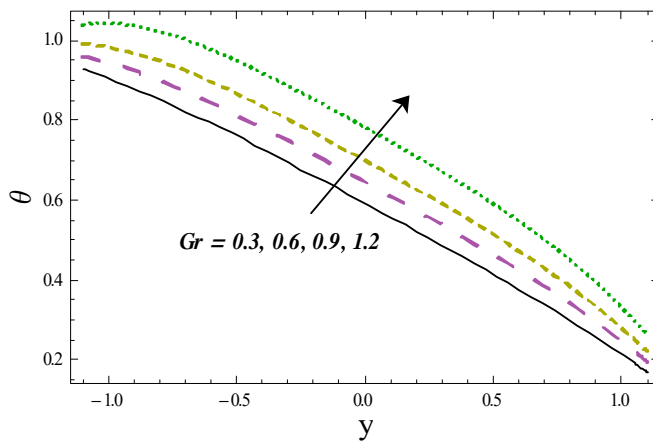


Fig. 10.9: Variation of Gr on θ

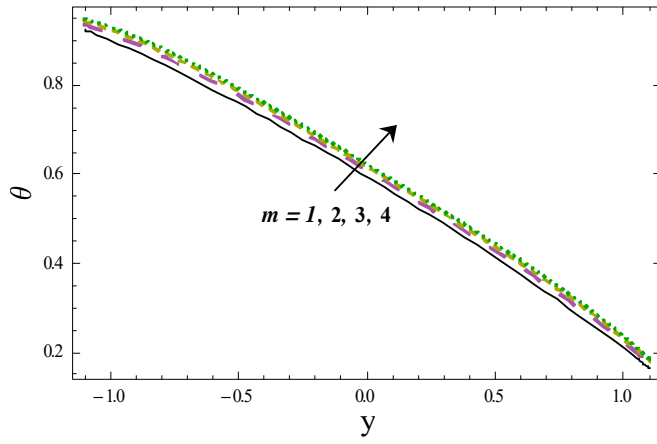


Fig. 10.10: Variation of m on θ

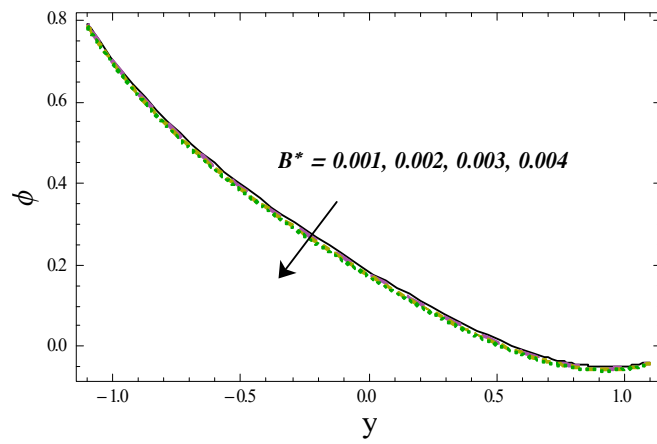


Fig. 10.11: Variation of B^* on ϕ

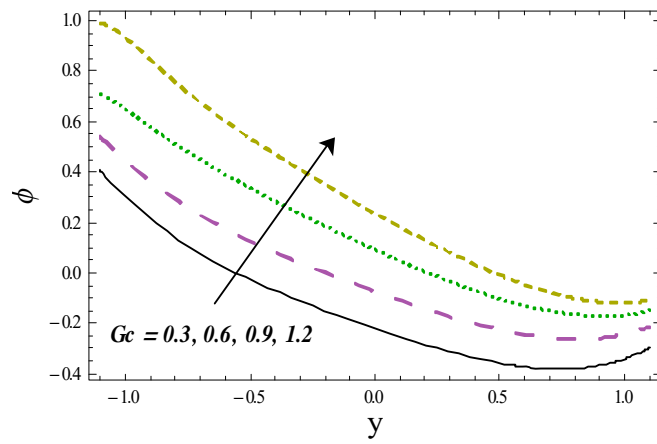


Fig. 10.12: Variation of Gc on ϕ

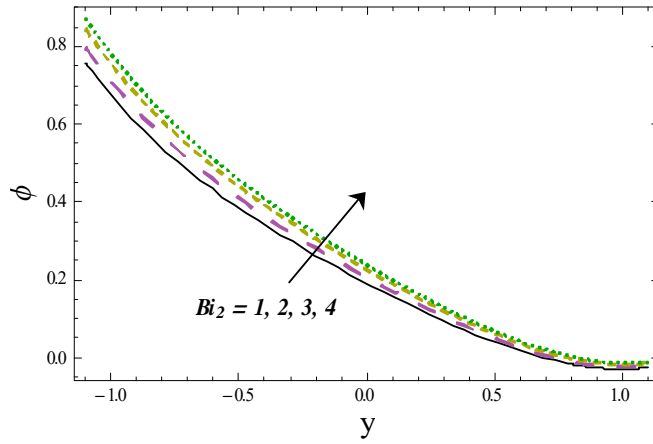


Fig. 10.13: Variation of Bi_2 on ϕ

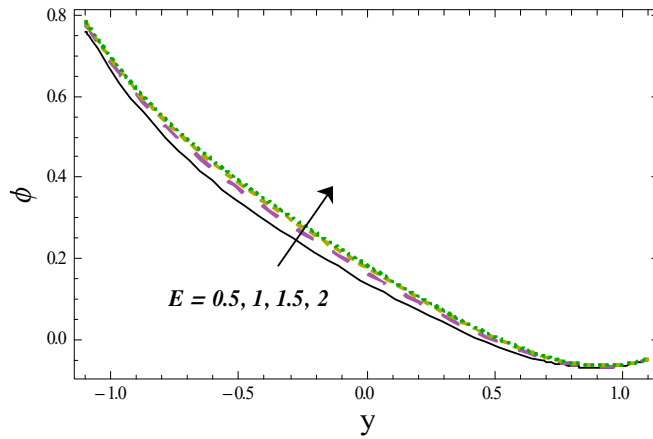


Fig. 10.14: Variation of E on ϕ

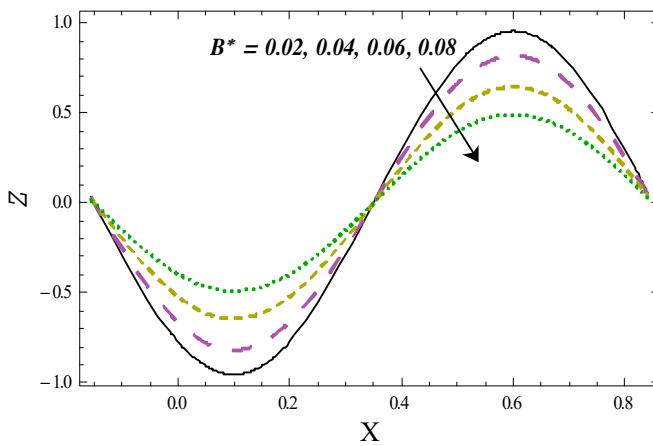


Fig. 10.15: Variation of B^* on Z

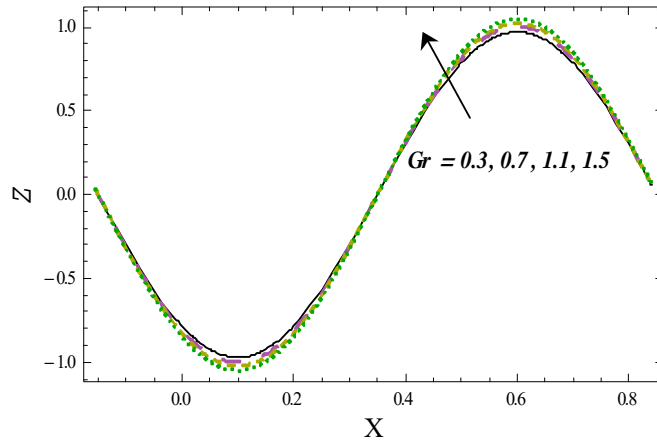


Fig. 10.16: Variation of Gr on Z

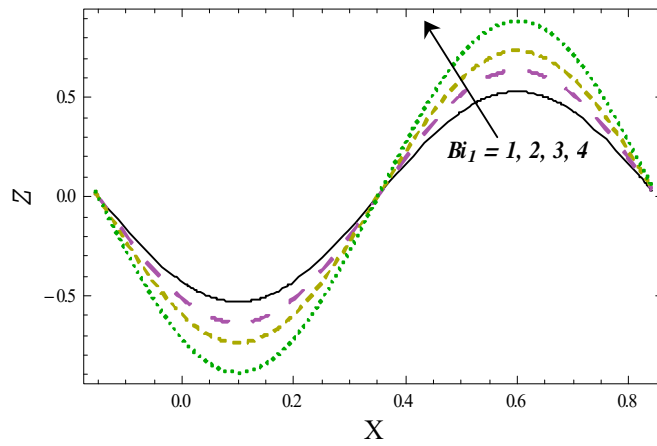


Fig. 10.17: Variation of Bi_1 on Z

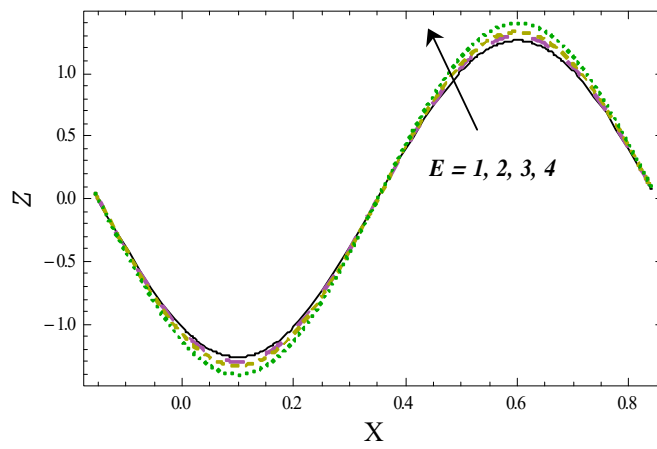


Fig. 10.18: Variation of E on Z

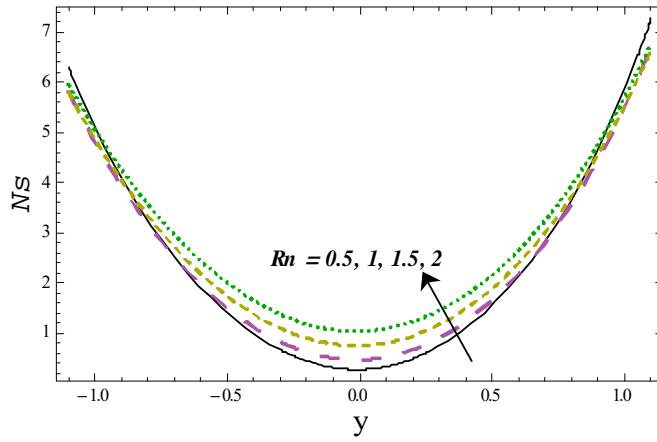


Fig. 10.19: Variation of Rn on Ns

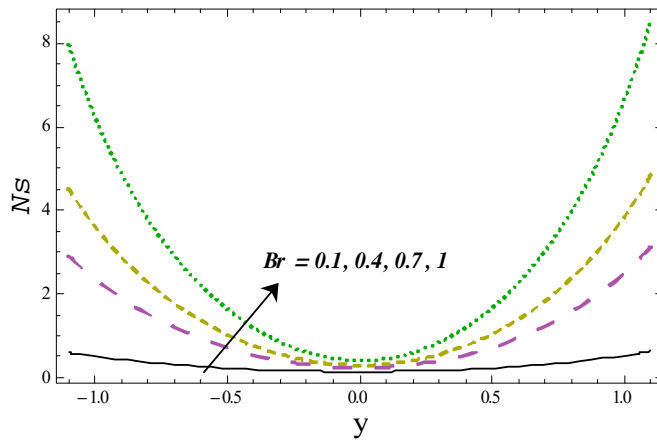


Fig. 10.20: Variation of Br on Ns

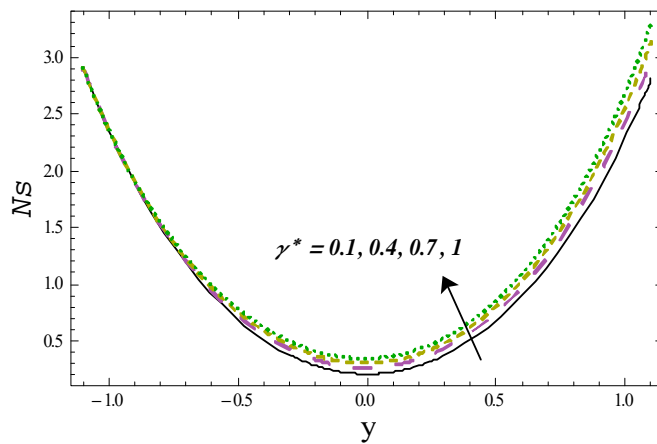


Fig. 10.21: Variation of γ^* on Ns

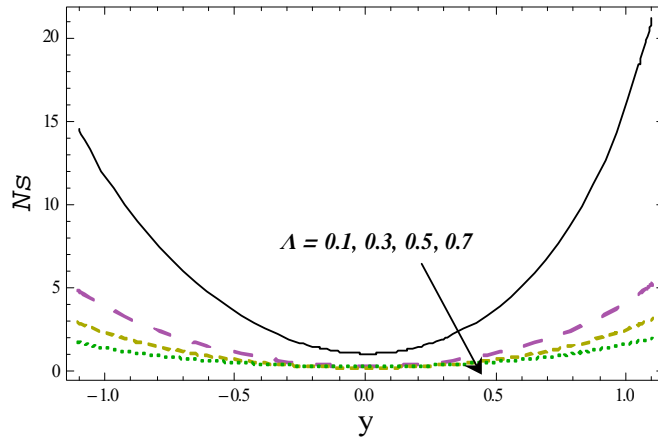


Fig. 10.22: Variation of Λ on Ns

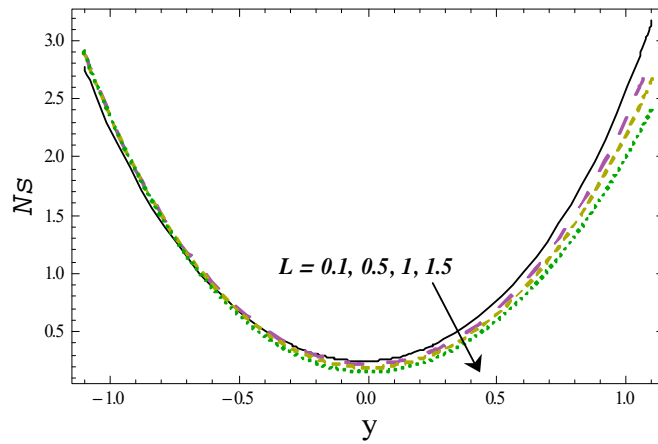


Fig. 10.23: Variation of L on Ns

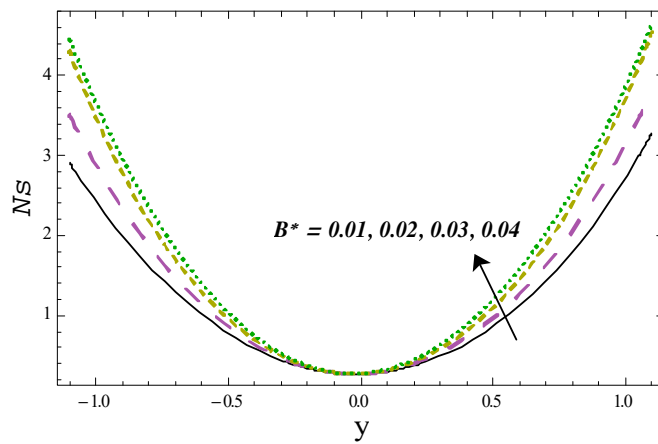


Fig. 10.24: Variation of B^* on Ns

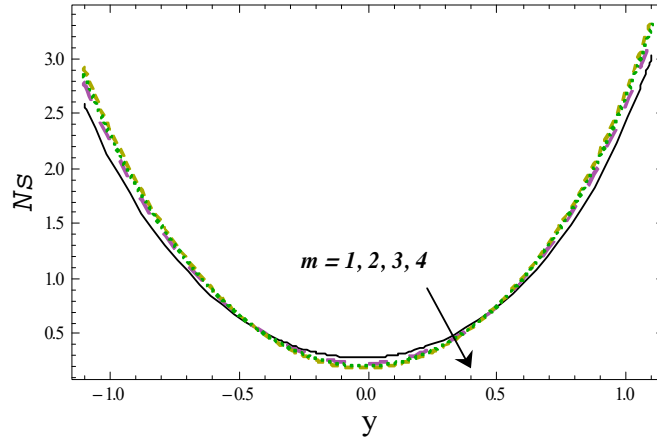


Fig. 10.25: Variation of m on Ns

10.6 Conclusions

The key points of current study are summarized below.

- Velocity is increased through Gr , B^* and m .
- Temperature rises with Gr and m .
- Concentration is decreased through B^* .
- Impact of E on concentration and heat transfer coefficient is qualitatively similar.
- Coefficient of heat transfer increases through larger Bi_1 , Gr and m .
- Entropy generation enhances for higher Rn and γ^* .
- Decreasing trend is noted for entropy generation against m , L and Λ .

Bibliography

- [1] T.W. Latham, Fluid motion in a peristaltic pump, MS Thesis, MIT Cambridge, MA, 1966.
- [2] J. C. Burns and T. Parkes, Peristaltic motion, *J. Fluid Mech.*, 29 (1967) 731-743.
- [3] A.H. Shapiro, M.Y. Jaffrin, S.L. Weinberg, Peristaltic pumping with long wavelength at low Reynolds number, *J. Fluid Mech.* 37 (1969) 799-825.
- [4] W.J. Dodds, W.J. Hogan, D.P. Reid, E.T. Stewart, R.C. Arndorfer, A comparison between primary esophageal peristalsis following wet and dry swallows, *J. Appl. Physiol.* 35 (1973) 851-857.
- [5] L.M. Srivastava, V.P. Srivastava, Peristaltic transport of a two-layered model of physiological fluid, *J. Biomech.* 15 (1982) 257-265.
- [6] E.F. El Shehawey, S.Z.A. Husseney, Effects of porous boundaries on peristaltic transport through a porous medium, *Acta Mech.* 143 (2000) 165-177.
- [7] J.C. Misra, S.K. Pandey, Peristaltic transport of blood in small vessels: Study of a mathematical model, *Comput. Math. with Appl.* 43 (2002) 1183-1193.
- [8] K.S. Mekheimer, Peristaltic flow of blood under effect of a magnetic field in a non-uniform channels, *Appl. Math. Comput.* 153 (2004) 763-777.
- [9] T. Hayat, N. Ali, S. Asghar, A.M. Siddiqui, Exact peristaltic flow in tubes with an endoscope, *Appl. Math. Comput.* 182 (2006) 359-368.
- [10] N. Ali, Q. Hussain, T. Hayat, S. Asghar, Slip effects on the peristaltic transport of MHD fluid with variable viscosity, *Phys. Lett. A* 372 (2008) 1477-1489.

- [11] D. Tripathi, S.K. Pandey, S. Das, Peristaltic flow of viscoelastic fluid with fractional Maxwell model through a channel. *Appl. Math. Comput.* 215 (2010) 3645-3654.
- [12] M. Mustafa, S. Hina, T. Hayat, A. Alsaedi, Slip effects on the peristaltic motion of nanofluid in a channel with wall properties, *J. Heat Transf.* 135 (2013) 041701.
- [13] F.M. Abbasi, T. Hayat, and B. Ahmad, Peristaltic transport of copper–water nanofluid saturating porous medium, *Physica E: Low-dimensional Systems and Nanostructures* 67 (2015) 47-53.
- [14] T. Hayat, Z. Nisar, H. Yasmin, A. Alsaedi, Peristaltic transport of nanofluid in a compliant wall channel with convective conditions and thermal radiation, *J. Mol. Liq.* 220 (2016) 448-453.
- [15] R. Ellahi, M.M. Bhatti, C. Fetecau, K. Vafai, Peristaltic flow of couple stress fluid in a non-uniform rectangular duct having compliant walls, *Commun. Theor. Phys.* 65 (2016) 66.
- [16] M.D. Sinnott, P.W. Cleary, S.M. Harrison, Peristaltic transport of a particulate suspension in the small intestine, *Appl. Math. Model.* 44 (2017) 143-159.
- [17] M.M. Bhatti, A. Zeeshan, R. Ellahi, G.C. Shit, Mathematical modeling of heat and mass transfer effects on MHD peristaltic propulsion of two-phase flow through a Darcy-Brinkman-Forchheimer porous medium, *Adv. Powder Techno.* 29 (2018) 1189-1197.
- [18] T. Hayat, B. Ahmed, F.M. Abbasi, A. Alsaedi, Peristalsis of nanofluid through curved channel with Hall and Ohmic heating effects, *J. Cent. South Univ.* 26 (2019) 2543-2553.
- [19] S.U.S. Choi, Enhancing thermal conductivity of fluids with nanoparticles, D.A. Siginer, H.P. Wang (Eds) *Developments and Applications of non-Newtonian Flows*, ASME FED. 231 (1995) 99-105.
- [20] H.U. Kang, S.H. Kim, J.M. Oh, Estimation of thermal conductivity of nanofluid using experimental effective particle volume, *Exp. Heat Transf.* 19 (2006) 181–191.
- [21] J. Buongiorno, Convective transport in nanofluids, *ASME J. Heat Transf.* 128 (2006) 240-250.

- [22] N.S. Akbar, S. Nadeem, T. Hayat, A.A. Hendi, Peristaltic flow of a nanofluid with slip effects, *Meccanica*, 47 (2012) 1283-1294.
- [23] S.Z. Heris, T.H. Nassan, S.H. Noie, H. Sardarabadi, Laminar convective heat transfer of Al₂O₃/water nanofluid through square cross-sectional duct, *Int. J. Numer. Methods Heat Fluid Flow*, 44 (2013) 375-382.
- [24] A. Ebaid, E.H. Aly, Exact analytical solution of the peristaltic nanofluids flow in an asymmetric channel with flexible walls and slip condition: application to the cancer treatment, *Comput. Math. Methods Med.* 2013 (2013) 825376.
- [25] N.S. Akbar, S. Nadeem, Z.H. Khan, Numerical simulation of peristaltic flow of a Carreau nanofluid in an asymmetric channel, *Alex. Eng. J.* 53 (2014), 191-197.
- [26] D. Tripathi, O.A. Bég, A study on peristaltic flow of nanofluids: Application in drug delivery systems, *Int. J. Heat Mass Transf.* 70 (2014) 61-70.
- [27] T. Hayat, F.M. Abbasi, M. Al-Yami, S. Monaquel, Slip and Joule heating effects in mixed convection peristaltic transport of nanofluid with Soret and Dufour effects, *J. Mol. liq.* 194 (2014) 93-99.
- [28] M. Kothandapani, J. Prakash, Effect of radiation and magnetic field on peristaltic transport of nanofluids through a porous space in a tapered asymmetric channel, *J. Magn. Magn. Mater.* 378 (2015) 152-163.
- [29] N.S. Akbar, M. Raza, R. Ellahi, Impulsion of induced magnetic field for Brownian motion of nanoparticles in peristalsis, *Appl. Nanosci.* 6 (2016) 359-370.
- [30] M.G. Reddy, O.D. Makinde, Magnetohydrodynamic peristaltic transport of Jeffrey nanofluid in an asymmetric channel, *J. Mol. Liq.* 223 (2016) 1242-1248.
- [31] T. Hayat, B. Ahmed, F.M. Abbasi, A. Alsaedi, Hydromagnetic peristalsis of water based nanofluids with temperature dependent viscosity: a comparative study, *J. Mol. Liq.* 234 (2017) 324-329.

- [32] D. Tripathi, A. Sharma, O.A. Bég, Electrothermal transport of nanofluids via peristaltic pumping in a finite micro-channel: Effects of Joule heating and Helmholtz-Smoluchowski velocity, *Int. J. Heat Mass Transf.* 111 (2017) 138-149.
- [33] F.M. Abbasi, M. Gul, S.A. Shehzad, Hall effects on peristalsis of boron nitride-ethylene glycol nanofluid with temperature dependent thermal conductivity, *Physica E*, 99 (2018) 275-284.
- [34] Kh S. Mekheimer, W.M. Hasona, R.E. Abo-Elkhair, A. Z. Zaher, Peristaltic blood flow with gold nanoparticles as a third grade nanofluid in catheter: Application of cancer therapy, *Phys. Lett. A* 382 (2018) 85-93.
- [35] M. Rafiq, H. Yasmin, T. Hayat, F. Alsaadi, Effect of Hall and ion-slip on the peristaltic transport of nanofluid: a biomedical application, *Chin. J. Phys.* 60 (2019) 208-227.
- [36] L.M. Srivastava, Peristaltic transport of a couple-stress fluid, *Rheol. Acta.* 25 (1986) 638-641.
- [37] K. Ramesh, Effects of slip and convective conditions on the peristaltic flow of couple stress fluid in an asymmetric channel through porous medium, *Comput. Meth. Prog. Biomed.* 135 (2016) 1-14.
- [38] T. Hayat, A. Tanveer, H. Yasmin, A. Alsaedi, Effects of convective conditions and chemical reaction on peristaltic flow of Eyring-Powell fluid, *Appl. Bionics Biomech.* 11 (2014) 221-233.
- [39] M.M. Bhatti, M.A. Abbas, M.M. Rashidi, Combine effects of magnetohydrodynamics (MHD) and partial slip on peristaltic blood flow of Ree-Eyring fluid with wall properties, *Eng. Sci. Technol. an Int.* 19 (2016) 1497-1502.
- [40] O.U. Mehmood, N. Mustapha, S. Shafie, Heat transfer on peristaltic flow of fourth grade fluid in inclined asymmetric channel with partial slip, *Appl. Math. Mech.* 33 (2012) 1313-1328.

- [41] M. Mustafa, S. Abbasbandy, S. Hina, T. Hayat, Numerical investigation on mixed convective peristaltic flow of fourth grade fluid with Dufour and Soret effects, *J. Taiwan. Inst. Chem. Eng.* 45 (2014) 308-316.
- [42] N.S. Akbar, S. Nadeem, Nano Sutterby fluid model for the peristaltic flow in small intestines, *J. Comput. Theor. Nanosci.* 10 (2013) 2491-2499.
- [43] F.M. Abbasi, T. Hayat, A. Alsaedi, Effects of inclined magnetic field and Joule heating in mixed convective peristaltic transport of non-Newtonian fluids, *B. Pol. Aca. Sci. Tech. Sci.* 63 (2015) 501-514.
- [44] S. Akram, S. Nadeem, Consequence of nanofluid on peristaltic transport of a hyperbolic tangent fluid model in the occurrence of apt (tending) magnetic field, *J. Magn. Magn. Mater.* 358 (2014) 183-191.
- [45] F.M. Abbasi, T. Hayat, A. Alsaedi, Numerical analysis for MHD peristaltic transport of Carreau–Yasuda fluid in a curved channel with Hall effects, *J. Magn. Magn. Mater.* 382 (2015) 104-110.
- [46] T.K. Mitra, S.N. Prasad, On the influence of wall properties and Poiseuille flow in peristalsis, *J. Biomech.* 6 (1973) 681-693.
- [47] G. Radhakrishnamacharya, Ch. Srinivasulu, Influence of wall properties on peristaltic transport with heat transfer, *Comptes Rendus Mecanique* 335 (2007) 369-373.
- [48] S. Srinivas, R. Gayathri, M. Kothandapani, The influence of slip conditions, wall properties and heat transfer on MHD peristaltic transport, *Comput. Phys. Commun.* 180 (2009) 2115-2122.
- [49] S. Srinivas, M. Kothandapani, The influence of heat and mass transfer on MHD peristaltic flow through a porous space with compliant walls, *Appl. Math. Comput.* 213 (2009) 197-208.
- [50] T. Hayat, S. Hina, A.A. Hendi, S. Asghar, Effect of wall properties on the peristaltic flow of a third grade fluid in a curved channel with heat and mass transfer, *Int. J. Heat Mass Transf.* 54 (2011) 5126-5136.

- [51] M. Mustafa, S. Hina, T. Hayat, A. Alsaedi, Influence of wall properties on the peristaltic flow of a nanofluid: analytic and numerical solutions, *Int. J. Heat Mass Transf.* 55 (2012) 4871-4877.
- [52] T. Hayat, M. Javed, S. Asghar, A.A. Hendi, Wall properties and heat transfer analysis of the peristaltic motion in a power-law fluid, *Int. J. Numer. Methods Fluids* 71 (2013) 65-79.
- [53] N.S. Gad, Effects of Hall currents on peristaltic transport with compliant walls, *Appl. Math. Comput.* 235 (2014) 546-554.
- [54] S. Nadeem, E.N. Maraj, N.S. Akbar, Investigation of peristaltic flow of Williamson nanofluid in a curved channel with compliant walls, *Appl. Nanosci.* 4 (2014) 511-521.
- [55] G. Sucharitha, P. Lakshminarayana, N. Sandeep. Joule heating and wall flexibility effects on the peristaltic flow of magnetohydrodynamic nanofluid, *Int. J. Mech. Sci.* 131 (2017) 52-62.
- [56] J.C. Umavathi, J.P. Kumar, A.J. Chamkha, I. Pop, Mixed convection in a vertical porous channel, *Transp. Porous Media*, 61 (2005) 315-335.
- [57] A. Akbarinia, A. Behzadmehr, Numerical study of laminar mixed convection of a nanofluid in horizontal curved tubes, *Appl. Therm. Eng.* 27 (2007) 1327-1337.
- [58] N.T.M. Eldabe, M.F.El-Sayed, A.Y. Ghaly, H.M. Sayed, Mixed convective heat and mass transfer in a non-Newtonian fluid at a peristaltic surface with temperature-dependent viscosity, *Arch. Appl. Mech.* 78 (2008) 599-624
- [59] S. Srinivas, R. Gayathri, M. Kothandapani, Mixed convective heat and mass transfer in an asymmetric channel with peristalsis, *Commun. Nonlinear Sci. Numer. Simul.* 16 (2011) 1845-1862.
- [60] S. Akram, A. Ghafoor, S. Nadeem, Mixed convective heat and mass transfer on a peristaltic flow of a non-Newtonian fluid in a vertical asymmetric channel, *Heat Transfer—Asian Research* 41 7 (2012) 613-633.
- [61] T. Hayat, F.M. Abbasi, B. Ahmad, A. Alsaedi, MHD mixed convection peristaltic flow with variable viscosity and thermal conductivity, *Sains Malays* 43 (2014) 1583-1590.

- [62] S. Noreen, Mixed convection peristaltic flow with slip condition and induced magnetic field, *Eur. Phys. J. Plus* 129 (2014) <https://doi.org/10.1140/epjp/i2014-14033-3>.
- [63] M. Mokhtari, M.B. Gerdroodbary, R. Yeganeh, K. Fallah, Numerical study of mixed convection heat transfer of various fin arrangements in a horizontal channel, *Eng. Sci. Technol. an Int. J.* 20 (2017) 1106-1114.
- [64] M. Turkyilmazoglu, Analytical solutions to mixed convection MHD fluid flow induced by a nonlinearly deforming permeable surface, *Commun. Nonlinear Sci. Numer. Simul.* 63 (2018) 373-379.
- [65] D. Pal, Combined effects of non-uniform heat source/sink and thermal radiation on heat transfer over an unsteady stretching permeable surface, *Commun. Nonlinear Sci. Numer. Simul.* 16 (2011) 1890-1904.
- [66] T. Hayat, A. Alsaedi, On thermal radiation and Joule heating effects in MHD flow of an Oldroyd-B fluid with thermophoresis, *Arab. J. Sci. Eng.* 36 (2011) 1113-1124.
- [67] A. Ara, N.A. Khan, H. Khan, F. Sultan, Radiation effect on boundary layer flow of an Eyring–Powell fluid over an exponentially shrinking sheet, *Ain Shams Eng. J.* 5 (2014) 1337-1342.
- [68] M. Kothandapani, J. Prakash, Effect of radiation and magnetic field on peristaltic transport of nanofluids through a porous space in a tapered asymmetric channel, *J. Magn. Magn. Mater.* 378 (2015) 152–163.
- [69] T. Latif, N. Alvi, Q. Hussain, S. Asghar, Peristaltic flow of nonconstant viscosity fluid with nonlinear thermal radiation, *J. Comput. Theor. Nanosci.* 14 (2017) 2681-2693.
- [70] J. Prakash, D. Tripathi, Electroosmotic flow of Williamson ionic nanoliquids in a tapered microfluidic channel in presence of thermal radiation and peristalsis, *J. Mol. Liq.* 256 (2018) 352-371.
- [71] W.K.H. Chu, J. Fang, Peristaltic transport in a slip flow, *Eur. Phys. J. B*, 16 (2000) 543-547.

- [72] N. Ali, Q. Hussain, T. Hayat, S. Asghar, Slip effects on the peristaltic transport of MHD fluid with variable viscosity, *Phys. Lett. A* 372 (2008) 1477-1489.
- [73] M.K. Chaube, S. K. Pandey, D. Tripathi, Slip effect on peristaltic transport of micropolar fluid, *Appl. Math. Sci.* 4 (2010) 2015-2117.
- [74] D. Tripathi, P.K.Gupta, S. Das, Influence of slip condition on peristaltic transport of a viscoelastic fluid with fractional Burger's model, *Therm. Sci.* 15(2011) 501-515.
- [75] N.S. Akbar, A.B. Huda, D. Tripathi, Thermally developing MHD peristaltic transport of nanofluids with velocity and thermal slip effects, *Eur. Phys. J. Plus.* 131 (2016) 332.
- [76] G. Sucharitha, M.M. Rashidi, S. Sreenadh, P. Lakshminarayana, Effects of magnetic field and slip on convective peristaltic flow of a non-Newtonian fluid in an inclined nonuniform porous channel with flexible walls, *J. Porous Media* 21 (2018) 895-910.

- Processed on 09-Jun-2022 15:16 PKT
- ID: 1853539166
- Word Count: 26316

Similarity Index
8%
Similarity by Source

Internet Sources:
5%
Publications:
5%
Student Papers:
2%

Palwan 14/06
Focal Person (Turnitin)
Quaid-i-Azam University
Islamabad

Zahid
3, 28

10/6/22

PROFESSOR
Department of Mathematics
Quaid-i-Azam University
Islamabad

sources:

- ✓ **1** 1% match (Internet from 24-Dec-2021)
<http://pr.hec.gov.pk/jspui/bitstream/123456789/17297/1/Sada%20Nawaz%20maths%202021%20qau%20isb.pdf>
- ✓ **2** 1% match (Internet from 16-Dec-2018)
<http://www.rpublication.com/ijeted/2014/march14/71.pdf>
- ✓ **3** < 1% match (Internet from 24-Dec-2021)
http://pr.hec.gov.pk/jspui/bitstream/123456789/9351/1/Anum%20Tanveer_Maths_2018_QAU_PRR.pdf
- 4** < 1% match (Internet from 27-Dec-2021)
http://pr.hec.gov.pk/jspui/bitstream/123456789/16733/1/Arsalan%20Aziz%20maths%202020%20qau%20isb%20%282021_02_17%2008
- 5** < 1% match (Internet from 17-Feb-2022)
<http://pr.hec.gov.pk/jspui/bitstream/123456789/9112/1/Azam.pdf>
- 6** < 1% match (Internet from 05-Oct-2017)
<http://pr.hec.gov.pk/Thesis/2927S.pdf>
- 7** < 1% match (Internet from 31-Oct-2021)
http://pr.hec.gov.pk/jspui/bitstream/123456789/11003/1/Arif%20Hussain_Maths_2019_QAU.pdf
- 8** < 1% match (student papers from 12-Jan-2018)
[Submitted to Higher Education Commission Pakistan on 2018-01-12](#)
- 9** < 1% match (student papers from 09-Apr-2018)
[Submitted to Higher Education Commission Pakistan on 2018-04-09](#)
- 10** < 1% match (student papers from 31-Jul-2018)
[Submitted to Higher Education Commission Pakistan on 2018-07-31](#)
- 11** < 1% match (student papers from 18-Dec-2017)
[Submitted to Higher Education Commission Pakistan on 2017-12-18](#)
- 12** < 1% match (student papers from 14-May-2018)
[Submitted to Higher Education Commission Pakistan on 2018-05-14](#)
- 13** < 1% match (student papers from 10-Sep-2009)
[Submitted to Higher Education Commission Pakistan on 2009-09-10](#)
- 14** < 1% match (student papers from 25-Dec-2016)
[Submitted to Higher Education Commission Pakistan on 2016-12-25](#)
- 15** < 1% match (student papers from 08-Apr-2017)
[Submitted to Higher Education Commission Pakistan on 2017-04-08](#)